Universidad Autónoma de Madrid

Departamento de Bioquímica

Estudio de las bases moleculares de los síndromes de Ellis-van Creveld y Weyers Acrofacial Dysostosis y análisis del papel de Evc en la placa de crecimiento

María Valencia Benítez

Madrid, 2012

Departamento de Bioquímica

Facultad de Medicina

Universidad Autónoma de Madrid

Estudio de las bases moleculares de los síndromes de Ellis-van Creveld y Weyers Acrofacial Dysostosis y análisis del papel de Evc en la placa de crecimiento

María Valencia Benítez

Licenciada en Biología

Director de Tesis: Dr. Víctor L. Ruíz Pérez

Instituto de Investigaciones Biomédicas “Alberto Sols”

CSIC-UAM

MINISTERIO
DE ECONOMÍA Y
COMPETITIVIDAD

CSIC

UAM UNIVERSIDAD AUTONOMA DE MADRID

INSTITUTO DE INVESTIGACIONES BIOMÉDICAS
"ALBERTO SOLS"

Víctor L. Ruíz Pérez, PhD
Instituto de Investigaciones Biomédicas
Arturo Duperier, 4.
E-28029 Madrid, SPAIN
Tel: 34 91 585 4387
Fax: 34 91 585 4401
e-mail:vlruiz@iib.uam.es

VÍCTOR L. RUÍZ PÉREZ, Científico Titular del Instituto de Investigaciones Biomédicas "Alberto Sols" CSIC-UAM,

certifico que:

MARÍA VALENCIA BENÍTEZ, Licenciada en Biología por la Universidad Autónoma de Madrid ha realizado, bajo mi dirección, el trabajo de investigación titulado:

"Estudio de las bases moleculares de los síndromes de Ellis-van Creveld y Weyers Acrofacial Dysostosis y análisis del papel de Evc en la placa de crecimiento"

Considero que el mencionado trabajo es satisfactorio y apto para poder optar al grado de Doctor por la Universidad Autónoma de Madrid.

Y para que conste a todos los efectos, firmo el presente certificado, en Madrid, a 14 de Febrero de 2012.

Fdo: Víctor L. Ruíz Pérez

Científico Titular, CSIC

Vº Bº: Jesús Cruces

Catedrático, UAM

Instituto de Investigaciones
Biomédicas "Alberto Sols".
C/Arturo Duperier, nº 4
28029 MADRID (ESPAÑA)
TEL.: 91 585 4400
FAX: 91 585 4401

A mis padres
A Sergio

"Lo importante es no dejar de hacerse preguntas".
-Albert Einstein-

Agradecimientos

Y como todo tiene su fin… aquí estoy escribiendo los agradecimientos de una etapa muy intensa tanto personal como profesionalmente, que termina después de 5 años y en la que en tengo que dar las gracias a muchas personas.

En primer lugar quiero agradecer a mi director de tesis, el Dr. Víctor L. Ruiz por darme la oportunidad de formar parte de tu laboratorio, por todo el apoyo de estos años, tu dedicación, tu tiempo, tu esfuerzo y tus enseñanzas. Gracias por confiar en mí.

No puedo olvidarme de mis primeros pasos en la ciencia en la Universidad Complutense. Gracias a la Dra. Julia Pérez-Miguelsanz que fuiste la primera persona que dejó un juego de pipetas en mis manos, y a Loli y Alicia porque me iniciasteis en el mundo de microtomo entre locura y locura. A mis "UCM Girls": a Arán, a Miriam y a Tamara, con las que he compartido tantos cafés, risas, charlas, si hablaran las paredes de ese despachito… y que habéis sido un apoyo importantísimo, porque aunque no nos veamos tan a menudo como nos gustaría, siempre os he sentido cerca. Y por supuesto a la Dra. Mª José Blanco, de la que tanto aprendí de la ciencia y de la vida, gracias por ser como eres.

Tengo que dar las gracias a muchas personas del IIB. Al servicio de Informática: a Javi, que inundas de buenas vibraciones todo tu alrededor; a Guti y a Alex, por salvarme en los momentos de colapso nervioso con el ordenador. Al servicio de Imagen, a Antonio, Dani y en especial a Javi, mi mano salvadora con el Ilustrator. Al servicio de Secuenciación, a Gema, a Conchi y a Diana, que siempre me habéis ayudado cuando os lo he pedido. A la gente del animalario, a Fernando que me recibes con una sonrisa cada vez que bajo, a Geni, a Graci, a Gus,… y sobre todo a Ili, por toda la paciencia que tuviste enseñándome a coger ratones, y por haber tenido que perseguir a alguno que otro que se escapó... A Dani y a Manolo de almacén, por el buen humor que tenéis ahí abajo. A los de Seguridad, Diego y a Carlos por traerme bombones para que me endulcen la escritura. Al servicio de Microscopía, a Lucía y sobre todo a Diego, por animarme en mi carrera como monologuista, y porque cada vez que voy con un reto nuevo estás dispuesto a echarme una mano. A Aida, porque intentas hacer del IIB un "mundo mejor" y porque te preocupas por nosotros.

Gracias a todos con los que en algún momento he intercambiado una conversación, unas palabras de ánimo o una sonrisa: Jose, Marina y a Diana (1.9); María, Ascen y Vero (1.11); Bea, Virginia y Jesús (1.7); Natalia (0.2); Yenni y Rafa (1.4.2); Carmen del 2.7, ahora al otro lado del charco, y Ana (2.9) con las que he compartido tantos momentos en células; Mª Carmen, porque desde esa noche en el Escorial….jaja descubrí a una gran persona; Dani (1.2.1) e Irene (1.8) por los pequeños momentos de relax en la biblioteca. Al 0.3, a Toño

y Laura, por brindarme su ayuda; a Merche por nuestras charlas, por tus consejos y por interesarte; a Patri, porque dentro de tu caos me has demostrado que hay un gran corazón. Al 1.4.1, Isa gracias por tus notitas, tus bailes, tus chistes… y tu optimismo, y a Albert mi "Maestro del HTC", compañero de células y de biblioteca, porque nadie baila como tú "Single Ladies" y porque tengo que darte las gracias muchas, muchas veces por tu ayuda impresindible en los últimos momentos.

A mis amigas de la Facultad a Anita, a Anette y a Vane, porque nunca olvidaré los buenos ratos que pasamos juntas: nuestros malabares con el Hacky, los bailes en los que fuisteis espectadoras y compañera, esas partidas interminables de mus, por los momentos de estrés previos a los exámenes, por vivir conmigo 5 años que fueron muy especiales.

A mis amigos de siempre con los que llevo 25 años, porque hemos crecido juntos y lo seguimos haciendo día a día: Sarita, Alicia, Rubén, José, María O, y en especial a Lucía, porque siempre estás a mi lado. Gracias por intentar entender lo que hago, por escucharme a pesar que os suene a chino lo que cuento, por preguntar cómo están mis ratones, por estar pendientes cada semana de mis avances, por animarme, por compartir nuestras preocupaciones y nuestros miedos, por tantos y tantos recuerdos!!

Volviendo al IIB tengo que dar las gracias a las personas con las que más momentos he vivido en esta etapa: hemos trepado por árboles, nos hemos tirado por toboganes como los niños y lo hemos dado todo bailando. Gracias a mis compañeros del "otro labo", el B15: a Pili porque eres una persona maravillosa (no me olvido de ti); a Irene, por todos los momentos compartidos, por estar, por ser confidente y porque te adoro, te echo mucho de menos!!!!; a Carlos por todo lo que he aprendido de moda (y de serpientes…) y porque siempre me haces reír; a Marta, por vivir juntas el estado catatónico que nos produce el cubículo con nuestras conversaciones sin sentido y por animarnos mutuamente. A María G. por no perderte una y recibirme siempre con los brazos abiertos cuando he acudido a ti. Trini, mucha suerte en esta etapa que empiezas

A mis compañeros de labo, mi familia del IIB. Edel, que con tu "ritmo sabrosón", me haces ver el lado positivo y me has enseñado a tomarme las cosas menos en serio. A María P, compañera y amiga en este viaje, gracias porque siempre has estado para escucharme, por aguantarme en los buenos y en los malos momentos, por aconsejarme, por reír y llorar conmigo, por preocuparte por mí, porque has sido imprescindible en esta tesis y muy importante también fuera. A Pepe porque eres una de las mejores personas que he conocido. Gracias porque siempre me haces sonreír incluso cuando parece misión imposible, por endulzarme la vida en los momentos de bajón,

porque siempre estás dispuesto a tenderme una mano cuando la necesito, por enseñarme con paciencia. Gracias porque tengo la suerte de poder decir que conocí compañeros y me llevo amigos!!!

A Sergio, porque llevamos mucho tiempo recorriendo juntos el camino, llevas apoyándome desde mi primer año de Facultad, pasando conmigo momentos malos y otros muy muy buenos. Gracias por no perder la paciencia en esta última etapa, por hacerme sentir especial, por cómo me quieres, porque nunca me has fallado y porque quiero que estés siempre a mi lado.

A mi "brother" por todo lo vivido, por tu sonrisa, por tu humor, por cómo te tomas las cosas, porque cuando te necesito estás y porque te quiero.

A mis padres, fundamentales en mi vida. Gracias por creer en mí, por hacerme crecer como persona, por ayudarme, por apoyarme siempre siempre siempre, por escucharme, por comprenderme, porque habéis hecho todo lo posible e inimaginable para hacerme feliz, porque esta tesis es tan mía como vuestra, porque sin vosotros no habría llegado donde estoy. Gracias por dejarme ser "la niña".

Resumen

El síndrome de Ellis-van Creveld (EvC; MIM 225500) es una enfermedad autosómica recesiva que afecta al desarrollo, la cual combina anormalidades esqueléticas con defectos ectodérmicos en uñas y dientes. Además el 60% de los casos también presentan malformaciones cardíacas. Los pacientes EvC portan mutaciones en los genes *EVC* o *EVC2,* las cuales en su mayoría introducen codones de fin de mensaje prematuros. Mientras la mayoría de las mutaciones encontradas en estos genes son recesivas, existen algunas mutaciones heterocigotas en el último exón de *EVC2* que dan lugar a un síndrome autosómico dominante denominado Weyers Acrofacial Dysostosis (Weyers; MIM # 193530). Los pacientes diagnosticados con Weyers manifiestan características clínicas muy similares a las del síndrome de EvC, aunque de menor gravedad. En esta tesis hemos llevado a cabo el análisis molecular de un número considerable de pacientes diagnosticados con EvC o Weyers, lo que nos ha permitido identificar 31 mutaciones nuevas en *EVC* y *EVC2,* incluidas 2 mutaciones dominantes Weyers en el último exón de *EVC2*. En este trabajo describimos por primera vez individuos con mutaciones en *EVC* y en *EVC2* como consecuencia de una deleción mediada por recombinación entre elementos LINE-1, la cual involucra a *EVC, EVC2* y los genes adyacentes *STK32B* y *C4orf6*. . El estudio del fenotipo de individuos portadores de este reordenamiento cromosómico indica que mientras que la deleción en heterocigosis no está asociada a defectos clínicos, individuos con la deleción en ambos cromosomas presentan EvC junto con un ligero retraso mental. Por otro lado, mediante experimentos en cultivo celular en los que usamos variantes murinas de mutaciones dominantes de *EVC2*, demostramos que el mecanismo molecular subyacente al síndrome de Weyers es una alteración en la respuesta a las señales Hh, y revelamos por primera vez un papel de Evc2 en esta vía. Anteriormente se había publicado que Evc se localiza en el cilio primario y es requerido en la vía de Hedgehog. Finalmente hemos llevado a cabo un estudio exhaustivo de la placa de crecimiento embrionaria de los huesos largos y sincrondrosis craneales del modelo animal *Evc-LacZ* en un fondo genético homogéneo C57BL/6J.Este estudio ha revelado que Evc juega un papel fundamental en el desarrollo del hueso, ya que actúa como mediador de prácticamente todas las funciones dependientes de Ihh en las placas de crecimiento.

Abstract

Ellis-van Creveld syndrome (EvC; MIM 225500) is a rare autosomal recessive chondroectodermal dysplasia which affects development of the skeleton, nails and teeth. 60% of EvC cases are also found with congenital heart defects. Patients with EvC are characterized with mutations either in *EVC* or *EVC2,* the majority of which result in the introduction of premature termination codons. While most of the mutations in *EVC* or *EVC2* are recessive, there are specific mutations in the last exon of *EVC2* which, in the heterozgyous state, are responsible for the autosomal dominant disorder named Weyers Acrofacial Dysostosis (Weyers; MIM # 193530). Weyers patients have features that are similar to, but milder than, EvC patients. In this thesis we have conducted an extensive molecular analysis of EvC and Weyers patients that has allowed us to identify 31 new mutations in *EVC* and *EVC2,* including 2 new dominant Weyers mutations. In addition we have detected 2 families with simultaneous mutations in *EVC* and *EVC2* owing to a contiguous gene deletion (*STK32B-EVC*) involving *EVC*, *EVC2* and the adjacent genes *STK32B* and *C4orf6*. Of note this is the first time that individuals with simultaneous mutations in *EVC* and *EVC2* have been reported. We demonstrate that in both families the deletion was caused by a recombination event between two neighboring LINE-1 retrotransposons. While heterozygous individuals for the *STK32B-EVC* deletion are asymptomatic, patients who were homozygous for the deletion had EvC and a borderline IQ, suggesting that this rearrangement could be associated with slight mental retardation. In addition cell culture experiments using murine variants of *EVC2* mutations demonstrated that the molecular mechanism underlying Weyers syndrome is a diminished response to Hh signals. These experiments also revealed for the first time an involvement of Evc2 in Hh signaling. Earlier publications had shown that Evc localizes at the primary cilium and that is required for Hedgehog signaling. Finally we have thoroughly analyzed the embryonic growth plate of the long bones and cranial synchondroses of *Evc*$^{-/-}$ mice in the homogenous genetic background C57BL/6J to fully understand the function of Evc in bone development. The result of this study have shown that *Evc* plays a key role in bone development by promoting all known regulatory aspects of Ihh signalling in the growth plates.

Índice

Clave de abreviaturas

Alkp: Fosfatasa alcalina (*Alkaline phosphatase*)

BAC: *Bacterial Artificial Chromosome*

BMP: *Bone Morphogenetic Protein*

BrdU: bromodesoxiuridina

CCP: Costillas-cortas polidactilia

Ci: *Cubitus interruptus*

CK1: caseína quinasa (*Casein Kinase 1)*

CNV: Variación en número de copias (*Copy Number Variation*)

Cos2: *Costal 2*

DBPO: borde distal de la osificación endocondral(*Distal Border of Perichondrial Ossification*)

Dhh*: Desert Hedgehog*

EvC: Ellis-Van Creveld

FGF: Factor de crecimiento de fibroblastos (*Fibroblast Growth Factor*)

FGFR: receptor de FGF (*Fibroblast Growth Factor Receptor*)

FISH: Fluorescent *In Situ* Hibridation (Hibridación *In situ* fluorescente)

Fu: *Fused*

GLI: *Glioma-associated oncogene*

GSK3β: glucógeno sintasa quinasa(*Glycogen synthase kinase 3 beta)*

Hh: *Hedgehog*

Hhip: *Hedgehog-interacting protein*

HIS: Hibridación *In Situ*

Ibsp: *Integrin binding sialoprotein*

IFT: Transporte intraflagelar (*intraflagellar transport*)

Ihh: *Indian Hedgehog*

LINE-1: Elementos nucleares largos intercalados 1 (*Long Interspersed Nuclear Element-1*)

MLPA: *Multiplex Ligation-dependent Probe Amplification*

NMD: *Non-Sense Mediated mRNA Decay*

Osp: Osteopontina (*Osteopontin*)

Osx: *Osterix*

Patch1: *Patched 1*

PCR: Reacción en cadena de la polimerasa (*Polymerase Chain Reaction*)

PKA: Proteína quinasa A (*Protein Kinase A*)

Pthrp: Hormona paratiroidea (*Parathyroid Hormone-like peptide*)

Pth1r: receptor de la hormona paratiroidea (*Parathyroid Hormone 1 receptor*)

qRT-PCR: PCR cuantitativa (*Real Time Quantitative-Polymerase Chain Reaction*)

RACE: *Rapid Amplification of cDNA Ends*

Shh: *Sonic Hedgehog*

Smo: *Smoothened*

SNP: Polimorfismo de un nucleótido (*Single Nucleotide Polymorphism*)

Sufu: *Suppressor of Fused*

VEGF: Factor de crecimiento vascular endotelial (*Vascular Endothelial Growth Factor*)

Introducción

1.- SÍNDROME DE ELLIS-VAN CREVELD

El síndrome de Ellis-van Creveld (EvC; MIM # 225500) o displasia condroectodérmica es una enfermedad rara autosómica recesiva, que afecta al desarrollo y cuya prevalencia en la población es de aproximadamente 7 casos por cada millón de nacimientos (Stoll et al., 1989). No obstante, en poblaciones con elevada consanguinidad, como en el caso de la comunidad Amish de Pensilvania, el número de afectados asciende a 5 casos por cada 1.000 nacimientos (McKusick et al., 1964). La primera descripción clínica de EvC data de 1940 y fue realizada por Richard Ellis y Simon van Creveld al documentar tres niños diagnosticados con condrodisplasia, uñas distróficas, anormalidades orales y una malformación cardíaca (Ellis and van Creveld, 1940). Más tarde, Victor A. McKusick publicó la descripción más exhaustiva que existe hasta la fecha de esta enfermedad, tras examinar 52 individuos con EvC pertenecientes a la comunidad Amish (McKusick et al., 1964). En función de la similitud del fenotipo, EvC junto con los síndromes de Saldino-Noonan (CCP tipo I, MIM # 263530), Majewski (CCP tipo II, MIM # 263520), Verma-Naumoff (CCP tipo III, MIM # 263510), Beemer-Langer (CCP tipo IV, MIM # 269860) y el síndrome de Jeune (MIM # 208500), forman el grupo de displasias esqueléticas autosómicas recesivas conocido como síndromes de costilla corta-polidactilia (CCP)(Baujat and Le Merrer, 2007).

1.1.- Características clínicas de EvC

Los pacientes con EvC se caracterizan por defectos a nivel del esqueleto y la ectodermis. Las características esqueléticas incluyen: estatura baja desproporcionada debido al acortamiento de los huesos largos de las extremidades, principalmente en su porción distal (talla final 1.0m-1.5m); tórax estrecho por acortamiento de las costillas (figura 1B); y polidactilia postaxial bilateral en manos y en ocasiones también en pies (10% de los casos aproximadamente) (figura 1D) (McKusick et al., 1964). Los estudios radiológicos demuestran la existencia de huesos tubulares cortos; pelvis poco desarrollada en su región supracetabular (pelvis en tridente); hipoplasia de las epífisis proximales tibiales, las cuales originan un defecto habitual en estos pacientes denominado "*genu valgo*" (figura 1A) y fusiones de los huesos carpianos (McKusick et al., 1964; Ruiz-Perez and Goodship, 2009).

Los defectos en la ectodermis afectan a uñas y dientes, siendo la distrofia de las uñas un rasgo distintivo de los pacientes con EvC (figura 1C). Las anormalidades dentales están presentes tanto en la dentición primaria como en la permanente e incluyen entre otros: dientes pequeños, cónicos y anormalmente posicionados (figura 1F); hipodoncia (ausencia de los incisivos maxilares y mandibulares generalmente) y aparición prematura de la dentición primaria antes del nacimiento (dientes neonatales). Otras características orofaciales son tabique nasal ancho, labio semi-leporino y desarrollo de múltiples frénulas entre la encía y el labio (figura 1G) (Baujat and Le Merrer, 2007; Cahuana et al., 2004; Hattab et al., 1998; Mostafa et al., 2005).

Además de las características clínicas mencionadas anteriormente, el 60% de los afectados con EvC presentan malformaciones cardíacas congénitas (Digilio et al., 1999; Giknis, 1963), siendo lo más común la existencia de una aurícula única como consecuencia de la formación incorrecta del tabique interauricular (figura 1E). Adicionalmente se han descrito pacientes con defectos en el tabique interventricular, transposición de las grandes arterias, atresia de la válvula tricúspide, conexión anómala de la vena pulmonar y estenosis de la arteria pulmonar entre otras (Hills et al., 2011). Ocasionalmente EvC puede ser una causa de letalidad neonatal, de hecho de los 52 casos estudiados por McKusick, 30 murieron a los 6 meses de vida por problemas respiratorios originados por el estrechamiento de la caja torácica y las malformaciones cardíacas (McKusick et al., 1964).

Figura 1. Características clínicas de pacientes afectados con EvC. A: *genu valgo*. **B:** tórax estrecho debido al acortamiento de las costillas. **C:** distrofia en las uñas. **D:** polidactilia postaxial en manos. **E:** malformación cardíaca: aurícula única. **F:** defectos dentales. **G:** múltiples frénulas entre la encía y el labio. Las flechas señalan la localización del rasgo clínico indicado en cada panel.

A día de hoy no hay tratamiento clínico para el síndrome de EvC, aunque cuidados médicos y quirúrgicos adecuados mejoran la calidad de vida de estos pacientes. Por ejemplo, la ortopedia puede corregir las deformidades óseas asociadas al "*genu valgo*" y la combinación de ortodoncia, cirugía y prótesis pueden subsanar en gran parte los defectos dentales (Baujat and Le Merrer, 2007; Cahuana et al., 2004; Jockel et al., 2011; Shibata et al., 1999).

1.2.- Weyers Acrofacial Dysostosis (Weyers Acrodental Dysostosis o síndrome de Curry-Hall).

Weyers Acrofacial Dysostosis (Weyers; MIM # 193530) es una enfermedad autosómica dominante descrita por primera vez en 1952 por H. Weyers (Weyers, 1952) y cuyas características clínicas son similares a EvC pero de menor gravedad. Los pacientes Weyers presentan polidactilia postaxial en ambas manos, uñas distróficas y defectos dentales (dientes pequeños e irregulares, único incisivo central o hipodoncia), sin embargo se diferencian de los afectados con Evc, en que su estatura se sitúa en el límite inferior de la media de la población control y tampoco se han detectado malformaciones cardiovasculares en afectados con Weyers (Howard et al., 1997; Ye et al., 2006). La prevalencia de Weyers es mucho menor que la de EvC, siendo muy pocas las familias descritas con este síndrome en la literatura (Curry and Hall, 1979; Roubicek and Spranger, 1984; Ruiz-Perez et al., 2000; Shapiro et al., 1984; Ye et al., 2006). Hoy se sabe que EvC y Weyers son enfermedades alélicas causadas por mutaciones en los mismos genes (Ruiz-Perez et al., 2000; Ye et al., 2006).

1.3.- Identificación de los genes causantes de EvC: *EVC* y *EVC2*

La identificación de los genes responsables de EvC se llevó a cabo mediante clonación posicional. Inicialmente el locus de EvC se mapeó en el brazo corto del cromosoma 4 entre los marcadores *D4S2957* y *D4S827* mediante análisis de ligamiento en 9 pedigrís de la comunidad Amish y en 3 familias de Méjico, Ecuador y Brasil (Ide et al., 1996; Polymeropoulos et al., 1996). El posterior acotamiento de la región crítica, la determinación de genes candidatos en ese intervalo y el análisis de mutaciones en los mismos, permitió identificar cambios patogénicos en pacientes en un gen nuevo que se denominó *EVC* y cuyo ADNc se generó a través de experimentos de RT-PCR y RACE (*Rapid*

Amplification of cDNA Ends) (Ruiz-Perez et al., 2000). La ausencia de mutaciones en *EVC* en aproximadamente el 50% de los casos, incluso en familias que mapeaban dentro del mismo intervalo crítico original, hizo que se examinasen de nuevo los genes contenidos en esa región y así se encontraron mutaciones en un segundo gen adyacente al anterior, el cual se denominó *EVC2* (Ruiz-Perez et al., 2003). La clonación de *EVC2* se vio favorecida al haberse descubierto con anterioridad mutaciones en el homólogo bovino de *EVC2* (*Limbin*) en una raza de ganado vacuno afectada con condrodisplasia (Takeda et al., 2002).

EVC (MIM # 604831) contiene 21 exones codificantes distribuidos a lo largo de 120 kb y produce dos variantes de ARNm las cuales dan lugar a dos proteínas de 992 ó 993 aminoácidos debido a un procesamiento (*splicing*) alternativo de su último exón. El *splicing* alternativo del último exón está conservado en ratón y produce en este organismo dos transcritos cuyos productos proteicos difieren en 13 aminoácidos (Ruiz-Perez et al., 2000). *EVC2* (MIM # 607261) comprende 150 kb y está compuesto de 22 exones que codifican para una proteína de 1.308 aminoácidos. Los dos genes se localizan en el brazo corto del cromosoma 4 (4p16.1) en orientación divergente, con sitios de inicio de la traducción separados por 2,6 kb en humanos y 1,7 kb en ratón (figura 2) (Ruiz-Perez et al., 2003).

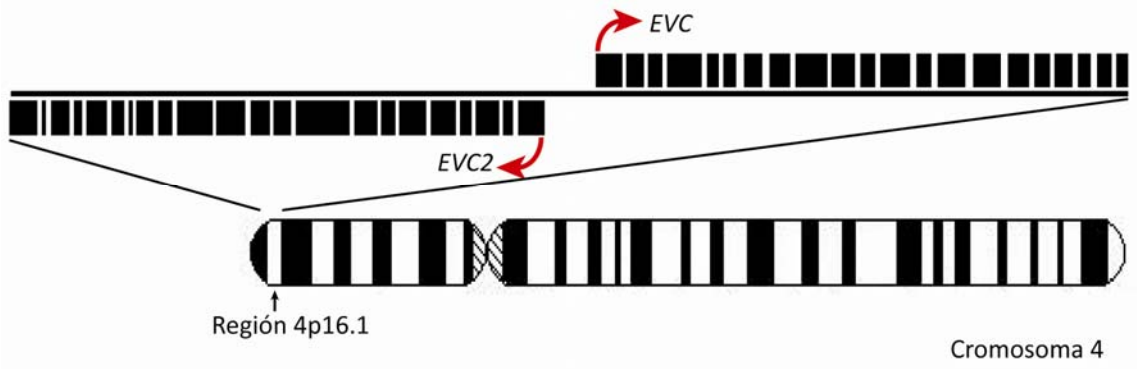

Figura 2. Estructura de los genes *EVC* y *EVC2* en la región 4p16.1. Las cajas negras representan los 21 y 22 exones de *EVC* y *EVC2* respectivamente. Las flechas rojas indican la orientación de transcripción de cada gen. Figura adaptada (Tompson et al., 2007)

El análisis de la secuencia de las proteínas EVC y EVC2 con programas de predicción de motivos estructurales proteicos muestra que ambas tienen dominios transmembrana (uno en EVC y dos en EVC2) y varias regiones de estructura *coiled-coiled*. Sin embargo no se encontró similitud con otras proteínas o motivos funcionales que ayudasen a esclarecer su función (Ruiz-Perez et al., 2003).

EVC y EVC2 no presentan un alto grado de homología entre sí por lo que en un principio fueron consideradas proteínas no homólogas, sin embargo un estudio reciente utilizando algoritmos especializados (PSI-BLAST) ha revelado que existe una similitud significativa ($E = 6 \times 10^{-14}$) entre EVC2 y EVC a lo largo de 550 aminoácidos. En este mismo estudio mediante el uso de herramientas bioinformáticas se dedujo que los genes *EVC* y *EVC2*, son el resultado de una duplicación génica ancestral (Blair et al., 2011), ya que se encontraron ortólogos de ambos genes en el genoma de cefalocordados (*Branchiostoma floridae*), equinodermos (*Strongylocenytrotus purpuratus*), moluscos (*Lottia gigantea*) y cnidarios (*Nematostella vectensis*), de ahí que se piense que la duplicación génica debió ocurrir en una especie ancestral a partir de la cual evolucionaron las distintas líneas de metazoos (Blair et al., 2011). De hecho el genoma del metazoo más primitivo conocido, el placozoo *Trichoplax adhaerens* (Dellaporta et al., 2006), contiene un gen muy similar a *EVC.* En cambio ambos genes están ausentes en el genoma de artrópodos (*Drosophilla melanogaster*) y en el de nemátodos (*Caenorhabditis elegans*) indicando que *EVC* y *EVC2* fueron delecionados en estos grupos (Blair et al., 2011).

1.4.- Espectro de mutaciones en *EVC* y *EVC2* en pacientes EvC y Weyers

Aproximadamente la mitad de los pacientes con EvC portan dos mutaciones en *EVC* y el otro 50% dos mutaciones en *EVC2* siendo los fenotipos asociados a mutaciones en uno u otro gen clínicamente indistinguibles (Tompson et al., 2007). Hasta la fecha el número de mutaciones distintas publicadas en *EVC* y *EVC2* es de 42 Y 51 respectivamente (Ali et al., 2010; Chen et al., 2010; Ruiz-Perez and Goodship, 2009; Shen et al., 2011; Umm et al., 2010). El espectro de mutaciones en ambos genes es idéntico y consiste en sustituciones puntuales de nucleótidos que introducen codones de terminación prematuros directamente (mutaciones *nonsense*) o bien alteran el sitio de *splicing*, microinserciones o microdeleciones que alteran la pauta de lectura del ARNm, deleciones de uno o más exones y unas pocas sustituciones de nucleótidos que conducen a cambios

de aminoácidos (*missense*) (figura 3) (Galdzicka et al., 2002; Ruiz-Perez and Goodship, 2009; Ruiz-Perez et al., 2000; Ruiz-Perez et al., 2003; Tompson et al., 2007). En consecuencia la gran mayoría de las mutaciones en pacientes con EvC dan lugar a codones de terminación prematuros (Tompson et al., 2007), siendo esperable que el ARN mensajero derivado de los alelos mutantes sea eliminado por la maquinaria NMD (*Non-sense mediated RNA decay*). Este mecanismo de control se encarga de degradar aquellos transcritos con codones de terminación prematuros evitando la formación de proteínas truncadas o no funcionales que pudieran interferir con los procesos normales que tienen lugar en la célula (Gehring et al., 2009; Hentze and Kulozik, 1999; Nagy and Maquat, 1998).

Respecto a los pacientes Weyers, sólo existen cinco casos caracterizados con mutaciones, las cuales han resultado ser cambios heterocigotos en *EVC* y en *EVC2*. Así se han descrito: una sustitución de aminoácido (S307P) en EVC (Ruiz-Perez et al., 2000), una deleción de un nucleótido (c.3793delC) en *EVC2* en dos familias no relacionadas (Ye, 2006 #2006 y en esta tesis) y dos mutaciones *nonsense* distintas, también en *EVC2,* en el codón contiguo al de la deleción c.3793delC que están descritas en esta tesis (c.3797T>A y c.3797T>G). Todas las mutaciones Weyers encontradas hasta ahora en *EVC2* originan proteínas truncadas que han perdido los últimos 43 aminoácidos, de lo que se deduce que estos residuos deben ser importantes para el funcionamiento de esta proteína.

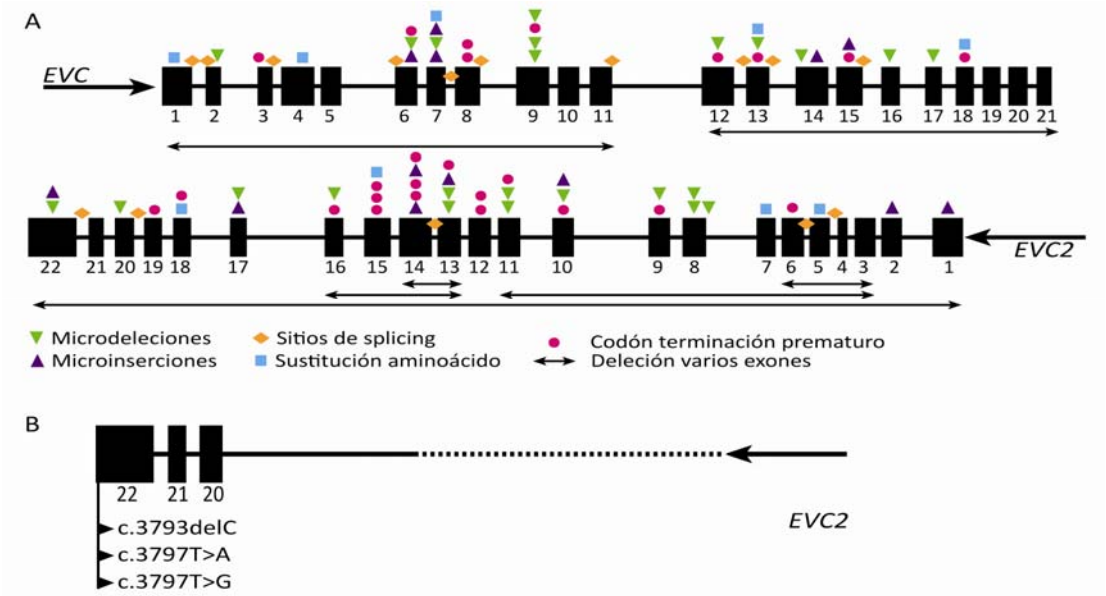

Figura 3. Espectro de mutaciones en los genes *EVC* y *EVC2.* A: mutaciones detectadas en pacientes EvC. **B**: mutaciones detectadas en pacientes Weyers. Figura adaptada (Ruiz-Perez and Goodship, 2009)

1.5.- Función de Evc y Evc2

Para conocer la función de Evc se generó un modelo experimental en ratón (*knockout*) en el que el exón 1 de *Evc* fue sustituido por el gen reportero *LacZ*, el cual queda bajo la dirección del promotor de *Evc.* La tinción con X-gal en embriones $Evc^{+/-}$ y $Evc^{-/-}$ demostró que *Evc*, se expresa principalmente en el hueso en crecimiento y en la región orofacial, coincidiendo con los tejidos en los que se manifiesta la enfermedad. Macroscópicamente los ratones $Evc^{-/-}$ reproducen el fenotipo esquelético de los pacientes y presentan huesos y costillas cortas junto con defectos dentales en incisivos y molares, sin embargo no desarrollan polidactilia, un rasgo constante en los pacientes EvC, ni poseen malformaciones cardíacas aparentes (Ruiz-Perez et al., 2007).

El posterior análisis histológico de la placa de crecimiento de embriones $Evc^{-/-}$ con fondo genético híbrido C57BL/6J; 129 reveló anormalidades propias de otros modelos murinos en los que la vía de señalización de Indian Hedgehog (Ihh) está reprimida (Long et al., 2004; Razzaque et al., 2005; St-Jacques et al., 1999), sugiriendo así que Evc se requiere para el funcionamiento correcto de esta ruta. Esto fue confirmado mediante estudios de hibridación *in situ* (HIS), en los que se demostró que la expresión de *Ihh* en los condrocitos hipertróficos de la placa de crecimiento de los huesos largos de ratones $Evc^{-/-}$ era normal, pero la expresión de los genes diana de esta ruta: *Patched1* (*Ptch1), Gli1* y *Parathyroid Hormone-like peptide* (*Pthrp*) se encontraba drásticamente disminuida (Ruiz-Perez et al., 2007). Por otra parte, anticuerpos policlonales desarrollados contra un fragmento de Evc localizaron esta proteína en la base del cilio primario (Ruiz-Perez et al., 2007), una organela clave para la transducción intracelular de la señalización Hedgehog (Hh) en vertebrados (Huangfu et al., 2003; Rohatgi et al., 2007).

Aunque a día de hoy se disponen de menos datos respecto a la función de Evc2, resultados preliminares publicados recientemente realizados en cultivo celular utilizando ARN de silenciamiento y células $Evc2^{-/-}$, han demostrado que Evc2 también se localiza en la base del cilio primario y actúa como mediador positivo en la vía de Hh. Además se ha observado que las proteínas Evc y Evc2 son capaces de interaccionar en el sistema de doble híbrido de levaduras y que co-immunoprecipitan al ser sobreexpresadas en la línea celular HEK293T. También se ha demostrado que ambas proteínas deben estar presentes en la célula para que se localicen en el cilio primario (Blair et al., 2011).

2.- CILIO PRIMARIO

2.1.- Estructura y biología de los cilios

Los cilios son proyecciones apendiculares hacia el exterior de la célula presentes tanto en organismos unicelulares eucariotas como en organismos multicelulares más complejos cuya estructura básica consiste en un axonema rodeado de una membrana plasmática especializada (Goetz and Anderson, 2010). El axomena está formado por nueve dobletes de microtúbulos periféricos y una pareja de microtúbulos centrales (9+2), que en algunos casos pueden estar ausentes (9+0), y descansa sobre un cuerpo basal constituido por nueve tripletes de microtúbulos embebidos en matriz pericentriolar. Entre el axonema y el cuerpo basal se encuentra la zona de transición que permite el anclaje del cilio a la membrana plasmática (Cardenas-Rodriguez and Badano, 2009; Fliegauf et al., 2007; Pedersen et al., 2008; Pedersen and Rosenbaum, 2008;). Se pueden identificar dos tipos principales de cilios: los considerados móviles cuya estructura es 9+2, como los cilios del tracto respiratorio, y los inmóviles con estructura 9+0, como el monocilio o cilio primario presente en la casi totalidad de las células de vertebrados (Fliegauf et al., 2007). No obstante existen algunas excepciones a esta norma y así existen cilios 9+0 móviles, como los del nodo embrionario; o cilios con estructura 9+2 inmóviles como el quinocilio de las células epiteliales de la cóclea (Fliegauf et al., 2007). Entre los dobletes de microtúbulos del axonema, los cilios móviles poseen brazos de dineína que participan en la generación de movimiento. Los cilios son desmantelados cuando comienza la división celular y ensamblados cuando la célula se encuentra en un estado quiescente o diferenciado (Cardenas-Rodriguez and Badano, 2009; Fliegauf et al., 2007).

2.2.- Transporte intraflagelar

Durante la formación del cilio, la elongación del axonema se realiza por la adición de nuevas subunidades de tubulina en su extremo distal. Puesto que los cilios carecen de la maquinaria necesaria para la síntesis proteica, requieren un aporte de proteínas desde el citoplasma, por lo que están provistos de un sistema de transporte de proteínas denominado sistema de transporte intraflagelar (IFT), el cual utiliza unidades motoras dependientes de los microtúbulos del axonema para desplazarse (Rosenbaum and Witman, 2002; Silverman and Leroux, 2009). Este mecanismo fue descrito por primera

vez en el alga *Chlamydomonas reinhardtii* y está conservado evolutivamente (Cole et al., 1998; Kozminski et al., 1993).

El transporte anterógrado, es decir, desde la base del cilio hasta su extremo distal, es llevado a cabo a través del complejo proteico IFTB, el cual está formado por once polipétidos (IFT172, IFT88, IFT81, IFT80, IFT74, IFT57, IFT54, IFT52, IFT46, IFT27, IFT20), mientras que el complejo IFTA formado por seis subunidades peptídicas (IFT144, IFT140, IFT139, IFT122, IFTA1 e IFT43) se encarga del transporte desde el extremo distal del cilio hasta su base, también denominado transporte retrógrado. El sistema IFTB utiliza para desplazarse al complejo motor quinesina-2 (también conocido como KIF3), formado por las proteínas KIF3A y KIF3B, y la proteína asociada a KIF3 (KAP3), y el movimiento del complejo IFTA depende del sistema motor dineína citoplasmática tipo 2, integrado por las proteínas DYNC2H1 y DYNC2L1 (Cardenas-Rodriguez and Badano, 2009; Goetz and Anderson, 2010; Pedersen and Rosenbaum, 2008; Scholey, 2008).

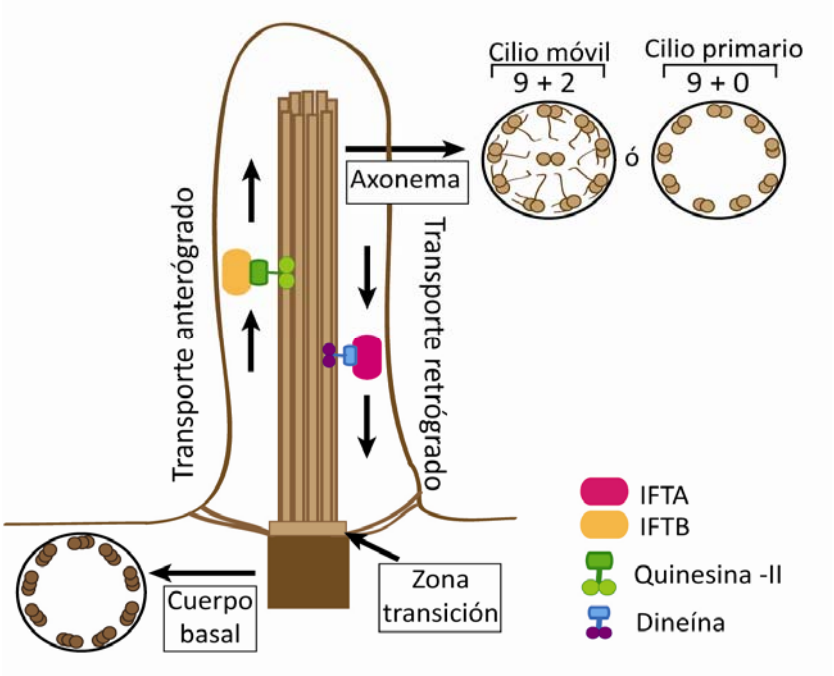

Figura 4. Estructura del cilio. Esquema gráfico donde se representan los diferentes elementos que componen el cilio: el axonema, la zona de transición y el cuerpo basal. También se muestran los complejos transportadores IFT y sus subunidades motoras. Figura adaptada (Cardenas-Rodriguez and Badano, 2009)

2.3.- Función del cilio primario.

La función del cilio primario es considerada fundamentalmente sensorial ya que está involucrado en la percepción y conversión de estímulos en cascadas de señalización hacia el interior de la célula (como la señalización Hh o Wnt) (Bergmann, 2011; Pedersen et al., 2008; Singla and Reiter, 2006). Un ejemplo representativo es el de las células fotorreceptoras de la retina, las cuales son neuronas sensoriales muy especializadas divididas en dos compartimentos funcional y morfológicamente distintos, que son el segmento interno y el externo. El segmento interno posee la maquinaria de biosíntesis proteica, y el segmento externo ó fotosensitivo, es un cilio primario modificado en el que se acumula el pigmento fotosensible, la rodopsina, necesaria para la transducción de la señal luminosa. La comunicación y transporte de proteínas entre ambos segmentos se realiza a través de una estructura denominada cilio conector, el cual es equivalente a la zona de transición (Deretic and Mazelova, 2009; Sedmak and Wolfrum, 2011; Wolfrum and Schmitt, 2000).

Recientemente el estudio del cilio primario ha adquirido especial relevancia, tras el descubrimiento de un número creciente de enfermedades humanas y murinas, las cuales son producidas por defectos en proteínas localizadas en esta estructura y que hoy se conocen con el nombre genérico de ciliopatías. Algunos ejemplos de este tipo de enfermedades son el síndrome de Bardel-Biedl (BBS; MIM # 209900), el síndrome de Joubert (JBTS; MIM # 213300), el síndrome de Meckel (MKS; MIM # 249000), el síndrome de Jeune (JATD; MIM # 208500) o los síndromes de riñón poliquístico. Las ciliopatías afectan a un número considerable de órganos e incluyen un amplio espectro de defectos entre los que se encuentran: malformaciones del sistema nervioso central, quistes renales, diabetes, malformación de las gónadas, malformación cardíaca, retraso mental, obesidad, polidactilia, disfunción pulmonar, degeneración retinal o anormalidades esqueléticas (Bergmann, 2011; Bisgrove and Yost, 2006; Cardenas-Rodriguez and Badano, 2009; Hildebrandt et al., 2011).

3.- VÍA DE LA SEÑALIZACIÓN Hh

Desde su descubrimiento en *Drosophila melanogaster* la vía de señalización de Hh es una de las rutas moleculares de comunicación intercelular más estudiadas en el campo

de la biología del desarrollo (Nusslein-Volhard and Wieschaus, 1980), ya que está implicada en la morfogénesis de prácticamente todos los tejidos y órganos de la gran mayoría de organismos (McMahon et al., 2003). El esquema básico de funcionamiento de esta ruta consta de un componente secretor en el que se sintetizan las moléculas Hh, las cuales son exportadas al exterior y difunden en forma de gradiente hasta alcanzar un componente receptor en el que a través de la acción de los factores de transcripción Ci (*Cubitus interruptus*) en *Drosophila* o las proteínas GLI (*Glioma-associated oncogene*; Gli1, Gli2 y Gli3) en vertebrados se induce la expresión de genes diana según la cantidad de morfógeno recibido (Lum and Beachy, 2004; Varjosalo et al., 2006).

Defectos en la transducción de la señales Hh durante el desarrollo embrionario se traducen en consecuencias drásticas para el feto como holoprosencefalia, microencefalia, anormalidades craniofaciales o defectos en la esqueletogénesis (Cohen, 2010). Esta ruta también está fuertemente asociada a cáncer, ya que mutaciones en algunos de sus componentes, como en *PATCHED1* (Hahn et al., 1996; Johnson et al., 1996) o en *SUFU* (Pastorino et al., 2009; Taylor et al., 2002), las cuales originan la desrepresión de la ruta, dan lugar al síndrome de Gorlin caracterizado por carcinomas de células basales, meduloblastomas y rabdomiosarcomas (BCNS, MIM # 109400). Asimismo se ha descrito que vía de Hh se encuentra constitutivamente activa en numerosos tipos de cánceres humanos de piel, cerebro, pulmón, próstata, páncreas y tracto gastrointestinal cuyo origen es diverso (Cohen, 2010; Li et al., 2011; Rohatgi and Scott, 2007). Tal es así que la vía de Hh está considerada actualmente una diana para el desarrollo de terapias antitumorales (Garber, 2008; Taipale et al., 2000). Finalmente esta vía de señalización también ha sido relacionada con la homeostasis celular, la renovación y reparación de tejidos en el adulto debido a su papel en el mantenimiento de las células madre (Hooper, 2005 #397).

3.1.- Síntesis, procesamiento y secreción de las proteínas Hh

Las proteínas Hh son inicialmente sintetizadas como una forma precursora de 45 kDa, la cual es convertida en un fragmento de 19 kDa correspondiente al extremo amino terminal (HhN) por autoprocesamiento. A continuación, el fragmento HhN sufre dos modificaciones postransduccionales que son críticas para su capacidad de difusión y posterior unión al receptor (Lee et al., 1994), consistentes en la adición de una molécula

de colesterol en su extremo carboxilo-terminal y otra de ácido palmítico en su extremo amino-terminal (Chen et al., 2004; Hall et al., 1995; Lewis et al., 2001; Porter et al., 1996). Las moléculas Hh son entonces secretadas al espacio extracelular con ayuda de la proteína de membrana Dispatched (Disp) (Kawakami et al., 2002; Ma et al., 2002) y difunden mediante un proceso en el que participan los proteoglicanos de heparán sulfato hasta alcanzar la célula receptora (The et al., 1999; Zhu and Scott, 2004). La unión de Hh a su receptor está facilitada por proteínas de membrana que incrementan la afinidad ligando-receptor como iHog y Boi en *Drosophila* o sus ortólogos Cdo y Boc en vertebrados (Tenzen et al., 2006; Yao et al., 2006; Zhang et al., 2006b).

3.2.- Señalización Hh en *Drosophila melanogaster*

En ausencia de señal el receptor de Hh, Ptch1, reprime al principal activador de la ruta Smoothened (Smo) y como consecuencia Costal 2 (Cos2), forma un complejo con las proteínas Fused (Fu), Supressor of Fused (Sufu) y el activador transcripcional bifuncional Ci, al cual se unen la proteína quinasa A (PKA), la caseína quinasa 1 (CK1) y la glucógeno sintasa quinasa 3 (GSK3β). El reclutamiento de estas quinasas al complejo Cos2-Fu-Sufu-Ci favorece la fosforilación de la forma larga de Ci (Ci155), lo que estimula su ubiquitinación y posterior procesamiento vía proteasoma hacia su forma represora (Ci75 o CiR) (figura 5A) (Aza-Blanc et al., 1997; Jia et al., 2005; Jiang and Struhl, 1998; Smelkinson and Kalderon, 2006; Zhang et al., 2005).

Cuando el ligando Hh se une al receptor Ptch1, éste deja de inhibir a Smo permitiendo su activación a través de la hiperfosforilación por PKA y CK1 de 26 residuos de serina/treonina de su extremo citoplasmático carboxilo terminal. Esto hace que el complejo de proteínas Cos2-Sufu-Fu se una al extremo carboxilo de Smo, liberando a Ci155 y evitando su fosforilación. De esta manera se bloquea la formación de CiR y se facilita la transformación de Ci155 a su forma activadora (CiA) por una reacción aún desconocida en la que participa activamente la quinasa Fused (figura 5B) (Jia et al., 2003; Jia et al., 2004; Lum and Beachy, 2004; Lum et al., 2003; Ohlmeyer and Kalderon, 1998; Wang and Holmgren, 1999).

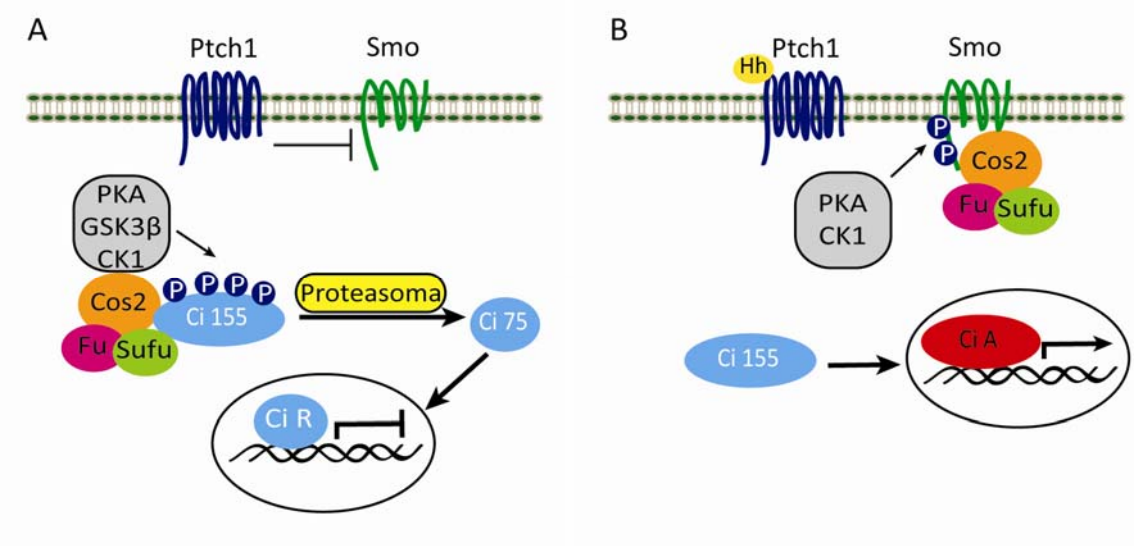

Figura 5. Señalización Hh en *Drosophila*. A: en ausencia de señal Ptch1 inhibe a Smo y Ci es procesado a su forma represora (CiR) tras ser fosforilado por PKA, GSK3β y CK1 las cuales son reclutadas por el complejo Cos2-Sufu-Fu. CiR viaja al núcleo donde reprime la transcripción de genes diana de Hh. **B:** Hh se une a Ptch1 y Smo es fosforilado por PKA y CK1, lo que permite el reclutamiento del complejo Cos-Sufu-Fu a su extremo carboxilo terminal. Como consecuencia Ci155 es transformado a CiA e induce la transcripción de genes diana de la ruta en el núcleo. Figura adaptada (Jia and Jiang, 2006).

3.3.- Señalización Hh en vertebrados

En vertebrados existen tres genes Hh: *Desert Hedgehog* (Dhh), esencial para el desarrollo de los nervios periféricos y la espermatogénesis; *Sonic Hedgehog* (Shh), involucrado en el establecimiento del patrón de simetría lateral, el eje antero-posterior de las extremidades y el desarrollo del sistema nervioso central; e *Indian Hedgehog* (Ihh), el cual dirige el proceso de osificación endocondral. Asimismo existen tres factores transcripcionales equivalentes a Ci denominados Gli1, Gli2 y Gli3 (McMahon et al., 2003). Mientras que Gli1 actúa como activador transcripcional, Gli3 y Gli2, al igual que Ci, pueden ser procesados a su forma represora y consecuentemente pueden ejercer un papel dual como activadores o represores de la transcripción. (Bai and Joyner, 2001; Buttitta et al., 2003; Huntzicker et al., 2006; Litingtung et al., 2002; McDermott et al., 2005; Pan et al., 2006; Wang et al., 2000).

El proceso de transducción de las señales Hh en vertebrados es similar a lo descrito para *Drosophila* pero difiere esencialmente en la participación del cilio primario (Huangfu et al., 2003). La primera asociación de esta estructura con la vía de Hh se descubrió al observar que mutantes murinos en proteínas del sistema IFT (Ift172 e Ift88),

los cuales carecían de cilios primarios en el nodo embrionario, mostraban defectos estructurales típicos de una señalización Hh alterada (Huangfu et al., 2003). Posteriormente se ha demostrado que las proteínas IFT se requieren tanto para la formación de proteínas Gli activadoras como represoras (May et al., 2005). Igualmente se ha visto que proteínas clave de la vía como Ptch1, Smo, Sufu o los factores Gli se localizan en el cilio primario (Corbit et al., 2005; Haycraft et al., 2005; Ocbina and Anderson, 2008; Rohatgi et al., 2007).

Según los hallazgos más recientes en la vía de Hh en vertebrados está aceptado que en ausencia de señal, Ptch1 se localiza en el cilio primario e inhibe la activación de Smo por un mecanismo aún desconocido en el que se cree que intervienen moléculas pequeñas (Bijlsma et al., 2006; Corcoran and Scott, 2006). Como consecuencia la forma no procesada de Gli3 (Gli3-FL) se encuentra unida a la proteína Sufu, formando un complejo inhibidor que estimula la formación vía proteasoma de su forma represora (Gli3-R). La fosforilación de Gli3-FL por las quinasas PKA, GSK3β y CK1 también favorece la formación de Gli3-R, el cual viaja al núcleo donde reprime la transcripción de genes diana de la ruta (figura 6A) (Humke et al., 2010; Jia et al., 2004; Tempe et al., 2006; Zhang et al., 2006a).

En presencia de Hh Ptch1 deja de reprimir a Smo, el cual se traslada ahora al cilio primario, mientras que Ptch1 unido a su ligando abandona la organela (Kovacs et al., 2008; Rohatgi and Scott, 2007). La activación de Smo recluta los complejos Gli3-FL/Sufu al cilio primario donde son disociados evitando así la formación de Gli3-R y provocando un enriquecimiento de Gli3-FL en el extremo distal del cilio. Una vez disociado de Sufu, Gli3-FL viaja al núcleo donde se postula que es fosforilado por un mecanismo aún no caracterizado y convertido en activador transcripcional (Gli3-A) de genes diana de la ruta (figura 6B) (Humke et al., 2010; Ingham et al., 2011; Merchant et al., 2004; Tukachinsky et al., 2010; Varjosalo et al., 2006).

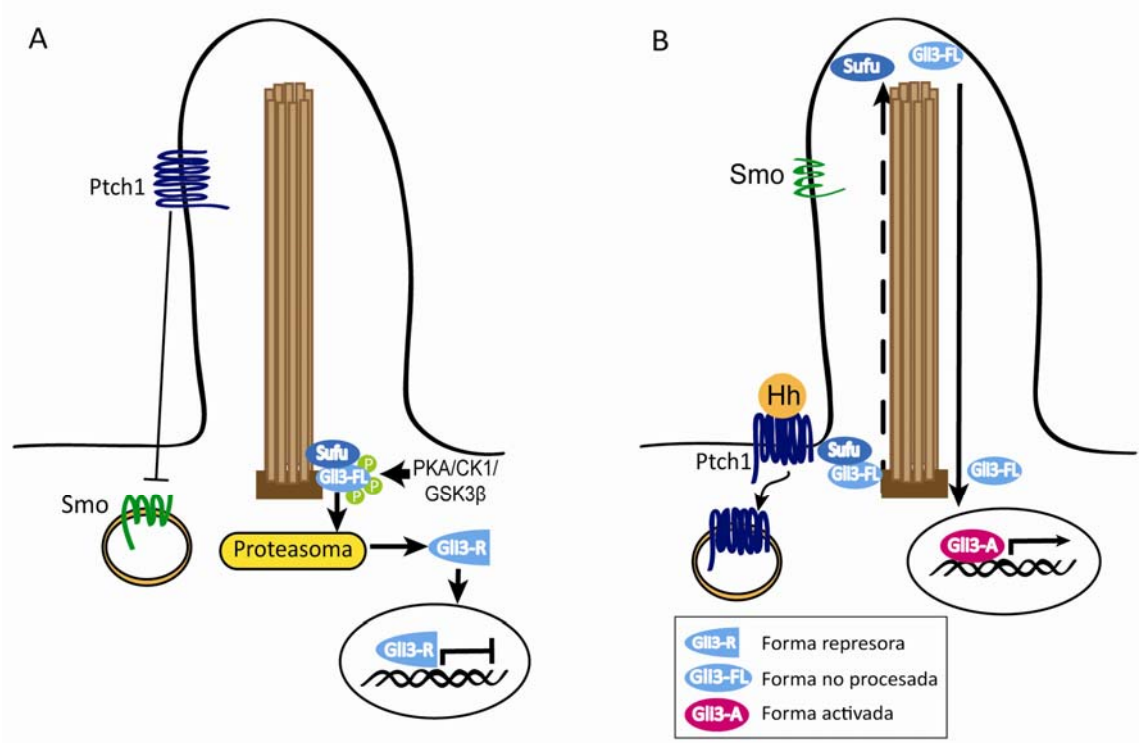

Figura 6. Señalización Hh en mamíferos. **A:** en ausencia de señal Ptch1, inhibe a Smo e impide su entrada al cilio primario. Gli3-FL se encuentra unido a Sufu y es fosforilado por PKA, GSK3β y CK1 lo que desencadena el procesamiento de Gli3-FL a Gli3-R, el cual reprime la transcripción de genes diana. **B:** Hh se une a Ptch1 y abandona el cilio permitiendo la entrada de Smo, lo que provoca la disociación del complejo Gli3-FL/Sufu en el cilio. Gli3-FL viaja al núcleo donde es transformado en activador Gli3-A e induce la transcripción de genes diana de la ruta.

A pesar que se trata de una ruta con un alto grado de conservación evolutiva existen varias diferencias entre vertebrados e invertebrados, además de la participación del cilio primario ya comentada. Una de ellas consiste en que mientras que la activación de Smo en *Drosophila* está acoplada a la hiperfosforilación de su extremo carboxilo terminal por las quinasas PKA y CK1 (Apionishev et al., 2005; Jia et al., 2004; Zhang et al., 2004), en vertebrados Smo ha perdido los sitios de fosforilación de PKA y uno de los dominios de unión a Cos2 (Jia et al., 2003). Igualmente la proteína Fused, la cual forma un complejo con Cos2 y es fundamental para la vía de Hh en *Drosophila*, no parece jugar un papel importante en vertebrados, como demuestran los mutantes murinos para *Fused,* los cuales no manifiestan alteraciones en la vía de Hh (Chen et al., 2005b; Merchant et al., 2005). Por último, la proteína Sufu es uno de los principales reguladores negativos de esta ruta en vertebrados, ya que su disrupción provoca embriones incompatibles con la vida (Svard et al., 2006), sin embargo no parece ser tan relevante en

invertebrados ya que los embriones de *Drosophila* carentes de esta proteína son perfectamente viables (Preat, 1992).

4.- DESARROLLO DEL HUESO.

Los huesos del esqueleto de los vertebrados se originan a partir de la diferenciación de células mesequimales mediante dos procesos distintos denominados osificación intramembranosa y osificación endocondral. En el primero de ellos, las células mesenquimales embrionarias se diferencian directamente a osteoblastos y está restringido a los huesos planos de la parte superior del cráneo y la clavícula (Olsen et al., 2000). El segundo es el mecanismo por el que se forman la mayor parte de los huesos del esqueleto incluidos los huesos largos de las extremidades y costillas, y se detalla a continuación (Kronenberg, 2003; Olsen et al., 2000).

4.1.- Osificación endocondral

La osificación endocondral comienza en etapas tempranas del embrión con la condensación de células mesenquimales en los diferentes puntos de la esqueletogénesis, tras lo cual dichas células se diferencian a condrocitos formando los moldes cartilaginosos de los futuros huesos (figuras 7A y 7B) (Kronenberg, 2003). Una vez diferenciados, los condrocitos proliferan activamente y secretan una matriz extracelular rica en colágeno tipo II, mientras que las células que rodean al molde cartilaginoso se diferencian en una estructura denominada pericondrio, formada por células fibroblásticas de las que posteriormente emergerán los osteoblastos del collar óseo (figura 7C) (Olsen et al., 2000). En una siguiente fase los condrocitos del centro del molde de cartílago sufren una segunda reprogramación genética, se hipertrofian y comienzan a secretar una matriz extracelular rica en colágeno tipo X que favorece la calcificación de la matriz extracelular. Los condrocitos hipertróficos también secretan otros factores específicos como *VEGF* (*Vascular Endothelial Growth Factor*) que fomentan la invasión del cartílago por vasos sanguíneos y osteoblastos, induciendo así la formación del centro de osificación primario o esponjosa primaria (figura 7D) (Kronenberg, 2003; Olsen et al., 2000). Finalmente los condrocitos hipertróficos mueren por apoptosis, produciéndose la sustitución de cartílago por tejido óseo. Más adelante a ambos lados del centro de

osificación primario surgen capas estratificadas de condrocitos de reserva (región distal del hueso en la que los condrocitos se dividen más lentamente), proliferativos e hipertróficos, que constituyen lo que se conoce como la placa de crecimiento (figura 7E). La proliferación continuada de condrocitos dentro de la placa, seguida de su hipertrofia y sustitución por tejido óseo constituye la base del crecimiento longitudinal del hueso (Kronenberg, 2003; Olsen et al., 2000).

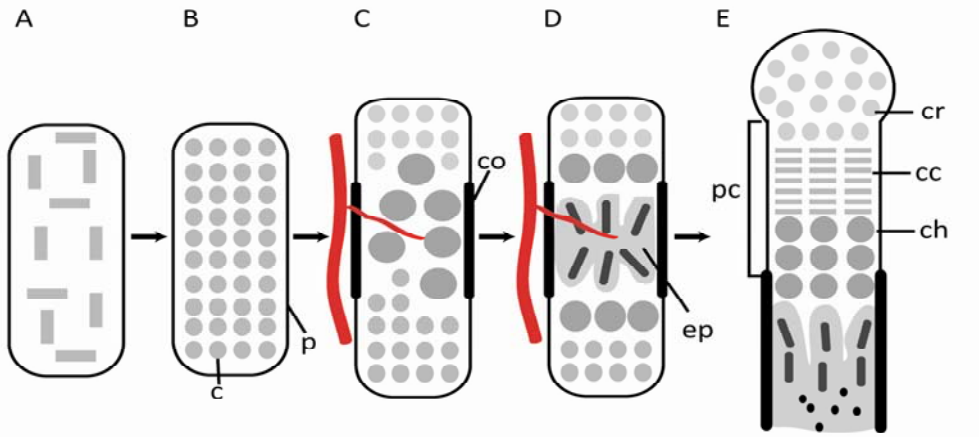

Figura 7. Proceso de osificación endocondral. **A y B:** condensación de células mesenquimales las cuales se diferencian a condrocitos (c) rodeados por el pericondrio (p). **C:** los condrocitos del centro se hipertrofian y fomentan la invasión vascular del cartílago, mientras que las células pericondriales se diferencian a osteoblastos para formar el collar óseo (co). **D:** los osteoblastos del pericondrio acompañan la invasión vascular del cartílago formando la esponjosa primaria (ep) **E:** en la región distal de hueso se forma la placa de crecimiento (pc), compuesta por capas de condrocitos de reserva (cr), columnares (cc) e hipertróficos (ch). Figura adaptada (Kronenberg, 2003).

4.2.- Papel de Ihh y otras vías de señalización en la osificación endocondral

Aunque son muchas las moléculas y rutas involucradas en el desarrollo del esqueleto, Ihh es el principal regulador de la formación del hueso. Las moléculas de Ihh son sintetizadas por los condrocitos prehipertróficos y una vez secretadas difunden a lo largo de la placa de crecimiento generando un gradiente de señal que coordina la diferenciación y proliferación de los condrocitos, así como la osificación del pericondrio (Kronenberg, 2003). Por un lado Ihh actúa sobre los condrocitos periarticulares estimulando la expresión de PTHrP, la cual a su vez difunde hacia el centro del hueso y actúa sobre su receptor (*Parathyroid Hormone 1 Receptor,* PTH1R) para retrasar la diferenciación de los condrocitos proliferativos a hipertróficos y por tanto la síntesis de Ihh (figura 8) (Vortkamp et al., 1996). De esta manera se establece un bucle de retroalimentación negativo entre PTHrP e Ihh que regula la diferenciación de los

condrocitos a lo largo del eje longitudinal del hueso (Vortkamp et al., 1996). Por otra parte se ha observado que Ihh también actúa estimulando la división de los condrocitos y la diferenciación de los osteoblastos del collar óseo, ya que los ratones *Ihh*$^{-/-}$ presentan una reducción del 50% de la división celular y carecen de osteoblastos (Razzaque et al., 2005; St-Jacques et al., 1999).

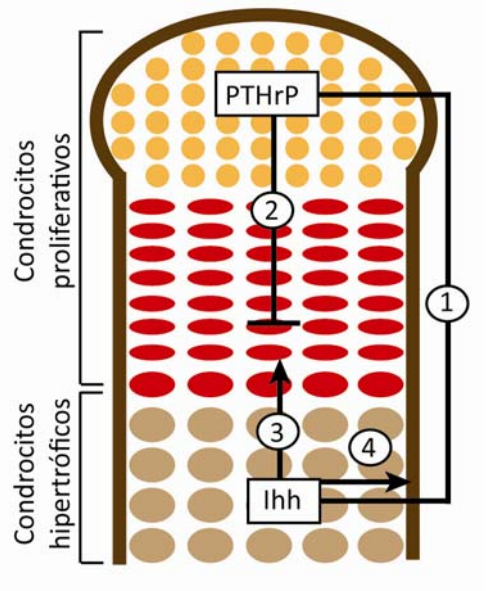

Figura 8. Papel de Ihh en la osificación endocondral. Ihh estimula la producción de PTHrP en las células de la zona distal del hueso (1). PTHrP actúa sobre los condrocitos proliferativos manteniéndolos en ese estado (2). Ihh también actúa directamente sobre los condrocitos columnares estimulando su división y sobre las células pericondriales induciendo su diferenciación a osteoblastos para formar el collar óseo (3 y 4). Figura adaptada (Kronenberg, 2003).

Además de Ihh, existen otras vías de señalización que regulan la osificación endocondral. Una de ellas es la señalización de los factores de crecimiento de fibroblastos (*Fibroblast Growth Factor*, FGF), cuyos receptores (FGFR) se expresan en diferentes regiones de la placa de crecimiento, así FGFR3 se expresa en los condrocitos proliferativos, FGFR1 en los pre-/hipertróficos y en los de reserva y FGFR2 en las células pericondriales (Ornitz and Marie, 2002). La función de FGFR3 es crucial en la fisiología de la placa de crecimiento ya que mutaciones en este gen son responsables de distintos tipos de condrodisplasias en humanos (Bellus et al., 1995; Rousseau et al., 1994; Shiang et al., 1994; Tavormina et al., 1995). Por el contrario la inactivación de FGR3 en ratón provoca una elongación mayor de lo habitual en los huesos largos (Colvin et al., 1996; Deng et al., 1996). La ruta canónica Wnt/β-catenina es otra vía de señalización clave en el desarrollo del hueso porque interviene en el proceso de diferenciación de los osteoblastos, como pone de manifiesto el fenotipo de los ratones condicionales para el gen de la *β-catenina* en los que las células mesenquimales que deberían dar lugar a osteoblastos se diferencian a condrocitos (Day et al., 2005; Hill et al., 2005; Logan and

Nusse, 2004). También las proteínas BMP (*Bone Morphogenetic Protein*) participan en el crecimiento y diferenciación del cartílago (Pathi et al., 1999). Se ha demostrado que para que el ritmo de proliferación de los condrocitos sea el adecuado se requiere la actuación en paralelo de la señalización BMP e Ihh (Minina et al., 2001). Estas proteínas se expresan de manera distinta en la placa de crecimiento, así BMP2, -3, -4, -5 y -7 se expresan en el pericondrio, BMP2 y -6 en los condrocitos hipertróficos y BMP7 en los proliferativos (Minina et al., 2002; Minina et al., 2001). Finalmente otros genes clave en el desarrollo óseo son los factores transcripcionales *Runx2* (también llamado Cbfa1) (Otto et al., 1997; Komori, 1997) y *Osterix* (Nakashima et al., 2002), los cuales son imprescindibles para la diferenciación de los osteoblastos, ó *Sox9* que está implicado en la formación de las condensaciones mesenquimales previas a la formación de los moldes cartilaginosos y es un marcador de los condrocitos proliferativos (Bi et al., 1999). En resumen la formación del hueso es un proceso complejo dirigido por Ihh pero en el que interviene un gran número de cascadas de señalización distintas, las cuales se encuentran perfectamente coordinadas entre ellas.

Objetivos

Los objetivos planteados en esta Tesis Doctoral han sido:

Objetivo 1

Estudio molecular de pacientes afectados con el síndrome de Ellis-van Creveld.

Objetivo 2

Estudio molecular de pacientes afectados con el síndrome de Weyers Acrofacial Dysostosis.

Objetivo 3

Estudio del efecto de las mutaciones Weyers sobre la vía de Hh.

Objetivo 4

Análisis funcional de Evc en la placa de crecimiento de los huesos largos y en las sincondrosis de la base del cráneo.

Materiales y Métodos
Resultados

Capítulo I

Long Interspersed Nuclear Element -1 (LINE-1)-Mediated Deletion of *EVC, EVC2, C4orf6* and *STK32B*in Ellis-van Creveld Syndrome With Borderline Intelligence

Temtamy, S.A.; Aglan, M.S.; **Valencia, M**.; Cocchi, G.; Pacheco, M.; Ashour, A.M.; Amr, K.S.; Helmy, S.M.; El-Gammal, M.A.; Wright, M.; Lapunzina, P.; Goodship, J.A.; Ruiz-Perez, V.L.

Human Mutation 29(7): 931-938 (2008)

En este trabajo hemos investigado mutaciones en *EVC* y *EVC2* en dos familias no relacionadas, una consanguínea de origen egipcio con dos hijos sanos y tres afectados con EvC y bajo cociente intelectual, y otra de origen italiano con un individuo también diagnosticado con EvC y padres no emparentados.

Al analizar el probando de la primera familia no pudimos amplificar por PCR ninguno de los exones de *EVC2* ni los 11 primeros exones de *EVC*, lo que nos hizo suponer, al tratarse de un caso consanguíneo, la existencia de una deleción en homocigosis de ambos genes. En el pedigrí italiano, la secuenciación de *EVC* y *EVC2* en el ADN del afectado, identificó sólo una mutación en homocigosis en el sitio 5´ de *splicing* del intrón 8 de *EVC* presente en el padre pero no en la madre. Para entender la homocigosidad de esta mutación llevamos a cabo un análisis de microsatélites y observamos que tanto la madre como el afectado eran homocigotos para un fragmento del cromosoma 4 en el cual el paciente parecía no haber heredado alelos maternos, apuntando también a una deleción de ADN en el cromosoma materno.

Demostramos la existencia de la deleción mediante un ensayo de hibridación *in situ* fluorescente sobre metafases de las madres e hijos afectados de ambos pedigrís. Para ello utilizamos una sonda marcada de ARN sintetizada a partir de un BAC (500H20) correspondiente a la región delecionada y una sonda control comercial de la región telomérica opuesta (4q). En el afectado del pedigrí italiano así como en las madres de ambas familias, la sonda sólo hibridó con uno de los dos cromosomas 4, mientras que en el afectado del pedigrí egipcio no detectamos señal en ninguno de los dos cromosomas 4. Es decir, los afectados del pedigrí egipcio tenían la deleción en homocigosis mientras que el paciente del pedigrí italiano y las madres de ambas familias eran heterocigotos. Para determinar el tamaño de la deleción y los puntos de ruptura de este reordenamiento, usamos ADN genómico de la madre italiana y de uno de los afectados egipcios y realizamos una hibridación en soporte sólido de SNPs utilizando un chip Illumina (Illumina Hap550 BeadArrays chip). Este estudio demostró que ambas familias portaban una deleción de tamaño similar (520 kb) que involucra al mismo número de genes (*EVC*, *EVC2*, *STK32B* y *C4orf6*). A continuación diseñamos parejas de *primers* en las regiones fronterizas de las SNPs delecionadas y no delecionadas y mediante PCR localizamos en ambas familias el punto de ruptura telomérico en un fragmento de 6 kb correspondiente a un elemento LINE-1 y el punto de ruptura centromérico en otro elemento LINE-1.

Ambos retrotransposones son 93% idénticos en su secuencia, lo que nos hizo pensar en un hecho de recombinación como causante de la pérdida de ADN. Para confirmarlo diseñamos *primers* específicos de secuencias únicas no delecionadas flanqueantes a los retrotransposones y realizamos PCR de larga de distancia en individuos portadores de la deleción de ambos pedigrís. Como resultado obtuvimos un fragmento de 8.5 kb cuya secuenciación reveló un único retrotransposón procedente de la fusión de los dos localizados en los bordes de la deleción en ambas familias. Comparando las secuencias de referencia de las bases de datos de los elementos L1 telomérico y centromérico con la de los elementos L1 híbridos de cada pedigrí y siguiendo el patrón de polimorfismos, observamos que el punto de recombinación entre los dos LINE-1 era diferente en cada familia, por lo que la deleción ocurrió de manera independiente en cada caso.

Este trabajo describe por primera vez individuos con mutaciones en *EVC* y en *EVC2* simultáneamente y revela que la inactivación de un alelo de *EVC* junto con la inactivación de un alelo de *EVC2* no provoca fenotipo. Asimismo, demuestra que la ausencia de alelos funcionales de ambos genes no agrava las características clínicas de EvC. Por otro lado es muy posible que la deleción *STK32B-EVC* esté asociada a bajo cociente intelectual, pero puesto que por RT-PCR observamos que todos los genes delecionados se expresan en cerebro no pudimos esclarecer qué gen o genes podrían ser responsables de dicho retraso. El fenotipo de los homocigotos para la deleción *STK32B-EVC* indica que la inactivación de *STK32B* o *C4orf6*, dos genes de función desconocida, conduce como máximo a un ligero retraso mental.

La doctoranda llevó a cabo los experimentos de FISH, la amplificación del fragmento de 8.5 kb resultante de la deleción en los pacientes y el diseño de los *primers* para su posterior secuenciación; el estudio y comparación de la secuencia nucleotídica entre ambos pedigrís para determinar el punto exacto de ruptura en los retrotransposones así como el estudio de la expresión de los cuatro genes delecionados en cerebro fetal. También participó en la composición de las figuras y discusión del artículo.

HUMAN MUTATION 29(7), 931–938, 2008

RAPID COMMUNICATION

Long Interspersed Nuclear Element-1 (LINE1)-Mediated Deletion of *EVC, EVC2, C4orf6,* and *STK32B* in Ellis–van Creveld Syndrome With Borderline Intelligence

Samia A. Temtamy,[1] Mona S. Aglan,[1] Maria Valencia,[2] Guido Cocchi,[3] Maria Pacheco,[2] Adel M. Ashour,[1] Khalda S. Amr,[1] Sanaa M.H. Helmy,[1] Mona A. El-Gammal,[1] Michael Wright,[5] Pablo Lapunzina,[4] Judith A. Goodship,[5] and Victor L. Ruiz-Perez[2]*

[1]Human Genetics and Genome Research Division, National Research Centre, Cairo, Egypt; [2]Instituto de Investigaciones Biomédicas, Consejo Superior de Investigaciones Científicas-Universidad Autónoma de Madrid and CIBER de Enfermedades Raras (CIBERER), Madrid, Spain; [3]Istituto Clinico di Pediatria Preventiva e Neonatología. Università di Bologna, Bologna, Italy; [4]Departamento de Genética, Hospital Universitario La Paz, Universidad Autónoma de Madrid and CIBER de Enfermedades Raras (CIBERER), Madrid, Spain; [5]Institute of Human Genetics, Newcastle University, Newcastle upon Tyne, United Kingdom

Communicated by Haig H. Kazazian

Previous work has shown Ellis–van Creveld (EvC) patients with mutations either in both alleles of *EVC* or in both alleles of *EVC2*. We now report affected individuals with the two genes inactivated on each allele. In a consanguineous pedigree diagnosed with EvC and borderline intelligence, we detected a 520-kb homozygous deletion comprising *EVC, EVC2, C4orf6,* and *STK32B*, caused by recombination between long interspersed nuclear element-1 (LINE-1 or L1) elements. Patients homozygous for the deletion are deficient in *EVC* and *EVC2* and have no increase in the severity of the EvC typical features. Similarly deletion carriers demonstrate absence of digenic inheritance in EvC. Further, the phenotype of these patients suggests that the *EVC-STK32B* deletion also leads to mild mental retardation and reveals that loss of the novel genes *C4orf6* and *STK32B* causes at most mild mental deficit. In an EvC compound heterozygote of different ethnic origin we identified the same LINE-to-LINE rearrangement due to a different recombination event. These findings highlight the importance of L1 repetitive sequences in human genome architecture and disease. Hum Mutat 29(7), 931–938, 2008. **© 2008 Wiley-Liss, Inc.**

KEY WORDS: Ellis–van Creveld syndrome; *EVC*; *EVC2*; 4p16.1 deletion; LINE-1 retrotransposons

INTRODUCTION

Ellis–van Creveld (EvC) syndrome (MIM# 225500) is an autosomal recessive skeletal dysplasia affecting development of the skeleton, teeth, and heart. Cardinal features of the condition include disproportionate short stature with short limbs and ribs, postaxial polydactyly, and dystrophic nails and teeth. Approximately two-thirds of EvC patients are born with congenital heart defects, most commonly an atrioventricular septal defect. Increased risk of neonatal mortality has also been reported in EvC, associated with respiratory problems resulting from the smaller rib cage and heart malformations [McKusick et al., 1964].

Two genes, *EVC* (MIM# 604831) and *EVC2* (MIM# 607261), are found mutated in EvC patients [Ruiz-Perez et al., 2000, 2003]. The recent generation of an $Evc^{-/-}$ mouse has revealed that defective hedgehog signaling underlies the clinical features of this disorder [Ruiz-Perez et al., 2007]. *EVC* and *EVC2* are arranged in a close divergent configuration suggestive of common transcriptional regulatory elements with the two genes separated by 2,624 bp in the human and 1,647 bp in the mouse. The majority of *EVC* and *EVC2* mutations introduce premature termination codons either directly or following a frameshift and thus they are predicted to be loss of function mutations. Mutations in both genes include single-basepair substitutions, microinsertions, microdeletions, and few deletions spanning more than one exon within the same gene [Tompson et al., 2007]. Two changes, S307P in *EVC* and c.3793delC in *EVC2*, were respectively found in pedigrees with autosomal dominant Weyer's acrodental dysostosis (MIM# 193530) demonstrating that specific mutations in *EVC* or *EVC2* have a dominant negative effect [Ruiz-Perez et al., 2000; Ye et al., 2006]. Weyer's patients have postaxial polydactyly and

Received 6 December 2007; accepted revised manuscript 11 February 2008.

*Correspondence to: Victor L. Ruiz-Perez; Instituto de Investigaciones Biomédicas, Consejo Superior de Investigaciones Científicas-Universidad Autónoma de Madrid, Arturo Duperier 4, Madrid 28029, Spain. E-mail: vlruiz@iib.uam.es

Grant sponsors: Ramón Areces Foundation; Spanish Ministry of Science and Education; European Union; Grant number: LSHM-CT-2007-03741.

DOI 10.1002/humu.20778

Published online 2 May 2008 in Wiley InterScience (www.interscience.wiley.com).

© 2008 WILEY-LISS, INC.

dental anomalies but not the short stature and cardiac manifestations of EvC. A considerable number of EvC cases have already been screened for mutations, including systematic screening of 65 EvC cases in which all coding exons of both genes were sequenced [Tompson et al., 2007]. Consistently EvC patients showed mutations either in *EVC* or *EVC2* with no previous reports of patients with mutations simultaneously in both genes. On this basis digenic inheritance was considered to be excluded in EvC, but the possibility remained that individuals carrying a defective copy of each gene could have a different phenotype. Likewise the phenotype of patients with biallelic inactivation of both genes was unknown.

MATERIALS AND METHODS

Patients

The study included patients from two unrelated pedigrees. The clinical features are described in Table 1. Ethical approval and appropriate informed consent was obtained from all human subjects or their parents.

Genomic Sequencing

Genomic DNA was extracted from peripheral blood by standard procedures. For mutation screening all coding exons of *EVC* and *EVC2*, the exon–intron boundaries, and at least 100 bp of the flanking introns were amplified by standard PCR (primers available on request). Prior to sequencing the PCR products were treated with shrimp alkaline phosphatase and exonuclease I (ExoSap-it; GE Healthcare, Piscataway, NJ) according to the manufacturer's instructions. Sequencing reactions were run on a ABI 3730 sequencer using a dye terminator cycle sequencing kit (Applied Biosystems, Foster City, CA). Chromatograms were aligned and compared with the reference nucleotide sequence for *EVC* and *EVC2* transcripts (GenBank AF216184 and AY185210) and with genomic sequence obtained from GenBank reference assembly NC_000004.10 using Sequencher (Gene Codes Corp, Ann Arbor, MI). For the c.1098+1G>A mutation, numbering started from the translation initiation codon of *EVC* being the A of the ATG nucleotide +1.

Fluorescence In Situ Hybridization

Metaphase spreads were prepared from peripheral blood by standard methods and BAC clones were purchased from Invitrogen (Carlsbad, CA). BAC DNAs were purified via Qiagen columns (Qiagen, Hilden, Germany) and labeled with SpectrumRed-dUTP by nick translation (Abbott Molecular Inc., Des Plaines, IL). BAC probes were preannealed with Cot-1 DNA and mixed with a commercial chromosome 4q–specific probe (Cytocell Technologies Ltd, Cambridge, United Kingdom) before being added onto denatured metaphases. The fluorescence in situ hybridization (FISH) procedure was performed overnight at 37°C

TABLE 1. Clinical Findings in Patients From Pedigrees 1 and 2

	Pedigree 1			Pedigree 2
Clinical features	Case 1	Case 2	Case 3	Proband
Age (years), sex	21, male	19, female	16, male	10, male
Height	−5.0 SD	−5.6 SD	−4.7 SD	−5.8 SD
Head circumference (HC)	+0.6 SD	−2 SD	−3 SD	−1.8 SD
Acromesomelic shortening	+	+	+	+
Long trunk, Narrow thorax	+	+	+	+
Knock knees	+	+	+	+
Postaxial polydactyly of fingers	+	+	+	+
Other hand/upper limb anomalies	Camptodactyly of fifth fingers	Camptodactyly and clinodactyly of fifth fingers	Camptodactyly of fifth fingers. Inability to full extension of elbows	Brachydactyly. Limitation to full extension of elbows
Broad hallux	+	+	+	–
Postaxial polydactyly of toes	+	+	+	–
Other foot anomalies	Soft tissue syndactyly between second and third toes, overriding toes, wide space between first and second toes, clinodactyly of fifth toes	Soft tissue syndactyly between second and third toes, overriding toes, wide space between first and second toes, clinodactyly of fifth toes	Soft tissue syndactyly between second & third toes, overriding toes, wide space between first and second toes, clinodactyly of fifth toes. Inability to full extension of knees	Wide space between first and second toes
Hypoplastic nails	+	+	+	+
Long face, prominent nose	+	+	+	+
Short philtrum	+	+	+	–
Mouth and lips	Thick lips, notched upper lip	Thick lips, notched upper lip	Thick lips, notched upper lip	–
Multiple frenula	+	+	+	+
Partial anodontia	+	+	+	+
Abnormal spaced teeth	+	+	+	+
Others dental anomalies	Taurodontism, delayed eruption	Taurodontism, delayed eruption	Supernumerary teeth, delayed eruption, enamel hypoplasia and hypocalcification	Delayed eruption, conical shaped teeth
Tongue	Median fissure of tongue with bifid tip	Median fissure of tongue with bifid tip	–	–
Intelligence	Borderline IQ 75	Borderline	Borderline	Normal
Echocardiography	Normal	Normal	Normal	Normal

+, present; –, not present.

in Abbott hybridization buffer and slides washed in 0.4 × SSC/0.3% NP-40 for 2 minutes at 73°C and in 2 × SSC/0.1% NP-40 for 1 minute at room temperature. Chromosomes were counterstained with DAPI and photographed using a Leica microscope and CytoVision software (Leica Microsystems, Wetzlar, Germany).

Microsatellite Analysis

Genotyping was performed using repeat-containing microsatellite markers from the EvC region. Sequence and position of the markers used are shown in the Ensembl genome browser (www.ensembl.org). *500H20P5* and *164F16* are markers that we described previously [Ruiz-Perez et al., 2000]. HEX or FAM fluorescently-labeled PCR products were run on a ABI 3730 sequencer and analyzed with GeneMapper (Applied Biosystems).

Array Hybridization Profiling and Data Analysis

DNAs were quantified using PicoGreen (Invitrogen) and a genome-wide scan of 550,163 tag SNPs was conducted using the Illumina Hap550 Bead Arrays according to the manufacturer's specifications (Illumina, San Diego, CA). DNA samples with GeneCall (Illumina) scores <0.15 at any locus were considered "no calls." Image data was analyzed using the Chromosome Viewer tool contained in Beadstudio 3.0 (Illumina). The metric used was the log *R* ratio, which is the log (base 2) ratio of the observed normalized *R* value for a SNP divided by the expected normalized *R* value [Simon-Sanchez, et al., 2007]. All genomic positions were based upon build 36 (dbSNP version 126).

Long-Range PCR

Long-range (LR) amplification was performed in patients and carriers of the *EVC-STK32B* deletion and in normal controls using the Expand Long Template PCR System (Roche Applied Science, Penzberg, Germany) following the instructions provided with the kit. The sequences of the forward 5′-TGAGTGTGCACCCAACTGAT-3′ and reverse 5′-GGTGGGATATTGATCGTCCA-3′ primers used for the LR amplification were designed from DNA previously masked with RepeatMasker (www.repeatmasker.org). LR-PCR products were run in a 1% agarose gel and extracted from the agarose using the QIAquick extraction kit (Qiagen). A total of two purified LR-PCR products, corresponding to a heterozygous member of each family, were directly sequenced by primer walking and compared to the sequence of the L1 breakpoint retrotransposons obtained from GenBank, reference assembly NC_000004.10.

RT-PCR

First strand cDNAs were synthesized with superscript II (Invitrogen) in 20-µl reactions containing 5 µg of total RNA from human fetal brain (Clontech Laboratories, Mountain View, CA) and 200 ng of random primers. RT-PCR amplification of *EVC* (AF216184), *EVC2* (AY185210), *C4orf6* (NM_005750), and *STK32B* (NM_018401) were performed for 35 cycles under standard PCR conditions. Human *Beta-actin* (*ACTB*; NM_001101) was used as loading control.

RESULTS

Patients and Mutation Analysis

Patients in this study included three affected siblings from a consanguineous Egyptian pedigree who had been reported with EvC syndrome and low intelligence quotient (IQ) [Mostafa et al., 2005] (Pedigree 1; Fig. 1; Table 1). Although EvC patients have normal intelligence, we were interested to determine if a specific mutation in *EVC* or *EVC2* could be responsible for this phenotype. We isolated DNA from the affected subjects and sought mutations in *EVC* and *EVC2* by PCR amplification of coding exons and sequencing. Whereas the last 12 exons of *EVC* were amplified normally, we could not obtain a PCR product from the preceding *EVC* exons 1 to 11 or from any of the *EVC2* exons in samples from the three affected individuals. Consequently a homozygous deletion involving both genes was suspected. To establish the boundaries of the deletion we performed PCR in the affected DNA using numerous primer pairs spaced between markers *D4S2925* and *D4S827*, so that we covered a larger 4p16.1 region. The PCR results revealed that in addition to *EVC* and *EVC2*, the contiguous gene *C4orf6* and coding exons 4 to 11 of *STK32B* were also missing in these patients. *C4orf6* and *STK32B* are novel genes of unknown function. *C4orf6* codes for a 93–amino acid protein and appears to be one of the few primate specific genes, since on database interrogation there is no recognizable homolog in the mouse or in any nonprimate vertebrate with genomic sequence currently available. *STK32B* encodes a protein with homology to serine-threonine protein kinases and accordingly it contains the 11 conserved amino acids motifs (I-XI) that constitute the hallmark of these enzymes [Hanks and Hunter, 1995]. In contrast, only kinase subdomains I, II, and III are present in the predicted peptide from the partially deleted *STK32B* allele of Pedigree 1 and hence it is nonfunctional. *STK32B* is part of a trio of adjacent genes coding for a serine-threonine kinase 32 (*STK32*(*A-C*)), a Collapsin response mediator protein (*CRMP*(*1,4,3*)), and a Janus kinase and microtubule interacting protein (*JAKMIP*(*1-2*) and *C10orf39*) that are duplicated in conserved orientation on human chromosomes 4, 5, and 10, with *C4orf6*, *EVC*, and *EVC2* inserted between *STK32B* and *CRMP1* exclusively on human chromosome 4.

In the light of the Egyptian pedigree we reviewed our data from a second EvC family of Italian origin (Pedigree 2; Table 1) . Direct sequencing of *EVC* and *EVC2* coding exons in the proband had revealed a novel homozygous 5′ splice-site mutation in intron 8 of *EVC*, c.1098+1G>A. However, as this was not a consanguineous family we searched for the mutation in both parental DNAs and found that the splice site change was present in the father but not in the mother. Microsatellite analysis showed mother and proband both homozygous for a 4p chromosomal fragment in which the child seemed not to have inherited any maternal alleles, pointing again to a chromosome deletion (Fig. 2A). To corroborate this, we obtained new samples from the family and developed metaphases to perform FISH. We purified DNA from two contiguous BAC clones mapping to the putative deleted region, 21912M1 and 500H20, and labeled it directly with spectrum red by nick translation. Whichever BAC probe was used, the red hybridization signal was always absent from one chromosome 4 in the affected child and his mother, thus confirming a 4p deletion carried on the maternal chromosome (Fig. 2B). When the same FISH experiments were repeated in patients from the Egyptian pedigree no BAC hybridization signal was observed, proving that the deletion was present in both chromosomes (Fig. 2D).

Characterization of a Large Chromosome 4 Interstitial Deletion Caused by Recombination Between Two Distant Long Interspersed Nuclear Element-1 (LINE-1) Retrotransposons

To measure the size of the rearrangement in both families, we took DNA from the heterozygous mother of Pedigree 2 and DNA from one of the affected siblings of Pedigree 1, and hybridized each of them to an Illumina HumanHap550 Genotyping BeadChip, previously shown useful for detecting chromosomal aberrations

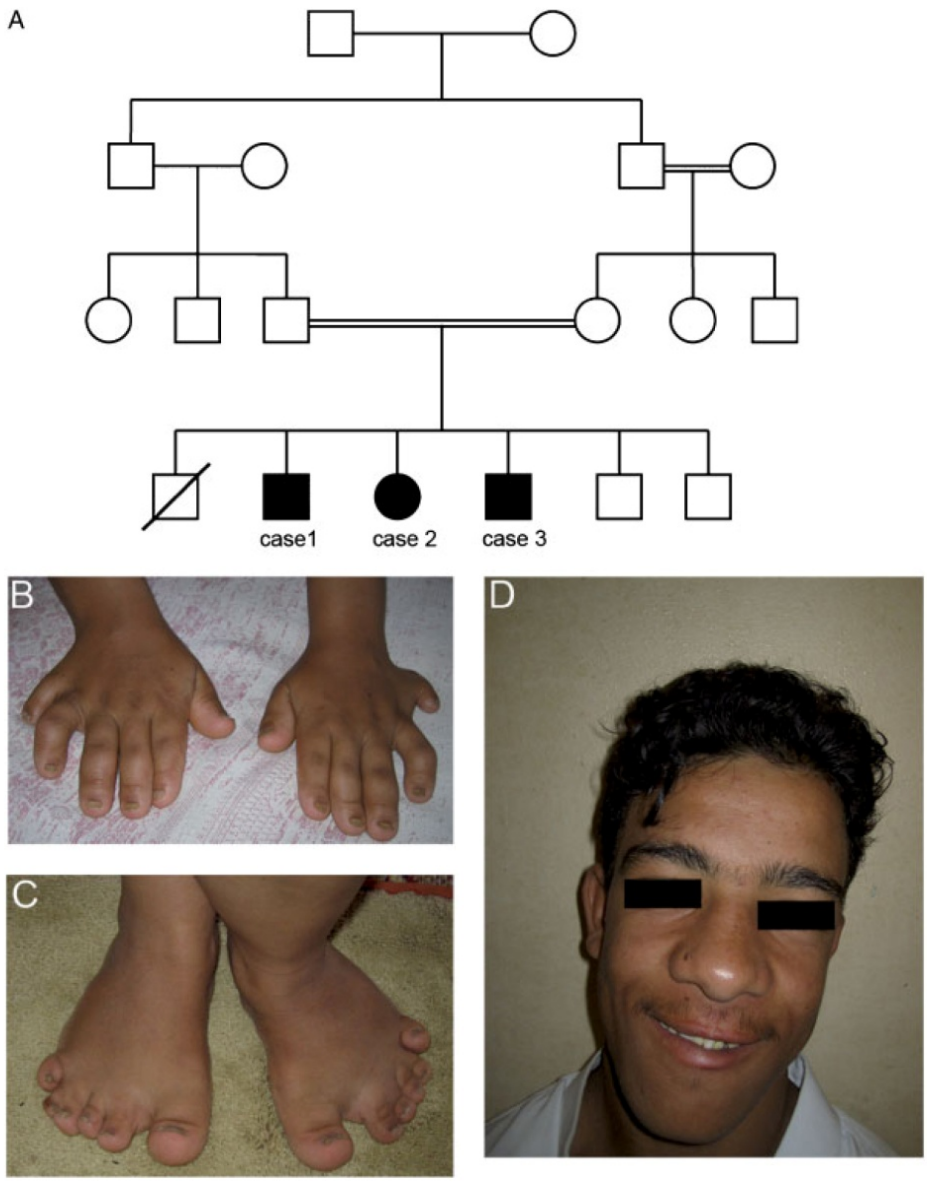

FIGURE 1. **Clinical features of the Egyptian family with EvC and borderline IQ (Pedigree 1). A: Pedigree of the family showing parental consanguinity and three affected sibs. B: Hands of Case 2 showing postaxial polydactyly, camptodactyly, and clinodactyly of fifth fingers with dysplastic nails. C: Feet of Case 2 showing postaxial polydactyly, brachydactyly, partial syndactyly of second and third toes and fourth and fifth toes, sandal gap between first and second toes, and dysplastic nails. D: Facial features of Case 3 with microcephaly and elongated face. [Color figure can be viewed in the online issue, which is available at www.interscience.wiley.com.]**

[Steemers and Gunderson, 2007]. We analyzed the hybridization data with the Illumina BeadStudio software that uses the log R ratio as a metric. The log R ratio represents the ratio of the observed to the expected SNP hybridization intensity and consequently it gives an indirect measure of copy number for each SNP. A drop in the log R ratio was observed across 529.023 kb between SNPs *rs6817353* and *rs4688960* in both samples tested, with the values of the log R ratio being lower in the Egyptian case as expected from a homozygous deletion (Fig. 2E). The BeadChip hybridizations confirmed our previous data in Pedigrees 1 and 2 and showed the two families carrying similar size deletion involving the same group of genes. As the genomic distance between the nondeleted and deleted SNPs on each side of the rearrangement was 15.7 kb and 7.6 kb, respectively, we refined the position of the deletion edges in an attempt to understand the mechanism causative of the deletion. For this we used primer pairs covering the gaps between deleted and nondeleted SNPs and checked amplification in DNA from consanguineous patients of Pedigree 1. By doing this we narrowed down the telomeric breakpoint to a 6-kb DNA fragment corresponding to a complete LINE-1 (or L1) and similarly we located the centromeric breakpoint within a second 6-kb full-length L1 retrotransposon (Fig. 3). Sequence alignment between the 5′ and 3′ L1 insertions demonstrates that they are 93% identical over their entire nucleotide length, making homologous recombination between LINE-1 elements the likely cause for the loss of DNA in these patients. Both L1 insertions were identified by BLAST and RepeatMasker and we used U93574 as the

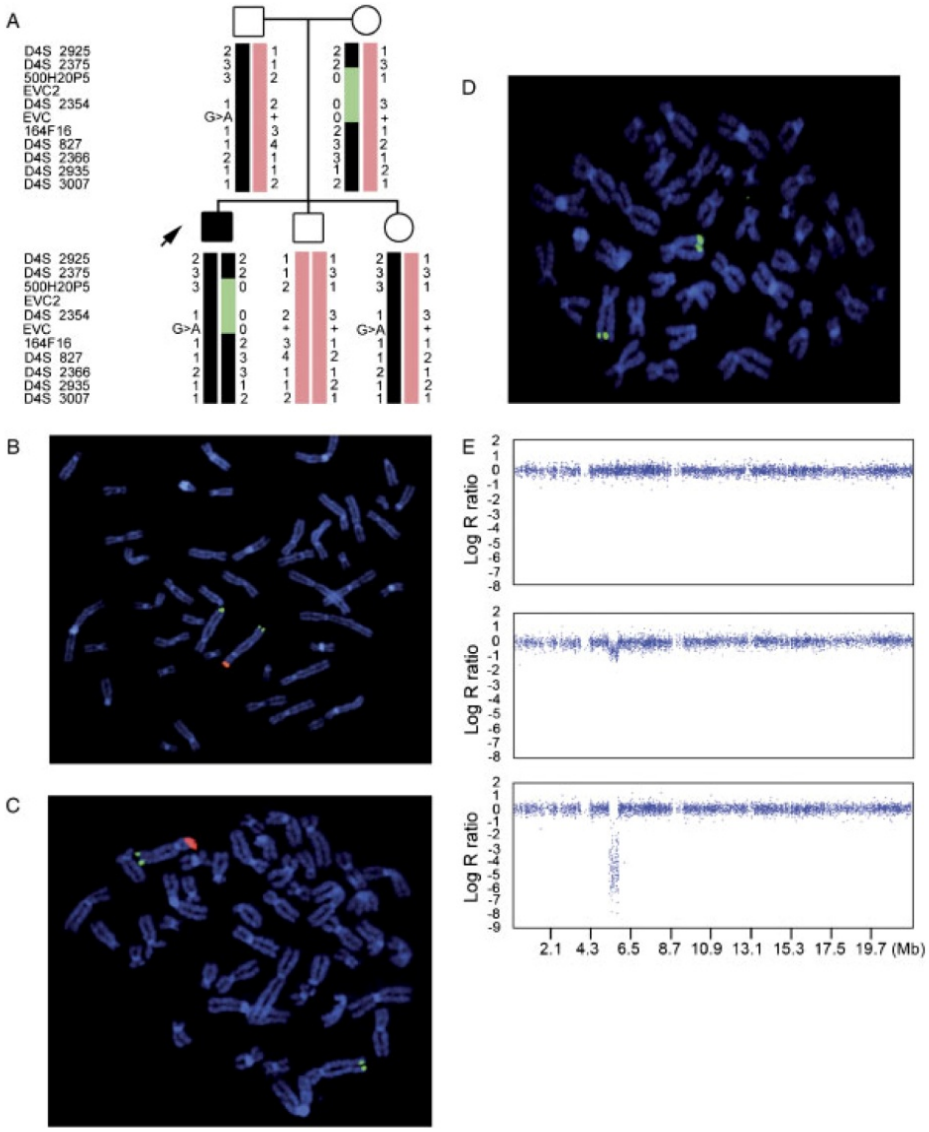

FIGURE 2. **Interstitial chromosome 4p deletion. A:** Haplotype analysis of Pedigree 2 showing a DNA region between markers *D4S2375* and *164F16* in which the proband and his mother are both homozygous but do not share a common haplotype due to the chromosome deletion (green area). Markers and haplotypes are shown from telomere to centromere. The disease haplotypes are in black, G>A is a splice site mutation in the nonrearranged chromosome and + indicates normal sequence at this position. **B**,**C:** FISH analysis demonstrating a chromosome 4p heterozygous deletion in the proband of Pedigree 2 (B) and mother of Pedigree 1 (C). **D:** 4p homozygous deletion in Case 1 of Pedigree 1. The green signal is a 4q telomere specific probe (Cytocell) and the red signal corresponds to 500H20 BAC probe. The same results were obtained for BAC 21912M1. **E:** HumanHap550 Genotyping BeadChip array profiles from a control subject (top panel), heterozygous mother of Pedigree 2 (medium panel), and homozygous Case 1 of Pedigree 1 (lower panel). Log R ratio values are in the y-axis and chromosome 4 genomic distance in abscises.

reference sequence for the full-length LINE-1 element. To identify the deletion junction in both families we performed LR-PCR with unique primers flanking the L1 retrotransposons placed at the edges of the deletion and obtained an 8.5-kb PCR product in affected and heterozygous individuals from both pedigrees but not in normal controls (Fig. 3C). Direct sequencing of the 8.5-kb junctional fragments revealed fusion of the two retrotransposons, while the DNA sequences upstream of the telomeric and downstream of the centromeric L1 insertions were intact. We next compared the nucleotide composition of the L1 recombinant element from each family with the sequences corresponding to both breakpoint retrotransposons obtained from GenBank. We focused on the trend of nucleotide mismatches and observed a different point of recombination in each pedigree (Fig. 4), so we concluded that the two families carry independently rearranged chromosomes rather than a common ancestral allele. This is supported by differences in the SNP haplotype between the two families all along their 8.5-kb deletion-junction fragments. We noticed that both L1 recombinant elements had a few sporadic positions containing single nucleotide variations that differed from the reference sequences of both the 5′ and the 3′ retrotransposons and a few others also randomly distributed that were placed within the context of one L1 insertion but matched the sequence of the other recombination partner (data not shown in Fig. 4). The

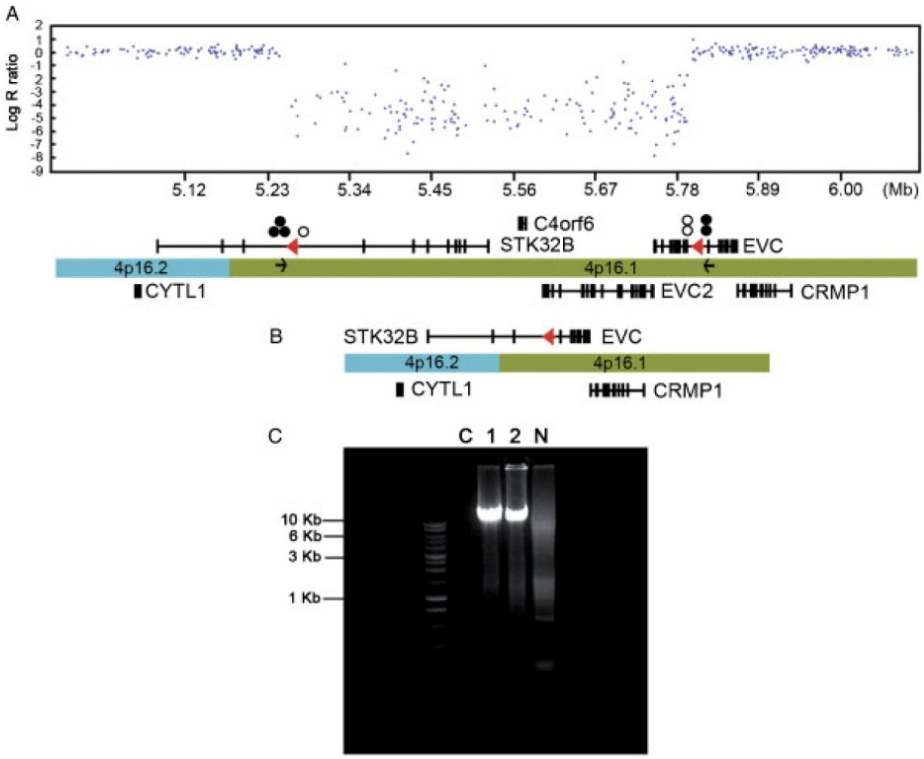

FIGURE 3. **Characterization of the *EVC-STK32B* deleted region. A: Magnification of the Beadchip hybridization plot from Case1, Pedigree 1, showing the region of interest and representation to scale of genes underneath. Genes transcribed from the forward or the reverse strands are shown above or below the cytogenetic bands. Shaded or open circles indicate positive or negative amplification of primers used to refine the deletion edges. LINE-1 elements that are inserted in reverse orientation to the transcriptional direction of *STK32B* and *EVC* are shown as gray/red arrows. Black arrows indicate the primers used for LR amplification of the deleted allele. B: Representation of the rearranged chromosome showing fusion of *STK32B* and *EVC*. Potential splicing between *STK32B* exon 3 and *EVC* exon 12 is not in frame and will lead to a stop codon 25 amino acids later. C: LR PCR using the primers shown in (A) produces an amplicon in DNA from heterozygotes from Pedigrees 1 and 2 but not in DNA from the normal control (N). A negative control with no DNA is labeled C. [Color figure can be viewed in the online issue, which is available at www.interscience.wiley.com.]**

number of these mismatching nucleotides was slightly higher in the recombinant element from Pedigree 2. This is not surprising since sequence polymorphisms are not an unusual finding in the L1 retrotransposons. In a recent survey in which three L1 insertions were sequenced among individuals of diverse geographic origins, the number of polymorphic sites in each retrotransposon ranged from 17 to 26 and a new allele for each locus was found in every three to five genomes [Seleme et al., 2006]. We named the mutations g.5295345_5815669del and g.5296396_5816718del for Pedigrees 1 and 2, respectively, following the recommended nomenclature guidelines [den Dunnen and Antonarakis, 2000] and numbered nucleotides according to human chromosome 4 reference sequence NC_000004.10 (NCBI Build 36.1). Nucleotides were counted from the start of the reference sequence. Finally, we searched the Database of Genomic Variants (http://projects.tcag.ca/variation), but the *EVC-STK32B* deletion has not been detected by any of the extensive screenings looking for copy number variations, indicating that it is not a frequent structural variation of the human genome [Redon et al., 2006; Wong et al., 2007].

DISCUSSION

The fact that heterozygous deletion carriers from both pedigrees show no phenotype and are normal demonstrates that *EVC*, *EVC2*, *C4orf6*, and *STK32B* hemizygosity has no clinical effect. In addition, as those individuals carry half of the genetic dosage of *EVC* and *EVC2*, they conclusively show that loss of function of one allele in each gene is not associated with a phenotype, formally excluding digenic inheritance in EvC. Affected individuals with mutations in *EVC* have the same typical spectrum of features as those with mutations in *EVC2* and are phenotypically indistinguishable [Tompson et al., 2007]. This also applies in the Italian case with classical EvC in which the deletion of *EVC* and *EVC2* occurs along with an *EVC* point mutation in the nonrearranged chromosome. Similarly, the three affected members from Pedigree 1, despite complete absence of functional EVC and EVC2 proteins, have typical skeletal and orofacial EvC features with no increase in severity. They did not have heart defects and we have seen pseudo-cleft lip and bifid tip of the tongue in EvC patients with mutations in only one of the EvC genes (our unpublished results). As the phenotype of Pedigree 1 is typical for EvC we conclude that there are no phenotypic features that in the absence of EVC are rescued by EVC2 or vice versa and so with the possible exception of the brain involvement there is no evidence of functional redundancy between the EvC proteins.

Borderline intelligence is a non-EvC feature that segregates with the homozygous deletion of *EVC*, *EVC2*, *C4orf6*, and *STK32B* in Pedigree 1. This was documented by two independent evaluators at two different time points. IQ evaluation using Wechsler Intelligence Scale for Children for Cases 1, 2, and 3 at the ages of 15, 13, and 11 years was 56, 53, and 64, respectively, and in a second more recent IQ assessment of Case 1 at the age of 21 years,

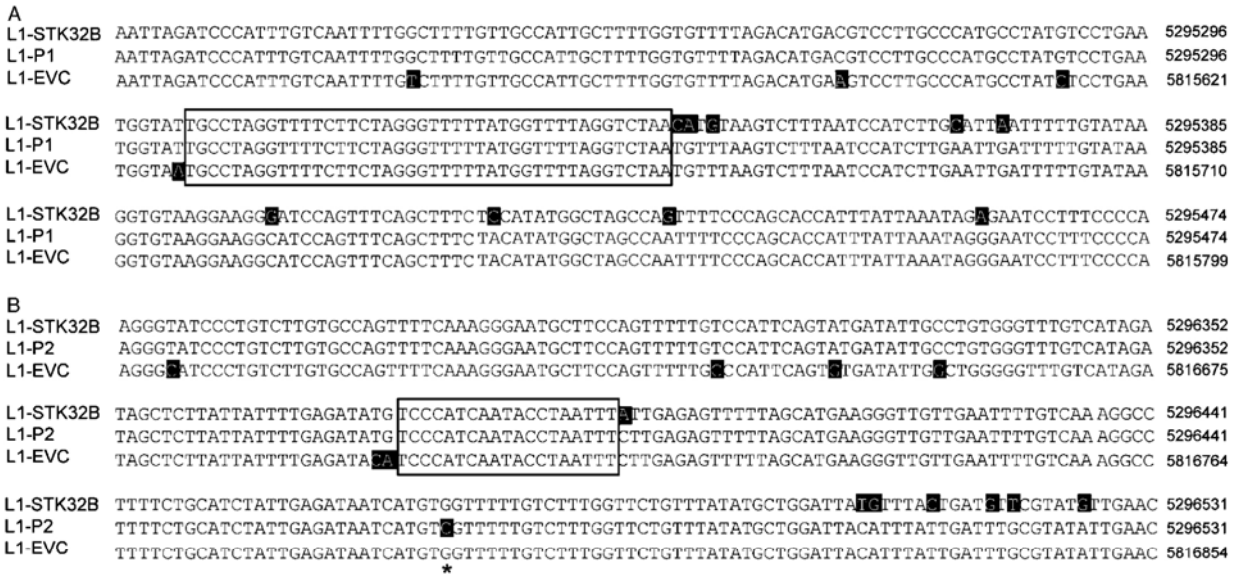

FIGURE 4. **The *EVC-STK32B* rearrangements in Pedigrees 1 and 2 resulted from independent recombination events. A,B:Two different regions of nucleotide alignment between the telomeric (L1-STK32B) and centromeric (L1-EVC) LINE-1 elements (GenBank reference sequence NC_000004.10) and the recombinant retrotransposons from Pedigrees 1 (L1-P1, panel A) and 2 (L1-P2, panel B). Mismatching nucleotides are shaded and nucleotide numbers on the right are based on genomic sequence from chromosome 4 (NC_000004.10). The area in which the recombination event took place in each family is indicated by a box. In each case the patient sequence to the left of the box matches the L1-STK32B element and the patient sequence to the right of the box matches the L1-EVC retrotransposon. The recombination intervals from Pedigrees 1 and 2 correspond in the reverse orientation to nucleotide positions 4854–4895 and 3803–3821, respectively, of the LINE-1 reference sequence U93574. A nucleotide mismatch in L1-P2 that diverges from the reference sequences of both L1 recombination partners is marked with an asterisk. Given that SNPs are not a rare finding in the LINE-1 insertions [Seleme et al., 2006], this is likely to represent a new polymorphic site in the *L1-EVC* locus rather than a nucleotide error induced by the recombination process.**

he scored 75 on the Wechsler adult scale with verbal IQ of 74 and performance IQ of 80. Clinical observations of the other two siblings also showed lower verbal IQ than performance IQ. In addition case 3 has microcephaly (Table 1: head circumference [HC] = –3.0 standard deviation [SD]; Fig. 1D). Variation in the IQ over the years can be explained by the social care, special schooling, and better environment provided to the patients after they were offered a diagnosis. Noncontrast brain MRI and video-electroencephalogram in Case 1 were normal. The fact that only the three EvC affected siblings in this pedigree also have slight mental retardation but not the other three non-EvC brothers, suggests that borderline intelligence in this family is a consequence of the chromosome 4p deletion and not due to an independent recessive mutation. For this reason we investigated brain expression of the four deleted genes by RT-PCR using cDNA generated from human fetal brain RNA. The RT-PCR results showed that all four genes are expressed in fetal brain, so they are all candidates based on their expression (data not shown). Mutations in *EVC* or mutations in *EVC2* do not cause a mental defect and head circumference in EvC is normal [Baujat and Le Merrer, 2007]; however, as the EvC proteins are involved in hedgehog signaling, which is crucial for neural patterning and brain size and shape [Agarwala et al., 2001; Dellovade et al., 2006], we cannot discard that the simultaneous loss of *EVC* and *EVC2* could lead to a brain phenotype. In the same way *STK32B* and *C4orf6* are both plausible candidates for mental defects. Kinases are key proteins in cell signaling and differentiation with involvement in synaptic plasticity, learning, memory, and neurodegeneration [Angelo et al., 2006; Grundke-Iqbal et al., 1986; Mayford et al., 1996; Mazzucchelli et al., 2002] and *C4orf6* was identified as one of the genes upregulated by retinoic acid–induced neuronal differentiation in SH-SY5Y human neuroblastoma cells [Kito et al., 1997]. Thus we cannot resolve which gene or combination of genes is responsible for the intellectual deficit, but what is clear from the phenotype of the Egyptian patients is that loss of *STK32B* and *C4orf6* cause no more than, at most, mild intellectual deficit.

LINE-1 repetitive elements comprise about 17% of the human genome and are considered a force driving human genome evolution [Kazazian, 2004; Lander et al., 2001]. They are recognized mutagenic agents capable of causing human disease as a result of de novo insertions and homologous recombination events between L1 sequences [Ostertag and Kazazian, 2001]. L1 elements have been shown implicated in several disease-related chromosomal deletions [Babushok and Kazazian, 2007; Chen et al., 2005]. In the majority of them, characterization of the deletion breakpoints identified L1 sequences on one side of the rearrangement, while unrelated sequence was present on the other. Occasionally, as in the cases reported here, the deletion is flanked by two neighboring LINE-1 retrotransposons [Babushok and Kazazian, 2007; Burwinkel and Kilimann, 1998; Segal et al., 1999]. To our knowledge this is the first example of a recurrent interstitial deletion involving two LINE-1 elements removing such large amount of DNA.

Mutations were not found in 20 cases when we sequenced all *EVC* and *EVC2* exons in a panel of 65 EvC patients, and in three patients only one mutation was identified [Tompson et al., 2007]. To address whether this LINE-1 mediated deletion is a common cause of EvC we set up a MLPA dosage assay for *EVC* and *EVC2* and undertook dosage analysis in 15 out of the 20 cases in which

we had failed to find causative mutations. One of these cases was found to have a heterozygous deletion encompassing all *EVC2* exons and the first 11 exons of *EVC*, which is compatible with the deletion we report here (our unpublished results). Thus we have results compatible with this large deletion occurring in another independent case (a third pedigree) but the MLPA data indicate that it is not a common cause of EvC.

In conclusion: we present a novel 4p16.1 contiguous gene deletion affecting four novel genes that is mediated by LINE-1 to LINE-1 homologous recombination and we describe the phenotype resulting from simultaneous heterozygous and homozygous ablation of these genes in humans. We demonstrate that patients with mutations in both *EVC* and *EVC2* have the same orofacial and skeletal features as those with mutations exclusively in *EVC* or *EVC2* and that it is likely that one or more of the deleted genes plays a role in brain development.

ACKNOWLEDGMENTS

We thank the patients for their contribution in this research. M.V. is supported by a grant from the European Union (LSHM-CT-2007-03741). We acknowledge Anna Gonzalez-Neira and Guillermo Pita for their contribution in the Beadchip hybridizations and Blanca Fernández and Teresa López for their help in preparing metaphases.

REFERENCES

Agarwala S, Sanders TA, Ragsdale CW. 2001. Sonic hedgehog control of size and shape in midbrain pattern formation. Science 291:2147–2150.

Angelo M, Plattner F, Giese KP. 2006. Cyclin-dependent kinase 5 in synaptic plasticity, learning and memory. J Neurochem 99:353–370.

Babushok DV, Kazazian Jr HH. 2007. Progress in understanding the biology of the human mutagen LINE-1. Hum Mutat 28:527–539.

Baujat G, Le Merrer M. 2007. Ellis-van Creveld syndrome. Orphanet J Rare Dis 2:27.

Burwinkel B, Kilimann MW. 1998. Unequal homologous recombination between LINE-1 elements as a mutational mechanism in human genetic disease. J Mol Biol 277:513–517.

Chen JM, Stenson PD, Cooper DN, Ferec C. 2005. A systematic analysis of LINE-1 endonuclease-dependent retrotranspositional events causing human genetic disease. Hum Genet 117:411–427.

Dellovade T, Romer JT, Curran T, Rubin LL. 2006. The hedgehog pathway and neurological disorders. Annu Rev Neurosci 29:539–563.

den Dunnen JT, Antonarakis SE. 2000. Mutation nomenclature extensions and suggestions to describe complex mutations: a discussion. Hum Mutat 15:7–12.

Grundke-Iqbal I, Iqbal K, Tung YC, Quinlan M, Wisniewski HM, Binder LI. 1986. Abnormal phosphorylation of the microtubule-associated protein tau (tau) in Alzheimer cytoskeletal pathology. Proc Natl Acad Sci USA 83:4913–4917.

Hanks SK, Hunter T. 1995. Protein kinases 6. The eukaryotic protein kinase superfamily: kinase (catalytic) domain structure and classification. FASEB J 9:576–596.

Kazazian Jr HH. 2004. Mobile elements: drivers of genome evolution. Science 303:1626–1632.

Kito K, Ito T, Sakaki Y. 1997. Fluorescent differential display analysis of gene expression in differentiating neuroblastoma cells. Gene 184:73–81.

Lander ES, Linton LM, Birren B, Nusbaum C, Zody MC, Baldwin J, Devon K, Dewar K, Doyle M, FitzHugh W, Funke R, Gage D, Harris K, Heaford A, Howland J, Kann L, and many others. 2001. Initial sequencing and analysis of the human genome. Nature 409:860-921.

Mayford M, Bach ME, Huang YY, Wang L, Hawkins RD, Kandel ER. 1996. Control of memory formation through regulated expression of a CaMKII transgene. Science 274:1678–1683.

Mazzucchelli C, Vantaggiato C, Ciamei A, Fasano S, Pakhotin P, Krezel W, Welzl H, Wolfer DP, Pages G, Valverde O, Marowsky A, Porrazzo A, Orban PC, Maldonado R, Ehrengruber MU, Cestari V, Lipp HP, Chapman PF, Pouysségur J, Brambilla R. 2002. Knockout of ERK1 MAP kinase enhances synaptic plasticity in the striatum and facilitates striatal-mediated learning and memory. Neuron 34:807–820.

McKusick VA, Egeland JA, Eldridge R, Krusen DE. 1964. Dwarfism in the Amish I. the Ellis-van Creveld syndrome. Bull Johns Hopkins Hosp 115:306–336.

Mostafa MI, Temtamy SA, el-Gammal MA, Mazen IM. 2005. Unusual pattern of inheritance and orodental changes in the Ellis-van Creveld syndrome. Genet Couns 16:75–83.

Ostertag EM, Kazazian Jr HH. 2001. Biology of mammalian L1 retrotransposons. Annu Rev Genet 35:501–538.

Redon R, Ishikawa S, Fitch KR, Feuk L, Perry GH, Andrews TD, Fiegler H, Shapero MH, Carson AR, Chen W, Cho EK, Dallaire S, Freeman JL, González JR, Gratacòs M, Huang J, Kalaitzopoulos D, Komura D, MacDonald JR, Marshall CR, Mei R, Montgomery L, Nishimura K, Okamura K, Shen F, Somerville MJ, Tchinda J, Valsesia A, Woodwark C, Yang F, Zhang J, Zerjal T, Zhang J, Armengol L, Conrad DF, Estivill X, Tyler-Smith C, Carter NP, Aburatani H, Lee C, Jones KW, Scherer SW, Hurles ME. 2006. Global variation in copy number in the human genome. Nature 444:444–454.

Ruiz-Perez VL, Ide SE, Strom TM, Lorenz B, Wilson D, Woods K, King L, Francomano C, Freisinger P, Spranger S, Marino B, Dallapiccola B, Wright M, Meitinger T, Polymeropoulos MH, Goodship J. 2000. Mutations in a new gene in Ellis-van Creveld syndrome and Weyers acrodental dysostosis. Nat Genet 24:283–286.

Ruiz-Perez VL, Tompson SW, Blair HJ, Espinoza-Valdez C, Lapunzina P, Silva EO, Hamel B, Gibbs JL, Young ID, Wright MJ, Goodship JA. 2003. Mutations in two nonhomologous genes in a head-to-head configuration cause Ellis-van Creveld syndrome. Am J Hum Genet 72:728–732.

Ruiz-Perez VL, Blair HJ, Rodriguez-Andres ME, Blanco MJ, Wilson A, Liu YN, Miles C, Peters H, Goodship JA. 2007. Evc is a positive mediator of Ihh-regulated bone growth that localises at the base of chondrocyte cilia. Development 134:2903–2912.

Segal Y, Peissel B, Renieri A, de Marchi M, Ballabio A, Pei Y, Zhou J. 1999. LINE-1 elements at the sites of molecular rearrangements in Alport syndrome-diffuse leiomyomatosis. Am J Hum Genet 64:62–69.

Seleme MC, Vetter MR, Cordaux R, Bastone L, Batzer MA, Kazazian HH, Jr. 2006. Extensive individual variation in L1 retrotransposition capability contributes to human genetic diversity. Proc Natl Acad Sci USA 103:6611–6616.

Simon-Sanchez J, Scholz S, Fung HC, Matarin M, Hernandez D, Gibbs JR, Britton A, de Vrieze FW, Peckham E, Gwinn-Hardy K, Crawley A, Keen JC, Nash J, Borgaonkar D, Hardy J, Singleton A. 2007. Genome-wide SNP assay reveals structural genomic variation, extended homozygosity and cell-line induced alterations in normal individuals. Hum Mol Genet 16:1–14.

Steemers FJ, Gunderson KL. 2007. Whole genome genotyping technologies on the BeadArray platform. Biotechnol J 2:41–49.

Tompson SW, Ruiz-Perez VL, Blair HJ, Barton S, Navarro V, Robson JL, Wright MJ, Goodship JA. 2007. Sequencing EVC and EVC2 identifies mutations in two-thirds of Ellis-van Creveld syndrome patients. Hum Genet 120:663–670.

Wong KK, deLeeuw RJ, Dosanjh NS, Kimm LR, Cheng Z, Horsman DE, MacAulay C, Ng RT, Brown CJ, Eichler EE, Lam WL. 2007. A comprehensive analysis of common copy-number variations in the human genome. Am J Hum Genet 80:91–104.

Ye X, Song G, Fan M, Shi L, Jabs EW, Huang S, Guo R, Bian Z. 2006. A novel heterozygous deletion in the EVC2 gene causes Weyers acrofacial dysostosis. Hum Genet 119:199–205.

Capítulo II

Widening the Mutation Spectrum of *EVC* and *EVC2.* Ectopic Expression of Weyer Variants in NIH3T3 Fibroblasts Hedgehog Signaling

Valencia, M.; Lapunzina, P.; Lim, D.; Zannolli, R.; Bartholdi, D.; Wollnik, B.; Al-Ajlouni, O.; Eid, S.S.; Cox, H.; Buoni, S.; Hayek, J.; Martinez-Frias, M.L.; Antonio, P.A.; Temtamy, S.; Aglan, M.; Goodship, J.A.; Ruiz-Perez, V.L.

Human Mutation 30(12): 1667-1675 (2009)

En este trabajo estudiamos 36 pacientes diagnosticados con EvC, de los cuales 18 resultaron poseer mutaciones en *EVC* (7 microdeleciones, 5 mutaciones *nonsense*, 4 que afectaban a sitios de *splicing*, 2 duplicaciones de un nucleótido y 2 mutaciones *missense*) y 18 en *EVC2* (8 mutaciones *nonsense* y una *missense,* 4 microdeleciones, 2 deleciones de más de un exón, una duplicación de nucleótido y un cambio en el sitio de *splicing*).

La secuenciación de la región codificante de *EVC* y *EVC2* en uno de estos pacientes, solo detectó una mutación en heterocigosis de origen materno en el sitio donador de *splicing* del exón 8 de *EVC*. Sin embargo al amplificar por RT-PCR un segmento de ADNc que abarca los exones del 6 al 11 de *EVC* obtuvimos un patrón de fragmentos distinto en la madre y en la paciente, sugiriendo un defecto adicional en el procesamiento del ARNm en la afectada. Tras secuenciar dos productos de RT-PCR presentes sólo en la paciente comprobamos que habían incorporado un segmento nuevo de ADN situado entre los exones 7 y 8 de *EVC*. Para entender la inclusión del nuevo segmento de ADN en *EVC,* amplificamos y secuenciamos en la paciente la región de ADN genómico correspondiente y encontramos un cambio heredado de su padre en el intrón 7 que generaba un sitio donador de *splicing* fuerte. Por lo que concluimos que la mutación paterna provocaba la transformación de un pseudoexón de *EVC* en un nuevo exón, lo que fue corroborado mediante un ensayo *in vitro.*

A su vez hemos llevado a cabo el análisis de mutaciones en 3 familias con fenotipo dominante Weyers. En una de ellas encontramos una deleción en heterocigosis ya descrita previamente en otro pedigrí (EVC2:c.3793delC, (Ye et al., 2006) y en las otras dos, dos mutaciones *nonsense* nuevas en *EVC2* (c.3797T>A y c.3797T>G) también en heterocigosis. En los tres casos las mutaciones se localizan en el último exón de *EVC2* y producen una proteína truncada carente de los últimos 43 aminoácidos (p.Evc2Δ43). Encontramos interesante el hecho que la mutación c.3660delC, la cual se localiza sólo 133 nucleótidos aguas arriba del cambio que provoca Weyers y da lugar a una proteína a la que le faltan los últimos 87 aminoácidos (p.Evc2Δ87), sea heredada de forma recesiva puesto que ambas mutaciones se sitúan en el último exón de *EVC2* y escaparían al mecanismo de NMD. Esto fue confirmado a través de la cuantificación de los niveles de ARNm de *EVC2* por qRT-PCR en fibroblastos de individuos portadores de las mutaciones c.3660delC y la c.3793delC (Weyers) en relación a fibroblastos control y observamos en todos los casos niveles semejantes de mensajero. La co-existencia de la forma salvaje de

EVC2 y de las mutantes c.3660delC y c.3793delC, también fue demostrada por secuenciación directa de ADNc. Por tanto ninguno de los dos transcritos con mutaciones en el último exón de *EVC2* es degradado.

Dado que Evc es un mediador positivo de la señalización Hh, investigamos si una mutación Weyers tendría un efecto sobre esta vía. Postulamos que si este efecto era específico debería distinguirse del de la mutación recesiva c.3660delC. Para ello generamos variantes murinas de *EVC2:* salvaje (p.Evc2wt) y las equivalentes a las mutaciones c.3660delC (p.Evc2Δ87) y Weyers (p.Evc2Δ43) y las co-transfectamos en la línea celular de fibroblastos de ratón (NIH3T3) junto con un plásmido que contiene el gen de la luciferasa (*Photinus pyralis*) bajo el control de un promotor inducible por la vía de Hh y otro plásmido que expresa luciferasa (*Renilla reniformis*) de manera constitutiva como control de la eficiencia de la transfección. A continuación estimulamos las células con un agonista químico de la vía de Hh (SAG) y medimos la actividad de luciferasa para conocer el grado de activación de la ruta. Este ensayo mostró un incremento en la actividad de luciferasa en las células transfectadas con Evc2wt y Evc2Δ87 tras la estimulación con SAG que no ocurría en las células que expresaban la variante Weyers, lo cual es consistente con el carácter dominante de esta mutación e indica que la patología Weyers también se debe a una disminución en la respuesta a las señales Hh.

La doctoranda, como autora de este trabajo, llevó a cabo los experimentos de RT-PCR que identificaron la mutación del intrón 7 de *EVC* así como el ensayo *in vitro* para demostrar la patogenicidad de la misma; los ensayos de qRT-PCR y análisis mediante secuenciación del ADNc obtenido del cultivo de los fibroblastos primarios de los pacientes. También puso a punto el sistema de co-transfección y medición de la actividad de la luciferasa en cultivo y los experimentos correspondientes realizados con el mismo. Realizó los análisis estadísticos y participó en la composición de figuras y en la escritura de los materiales y métodos así como en la discusión del trabajo.

RESEARCH ARTICLE

Human Mutation

OFFICIAL JOURNAL
HGVS
HUMAN GENOME VARIATION SOCIETY
www.hgvs.org

Widening the Mutation Spectrum of *EVC* and *EVC2*: Ectopic Expression of Weyer Variants in NIH 3T3 Fibroblasts Disrupts Hedgehog Signaling

Maria Valencia,[1] Pablo Lapunzina,[2] Derek Lim,[3] Raffaella Zannolli,[4] Deborah Bartholdi,[5] Bernd Wollnik,[6] Othman Al-Ajlouni,[7] Suhair S. Eid,[7] Helen Cox,[3] Sabrina Buoni,[4] Joseph Hayek,[4] Maria L. Martinez-Frias,[8] Perez-Aytes Antonio,[9] Samia Temtamy,[10] Mona Aglan,[10] Judith A. Goodship,[11] and Victor L. Ruiz-Perez[1]*

[1]Instituto de Investigaciones Biomédicas, Consejo Superior de Investigaciones Científicas-Universidad Autónoma de Madrid and CIBER de Enfermedades Raras (CIBERER), Madrid, Spain; [2]Departamento de Genética, Hospital Universitario La Paz, Universidad Autónoma de Madrid and CIBER de Enfermedades Raras (CIBERER), Madrid, Spain; [3]West Midlands Regional Genetics Service, Birmingham Women's Hospital, Edgbaston, Birmingham, United Kingdom; [4]Department of Pediatrics, Child Neurology and Psychiatry, Azienda Ospedaliera Universitaria Senese, Policlinico Le Scotte, Siena, Italy; [5]Institute of Medical Genetics, University of Zürich, Schwerzenbach, Switzerland; [6]Center for Molecular Medicine Cologne (CMMC), Institute of Human Genetics and Cologne Excellence Cluster on Cellular Stress Responses in Aging-Associated Diseases (CECAD), University of Cologne, Cologne, Germany; [7]King Hussein Medical Center, Royal Medical Services, Amman, Jordan; [8]Estudio Colaborativo Español de Malformaciones Congénitas (ECEMC) del Centro de Investigación sobre Anomalías Congénitas (CIAC) and CIBER de Enfermedades Raras (CIBERER), Instituto de Salud Carlos III, Ministerio de Sanidad y Consumo, Madrid, Spain; [9]Hospital Universitario La Fé, Valencia, Spain; [10]Human Genetics and Genome Research Division, National Research Centre, Cairo, Egypt; [11]Institute of Human Genetics, Newcastle University, Newcastle upon Tyne, United Kingdom

Communicated by Iain McIntosh

Received 12 April 2009; accepted revised manuscript 12 August 2009.
Published online in Wiley InterScience (www.interscience.wiley.com). DOI 10.1002/humu.21117

ABSTRACT: Autosomal recessive Ellis-van Creveld syndrome and autosomal dominant Weyer acrodental dysostosis are allelic conditions caused by mutations in *EVC* or *EVC2*. We performed a mutation screening study in 36 EvC cases and 3 cases of Weyer acrodental dysostosis, and identified pathogenic changes either in *EVC* or in *EVC2* in all cases. We detected 40 independent *EVC/EVC2* mutations of which 29 were novel changes in Ellis-van Creveld cases and 2 were novel mutations identified in Weyer pedigrees. Of interest one EvC patient had a T>G nucleotide substitution in intron 7 of *EVC* (c.940−150T>G), which creates a new donor splice site and results in the inclusion of a new exon. The T>G substitution is at nucleotide +5 of the novel 5′ splice site. The three Weyer mutations occurred in the final exon of *EVC2* (exon 22), suggesting that specific residues encoded by this exon are a key part of the protein. Using murine versions of *EVC2* exon 22 mutations we demonstrate that the expression of a Weyer variant, but not the expression of a truncated protein that mimics an Ellis-van Creveld syndrome mutation, impairs Hedgehog signal transduction in NIH 3T3 cells in keeping with its dominant effect.
Hum Mutat 30:1–9, 2009. © 2009 Wiley-Liss, Inc.

KEY WORDS: Ellis-van Creveld syndrome; Weyer acrodental dysostosis; EVC; EVC2; Hedgehog signaling

Additional Supporting Information may be found in the online version of this article.

*Correspondence to: Victor L. Ruiz-Perez, Instituto de Investigaciones Biomédicas, Consejo Superior de Investigaciones Científicas-Universidad Autónoma de Madrid, Arturo Duperier 4, Madrid 28029, Spain. E-mail: vlruiz@iib.uam.es

Introduction

EVC (MIM# 604831) and *EVC2* (MIM# 607261) are adjacent genes that lie in divergent orientation on the short arm of human chromosome 4. Mutations in *EVC* or *EVC2* are associated with Ellis-van Creveld syndrome (EvC; MIM# 225500) and Weyer acrodental dysostosis (Weyer; MIM# 193530), two conditions that differ in the severity of the phenotype and the pattern of inheritance [Ruiz-Perez et al., 2000, 2003; Ye et al., 2006]. EvC is a recessive disorder whereas Weyer acrodental dysostosis is a dominant trait. The skeletal features of EvC are disproportionate short stature (reported adult height range 106–160 cm) with acromesomelic shortening of limbs, short ribs, and postaxial polydactyly of hands and feet. Tooth abnormalities, multiple oral frenulae, and hypoplastic nails are consistent findings in EvC and congenital heart defects, typically an atrial or atrioventricular septal defect, are another common feature that is present in approximately two-thirds of the patients [da Silva et al., 1980; McKusick et al., 1964]. Weyer patients also have postaxial polydactyly of hands and feet, dental abnormalities, and nail dystrophy. Oral frenulae seem less common than in EvC, and the height of affected individuals is typically in the lower half of the normal range (reported adult range 140–171 cm) [Curry and Hall, 1979; Roubicek and Spranger, 1984; Ye et al., 2006]. Congenital heart disease has not been reported in Weyer acrodental dysostosis. To date, only two mutations, S307P in EVC and c.3793delC in *EVC2*, had been found in patients with Weyer syndrome [Ruiz-Perez et al., 2000; Ye et al., 2006].

The vast majority of EvC patients have mutations either in *EVC* or *EVC2* and the phenotypes associated with mutations in these genes are clinically indistinguishable [Tompson et al., 2007]. Recently, two families have been identified as having LINE-1 mediated chromosome 4 interstitial deletions removing *EVC* and *EVC2* along with the adjacent transcripts *C4orf6* and *STK32B* [Temtamy et al., 2008].

© 2009 WILEY-LISS, INC.

Three consanguineous siblings homozygous for this deletion were diagnosed with classical Ellis-van Creveld syndrome and borderline intelligence indicating that the simultaneous loss of *EVC* and *EVC2* does not worsen the skeletal, orofacial, or cardiac features of EvC or, with the possible exception of the learning difficulties, lead to additional phenotypes. As all subjects heterozygous for the *EVC-STK32B* rearrangement were normal, it became apparent that *EVC* and *EVC2* hemizygosity causes no clinical phenotype excluding *EVC/EVC2* digenic inheritance in EvC. A previous mutation screen in EvC patients in which all coding exons of *EVC* and *EVC2* were sequenced detected mutations in only two-thirds of cases, raising the possibility of further genetic heterogeneity in EvC [Tompson et al., 2007]. Here we have addressed this question by carrying out a new mutation study in an independent cohort of patients enriched for consanguineous samples and have found no support for this hypothesis.

The analysis of an Ellis-van Creveld syndrome mouse model in which the first exon of *Evc* was replaced by the *LacZ* cassette demonstrated that Evc is required for the transduction of the Hedgehog (Hh) signal [Ruiz-Perez et al., 2007]. Because nearly all the mutations identified in EvC patients are predicted to be loss of function mutations and cause no phenotype in the heterozygous state, we postulated that mutations associated with Weyer acrodental dysostosis might be dominant negatives and could disturb Hedgehog signaling. We have now confirmed this in in vitro studies.

Materials and Methods

Genomic Sequencing

We used genomic DNA isolated from peripheral blood to amplify all coding exons of *EVC* and *EVC2* and the exon–intron boundaries by standard polymerase chain reaction (PCR). Before sequencing, the PCR products were treated with shrimp alkaline phosphatase and exonuclease I (ExoSap-it, GE Healthcare, Piscataway, NJ) according to the manufacturer's instructions. Sequencing reactions were carried out using a dye terminator cycle sequencing kit (Applied Biosystems, Bedford, MA) and run on a ABI 3730 sequencer. The resulting sequencing chromatograms were aligned and compared with the reference nucleotide sequence of *EVC* and *EVC2* transcripts (NM_153717.2 and NM_147127.3) and with genomic sequence obtained from the GenBank reference assembly NC_000004.10 using Sequencher (Gene Codes Corp., Ann Arbor, MI). For numbering the mutations we considered the A of the ATG translation initiation codon of *EVC* and *EVC2* as nucleotide +1. The mutations are described following the recommended nomenclature guidelines [den Dunnen and Antonarakis, 2000; den Dunnen and Paalman, 2003], and were checked using the Mutalizer program (http://www.LOVD.nl/mutalyzer) [Wildeman et al., 2008].

cDNA Analysis

We cultured primary skin fibroblasts in F-10 Nutrient Mixture (Ham) supplemented with 23% of fetal calf serum (FCS); 2 mM Glutamine, and 25 mM of HEPES, and extracted RNA with Trizol (Invitrogen, Carlsbad, CA, USA) as described by the manufacturer. Fibroblast first-strand cDNA was synthesized from 5 μg of total RNA with superscript II (Invitrogen) and 250 ng of random primers. For patient 07 a cDNA fragment extending from *EVC* exon 6 to 11 was amplified with Pfu DNA polymerase (Invitrogen) and the resulting PCR products were gel purified and cloned in pCR-Blunt (Invitrogen) before being sequenced. The main RT-PCR fragment from the carrier of case 07 was extracted from the agarose and analyzed by direct sequencing. cDNA analysis of *EVC2* in a carrier of the c.3660delC mutation and in a Weyer patient heterozygous for the c.3793delC mutation was performed by RT-PCR on RNA extracted from primary skin fibroblasts using a forward PCR primer from *EVC2* exon 12 and a reverse primer from the 3′ untranslated region of *EVC2* exon 22. The RT-PCR products from both samples were sequenced directly after agarose purification. Relative quantification of *EVC2* mRNA in fibroblast cultures was performed by quantitative RT-PCR (qRT-PCR) using TaqMan real-time PCR gene expressions assays Hs00377633_m1 for *EVC2* and Hs99999909_m1 for the housekeeping gene *HPRT-1* (Applied Biosystems). For each individual we obtained qRT-PCR data from three independent experiments using each time a different RNA sample isolated from a separate culture flask. All RNA samples were analyzed in triplicate.

In Vitro Splicing Assay

To demonstrate the effect of the c.940−150T>G *EVC* mutation on splicing we used Pfu DNA polymerase to amplify a 1,316-bp genomic fragment corresponding to nucleotides 41320 to 42635 of the NG_008843.1 reference sequence in a control subject and in patient 07. The products from the two PCR reactions were cloned into the multiple cloning site of the exon trapping vector pSPL3 using *XhoI* and *BamHI* (Fig. 1E; Life Technologies, Baltimore, MD, USA) and two pSPL3/*EVC* minigenes, one of them carrying the c.940−150T>G mutation and another one a wild-type sequence were selected by sequencing. Normal and mutant minigenes were transfected in COS-7 cells using Lipofectamine 2000 (Invitrogen) and 24 hr later we isolated RNA with Trizol. cDNA was synthesized from each transfection with superscript II and random primers and used to carry out 35 cycles of PCR reaction using vector exonic primers. The resulting RT-PCR products from the transfections with the normal and mutant minigenes were purified from the gel and directly sequenced.

Generation of Evc2 Expression Constructs

We generated wild-type and mutant Evc2 expression constructs by PCR. To do this the image clone 4237472 (BC037473) was used as a template to amplify the *Evc2* coding region with the same forward primer and specific reverse primers for each construction harboring a wild-type sequence or the desired mutations. Pfx50 DNA polymerase (Invitrogen) was used to minimize amplification errors. The forward primer was 5′-GCGGCCGCGGGTCTGTAGCCACCAGATG-3′ and the reverse primers designed to PCR the entire *Evc2* coding region and to create the *Evc2*: c.3396delC (Evc2: p.I1133YfsX2; Evc2Δ87) and *Evc2*: 3533T>A (Evc2: p.L1178X; Evc2Δ43) truncation mutations were respectively 5′-CTCGAGCTTCCCCCTGGGT-CAGTC-3′, 5′-CTCGAGTTCTTCAATATCGCTCCTTCTTC-3′, and 5′-CTCGAGTTTTATATGTCCATAGCGTCTGC-3′. Numbering of the mouse *Evc2* mutations starts from the translation initiation codon of the reference sequence NM_145920.2. *NotI* and *XhoI* restriction sites were added at the end of the primers to facilitate the cloning of the three amplified fragments into a pCAGGS-derivate eukaryotic expression vector containing the CMV-EI enhancer and the chicken β-actin promoter and intron 1 [del Mar Lorente et al., 2000]. The three expression constructs were sequenced to confirm the presence of the mutations and to ensure that there were no other nucleotide changes in the cDNA.

Luciferase Assay

Luciferase reporter assays were conducted as described earlier [Ocbina and Anderson, 2008]. We seeded NIH 3T3 murine

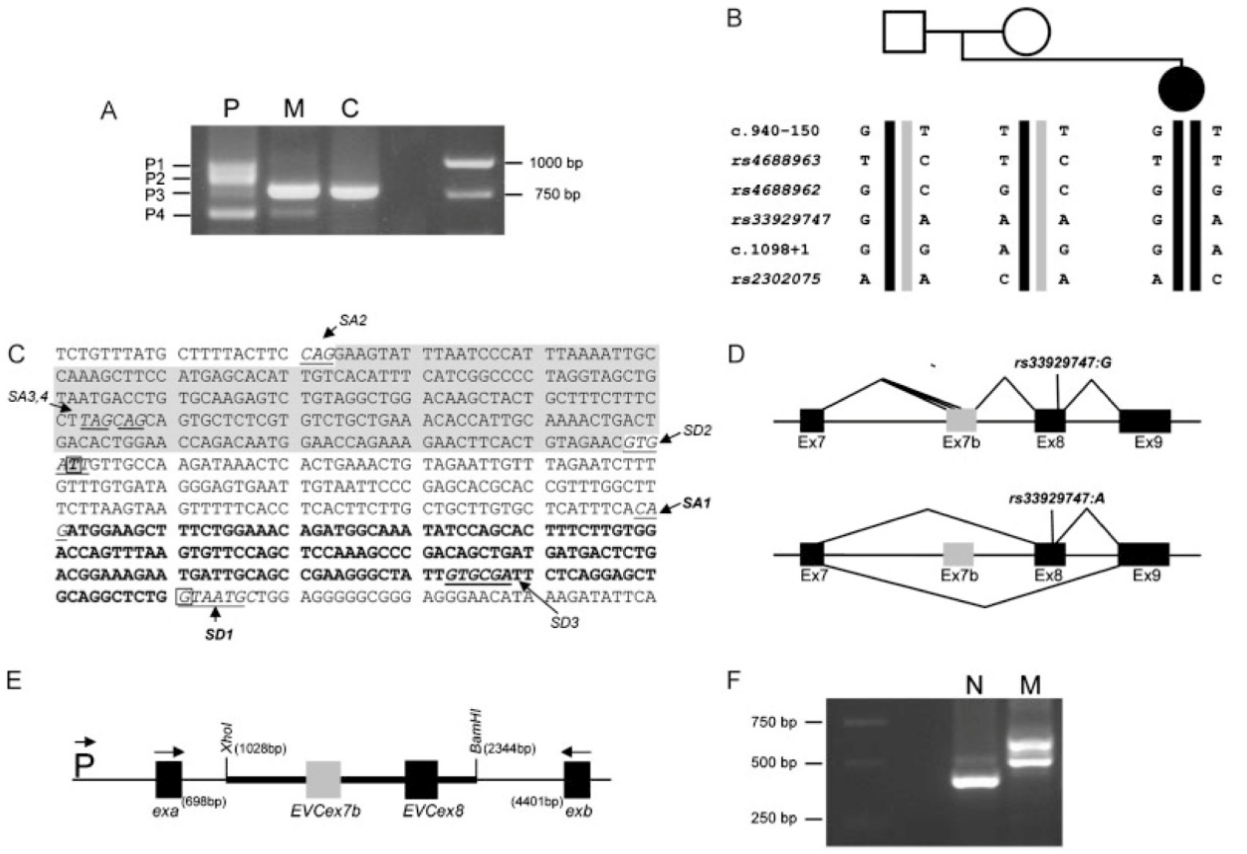

Figure 1. Characterization of mutations in patient 07. **A:** RT-PCR amplification from primary fibroblast cDNA of an *EVC* fragment spanning from exon 6 to 11 showing a different amplification pattern in patient 07 (P) and her mother (M), who is a carrier of the *EVC* exon 8 donor splice site mutation c.1098+1G>A. The same RT-PCR experiment performed in normal fetal brain cDNA (Clontech) is shown in lane C. P1–4 designate each of the RT-PCR products obtained in the patient. **B:** SNP haplotype construction of pedigree 07. *rs4688963*, *rs4688962*, and *rs33929747* are polymorphic sites located in *EVC* exon 8 and *rs2302075* is a nucleotide polymorphism in exon 10. The paternal, c.940−150T>G, and maternal, c.1098+1G>A, mutations are also indicated. The disease haplotypes are shown in black. **C:** Wild-type genomic sequence encompassing *EVC* exon 8 (bold letters) and exon 7b (gray box). Acceptor (*SA*) and donor (*SD*) splice sites are in italics and underlined, the nucleotide position of the maternal G>A mutation is squared and the position of the paternal T>G nucleotide substitution is boxed and gray. *SA1* and *SD1* are the natural splice sites of exon 8. The maternal mutation causes skipping of exon 8 resulting in P4 and activates the cryptic 5′ splice site *SD3* (P3). The paternal mutation creates a new donor splice site (*SD2*), which, in combination with *SA2*, leads to P1 and in conjunction with *SA3* or *SA4* gives rise to P2. **D:** Exon structure of the paternal and maternal *EVC* transcripts from patient 07 between exons 7 to 9. The top part corresponds to the paternal transcripts P1 and P2 and the picture underneath represents the maternally transcribed mRNAs P3 and P4. The haplotype of the *rs33929747* SNP is indicated. **E:** Representation of the pSPL3/*EVC* minigene constructs used to study the c.940−150T>G mutation. The two pSPL3 exons, exa and exb, are separated by an intron containing a multiple cloning site in which genomic *EVC* fragments running from −632 exon 8 to +525 exon 8 carrying wild-type or c.940−150T>G sequence were inserted using *XhoI* and *BamHI*. RT-PCR primers are indicated by arrows. P symbolizes the promoter and the arrow on the top the direction of transcription. **F:** RT-PCR results from COS-7 cells transfected with normal (N) or mutant (M) minigenes using primers from exons a and b. There is no normally spliced product in the lane corresponding to mutant sequence, instead two larger fragments due to inclusion of different 3′ alternative splice forms of exon 7b were amplified.

fibroblasts in 24-well tissue culture dishes at a initial density of 1.0×10^5 cells/well in DMEM supplemented with 10% fetal calf serum, 100 units/ml penicillin, 100 µg/ml streptomycin, 0.25 µg/ml amphotericin B, 2 mM L-glutamine, and nonessential amino acids 1× (Invitrogen). After 18 hr the cells were transfected with 1 µg per well of a plasmid DNA mix using Fugene 6 (Roche, Indianapolis, IN). The proportion of the plasmids included in the DNA transfection mix was: 8×3′ Gli-BS-Luc luciferase reporter 40% [Sasaki et al., 1997], *Renilla* luciferase pRL-TK (Promega, Madison, WI) 10% and the plasmid of interest expressing wild-type or mutant *Evc2* or the empty vector 50%. Twelve hours after transfection the growth medium was changed to low serum medium (0.5% FCS) supplemented with 100 nM of SAG (Calbiochem, LaJolla, CA) or its vehicle (DMSO). The cells were maintained for a further 48 hr before they were lysed and processed for firefly and *Renilla* luciferase readings using the Dual-Luciferase Reporter Assay System (Promega) on a Glomax 96 Microplate Luminometer 8 (Promega) following manufacturer's instructions. The reporter assays were done in triplicate wells in three independent experiments, and the results were normalized for transfection efficiency using *Renilla* luciferase values.

Results

Patients and Mutation Analysis

We have studied 36 independent EvC patients, 23 of whom were known to be from consanguineous families, and 3 patients with Weyer acrodental dysostosis. Mutation analysis was performed by

direct sequencing of all the 21 coding exons of *EVC* and the 22 coding exons of *EVC2* including the exon–intron junctions. Ethical approval and appropriate informed consent was obtained from all human subjects or their parents. When possible the mutations were confirmed in parental DNA.

Mutations in EvC Patients

Mutations were identified in all 36 EvC cases (Table 1, Table 2, and Fig. 2A). Eighteen patients had mutations in *EVC* and 18 patients had mutations in *EVC2*, with none of the samples having mutations in both genes. In total, in this cohort we isolated 20 independent *EVC* mutations (15 novel) and 17 independent *EVC2* mutations (14 novel). Mutations in *EVC* comprised seven microdeletions, five nonsense mutations, four splice site mutations, two mono-nucleotide duplications, and two missense mutations. The *EVC2* mutations comprised eight nonsense mutations, four microdeletions, two deletions affecting more than one exon, one mono-nucleotide duplication, one missense mutation, and one splice site change. The following previously reported *EVC* mutations were observed: p.K302del, c.1098+1G>A, c.873dupT, p.R340X, and p.L623P [Ruiz-Perez et al., 2000; Temtamy et al., 2008; Tompson et al., 2007; Ulucan et al., 2008]. p.R340X and p.L620_L626del occurred twice in this study. As p.L623P was found in a Turkish family we sequenced 100 healthy Turkish control individuals for this change and did not detect it. Of the *EVC2* mutations, p.Q249X, p.I283R, and c.3660delC have been reported previously [Ruiz-Perez et al., 2003; Tompson et al., 2007]. c.3660delC was first identified in a Spanish gypsy pedigree, and here it was found in homozygosity or in combination with a second *EVC2* mutation in 6 out of the 12 Spanish cases that are part of this study but not in patients of other nationalities. The pedigrees carrying the c.3660delC mutation were from different parts of the country and only case 16 was of gypsy origin. We observed variability in the severity of the phenotype and in the presence of heart defects among EvC patients that were independent of the mutation class, and as described earlier, there were no clinical features that distinguished patients with mutations in *EVC* from those with mutations in *EVC2* [Tompson et al., 2007].

Characterization of a Deep Intronic Mutation in *EVC* in a Patient with Ellis-van Creveld Syndrome

Genomic sequencing of *EVC* and *EVC2* in case 07 revealed only a heterozygous donor splice site mutation in intron 8 of *EVC*, c.1098+1G>A, inherited from the unaffected mother. To check the effect of this mutation in the *EVC* mRNA and to look for the paternal change we generated fibroblast cDNA from the patient and her mother and amplified the *EVC* region comprised between exons 6 and 11. We obtained a main product of normal size in the mother but four different PCR fragments in the patient, hereafter referred to as P1–P4, revealing the presence of an additional change in the patient cDNA (Fig. 1A). SNP haplotype construction of the pedigree was used to differentiate the allelic origin of the cDNA fragments amplified after they were sequenced (Fig. 1B). Direct sequencing of the main amplicon from the maternal sample demonstrated that it was derived from the normal allele. Subsequently, the four RT-PCR fragments from the proband were cloned and sequenced. PCR products 1 and 2 were larger than the size expected for a normal exon structure and sequencing revealed that they were aberrant *EVC* spliced variants that had incorporated an additional DNA segment from *EVC* intron 7 between exons 7 and 8. Product 2 was a mixture of two transcripts carrying intron 7 insertions 5′ nested to the sequence included in P1. P3 was a spliced variant missing the last 28 nucleotides of exon 8 due to the usage of a cryptic donor splice site (*SD3*, Fig. 1C) and P4 resulted from exon 8 skipping. PCR products 1 and 2 carried the paternal alleles G and A in *rs33929747* and in *rs2302075*, respectively, so they were of paternal origin, whereas P3 and P4 contained the maternal alleles A and C in the positions corresponding to the same SNPs (Fig. 1B and D). *rs33929747* is an

Table 1. Mutations Identified in *EVC*

				EvC patients			
Case	Origin	Consanguinity	Mutation status	Exon/intron	Nucleotide change	Protein effect	Novel mutation or previously reported
29	Turkey	C	Homozygous	Exon1	c.2T>A	p.M1?	Novel
30	Turkey	C	Homozygous	Intron1	c.175−2A>G		Novel
08	Spain	NC	Compound	Exon2	c.203delA	p.N68IfsX48	Novel
			Heterozygous	Exon9	c.1114_1122del	p.T372_G374del	Novel
21	Mexico	NC	Compound	Exon3	c.363C>A	p.Y121X	Novel
			Heterozygous	Exon12	c.1678G>T	p.E560X	Novel
12	Egypt	C	Homozygous	Exon6	c.708dupT	p.I237YfsX5	Novel
18	Spain	NC	Compound	Exon7	c.873dupT	p.E292X	Tompson et al. (2007)
			Heterozygous	Exon8	c.1060G>T	p.E354X	Novel
05	Spain	C	Homozygous	Exon7	c.904_906del	p.K302del	Ruiz-Perez et al. (2000)
07	Spain	NC	Compound	Intron7	c.940−150T>G		Novel
			Heterozygous	Intron8	c.1098+1G>A		Temtamy et al. (2008)
38	Jordan	C	Homozygous	Exon8	c.1018C>T	p.R340X	Ruiz-Perez et al. (2000)
39	Jordan	C	Homozygous	Exon8	c.1018C>T	p.R340X	Same as case 38
03	Spain	NC	Homozygous	Exon9	c.1217delT	p.L406RfsX94	Novel
22	Qatar	C	Homozygous	Exon9	c.1255G>T	p.E419X	Novel
13	Egypt	C	Homozygous	Exon9	c.1269_1278del	p.Q424RfsX73	Novel
37	Jordan	C	Homozygous	Intron11	c.1563+1G>C		Novel
31	Israel	C	Homozygous	Exon13	c.1858_1878del	p.L620_L626del	Novel
36	Netherlands	NC	Homozygous	Exon13	c.1858_1878del	p.L620_L626del	Same as case 31
34	Turkey	C	Homozygous	Exon13	c.1868T>C	p.L623P	Ulucan et al. (2008)
20	Egypt	C	Homozygous	Exon16	[c.2344_2345del; c.2357_2370del]	p.T782QfsX26	Novel

C, consanguineous; NC, nonconsanguineous.

Table 2. Mutations Identified in *EVC2*

Case	Origin	Consanguinity	Mutation status	Exon/intron	Nucleotide change	Protein effect	Novel mutation or previously reported
				EvC patients			
24	Turkey	C	Homozygous	Exon3_6	Ex3_6del		Novel
15	Brazil	NC	Homozygous	Exon6	c.745C>T	p.Q249X	Tompson et al. (2007)
02	UK[a]	C	Homozygous	Exon7	c.848T>G	p.I283R	Ruiz-Perez et al. (2003)
19	Egypt	C	Homozygous	Exon12	c.1828C>T	p.Q610X	Novel
23	Brazil	C	Homozygous	Exon13_16	Ex13_16del		Novel
25	Spain	NC	Compound	Exon13	c.1918delA	p.M640CfsX21	Novel
			Heterozygous	Exon22	c.3660delC	p.S1220RfsX3	Ruiz-Perez et al. (2003)
09	Spain	NC	Homozygous	Exon13	c.2029C>T	p.R677X	Novel
32	France[b]	C	Homozygous	Exon14	c.2365G>T	p.E789X	Novel
10	Egypt	C	Homozygous	Exon14	c.2476C>T	p.R826X	Novel
17	Spain	NC	Compound	Exon15	c.2652G>A	p.W884X	Novel
			Heterozygous	Exon22	c.3660delC	p.S1220RfsX3	Same as case 25
11	Egypt	C	Homozygous	Exon16	c.2710C>T	p.Q904X	Novel
04	Spain	NC	Compound	Exon17	c.2885delG	p.G962AfsX17	Novel
			Heterozygous	Exon22	c.3660delC	p.S1220RfsX3	Same as case 25
01	USA	NC	Compound	Exon19	c.3283G>T	p.E1095X	Novel
			Heterozygous	Exon20	c.3405_3411del	p.G1136RfsX6	Novel
28	Turkey	C	Homozygous	Intron19	c.3360+1G>A		Novel
06	Spain	NC	Homozygous	Exon22	c.3660delC	p.S1220RfsX3	Same as case 25
14	Spain	C	Homozygous	Exon22	c.3660delC	p.S1220RfsX3	Same as case 25
16	Spain	C	Homozygous	Exon22	c.3660delC	p.S1220RfsX3	Same as case 25
35	Jordan	C	Homozygous	Exon22	c.3731dupT	p.S1245VfsX20	Novel
				Weyer patients			
33	UK	NC	Heterozygous	Exon22	c.3793delC	p.L1265YX2	Ye et al. (2006)
26	Switzerland	NC	Heterozygous	Exon22	c.3797T>A	p.L1266X	Novel
27	Italy	NC	Heterozygous	Exon22	c.3797T>G	p.L1266X	Novel

[a]Family of Pakistani origin, living in UK.
[b]Family of Algerian origin, living in France.
C, consanguineous; NC, nonconsanguineous.

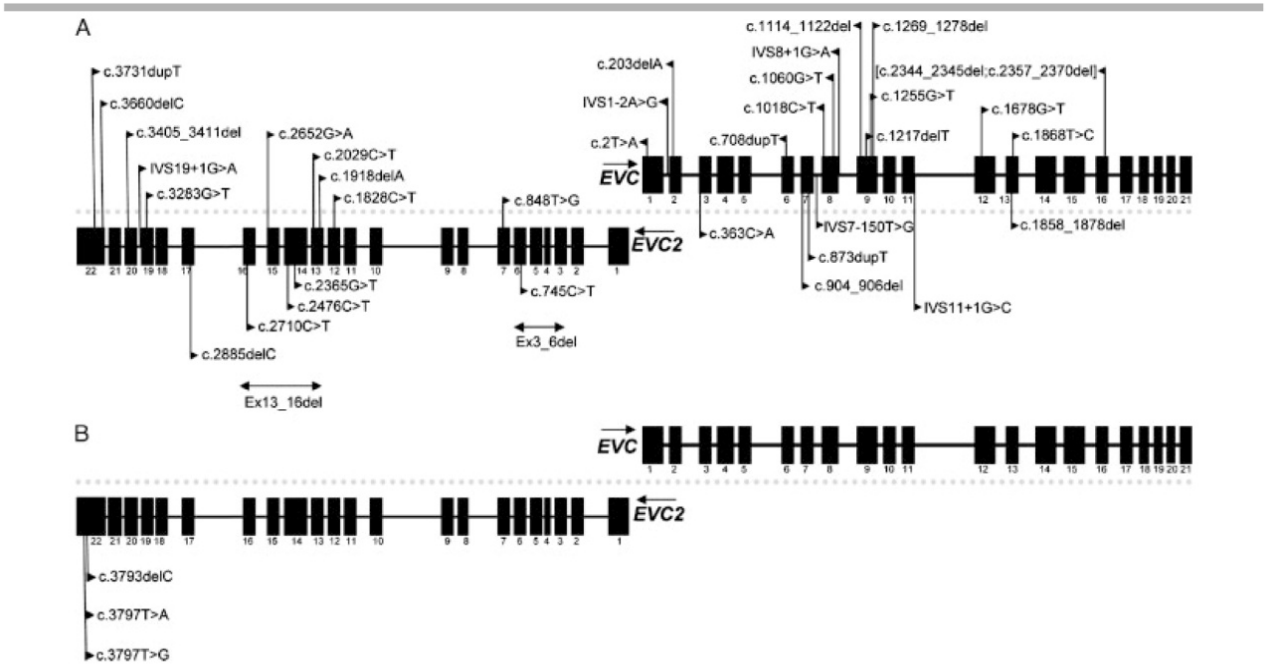

Figure 2. Schematic representation of *EVC* and *EVC2* illustrating the location of the mutations identified in this study. The changes identified in Ellis-van Creveld patients are shown in **A** and the changes detected in Weyer cases are indicated in **B**. 4p telomere is on the left and centromere on the right. Exons are represented by black boxes and their position relative to the dashed line indicates the different transcription orientation, *EVC* is expressed from the forward strand and *EVC2* is transcribed in the reverse orientation (NC_000004.10 reference assembly).

exon 8 polymorphism, so it is not present in P4. All PCR products from the patient excepting P4 lead to early termination codons. To find out the change responsible for the inclusion of the new exon (exon 7b) in the paternal *EVC* mRNA we aligned the intronic sequences from P1 and both P2 fragments against normal genomic DNA. By doing this we observed that the three DNA insertions were preceded by consensus acceptor splice sites (*SA2*, *SA3*, and *SA4*, Fig. 1C), whereas none of the splice site predictor programs we used detected a donor splice site at the end of exon 7b in the normal DNA. Amplification followed by sequencing of the genomic region corresponding to exon 7b, and adjacent sequences in the three members of pedigree 07 showed a heterozygous T>G transversion 5 nucleotides downstream of the 3′ end of exon 7b in the father and the patient but not in the mother. Direct sequencing did not detect this change in 186 ethnically matching control chromosomes. The T>G substitution created a strong donor splice site (SD2, Fig. 1C) that was recognized by the NNSPLICE 0.9 splice site predictor program (score 0.95) (www.fruitfly.org/seq_tools/splice.html) [Reese et al., 1997] and has a high Shapiro score of 83.2 [Shapiro and Senapathy, 1987]. This mutation corresponds to c.940−150T>G following the recommended nomenclature guidelines.

We corroborated the effect of the paternal mutation in an in vitro splicing assay. For this we amplified the genomic region from −632 exon 8 to +525 exon 8, which includes the additional exon 7b in a control individual and in patient 07 and subcloned the amplification fragments into the exon trapping vector pSPL3 to generate pSPL3/*EVC* hybrid minigenes (Fig. 1E). Minigenes carrying the c.940−150T>G paternal mutation or wild-type sequence were transfected into COS-7, and we analyzed splicing between the pSPL3 exons a and b by RT-PCR. This showed a single PCR product of the expected size in the transfections with the control minigene and two larger DNA fragments in the transfections with the c.940−150T>G construct (Fig. 1F). Direct sequencing of the product obtained in the control transfections confirmed that it corresponded to inclusion of exon 8 between the two vector exons, whereas direct sequencing of the products generated in the transfections with the mutant minigene proved that, as in the patient fibroblasts, they resulted from the inclusion of different 3′ alternative spliced forms of exon 7b between pSPL3 exon a and *EVC* exon 8.

Mutations in Weyer Acrodental Dysostosis Patients

Weyer acrodental dysostosis has a much lower prevalence than EvC, and consequently, we have studied only three families with this disorder (Fig. 3). The phenotype of patients from pedigree 27 (Fig. 3C) has been described in detail [Zannolli et al., 2008], and the clinical features of the two new families are in Table 3. Sequencing of *EVC* and *EVC2* in the proband of each family identified three different *EVC2* heterozygous mutations that were tightly clustered in the last exon of this gene indicating a Weyer mutation hotspot at the 3′ end of *EVC2* (Table 2, Figs. 2B and 3). In case 33, we found the same heterozygous frameshift mutation, c.3793delC, as that found earlier in a Chinese pedigree with Weyer acrodental dysostosis [Ye et al., 2006]. This mutation changes Leucine 1265 to Tyrosine and introduces a stop codon in the next triplet. The structure of pedigree 33 shows the first affected member in the second generation (Fig. 3); this, and the different ethnic background of the two families with the same mutation (case 33 is a Caucasian UK family), suggest that the c.3793delC nucleotide deletion happened independently in the two pedigrees rather than the two families sharing a common ancestor. Pedigrees 26 and 27 were characterized with two different heterozygous nonsense mutations of the same nucleotide position, c.3797T>A and c.3797T>G, respectively, which truncate the protein at L1266. We verified the presence of the c.3797T>G mutation in the affected mother and brother of proband 27, but neither of the parents of proband 26 had the c.3797T>A change indicating that this is a de novo mutation (microsatellite analysis of these samples was consistent with the pedigree). The mother of case 26 has no phenotypic abnormalities, and the father has three missing teeth and transposition of the great arteries but does not have short stature or polydactyly. Although his phenotype is not typically Weyer, the possibility of the father being a mosaic has not been excluded.

Weyer Acrodental Dysostosis Mutations Impair Hedgehog Signaling

Given that Evc is an intracellular mediator of Hedgehog signaling [Ruiz-Perez et al., 2007], we investigated the effect of a Weyer mutation and a recessive EvC mutation on Hedgehog signal

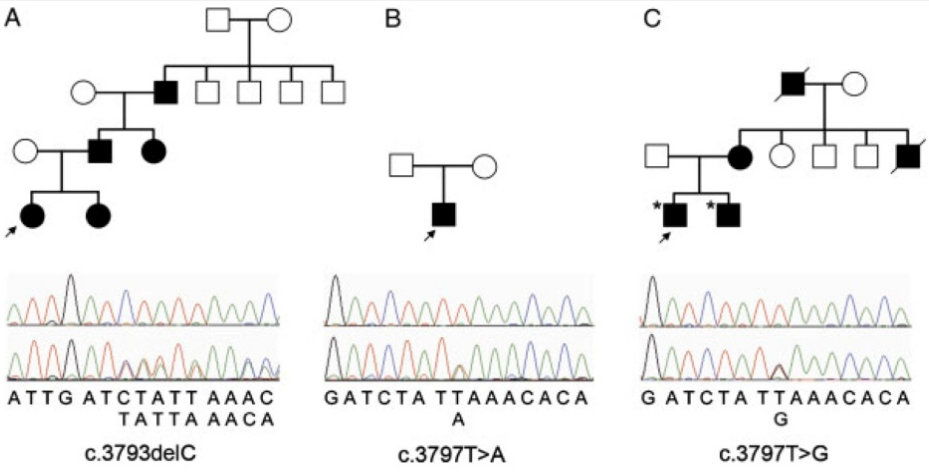

Figure 3. Pedigree structure and mutations of Weyer cases. **A**, **B**, and **C** represent cases 33, 26, and 27, respectively (Table 2). Mutant sequence from each case is shown below wild-type sequence. The asterisk indicates that patients III-1 and III-2 (panel C) have mental retardation in addition to Weyer syndrome [Zannolli et al., 2008].

Table 3. Clinical Features Observed in Weyer Acrodental Dysostosis Patients

	Case 33					Case 26
Individual Age	IV:I 15 months	IV:2 2 months	III:2 25 years	III:3 22 years	II:2 49 years	Proband 2.5 years
Postaxial polydactyly	+All 4 limbs	+All 4 limbs	+All four limbs	+All 4 limbs	+All 4 limbs	+All 4 limbs
Syndactyly	2–3 toe syndactyly bilaterally	2–3 toe syndactyly bilaterally	2–3 toe syndactyly bilaterally & syndactyly of 4th and 5th digit of right hand	2–3 toe syndactyly bilaterally	2–3 toe syndactyly bilaterally	–
Nails	Thin	Thin	Thin and dysplastic. Splitting of thumb nails	Thin and dysplastic. Splitting of thumb nails	Thin and dysplastic. Splitting of most finger nails	Small nails with grooves
Dentition	Delayed primary dentition	–	Widely spaced, small incisors	Abnormal presentation, small incisors	Widely spaced, small incisors	Delayed dentition, oligodonthia, small peg-shaped teeth
Height	25th centile	25th centile	2nd to 9th centile	50th centile	2nd to 9th centile	50th centile
Other bone abnormalities	–	–	Duplication of terminal phalange of 5th digit of right hand	–	–	–
Multiple oral frenulae	–	–	–	–	–	+
Heart defects	–	–	–	–	–	–

+, present; – not present. Family pedigrees are shown in Fig. 3.

transduction in a cell culture model. To do this we used NIH 3T3 mouse embryonic fibroblasts because the transcription of Hh target genes such as *Ptch1* and *Gli1* has been shown to increase in response to Hh signaling in these cells [Rohatgi et al., 2007; Taipale et al., 2000]. RT-PCR verified that *Evc* and *Evc2* are expressed in NIH 3T3 cells (data not shown). As NIH 3T3 fibroblasts are a mouse cell line we used PCR to generate a murine Evc2 Weyer variant missing the last 43 amino acids (*Evc2*:c.3533-T>A; Evc2: p.L1178X; Evc2Δ43) to mimic the effect of the mutations observed in patients with Weyer syndrome and a second C-terminal truncation mutation (*Evc2*: c.3396delC; Evc2:p.I1133YfsX2; Evc2Δ87) equivalent to the human *EVC2* c.3660delC change. The two mutations chosen to be tested occur in the last exon of *EVC2* and so they are predicted to escape nonsense mediated decay [Nagy and Maquat, 1998]. Consistent with this RT-PCR amplification of the 3′ half of *EVC2* (exons 12–22) in primary skin fibroblasts from a c.3660delC heterozygote followed by direct sequencing confirmed the presence of wild-type and mutant *EVC2* mRNA species in these cells. Sequencing of the same RT-PCR product in a Weyer patient heterozygous for the c.3793delC mutation also demonstrated coexistence of normal and mutant *EVC2* transcripts in primary skin fibroblasts. Additionally, relative quantification of the *EVC2* mRNA levels with respect to an endogenous control (*HPRT-1*) by qRT-PCR did not reveal significant differences in *EVC2* expression between cultured fibroblasts from a normal subject and the cells derived from the carrier of the c.3660delC EvC mutation or the c.3793delC Weyer patient (Supp. Fig. S1). Thus, the carriers of the c.3660delC or the c.3793delC mutations are both expected to produce the corresponding EVC2 truncated protein (Table 2). c.3660delC is the prevalent Ellis-van Creveld mutation within the Spanish population and because none of the carriers of this change manifest features of EvC or Weyer, we are confident that heterozygosity for this change does not cause a phenotype. Introduction of the c.3396delC frameshift mutation in the mouse changes Isoleucine 1133 to Tyrosine and deletes the last 87 residues of Evc2, thus causing the same protein effect as the c.3660delC nucleotide deletion in humans. A sequence alignment between normal and mutant EVC2 proteins from human and mouse is shown in Fig. 4. Once the mutations were generated, we cloned the full-length *Evc2* coding region and the cDNAs encoding Evc2Δ43 and Evc2Δ87 in a pCAGGS-derived eukaryotic expression vector [del Mar Lorente et al., 2000], and each of these constructs was transfected into NIH 3T3 cells together with a Hedgehog luciferase reporter carrying 8 Gli1 consensus binding sites in its promoter [Sasaki et al., 1997] and a plasmid expressing *Renilla* luciferase constitutively. We treated the transfected cells with the Hedgehog agonist SAG to activate the pathway [Chen et al., 2002], and we determined Gli1 activity in each culture by measuring the relative luciferase expression. *Gli1* is a transcriptional target of Hedgehog signaling that is widely used as a sensitive readout of the pathway [Ruiz i Altaba et al., 2007]. The result of this analysis showed that after the SAG treatment there was almost no activation of the Gli1-luciferase reporter in the cells transfected with the *Evc2Δ43* Weyer cDNA, whereas the Hedgehog pathway was fully active in the cells expressing the complete *Evc2* coding region, or the *Evc2Δ87* cDNA or the empty vector, hence indicating that expression of the Evc2 Weyer protein disrupts Hedgehog signaling (Fig. 4C).

Discussion

In this report we have characterized 40 *EVC/EVC2* independent mutations, 31 of them being novel in 36 Ellis-van Creveld patients and 3 patients with Weyer acrodental dysostosis. In addition to single-base substitutions, microdeletions, and microinsertions, the spectrum of *EVC* and *EVC2* mutations found in this cohort included a deep intronic mutation in *EVC* and two larger deletions

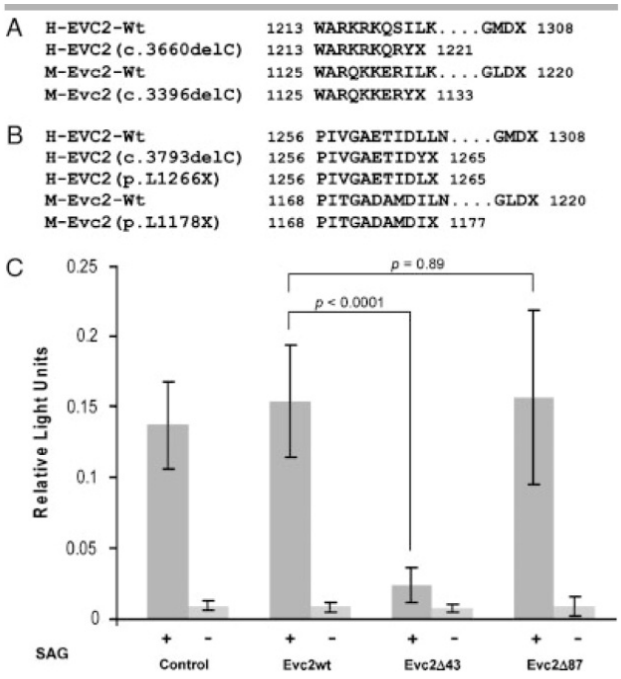

Figure 4. Effect of Evc2 truncated proteins on Hedgehog signaling. **A**, **B**: Protein sequence alignment of the C-terminal region of wild-type (Wt) and mutant EVC2 protein variants from human (H, NP_667338.3) and mouse (M, NP_666032.1). An EvC change is shown in panel A and Weyer changes are shown in panel B. Numbers of residues are indicated before and after each stretch of amino acids. Stop codons are represented by an X. *Evc2*:c.3396delC (Evc2Δ87) and Evc2:p.L1178X (Evc2Δ43) are the mouse truncation mutations generated by PCR for in vitro studies. **C:** Relative luciferase readings obtained in protein extracts from NIH 3T3 cells cotransfected with a Gli1-luciferase reporter, pRL-TK (*Renilla* luciferase) and a expression construct carrying either the normal coding sequence of *Evc2* (Evc2wt), or the *Evc2Δ87* or *Evc2Δ43* cDNAs. Symbols + and − indicate whether SAG (+) or its vehicle (−) were added to the cultures and transfections with the empty vector are referred as control. Data are expressed as mean ± standard deviation and the *P*-values from the statistical analysis of the differences in luciferase activity between SAG treated cultures are also indicated. *P*-Values were calculated using a two-tailed Student's *t*-test. A *P*-value <0.05 was considered statistically significant.

of several exons in *EVC2*. This spectrum has to be considered when designing a strategy for diagnostic service. Deletions could be detected by incorporating a dosage sensitive technique such as MLPA into the strategy, but the intronic change could only be detected by cDNA analysis. Because pathogenic changes either in *EVC* or *EVC2* were found in all affected subjects, our study gives no support for further genetic heterogeneity in Weyer or Ellis-van Creveld syndrome patients with classical chondroectodermal phenotype. The high proportion of consanguineous families in this cohort in which the exon deletions are more easily detected and the availability of fibroblasts for cDNA analysis in the one EvC sample in which only one mutation had been found are likely to be the reason for the mutation detection rate of this analysis being higher than the 69% reported in our earlier study [Tompson et al., 2007].

The previous finding that a homozygous chromosomal deletion involving all exons of *EVC2* and the first 11 exons of *EVC* results in EvC [Temtamy et al., 2008] is a clear demonstration that Ellis-van Creveld syndrome is caused by a loss of function mechanism. This is supported by the large number of mutations found in EvC patients that give rise to mRNAs containing premature termination codons that would be subject to nonsense-mediated mRNA decay (NMD), and hence leading to the loss of gene function. In agreement with this in the carrier of the c.1098+1G>A mutation (pedigree 07, Fig. 1A) we amplified a main RT-PCR fragment corresponding to transcription from the wild-type chromosome, and there were no other additional product observed excepting for a faint band of the size of patient product 4, which does not include an early termination codon. In fibroblasts from the affected daughter, however, we amplified some fainter spliced transcripts containing premature termination codons. We think that without a major normal transcript competing for amplification, primers bind to underrepresented transcripts that are then amplified.

As carriers of EvC mutations are phenotypically normal the dominant Weyer phenotype cannot be due to haploinsufficiency, instead Weyer changes represent dominant negative mutations that cause a phenotype by a gain of function mechanism or by interfering with the function of the product coming from the normal allele. Considering the two new changes reported here there are now four different mutations identified in Weyer families: these are an amino acid substitution in EVC and one frameshift and two nonsense mutations in the last exon of *EVC2*. In the published pedigree [Ye et al., 2006] and the cases described here all carriers of *EVC2* Weyer mutations manifest features of the condition. The S307P Weyer change in EVC has a more enigmatic nature, which seems to be influenced by the genetic context of each individual as some carriers of this change have no clinical features [Tompson et al., 2007]. Although the four Weyer mutations are predicted to escape from NMD, not all the *EVC* or *EVC2* mutations avoiding the NMD machinery cause a dominant phenotype. c.3660delC and c.3731dupT (Table 2) are two *EVC2* frameshift mutations introducing premature termination codons within the last exon of *EVC2* (only a few nucleotides upstream of the cluster of *EVC2* Weyer mutations) that should not be subject to NMD [Nagy and Maquat, 1998], and yet are not associated with a phenotype in heterozygotes. cDNA sequencing and qRT-PCR analysis in cultured fibroblasts verified that neither the c.3660delC nor the c.3793delC transcripts undergo nonsense-mediated decay. Similarly, there are in-frame deletions and missense changes in EVC and EVC2 (Tables 1 and 2) that do not result in a heterozygous phenotype.

The fact that the three Weyer associated changes in *EVC2* exon 22 produce a protein 43 amino acids shorter than normal, whereas the two neighboring truncation mutations located in the same exon act as typical recessive Ellis-van Creveld syndrome mutations (Table 2) prompted us to investigate a molecular explanation for the dominant inheritance of Weyer acrodental dysostosis. Using a cell culture model we found that expression of a murine Evc2 protein missing the final 43 amino acids interferes with Hh signaling in NIH 3T3 cells. This suggests that Evc2, like Evc, is also involved in Hh signal transduction. Because SAG activates the pathway at the level of Smo, a protein that is the major activator of the pathway [Hooper and Scott, 2005], the effect of the dominant Evc2 mutations is presumably downstream of Smo. Interestingly, the expression of an Evc2 protein lacking the last 87 residues in NIH 3T3 fibroblasts has no effect on Hedgehog signaling, which is in agreement with the lack of phenotype observed in carriers of the equivalent human mutation (*EVC2*: c.3660delC). This data indicates that the 44 residues between Evc2Δ87 and Evc2Δ43 can modify Evc2 function in the absence of the final 43 amino acids of the protein. At this stage we can only speculate on the molecular mechanism by which Weyer variants affect Hedgehog signaling. It

might be that Evc2 functions as a homodimer that could work alone or/and in association with other proteins such as Evc, and that the fragment between Evc2Δ43 and Evc2Δ87 is necessary for dimerization but insufficient to create a functional protein complex without the last 43 amino acids. In this scenario the EVC2Δ43 mutant protein would reduce the amount of functional homodimers as only a quarter of the dimers that would normally form in the case that two wild-type molecules would be made. The same reduction in the number of functional complexes would occur if the putative EVC2 protein conglomerates are targeted for proteolytic degradation following the incorporation of a Weyer mutant EVC2 subunit. Alternatively, a gain of function mechanism triggered by the loss of the final 43 residues but not by the loss of the last 87 amino acids is also a plausible explanation for the Weyer dominant phenotype. Protein stability could also play a role in determining the pattern of inheritance of *EVC2* exon 22 mutations in vivo. As the final exon mutations escape NMD, there exists the possibility that the exon 22 recessive changes lead to the synthesis of C-terminal truncated EVC2 proteins that may be less stable than the slightly larger Weyer EVC2 polypeptides. If this is the case, the *EVC2* exon 22 recessive mutations could, in effect, be loss-of-function mutations, which would then explain the lack of phenotype in the heterozygous carriers of these mutations. In contrast, the more stable EVC2 Weyer proteins would cause the dominant phenotype by one of the mechanisms described above.

Defects in Hedgehog signaling have been shown implicated in a variety of skeletal, craniofacial, and dental abnormalities [Cordero et al., 2006; Ehlen et al., 2006; McMahon et al., 2003; Varjosalo and Taipale, 2008] and we previously demonstrated in in vivo and in vitro murine studies that Evc is a positive mediator of Hh signaling, which is required for normal transcriptional activation of Hh target genes [Ruiz-Perez et al., 2007]. The in vitro data we present here indicates that Evc2 also plays a role in Hh signal transduction, and furthermore, that disruption of Hedgehog signaling is the likely causative mechanism of the Weyer acrodental dysostosis phenotype.

Acknowledgments

We thank the patients and their families for their contribution to this research. This work was funded by the Spanish Ministry of Science and Innovation (SAF-62291), Ramon Areces Foundation, and the European Union (LSHM-CT-2007-03741). We acknowledge the following clinicians who sent one or two EvC samples: Georgina Arteaga, Merçè Artigas-López, Valerie Cormier-Daire, Nursel Elcioglu, Javier Egües, Joaquin Fernandez-Toral, Juan Fondevilla, Esther Gean, Jung Hokhim, Bob Lebel, Isabel Lorda, Victor Marugan, Salvador Martinez-Santana, Jose Antonio Sanz, and Ineke van der Burgt. We thank Dr. Hiroshi Sasaki for the kind gift of the Gli1-luciferase reporter, Dr. Miguel Vidal for the pCAGGS-derivate expression vector and Mónica Roselló and Carmen Sánchez-Gómez for their help with the primary skin fibroblast cultures.

References

Cordero D, Tapadia M, Helms JA. 2006. Sonic Hedgehog signalling in craniofacial development. In: Ruiz i Altaba A, editor. Hedgehog-Gli signaling in human disease. New York: Springer Science+Business Media. p 153–176.

Curry CJ, Hall BD. 1979. Polydactyly, conical teeth, nail dysplasia, and short limbs: a new autosomal dominant malformation syndrome. Birth Defects Orig Artic Ser 15:253–263.

Chen JK, Taipale J, Young KE, Maiti T, Beachy PA. 2002. Small molecule modulation of Smoothened activity. Proc Natl Acad Sci USA 99:14071–14076.

da Silva EO, Janovitz D, de Albuquerque SC. 1980. Ellis-van Creveld syndrome: report of 15 cases in an inbred kindred. J Med Genet 17:349–356.

del Mar Lorente M, Marcos-Gutierrez C, Perez C, Schoorlemmer J, Ramirez A, Magin T, Vidal M. 2000. Loss- and gain-of-function mutations show a polycomb group function for Ring1A in mice. Development 127:5093–5100.

den Dunnen JT, Antonarakis SE. 2000. Mutation nomenclature extensions and suggestions to describe complex mutations: a discussion. Hum Mutat 15:7–12.

den Dunnen JT, Paalman MH. 2003. Standardizing mutation nomenclature: why bother? Hum Mutat 22:181–182.

Ehlen HW, Buelens LA, Vortkamp A. 2006. Hedgehog signaling in skeletal development. Birth Defects Res C Embryo Today 78:267–279.

Hooper JE, Scott MP. 2005. Communicating with hedgehogs. Nat Rev Mol Cell Biol 6:306–317.

McKusick VA, Egeland JA, Eldridge R, Krusen DE. 1964. Dwarfism in the Amish I. The Ellis-Van Creveld Syndrome. Bull Johns Hopkins Hosp 115:306–336.

McMahon AP, Ingham PW, Tabin CJ. 2003. Developmental roles and clinical significance of hedgehog signaling. Curr Top Dev Biol 53:1–114.

Nagy E, Maquat LE. 1998. A rule for termination-codon position within intron-containing genes: when nonsense affects RNA abundance. Trends Biochem Sci 23:198–199.

Ocbina PJ, Anderson KV. 2008. Intraflagellar transport, cilia, and mammalian Hedgehog signaling: analysis in mouse embryonic fibroblasts. Dev Dyn 237: 2030–2038.

Reese MG, Eeckman FH, Kulp D, Haussler D. 1997. Improved splice site detection in Genie. J Comput Biol 4:311–323.

Rohatgi R, Milenkovic L, Scott MP. 2007. Patched1 regulates hedgehog signaling at the primary cilium. Science 317:372–376.

Roubicek M, Spranger J. 1984. Weyers acrodental dysostosis in a family. Clin Genet 26:587–590.

Ruiz i Altaba A, Mas C, Stecca B. 2007. The Gli code: an information nexus regulating cell fate, stemness and cancer. Trends Cell Biol 17:438–447.

Ruiz-Perez VL, Blair HJ, Rodriguez-Andres ME, Blanco MJ, Wilson A, Liu YN, Miles C, Peters H, Goodship JA. 2007. Evc is a positive mediator of Ihh-regulated bone growth that localises at the base of chondrocyte cilia. Development 134:2903–2912.

Ruiz-Perez VL, Ide SE, Strom TM, Lorenz B, Wilson D, Woods K, King L, Francomano C, Freisinger P, Spranger S, Marino B. 2000. Mutations in a new gene in Ellis-van Creveld syndrome and Weyers acrodental dysostosis. Nat Genet 24:283–286.

Ruiz-Perez VL, Tompson SW, Blair HJ, Espinoza-Valdez C, Lapunzina P, Silva EO, Hamel B, Gibbs JL, Young ID, Wright MJ, Goodship JA. 2003. Mutations in two nonhomologous genes in a head-to-head configuration cause Ellis-van Creveld syndrome. Am J Hum Genet 72:728–732.

Sasaki H, Hui C, Nakafuku M, Kondoh H. 1997. A binding site for Gli proteins is essential for HNF-3beta floor plate enhancer activity in transgenics and can respond to Shh in vitro. Development 124:1313–1322.

Shapiro MB, Senapathy P. 1987. RNA splice junctions of different classes of eukaryotes: sequence statistics and functional implications in gene expression. Nucleic Acids Res 15:7155–7174.

Taipale J, Chen JK, Cooper MK, Wang B, Mann RK, Milenkovic L, Scott MP, Beachy PA. 2000. Effects of oncogenic mutations in Smoothened and Patched can be reversed by cyclopamine. Nature 406:1005–1009.

Temtamy SA, Aglan MS, Valencia M, Cocchi G, Pacheco M, Ashour AM, Amr KS, Helmy SM, El-Gammal MA, Wright M, Lapunzina P. 2008. Long interspersed nuclear element-1 (LINE1)-mediated deletion of EVC, EVC2, C4orf6, and STK32B in Ellis-van Creveld syndrome with borderline intelligence. Hum Mutat 29:931–938.

Tompson SW, Ruiz-Perez VL, Blair HJ, Barton S, Navarro V, Robson JL, Wright MJ, Goodship JA. 2007. Sequencing EVC and EVC2 identifies mutations in two-thirds of Ellis-van Creveld syndrome patients. Hum Genet 120:663–670.

Ulucan H, Gul D, Sapp JC, Cockerham J, Johnston JJ, Biesecker LG. 2008. Extending the spectrum of Ellis van Creveld syndrome: a large family with a mild mutation in the EVC gene. BMC Med Genet 9:92.

Varjosalo M, Taipale J. 2008. Hedgehog: functions and mechanisms. Genes Dev 22:2454–2472.

Wildeman M, van Ophuizen E, den Dunnen JT, Taschner PE. 2008. Improving sequence variant descriptions in mutation databases and literature using the Mutalyzer sequence variation nomenclature checker. Hum Mutat 29:6–13.

Ye X, Song G, Fan M, Shi L, Jabs EW, Huang S, Guo R, Bian Z. 2006. A novel heterozygous deletion in the EVC2 gene causes Weyers acrofacial dysostosis. Hum Genet 119:199–205.

Zannolli R, Buoni S, Viviano M, Macucci F, D'Ambrosio A, Livi W, Mazzei MA, Mazzei F, Sacco P, Volterrani L, Vonella G, Orsi A, Zappella M, Hayek J. 2008. Polydactyly with ectodermal defect, osteopenia, and mental delay. J Child Neurol 23:683–689.

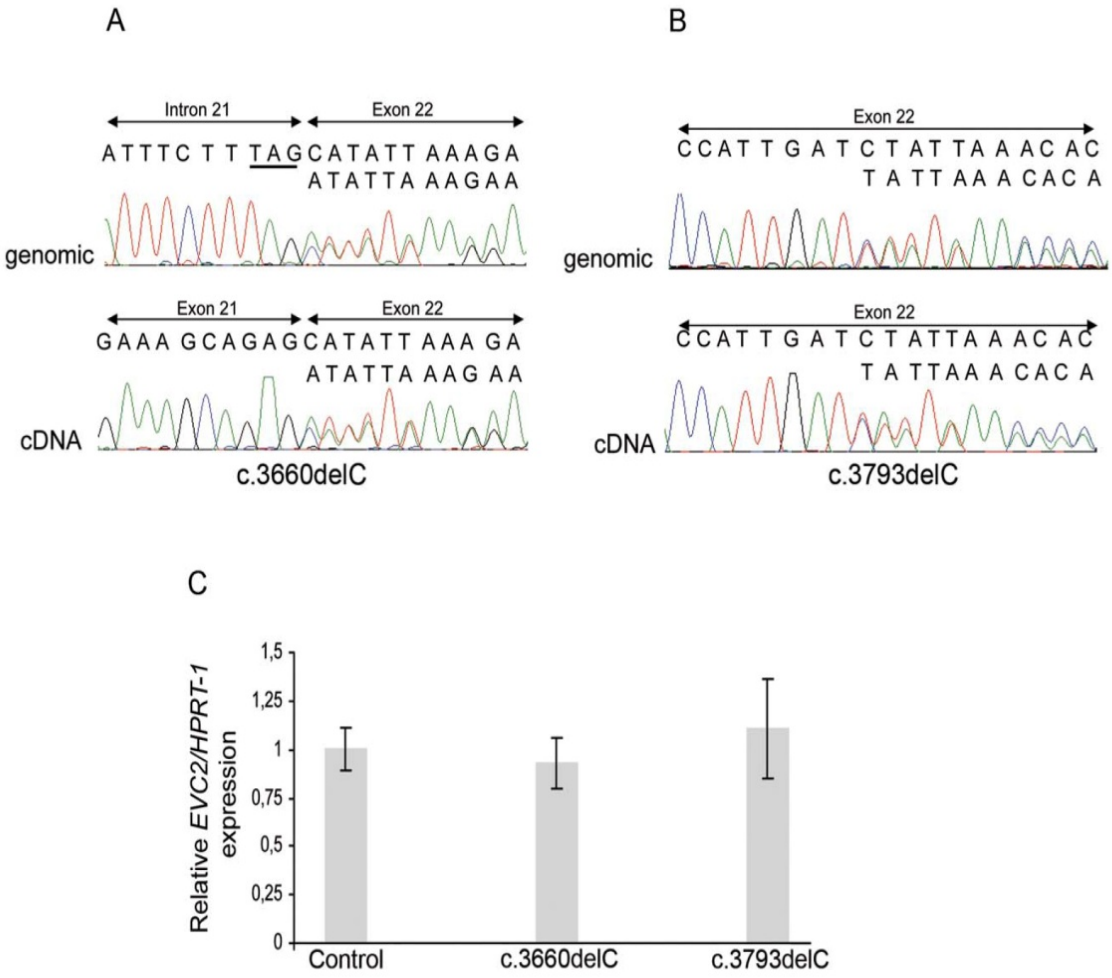

Supp. Figure S1. A and B. Direct sequencing of genomic and cDNA (exons 12-22) PCR products encompassing *EVC2* exon 22 in fibroblasts from the c.3660delC **(A)** and c.3793delC **(B)** heterozygotes demonstrating the presence of mutant *EVC2* transcripts in the cDNA from both individuals. The 3´splice site of *EVC2* exon 22 is underlined. For each individual the height of the double peaks downstream of the corresponding mutation in the cDNA sequencing chromatograms is equivalent to the height of the double peaks in the genomic chromatograms, suggesting a similar proportion of mutant and normal cDNA templates in the heterozygous cultures. **C.** Relative quantification of the *EVC2* mRNA levels in normal control fibroblasts and in fibroblasts derived from the c.3660delC and c.3793delC heterozygotes by qRT-PCR. For each individual we studied 3 different RNA samples that were run in triplicates and analyzed by the $2^{-(\Delta Ct\ sample-\ \Delta Ct\ calibrator\ sample)}$ method. The ΔCt for each of the RNA samples was calculated as the Ct value for *EVC2* minus the Ct value for *HPRT-1* and we considered the ΔCt average from the three normal control samples as the calibrator sample. The y axis represents the mean of the $2^{-\Delta\Delta Ct}$ values ± SD. Statistical analysis using Student´s t-test showed no significant differences in the relative expression of *EVC2* between normal fibroblasts and the c.3660delC or c.3793delC heterozygous cultures (p= 0.47 and p=0.55 respectively).

Capítulo III

Evc works in chondrocytes ans osteoblasts to regulate multiple aspects of growth plate development in the apendicular skeleton and cranial base

Pacheco, M.*; **Valencia, M.***;Caparrós-Martín, J.A.; Mulero, F.; Goodship, J.A.; Ruiz-Perez, V.L.

Bone 50(1): 28-41 (2012)

En este trabajo analizamos en detalle las placas de crecimiento embrionarias de los huesos largos y las sincondrosis craneales en ratones *Evc* $^{-/-}$ con fondo genético homogéneo C57BL/6J para profundizar en el conocimiento de la patología asociada a EvC.

Utilizando técnicas histológicas e HIS corroboramos la disminución de la expresión de genes diana de la ruta (*Ptch1, Gli1, Pthrp* y *Hhip*) en los huesos largos de las extremidades superiores, la cual había sido observada anteriormente en la tibia de los ratones *Evc*$^{-/-}$ de fondo genético mixto (C57BL/6J; 129). Sin embargo a diferencia del estudio anterior encontramos una disminución de la proliferación en los condrocitos de reserva y en los columnares (56% y 33% respectivamente) y un retraso en la incorporación de condrocitos de la región distal a la proliferativa. Para conocer el papel de Evc durante las primeras etapas de osificación estudiamos los metatarsos y falanges a estadio 18.5. Este estudio puso de manifiesto que la ausencia de Evc provoca un retraso en la mineralización del pericondrio que rodea el centro de osificación primario y en la diferenciación de los condrocitos adyacentes a esa región. También analizamos el desarrollo del pericondrio una vez formada la placa de crecimiento (E16.5) mediante la expresión de marcadores de osteoblastos tempranos (*Alkp*, *Col1a1* y *Runx2)*, intermedios (*Osx* y *Pth1r*) y tardíos (*Ibsp* y *Osp*). Este análisis demostró que el extremo distal de expresión de estos genes se encuentra situado más cerca a la esponjosa primaria en los mutantes. No obstante la intensidad de hibridación de los marcadores de osteoblastos era similar a la de los individuos normales, salvo en el extremo distal del frente de osificación pericondrial (DBPO). Por tanto deducimos que Evc regula la diferenciación de osteoblastos principalmente en la región DBPO pero es prescindible en la esponjosa primaria o en regiones del pericondrio más maduras. En esta región también encontramos menor número de células positivas para Osx y la señal de genes diana de la ruta β-catenina (*Tcf1*, *Dkk1* y *Apcdd1*) es más débil (tanto Osx como la ruta de la β-catenina son fundamentales para la diferenciación de los osteoblastos). Posteriormente usando un anticuerpo monoclonal demostramos mediante *western blot* que Evc se expresa en osteoblastos en cultivo desarrollados a partir de calvarias (E18.5) y que en estas células Evc se localiza a lo largo del cilio primario. También demostramos mediante

qRT-PCR que la respuesta de los cultivos de osteoblastos primarios *Evc*$^{-/-}$ a la estimulación de la ruta con un agonista químico (purmorfamina) se encuentra disminuida.

Dado que la ausencia de *Evc* afecta a la señalización Hh y el gen *Ptch1* es diana de la misma, generamos una línea doble heterocigota *Ptch1-Evc* y usamos la actividad de la *β-galactosidasa* dependiente de *Ptch1* para caracterizar los distintos tipos celulares que responden a Hh en el pericondrio. En los embriones *Ptch1* $^{+/-}$*; Evc* $^{-/-}$ observamos una disminución de la actividad *Ptch1-LacZ* respecto a los embriones *Ptch1* $^{+/-}$*; Evc* $^{+/+}$ en los condrocitos y en los osteoblastos pero no en las células fibroblásticas de las capas más externas del pericondrio, indicando que en esa región la vía de Hh no depende de Evc.

Los huesos de la base cráneo también se forman por osificación endocondral pero presentan placas de crecimiento distintas a las de los huesos largos denominadas sincondrosis. Los estudios histológicos demuestran que el desarrollo de la región basioccipital de los ratones *Evc*$^{-/-}$ es prácticamente normal, pero existen importantes defectos morfológicos en la parte frontal entre los que cabe destacar la ausencia de la sincondrosis intraesfenoidal, la presencia de un orificio en el centro del hueso basiesfenoides y una hendidura en la línea media a nivel del preesfenoides. Mediante HIS e inmunohistoquímica observamos que las sincondrosis *Evc*$^{-/-}$ presentan los mismos defectos descritos en los huesos largos, como retraso en la diferenciación de los osteoblastos del pericondrio, disminución de la proliferación y disminución de la expresión de las dianas de Ihh.

La doctoranda, como co-autora del trabajo, llevó el mantenimiento de las colonias de ratones usados en este trabajo incluyendo los dobles cruces. Puso a punto el sistema de cultivo de osteoblastos primarios a partir de calvarias de embriones de E18.5, de los que extrajo ARN para las qRT-PCR, proteínas para los western blots y realizó los estudios de inmunofluorescencias. También llevó a cabo los estudios de proliferación con BrdU y el procesamiento de muestras para histología así como la captura de imágenes. Realizó los análisis estadísticos y participó en la composición de las figuras, escritura y discusión.

Bone 50 (2012) 28–41

Contents lists available at SciVerse ScienceDirect

Bone

journal homepage: www.elsevier.com/locate/bone

Original Full Length Article

Evc works in chondrocytes and osteoblasts to regulate multiple aspects of growth plate development in the appendicular skeleton and cranial base

María Pacheco [a,1], María Valencia [a,1], José A. Caparrós-Martín [a], Francisca Mulero [b], Judith A. Goodship [c], Victor L. Ruiz-Perez [a,*]

[a] Instituto de Investigaciones Biomédicas, Consejo Superior de Investigaciones Científicas-Universidad Autónoma de Madrid and Ciber de enfermedades raras, Arturo Duperier 4, Madrid 28029, Spain
[b] Spanish National Cancer Research Centre (CNIO), Melchor Fernández Almagro, 3. E-28029 Madrid, Spain
[c] Institute of Human Genetics, Newcastle University, Central Parkway, Newcastle upon Tyne NE1 3BZ, UK

ARTICLE INFO

Article history:
Received 13 May 2011
Revised 2 August 2011
Accepted 24 August 2011
Available online 31 August 2011

Edited by: Bjorn Olsen

Keywords:
Growth plate
Indian hedgehog signaling
Primary cilia
Ellis-van Creveld
Evc

ABSTRACT

Ellis-van Creveld syndrome protein homolog (Evc) was previously shown to mediate expression of Indian hedgehog (Ihh) downstream targets in chondrocytes. Consequently disruption of the Ihh/Pthrp axis was demonstrated in *Evc*$^{-/-}$ mice, but the full extent of Evc involvement in endochondral development was not totally characterized. Herein we have examined further the *Evc*$^{-/-}$ growth plate in a homogeneous genetic background and show that Evc promotes chondrocyte proliferation, chondrocyte hypertrophy and the differentiation of osteoblasts in the perichondrium, hence implicating Evc in both Pthrp-dependent and Pthrp-independent Ihh functions. We also demonstrate that Evc, which localizes to osteoblast primary cilia, mediates Hedgehog (Hh) signaling in the osteoblast lineage. In spite of this, bone collar development is mildly affected in *Evc*$^{-/-}$ mutants. The onset of perichondrial osteoblastogenesis is delayed at the initial stages of endochondral ossification in *Evc*$^{-/-}$ mice, and in later stages, the leading edge of expression of osteoblast markers and Wnt/β-catenin signaling components is located closer to the primary spongiosa in the *Evc*$^{-/-}$ perichondrium owing to impaired osteoblast differentiation. Additionally we have used *Ptch1-LacZ* reporter mice to learn about the different types of Hh-responsive cells that are present in the perichondrium of normal and *Evc*$^{-/-}$ mice. Evc mediates Hh target gene expression in inner perichondrial cells, but it is dispensable in the external layers of the perichondrium. Finally, we report cranial base defects in *Evc*$^{-/-}$ mice and reveal that Evc is essential for intrasphenoidal synchondrosis development.

© 2011 Published by Elsevier Inc.

Introduction

The majority of bones of the appendicular skeleton are formed by endochondral ossification. This process commences in the early embryo with the condensation of mesenchymal cells at the different sites of skeletogenesis, which then differentiate into proliferating chondrocytes giving rise to the cartilage templates of the future bones. In the meantime mesenchymal cells surrounding the chondrocytes develop into the perichondrium, a structure composed of a few fibroblast-like cell layers from which bone collar osteoblasts differentiate. As the incipient skeletal elements enlarge, chondrocytes in the center of the bone anlagen start to hypertrophy. Hypertrophic chondrocytes synthesize a type X collagen-rich extracellular matrix, which later becomes mineralized, and produce specific factors that attract blood vessels, osteoblasts and osteoclasts, promoting the formation of the primary ossification center, before undergo terminal differentiation and apoptosis. Finally in the developing long bones stratified layers of resting, proliferating and hypertrophic chondrocytes emerge at each end of the primary ossification center, and these comprise the growth plate. Continuous proliferation and hypertrophy of chondrocytes in the growth plate and their subsequent replacement by bone cells results in bone growth [1].

The development of the growth plate is orchestrated by Indian hedgehog (Ihh). Ihh is secreted by prehypertrophic chondrocyes and controls the rate of chondrocyte hypertrophy along the longitudinal axis of the bone by establishing a negative feedback loop with the Parathyroid hormone related peptide (Pthrp) [2]. Pthrp is produced in resting chondrocytes in response to Ihh and diffuses back toward the hypertrophic region preventing proliferating chondrocytes from entering into hypertrophy and thus postponing *Ihh* expression. In addition, Ihh also regulates skeletal development by stimulating chondrocyte division and the differentiation of bone collar osteoblasts. *Ihh*$^{-/-}$ endochondral bones were demonstrated having a 50% fall in chondrocyte proliferation and lacking bone collars [3,4]. More recently in vitro and in vivo experiments in which Hedgehog (Hh) signaling was either blocked or activated in a *Pthrp*$^{-/-}$ background demonstrated that Ihh

* Corresponding author. Fax: +34 91585 4401.
E-mail address: vlruiz@iib.uam.es (V.L. Ruiz-Perez).
[1] These authors contributed equally to this work.

8756-3282/$ – see front matter © 2011 Published by Elsevier Inc.
doi:10.1016/j.bone.2011.08.025

promotes chondrocyte hypertrophy independently of Pthrp, thus extending further the roles of Ihh in the growth plate and revealing opposing functions of Ihh in the control of hypertrophy [5]. Differentiation of osteoblasts in the perichondrium also requires the participation of the canonical Wnt/β-catenin signaling. Activation of this pathway by Wnt ligands culminates in β-catenin translocating into the nucleus and activating the transcription of target genes through the interaction with the Lef/Tcf family of transcription factors [6]. Conditional ablation of β-catenin from mesenchymal precursors using either *Dermo1-Cre* or *Prx1-Cre* results in loss of mature osteoblasts and transformation of osteoblast precursors in the perichondrium to chondrocytes [7,8].

Primary cilia are indispensable for Hh signal transduction in vertebrates [9]. Key proteins of the pathway such as Ptch1, Smo, and the Gli factors have been shown to enter or leave the cilium in the presence of Hh and both Gli processing and the generation of functionally competent Gli-full length activators depend on this organelle [10–13]. Accordingly mice with conditional ablation of proteins that are involved in cilia assembly and function, like the components of the intraflagellar transport system (IFT) or the IFT motor proteins, manifest skeletal abnormalities secondary to growth plate defects that are consistent with impaired Ihh signaling. Examples of the latest include the *Ift88* and *Kif3A; Prx1-Cre* conditional knockouts [14,15].

EVC and *EVC2* are adjacent genes responsible for the recessive skeletal dysplasia Ellis-van Creveld syndrome (EvC; MIM: 225500) [16,17] with homozygous loss-of function mutations in either gene leading to the same condition [18,19]. We generated an *Evc* null allele by replacing the first exon of this gene with a *LacZ* reporter [20]. Mice homozygous for this allele phenocopy the short limbs and short ribs of EvC patients. Preliminary work performed in the embryonic tibia of $Evc^{-/-}$ mice demonstrated that the expression of three Ihh-downstream targets *Ptch1*, *Gli1* and *Pthrp* was diminished in the Evc knockouts. Similarly $Evc^{-/-}$ chondrocyte cultures treated with purmorphamine, a chemical agent that activates the Hh pathway at the level of Smo, were unable to upregulate the mRNA levels of the downstream targets of Hh signaling, proving that Evc is required for the intracellular transduction of the Hh signal, rather than for Ihh synthesis or secretion. Consistent with this Evc was localized at the base of chondrocyte cilia [20]. Nevertheless, the level of involvement of Evc in each one of the different aspects of Ihh signaling including stimulation of chondrocyte hypertrophy and osteoblast differentiation; the state of other key pathways of bone development such as canonical Wnt/β-catenin signaling in *Evc* depleted mice; or whether Evc was needed in other parts of the skeleton like the bones of the base of the cranium, were all unknown. Thus a more comprehensive examination of the $Evc^{-/-}$ growth plate was needed for better understanding of the bone pathology associated to EvC. Herein we undertook an in depth analysis of the $Evc^{-/-}$ growth plates in a homogeneous genetic background and have identified Evc as an important and general regulator of endochondral ossification.

Materials and methods

Transgenic mice

The generation of $Evc^{-/-}$ mice has been reported earlier and the *Ptch1-LacZ* mouse line was obtained from the Jackson Laboratories [20,21]. Cranial base studies in $Evc^{-/-}$ mice were conducted in a hybrid C57BL/6J;129 background and for the remaining studies $Evc^{-/-}$ mice were on a C57BL/6J background. Due to perinatal lethality, $Evc^{-/-}$ embryos were generated by crossing $Evc^{+/-}$ mice. *Ptch1-LacZ* mice were maintained in a C57BL/6J;129 mixed background.

Histology and immunohistochemistry

Forelimbs, heads and dissected digits of mouse embryos were fixed in 4% PFA/PBS, decalcified in 12% EDTA/PBS and embedded in paraffin prior to sectioning. 5 μm thick serial sections were stained with Haematoxylin–Eosin or with the von-Kossa technique following standard methods. Tissues were not decalcified when used for von-Kossa staining. The following antibodies were used: mouse anti-β-catenin (1:200; BD Biosciences), rabbit anti-Col I (1:40, Chemicon), rabbit anti-Osx (1: 125, Abcam) and rabbit anti-Col X (a kind gift from Dr. Danny Chan). Biotinylated secondary antibodies in conjunction with the ABC elite kit (Vector) or the K-0673 kit (DAKO) were applied following the manufacturer specifications. An antigen retrieval protocol consisting in heating the samples at 120 °C for 2 min in 10 mM citrate buffer (pH 6.0) was conducted for β-catenin detection and a hyaluronidase treatment (0.8 mg/ml for 30 min at 37 °C) was used for Col-X immunohistochemistry. Tartrate-Resistant Acid Phosphatase (TRAP) staining was performed on paraffin sections using the acid phosphatase staining kit from Sigma according to the manufacturer instructions.

In situ hybridization

Tissues were fixed overnight in 4% PFA in PBS (DEPC treated) at 4 °C, decalcified in 12% EDTA/PBS, embedded in paraffin and sectioned at 10 μm thickness under RNAse free conditions. Depending on the expression levels of the gene tested sections were hybridized with radioactively labeled (^{35}S or ^{33}P, 2×10^7 cpm/ml) or digoxigenin labeled (3 ng/μl) antisense riboprobes. Hybridization steps were performed as in Lescher et al., [22] with the exception that 10% of dextran sulfate was included in the radioactive hybridization buffer. For radioactive ISH sections were coated with Kodak nuclear emulsion NBT after dehydration and exposed for 2–6 weeks at 4 °C. Radioactive signals were developed in Kodak D-19 developer (Sigma) and fixed. Before mounting, sections were counterstained with nuclear Fast Red. For non-radioactive ISH, probes were fabricated with the digoxigenin labeling kit from Roche and hybridization signals were detected using an alkaline phosphatase (AP) labeled antidigoxigenin antibody (Roche) and the AP substrates BM-purple or NBT/BCIP (Roche). Template plasmids containing the hybridization probes were obtained by request or generated by RT-PCR amplification and confirmed by sequencing. At least three wild-type and three mutant littermates were analyzed for each probe and representative images are reported here. Bright-field images were captured on a Nikon DS-5L1 digital camera.

BrdU labeling

E16.5 pregnant mice were injected with 1 ml of Cell Proliferation Labelling Reagent (GE healthcare)/100 g of body weight 2 h before sacrifice. Embryos were dissected and forelimbs and heads fixed, decalcified and paraffin embedded. BrdU immunodetection was performed on 5 μm thick paraffin sections using the BrdU detection kit from Invitrogen. Sections were counterstained with Haematoxylin and all BrdU-positive and non-positive nuclei counted separately with the help of Image J software in the resting and columnar regions of the growth plate defined by morphology. To study proliferation in the forelimbs 3 embryos of each genotype from 3 different litters were analyzed and 9 sections per embryo were counted. For synchondrosis proliferation analysis a minimum of 3 embryos of each genotype and 3 sections per embryo were counted.

Antibody development

A His-tagged fragment of the Evc protein (NP_067267) comprising the last 258 amino acids was purified from bacteria by IMAC chromatography (Biomedal) and used to immunize mice. Following hybridoma development (Immunostep) a clone was selected and subsequently subcloned to ensure the purity of the hybridoma. Anti-Evc immunoglobulins were purified from cell culture supernatant by protein A/G affinity purification.

Primary cultures

Primary osteoblasts were isolated from the skull of E18.5 embryos. Briefly calvaria were dissected and incubated in 0.1% collagenase P (Roche) and 0.2% dispase (Invitrogen) in Hank's Balance Salt Solution (Invitrogen) during 10 min at 37 °C with rocking. This process was repeated 4 times and cells from the second to the fourth digestions were collected. Osteoblasts were cultured in 24-well plates at a density of 1 10^5 cells/well in α-minimum essential medium (α-MEM, Invitrogen) supplemented with 10% fetal bovine serum and 1× antibiotic/antimycotic solution (Invitrogen). 16 h later the media was replaced with new fresh media containing ascorbic acid (50 μg/ml; Sigma) and ß-glycerol phosphate (10 mM; Sigma) to avoid any possible dedifferentiation of osteoblasts.

Immunofluorescence

Fresh primary osteoblasts were seeded in 12 mm glass coverslips (24-well plates, 5 10^4 cells/well) in osteoblast medium and after 24 h fixed in 4% PFA/PBS for 10 min at room temperature. Osteoblasts were permeabilised and blocked in 4% goat serum, 0.05% Triton X-100 for 30 min. Subsequently cells were incubated with anti-Evc monoclonal antibody (5 μg/ml) and rabbit polyclonal anti-detyrosinated tubulin (Glu-tubulin 1:350, Millipore) diluted in blocking solution followed by secondary antibodies Alexa Fluor 488 goat anti-mouse (Molecular Probes) and Alexa Fluor 594 goat anti-rabbit (Molecular Probes). For Osx staining, rabbit anti-Osx (1:125, Abcam) was included in the primary antibody incubation step. Coverslips were mounted with Vectashield with DAPI (Vector) and images captured in a Nikon microscope with the NIS-Elements software.

Western blot analysis

Primary calvarial osteoblast cultures were lysed in RIPA buffer supplemented with complete protease inhibitor cocktail (Roche) and 1 mM PMSF. Cell lysates were clarified by centrifugation and 20 μg of total protein were subjected to 10% SDS-PAGE gel electrophoresis and transferred to Hybond-C Extra membrane (GE Healthcare). Evc was detected using an anti-Evc mouse monoclonal antibody (1 μg/ml) and a HRP-conjugated goat anti-mouse (Jackson Immunoresearch). Antibody signals were developed using the ECL Western Blotting Detection kit (GE Healthcare). Mouse monoclonal anti-α-tubulin (Sigma, 1:10000) was used as protein loading control.

Quantitative RT-PCR

To assay the Hh pathway in osteoblasts 2 μM of purmorphamine or its carrier (DMSO) were added to calvarial osteoblast cultures and 72 h later we isolated RNA with Trizol as described by the manufacturer (Invitrogen). Relative quantification of gene expression was performed using gene specific Taqman gene-expression assays purchased from Applied Biosystems. The following assays were used: *Ptch1* (Mm00436026_m1), *Gli1* (Mm00494645_m1), *Hhip1* (Mm00469580_m1) and *Evc* (Mm00469587_m1). The *Hprt1* (Mm00446968_m1) housekeeping gene was used to normalize expression. For each genotype we studied 4 different RNA samples corresponding to mice from 4 different litters, which were run in triplicates and analyzed by the $2^{-(\Delta Ct\ sample - \Delta Ct\ calibrator\ sample)}$ method. The ΔCt of each sample was calculated by subtracting to the average Ct value of this sample the average Ct value of *Hprt1*. The corresponding untreated normal control of the same litter was considered as the calibrator sample.

X-Gal staining and whole mount Alcian-blue/Alizarin preps

For LacZ staining dissected E16.5 forelimbs or E18.5 digits were fixed in 0.2% of glutaraldehyde for 4 h. Tissues were transferred to a series of 15% and 30% sucrose solutions at 4 °C and then frozen in OCT-compound (Takara). 10 μm thick cryostat sections were briefly fixed, washed and stained overnight at 37 °C in X-Gal solution as described previously [23]. Sections were mounted in Aquatex (Merck) for microscope visualization. Whole mount Alcian blue/Alizarin red staining was performed as described earlier [20].

Micro-computed tomography

Embryos were fixed overnight in 4% PFA at 4 °C and subjected to micro-computed tomography using the GE eXplore Locus micro-CT scanner (GE Healthcare) at 80 kvolts of energy and 450 μA of current. Micro-CT image acquisition consisted of 400 projections collected in one full rotation of the gantry in 20 min. The resulting raw data were reconstructed using a filtered back-projection algorithm to a final image volume of 875×875×465 slices at (93 μm) 3 voxel dimensions. Reconstructed images were viewed using MicroView analysis software ABA (Advanced Bone Analysis) version 2.2 (GE Healthcare).

Statistical analysis

Statistical analysis was performed by the Student's *t*-test in a minimum of 3 individuals for each genotype. A p-value$<$0.05 was considered statistically significant.

Results

The $Evc^{-/-}$ growth plate is characterized by a wide-range of Ihh signaling associated defects

We commenced this study by reviewing the extent of Ihh-associated defects in the forelimbs of E16.5 $Evc^{-/-}$ embryos maintained on a C57BL/6J homogeneous background. The C57BL/6J phenotype being more severe than the mixed background phenotype of the mice used in our earlier study [20]. Similar to the tibia, the growth plates of the $Evc^{-/-}$ ulna and radius are shorter than that of their wild-type littermates and have reduced regions of proliferative and hypertrophic chondrocytes (Fig. 1A and Supplementary Fig. S1). Likewise in situ hybridization (ISH) in the $Evc^{-/-}$ forelimbs confirmed *Ihh* expression to be normal, but expression of the Ihh downstream targets *Ptch1*, *Gli1* and *Pthrp* in chondrocytes to be diminished. Decreased levels of *Ptch1*, *Gli1 and Hedgehog interacting protein* (*Hhip*) [24], were also detected in the inner perichondrium and primary spongiosa osteoblasts of the mutant bones. Conversely the expression of *Ptch1*, *Gli1* and *Pthrp* was upregulated in the outer perichondrial cell layers (Fig. 1B, black arrows). Of note, in all of the bones examined of the knockouts (ulna/radius and digital bones), the reduction of *Ptch1* expression was greater in the distal growth plate (Fig. 2B and Supplementary Fig. S3). Incorporation of resting chondrocytes into the columnar zone is stimulated by Ihh [25,26]. Analysis of this process in C57BL/6J mice using *Fgfr3* and *Fgfr1* as markers for columnar and resting chondrocytes respectively, showed expansion of the *Fgfr1* expression domain in $Evc^{-/-}$ forelimbs, indicating delayed differentiation of resting chondrocytes into columnar chondrocytes in the absence of Evc (Fig. 1D). The *Fgfr3* positive region was markedly shortened in $Evc^{-/-}$ forelimbs, a defect primarily associated to low Pthrp levels [20]. Failure to detect expansion of the *Fgfr1* domain in the tibia of C57BL/6J;129 $Evc^{-/-}$ mice is likely to result from background differences [20]. Phenotypic variability is also a common feature among EvC patients. *Bmp2*, *Bmp4* and *Wnt7b* are genes which have been suggested to be regulated by Ihh in the perichondrium, so we checked their expression in $Evc^{-/-}$ mice [27–29]. *Bmp2* was expressed normally in perichondrial and hypertrophic cells of Evc deficient mice, but the amount of *Bmp4* and *Wnt7b* transcripts was diminished in the $Evc^{-/-}$ perichondrium (Fig. 1C). Thus these data are consistent with *Bmp4* and *Wnt7b*, but not *Bmp2* being regulated

by Evc-mediated Ihh signaling. Examination of the area of terminally differentiated chondrocytes revealed no differences in the expression of the angiogenesis marker *Vegf* (Vascular endothelial growth factor) and the metalloproteinase *Mmp13* between normal and mutant embryos at E16.5. The mRNA levels of the *Mmp9* metalloproteinase were also unchanged in the $Evc^{-/-}$ primary spongiosa, but were

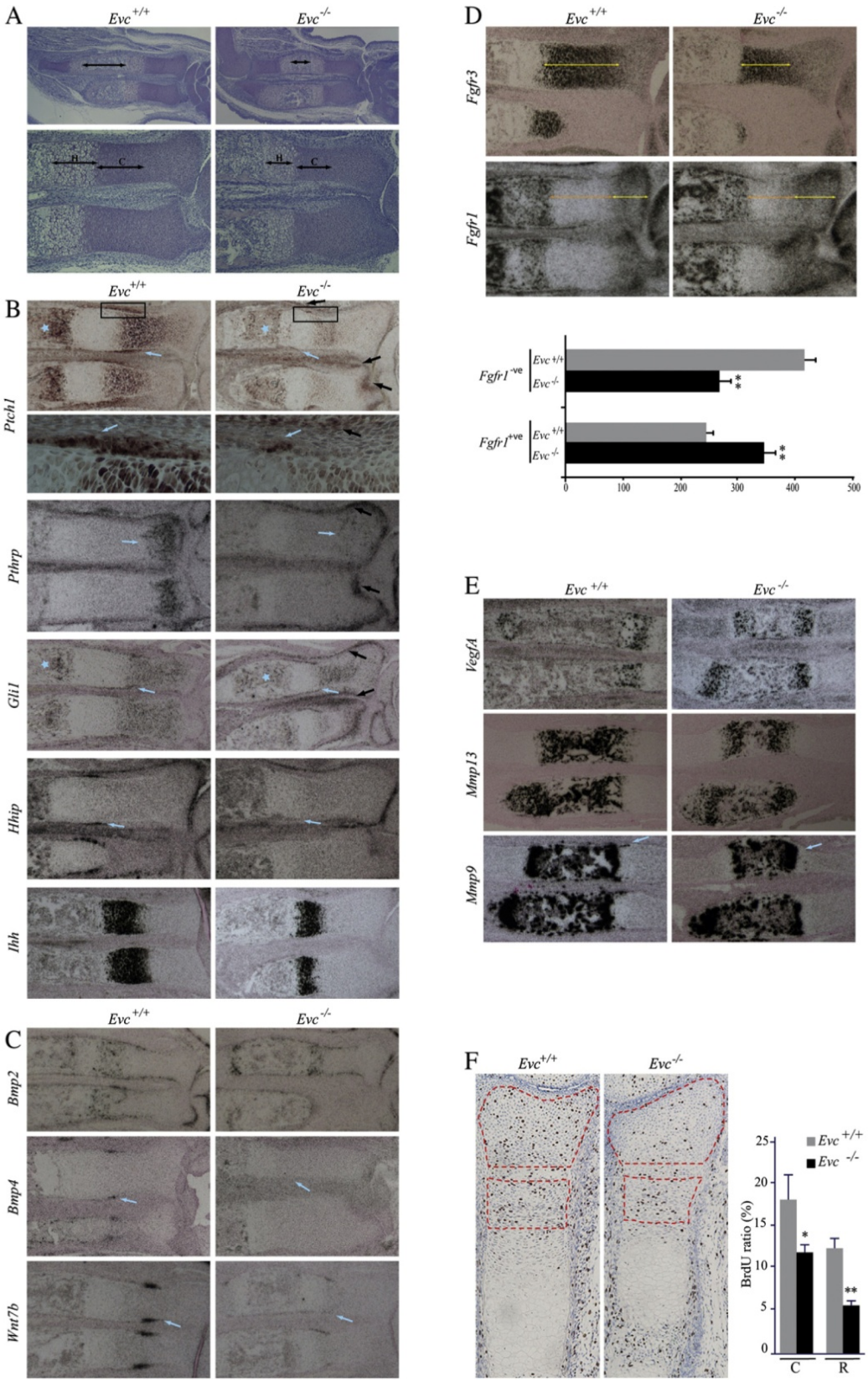

diminished in the region of the *Evc*$^{-/-}$ perichondrium surrounding the hypertrophic chondrocytes (Fig. 1E). Since *Mmp9* was shown ectopically expressed in the perichondrium of *Ptch1*$^{c/-}$*;Col2a1-Cre* conditional mice, which are characterized by increased Ihh signaling, this data provides further evidence that perichondrial *Mmp9* expression is Ihh dependent [30]. Expression of cartilage extracellular matrix genes was unaffected in *Evc*$^{-/-}$ embryos except for chondrocytes immediately adjacent to the perichondrium, which in some sections, were found retaining *Aggrecan* and *Link protein* expression, suggesting delayed maturation of these cells (Supplementary Fig. S2, black arrows).

Chondrocyte proliferation is regulated by Evc

We previously described chondrocyte proliferation to be normal in *Evc*$^{-/-}$ mice based on BrdU uptake in a fixed area of the columnar region [20]. Here we have evaluated the percentage of BrdU positive nuclei in the new C57BL/6J genetic background by counting the total number of labeled and non-labeled nuclei in both the columnar and resting zones of the growth plate separately. This analysis showed that the proliferation rate of *Evc*$^{-/-}$ chondrocytes is reduced, this being more pronounced in the resting zone (Fig. 1F). A 56% drop in cell division was detected in the resting region ($p = 0.0008$) and a 33% drop was recorded in the columnar zone ($p = 0.038$).

Evc is required for chondrocyte hypertrophy and induces bone collar and primary spongiosa formation at the early stages of endochondral ossification

To study the role of Evc during the first stages of ossification we analyzed the skeletal rudiments inside the central digit of the E18.5 hindpaws which at this time are undergoing sequential endochondral ossification. Whole mount Alcian blue/Alizarin red staining of E18.5 *Evc*$^{-/-}$ hindpaws showed delayed bone mineralization and ISH analysis proved deficient *Ptch1* expression in the mutant digital bones (Figs. 2A, B and Supplementary Fig. S3). Molecular analysis of E18.5 central metatarsals demonstrated that chondrocytes located at the periphery of the primary ossification center were decelerated in their progression toward terminal differentiation in the knockouts. They did not have the characteristic shape of hypertrophic chondrocytes and expressed proliferative (*Sox9* and *Col2a1*), prehypertrophic (*Ihh* and the Pth/Pthrp receptor gene, *Pth1r*) and hypertrophic (*Col10a1*) markers simultaneously. In contrast in the equivalent metatarsal of control mice there were two regions of *Col10a1* expressing chondrocytes separated by primary spongiosa (Fig. 2C). Clear transitions between proliferative, prehypertrophic and hypertrophic chondrocytes were already established across the template of the first phalanx of the same digit in normal mice despite this element being at an earlier point of development (Supplementary Fig. S3). Delayed hypertrophy of the more peripheral chondrocytes was also found in the ulna and radius of *Evc*$^{-/-}$ mutants at E14.5 demonstrating that this defect is not metatarsal bone-specific (Supplementary Fig. S3).

Subsequently we compared the normal and mutant E18.5 middle metatarsal perichondriums. While in wild-type embryos the osteoblast marker *Pth1r* was expressed in the perichondrial cells of this bone and the von-Kossa technique revealed the presence of a mineralized bone collar, no *Pth1r* expression or mineralization was detected in the mutant perichondrium (Figs. 2D and F). Expression of the transcription factor *Runx2*, a principal trigger of osteoblast differentiation and a perichondrial target of Ihh signaling, was also reduced in the *Evc*$^{-/-}$ perichondrium (Fig. 2D) [31]. Therefore the onset of osteoblastogenesis is delayed in *Evc*$^{-/-}$ mice. Moreover the morphological appearance of E18.5 *Evc*$^{-/-}$ metatarsals on paraffin sections suggested delayed primary spongiosa development in the knockout mice. To confirm this we performed TRAP staining, a technique that specifically labels chondroclasts and osteoclasts. These cells emerge after the invasion of the bone elements by blood vessels and thus are markers for primary spongiosa. TRAP-positive cells were present in the normal metatarsal but were absent from the mutant bone indicating delayed blood vessel invasion of the *Evc*$^{-/-}$ primary ossification center (Fig. 2F).

Osteoblast differentiation at the leading edge of the bone collar is impaired in Evc$^{-/-}$ *mice*

A hallmark of *Evc*$^{-/-}$ bones is the presence of a shorter region of mineralization in the perichondrium adjacent to the pre-hypertrophic chondrocytes (Fig. 3A) [20]. In order to clarify the molecular basis of this defect and to gain insight into the development of the *Evc*$^{-/-}$ perichondrium we studied the expression of early (*Alkaline phosphatase (Alkp)*, *Col1a1* and *Runx2*), intermediate (*Osx* and *Pth1r*) and late (*Integrin binding sialoprotein* (*Ibsp*), and *Osteopontin (Osp)*) osteoblast markers in E16.5 forelimbs. The result of this analysis showed that the leading edge of expression of all of these genes in the perichondrium did not extend as far from the primary spongiosa in Evc mutants as in controls (Figs. 3B–D). However, despite the loss of Hh signaling in perichondrial and bone core *Evc*$^{-/-}$ osteoblasts, the intensity of the hybridization signals corresponding to osteoblast markers was similar between mutant and normal bones, apart from a small area of the perichondrium adjacent to the late proliferative chondrocytes which correlates with the distal border of perichondrial osteoblastogenesis (from now on DBPO). In the DBPO, the expression patterns of *Pth1r* and *Osx* are expanded in wild-type mice revealing the presence in this position of a cluster of cells of the osteoblast lineage (red arrowheads, Fig. 3C). In contrast in mutant mice the DBPO enlargements of the *Pth1r* and *Osx* hybridization signals were less noticeable (Fig. 3C). Anti-Osx immunohistochemistry confirmed reduced number of differentiated osteoblasts in the *Evc*$^{-/-}$ DBPO (Figs. 4E and H).

The onset of canonical Wnt/β-catenin signaling in the perichondrium is regulated by Evc

We used E16.5 forelimbs to investigate the expression of the β-catenin downstream targets *Tcf1*, *Dkk1* and *Apcdd1*, which are known to be expressed in bone [27,32]. Just as we observed for the osteoblast markers, the distal edge of expression of the β-catenin targets in the perichondrium did not extend as far from the primary spongiosa in the Evc knockouts as in normal mice. *Tcf1* and *Apcdd1*

Fig. 1. Ihh signaling defects in the *Evc*$^{-/-}$ embryonic growth plate. A. H-E staining of E16.5 forelimb paraffin sections showing shortening of bones and reduced region of hypertrophic (H) and columnar (C) chondrocytes in *Evc*$^{-/-}$ mutants. B. Gene expression analysis by radioactive and non-radioactive ISH on paraffin sections demonstrating diminished expression of Ihh downstream targets in the forelimbs of E16.5 *Evc*$^{-/-}$ embryos. The boxed region is shown at higher magnification in the underneath panel (note residual expression of *Ptch1* in the *Evc*$^{-/-}$ perichondrium). Hybridization differences are indicated by blue arrows and the asterisk designates primary spongiosa osteoblasts. Black arrows point to increased Hh-response in the outer perichondrium of Evc mutants. C. Paraffin sections of E16.5 forelimbs hybridized with *Bmp2*, *Bmp4* and *Wnt7b* radioactively labeled riboprobes. Blue arrows indicate expression differences. D. Radioactive ISH on paraffin sections showing reduction of the *Fgfr3* expression domain and expansion of the *Fgfr1* expression pattern in the mutant forelimbs at E16.5. The lower panel represents a comparison of the length (abscise axis, μm) of the *Fgfr1* positive (+ve, yellow arrow) and negative (− ve, orange arrow) regions of the radius between normal and mutant mice. Measurements were taken from 3 different pairs of littermates, ** = $p < 0.001$. E. Radioactive ISH analysis on E16.5 forelimb paraffin sections using markers for terminally differentiated chondrocytes. Diminished expression of *Mmp9* in the *Evc*$^{-/-}$ perichondrium is indicated by an arrow. H. BrdU immunohistochemistry and percentages of labeled chondrocytes measured in the resting (R) and columnar (C) regions of the distal growth plate of the radius at E16.5. Dotted lines delineate the two regions that were counted separately. $n = 3$, * = $p < 0.05$, ** = $p < 0.001$. (For interpretation of the references to color in this figure legend, the reader is referred to the web version of this article.)

were strongly expressed in the DBPO in normal embryos, but the expression of these genes was weaker in the equivalent region of the knockouts (Fig. 3E). Consistent with this, the number of cells in which β-catenin localized to the nucleus was higher in wild-type embryos (Fig. 3F). Excluding the DBPO, the expression levels of β-catenin signaling components in the remaining cortical and primary spongiosa

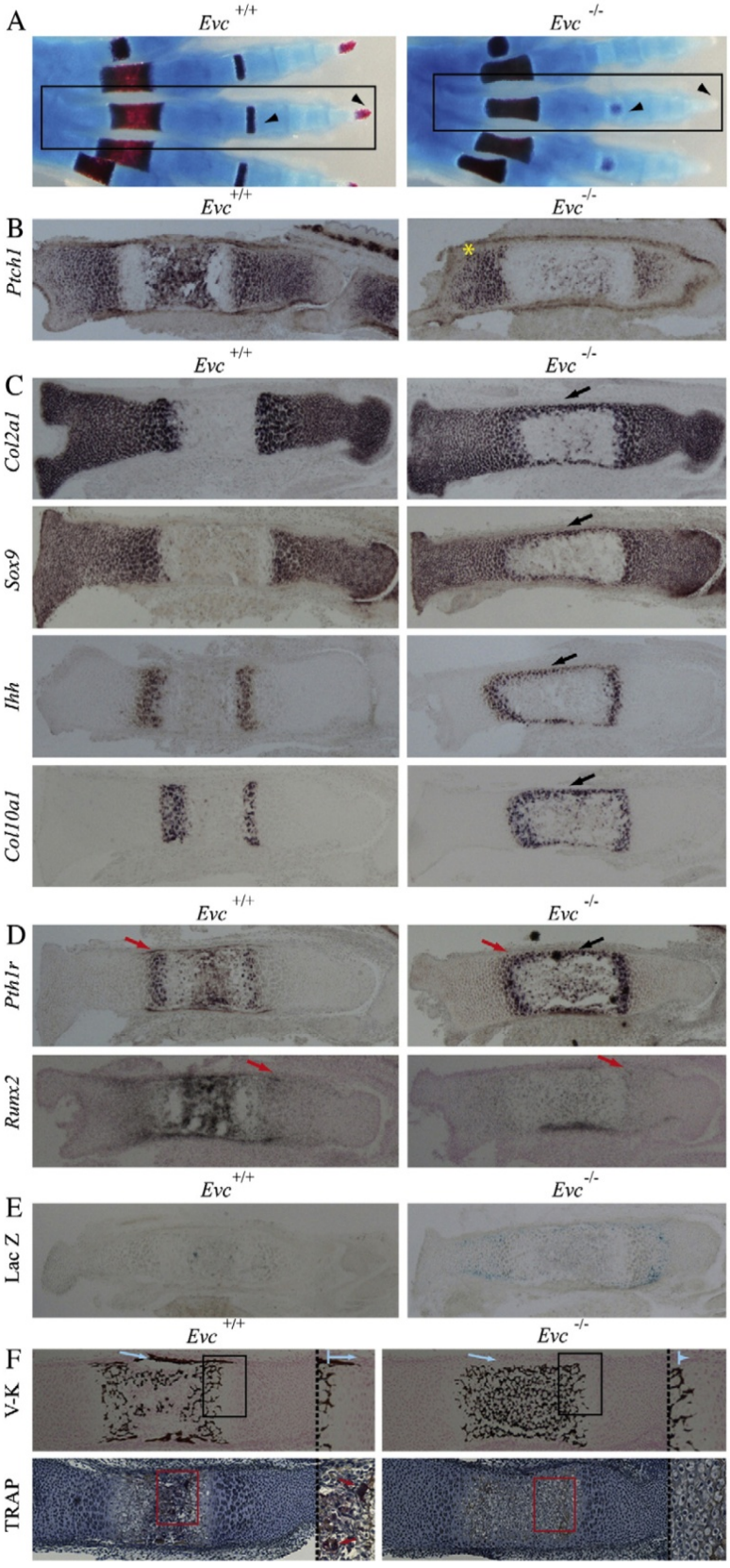

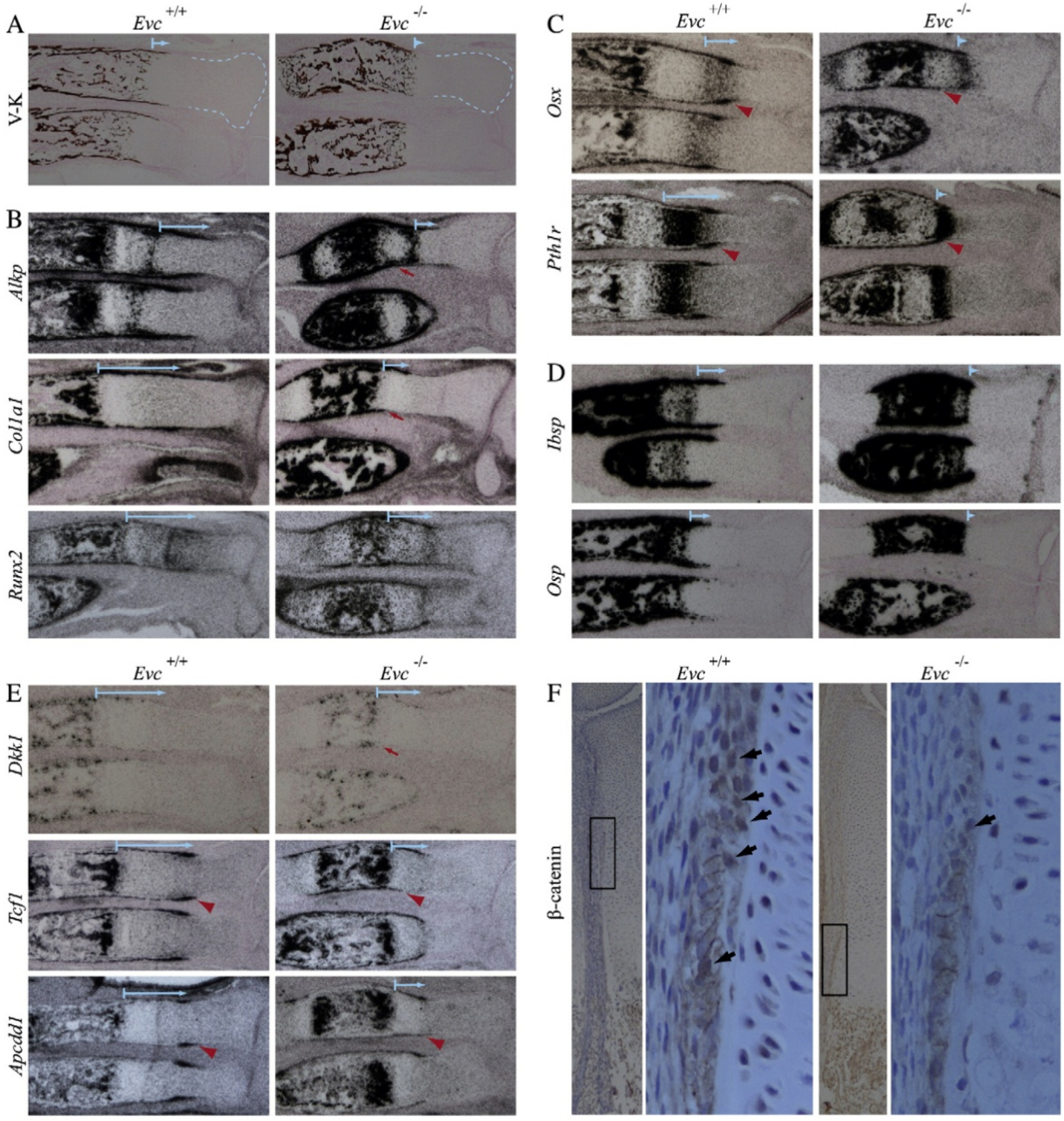

Fig. 3. Osteoblast development is impaired at the leading edge of the *Evc*$^{-/-}$ bone collar. A. E18.5 forelimb sections stained with von-Kossa. B–E. E16.5 forelimb paraffin sections hybridized with radioactively labeled riboprobes corresponding to early (B), intermediate (C) and late (D) osteoblast markers and Wnt/β-catenin target genes (E). The extent of the expression domain of each gene in the perichondrium starting from the hypertrophic chondrocytes or the primary spongiosa is shorter in Evc mutants than in controls and is indicated by blue arrows. Red arrowheads point to the widening of the *Osx*, *Pth1r*, *Tcf1* and *Apcdd1* hybridization signals in the DBPO. The red arrows designate asymmetrical expression of markers in the *Evc*$^{-/-}$ radius. F. β-catenin immunohistochemistry showing membrane staining in normal and mutant DBPO cells at E16.5 but increased number of cells with β-catenin in the nucleus (arrows) in wild-type mice. Boxed areas are enlarged on the right panels. (For interpretation of the references to color in this figure legend, the reader is referred to the web version of this article.)

osteoblasts showed no differences between normal and mutant littermates. Asymmetrical expression of Wnt/β-catenin signaling targets and osteoblast markers was consistently observed in the mutant radius (Fig. 3, red arrows). Whilst the mechanism for this is unclear, it could be one of the factors contributing to the bowing of this bone that occurs in C57BL/6J *Evc*$^{-/-}$ mice (data not shown).

Fig. 2. Evc promotes chondrocyte hypertrophy and stimulates development of both bone collar and primary spongiosa at the early stages of endochondral ossification. A. Whole mount Alcian blue/Alizarin red staining of E18.5 hindpaws. The central digit is squared and ossification differences are indicated by arrowheads. B–D. ISH analysis on E18.5 central metatarsal paraffin sections with the indicated probes showing reduced response to Ihh (B), hypertrophic delay of chondrocytes surrounding the primary ossification center (C) and impaired osteoblast differentiation (D). Black and red arrows highlight differences in chondrocyte hypertrophy and osteoblast differentiation respectively. The asterisk indicates less reduction of *Ptch1* expression in the proximal growth plate of this bone. E. X-Gal staining of E18.5 central metatarsal cryosections reports *Evc*-driven LacZ expression, wild-type cryosections were stained as control. F. Paraffin sections of E18.5 middle metatarsal stained with von-Kossa (V-K, top panels) or TRAP-staining (lower panels) demonstrating delayed formation of both bone collar and primary spongiosa in the knockouts. Higher magnifications of the squared regions are separated by dashed lines. Arrows point to mineralization and TRAP positive cells. (For interpretation of the references to color in this figure legend, the reader is referred to the web version of this article.)

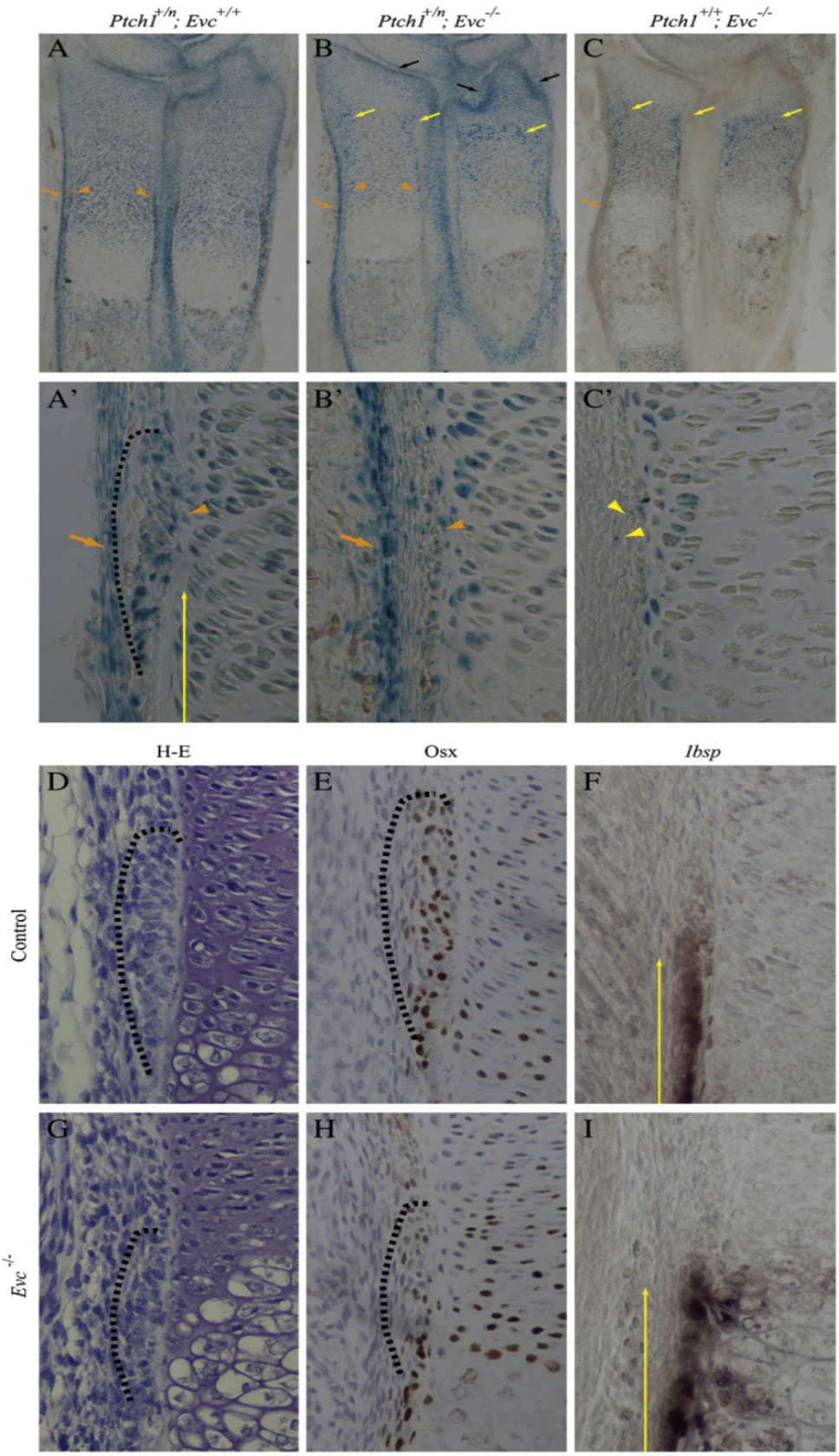
Ptch1+/n; Evc+/+
Ptch1+/n; Evc-/-
Ptch1+/+; Evc-/-
A
B
C
A'
B'
C'
H-E
Osx
Ibsp
D
E
F
G
H
I
Control
Evc-/-

Evc mediates Hh signaling in the osteogenic perichondrium but not in the external perichondrial region

In order to characterize the different types of Hh-responsive cells that are present in the embryonic perichondrium we used β-galactosidase staining in forelimb cryostat sections from E16.5 *Ptch1-LacZ* reporter mice (*Ptch1*$^{+/n}$). These mice carry the β-galactosidase reporter under control of the *Ptch1* promoter [21]. Robust LacZ activity in the inner perichondrium of *Ptch1*$^{+/n}$ embryos begins in a clump of tightly packed cells adjacent to the late proliferative chondrocytes which are arranged in a half-moon-like shape with respect to the longitudinal axis of the growth plate (Figs. 4A and A′, orange arrowheads). Immunohistochemistry in parallel sections showed that these cells correlate with the leading edge of nuclear Osx staining and so their position matches the DBPO (Figs. 4D–E). In the equivalent region of *Evc*$^{-/-}$ embryos there are fewer Osx positive cells which on H–E examination appeared to have lost the wild-type organization (Figs. 4G–H). Perichondrial cells immediately beneath the DBPO have stronger β-galactosidase activity than DBPO cells, and are positive for the bone matrix gene *Ibsp*, so they are in a more advanced stage of osteogenic differentiation (Figs. 4A′ and F, vertical yellow arrow). Looking at the outer layers of the perichondrium we observed a string of elongated fibroblastic-like cells with high β-galactosidase activity that encompasses the entire bone element. Interestingly these cells lie adjacent to the differentiating bone collar osteoblasts of the inner perichondrium in the central region of the bone (Figs. 4A, A′ and Supplementary Fig. S4). To assess the effect of the Evc mutation on *Ptch1* driven β-galactosidase in the perichondrium we generated double heterozygous *Ptch1*$^{+/n}$;*Evc*$^{+/-}$ mice and crossed the males from this genotype to *Evc*$^{+/-}$ females. Although both the *Ptch1* and the *Evc* targeted alleles carry a *LacZ* reporter controlled by their respective promoters, the β-galactosidase activity from the *Evc* allele is considerably weaker than the LacZ activity driven by the *Ptch1* promoter, so we were able to recognize differences in *Ptch1-LacZ* expression between *Ptch1*$^{+/n}$;*Evc*$^{+/+}$ and *Ptch1*$^{+/n}$;*Evc*$^{-/-}$ mice. As expected, *Ptch1-LacZ* activity was reduced in *Ptch1*$^{+/n}$;*Evc* $^{-/-}$ chondrocytes and osteoblasts, but it was not inhibited in the outer regions of the *Ptch1*$^{+/n}$;*Evc* $^{-/-}$ perichondrium. Thus Evc is not required for Hh signaling in the external perichondrial layers (Figs. 4B, B′ and Supplementary Fig. S4). No staining was observed in the outer perichondrium of *Ptch1*$^{+/+}$;*Evc*$^{-/-}$ mice indicating that *Evc* is expressed at lower levels if at all in this region (Figs. 4C, C′ and Supplementary Fig. S4). The skeletal phenotype of *Ptch1*$^{+/n}$;*Evc*$^{-/-}$ mice recapitulates the *Evc*$^{-/-}$ phenotype.

Evc is expressed along the osteoblast primary cilium and is required for transduction of the Hh signal in osteoblasts

To establish whether Evc is directly required in osteoblasts for the intracellular transduction of the Hh signal, we assayed the state of Hh signaling in cultured osteoblasts from mutant embryos. To do this we developed primary osteoblast cultures from the calvaria of E18.5 embryos and we treated them with the Smo agonist purmorphamine or its carrier DMSO [33]. 72 h later we isolated RNA and performed quantitative RT-PCR. Following purmorphamine treatment induction of *Ptch1*, *Gli1* and *Hhip* expression was significantly lower in *Evc*$^{-/-}$ osteoblasts than in wild-type cells, confirming that Evc is required for Hh signal transduction at a level downstream of Smo in osteoblasts (Fig. 5A). *Evc* expression remained unchanged following the activation of the Hh pathway (Fig. 5A). To learn about the Evc subcellular localization in osteoblasts we generated an anti-Evc monoclonal antibody. On Western blot analysis this detected a band of the expected size (113 kD) in protein extracts from wild-type and heterozygous primary osteoblast cultures but not in the corresponding lysates from mutant cells demonstrating both that Evc is expressed in osteoblasts and the specificity of the antibody (Fig. 5B). Immunofluorescence analysis using this antibody identified Evc along osteoblast primary cilia in keeping with its localisation in chondrocytes and the role of primary cilia in Hh signal transduction [20]. No signal was observed in cilia of *Evc*$^{-/-}$ osteoblasts (Figs. 5C–D).

Evc$^{-/-}$ *mice exhibit morphological defects at the base of the cranium*

Bones of the base of the cranium are formed by endochondral ossification and have growth plates known as synchondroses. Each synchodrosis consisting in two mirror-image growth plates which share a common central zone of reserve cartilage and have opposite regions of proliferating and differentiating chondrocytes [34]. As Ihh regulates cranial base development, we investigated whether Evc is required for this process [35]. Comparison of the base of the cranium between normal and *Evc*$^{-/-}$ littermates by whole-mount Alcian blue/Alizarin red staining and micro-CT scanning revealed normal development of the basioccipital region, but notable morphological defects at the frontal side of the cranial base in the mutant embryos (Fig. 6). At E17.5 there is a hole in the basisphenoid bone of the Evc knockouts and the presphenoid ossification center has not yet been developed. In addition a midline gap in the presphenoidal cartilage was noticed in the mutant genotype (Fig. 6A). At the neonatal stage the hole in the basisphenoid still persists in *Evc*$^{-/-}$ pups and the presphenoid bone now appears morphologically altered and partially fused to the basisphenoid leaving almost no intrasphenoidal (IS) cartilage in between. In three out of the five *Evc*$^{-/-}$ newborn mice analyzed the presphenoid bone was split in the middle (Fig. 6B).

Histological and gene expression analysis of the base of the cranium at E18.5 showed that while in control mice the basisphenoid bone was preceded by a well-defined region of *Col2a1* expressing chondrocytes flanked by hypertrophic chondrocytes (the IS synchondrosis), in the equivalent region of *Evc*$^{-/-}$ mice, chondrocytes were not arranged in a characteristic synchondrosis, and instead there was widespread expression of *Col2a1*, *Col10a1* and *Ihh* (Fig. 7). *Ptch1* expression was downregulated in perichondrial and primary spongiosa osteoblasts and in chondrocytes of the mutant cranial base. The reduction of *Ptch1* expression in *Evc*$^{-/-}$ spheno-occipital (SO) chondrocytes is less severe than in chondrocytes from the more anterior part of the cranium or than in osteoblasts, but the gradient of *Ptch1* expression is disrupted in the SO synchondrosis. As a result chondrocytes in the center of the SO synchondrosis were found expressing abnormal increased levels of *Ptch1* in some mutant sections (Fig. 7B). This is equivalent to the overexpression of Hh targets that takes place in the articular perichondrium of *Evc*$^{-/-}$ tubular bones. In keeping with the role of Evc in promoting hypertrophy,

Fig. 4. Hh-responsive cells in normal and *Evc*$^{-/-}$ embryonic perichondrium. A–C′. X-Gal staining of *Ptch1*$^{+/n}$;*Evc*$^{+/+}$, *Ptch1*$^{+/n}$;*Evc*$^{-/-}$ and *Ptch1*$^{+/+}$;*Evc*$^{-/-}$ E16.5 forelimb cryostat sections showing reduced expression of *Ptch1*-driven β-galactosidase in osteoblasts and chondrocytes but not in outer perichondrial cells (orange arrows) of the *Ptch1*$^{+/n}$;*Evc*$^{-/-}$ genotype. Yellow arrows designate LacZ activity controlled by the *Evc* promoter and black arrows indicate increased Hh-response in the outer perichondrium in the absence of Evc. Orange arrowheads point to the DBPO to highlight the reduction of *Ptch1*-dependent X-Gal staining in DBPO cells of the *Ptch1*$^{+/n}$;*Evc*$^{-/-}$ genotype. Panels A′–C′ are higher magnification representative images of the DBPO of E16.5 radius from each genotype. Yellow arrowheads in C′ indicate weak *Evc-LacZ* expression in *Ptch1*$^{+/+}$;*Evc*$^{-/-}$ DBPO perichondrial cells proving positive transcriptional activity of the *Evc* promoter in these cells. D–I. From left to right, H-E staining (D and G), Osx immunohistochemistry (E and H) and non-radioactive ISH for *Ibsp* (F and I) performed on paraffin sections of the DBPO of E16.5 radius. The half-moon arrangement of osteoblast precursors at the DBPO which is disrupted in the knockouts is encircled by a dashed line. Note that there are less Osx-positive cells in the mutant DBPO. The vertical long yellow arrow in A', F and I designates cells with strong LacZ activity beneath the DBPO that express *Ibsp*. Control refers to wild-type littermates of the mutant embryos excepting for the Osx panel (G) in which the control is an *Evc*$^{+/-}$ heterozygote (*Evc*$^{+/-}$ heterozygous mice are phenotypically indistinguishable from wild-type mice). (For interpretation of the references to color in this figure legend, the reader is referred to the web version of this article.)

we detected residual expression of *Col2a1*, *Col10a1* and prehypertrophic markers in the periphery of the mutant basisphenoid ossification center (Fig. 7B, black arrows). Analysis of the SO perichondrium recapitulates the long bone phenotype, and so the leading edge of expression of *Tcf1*, *Apcdd1* and *Pth1r* and the distal border of von-Kossa staining were located nearer to the primary spongiosa in the *Evc*$^{-/-}$ SO

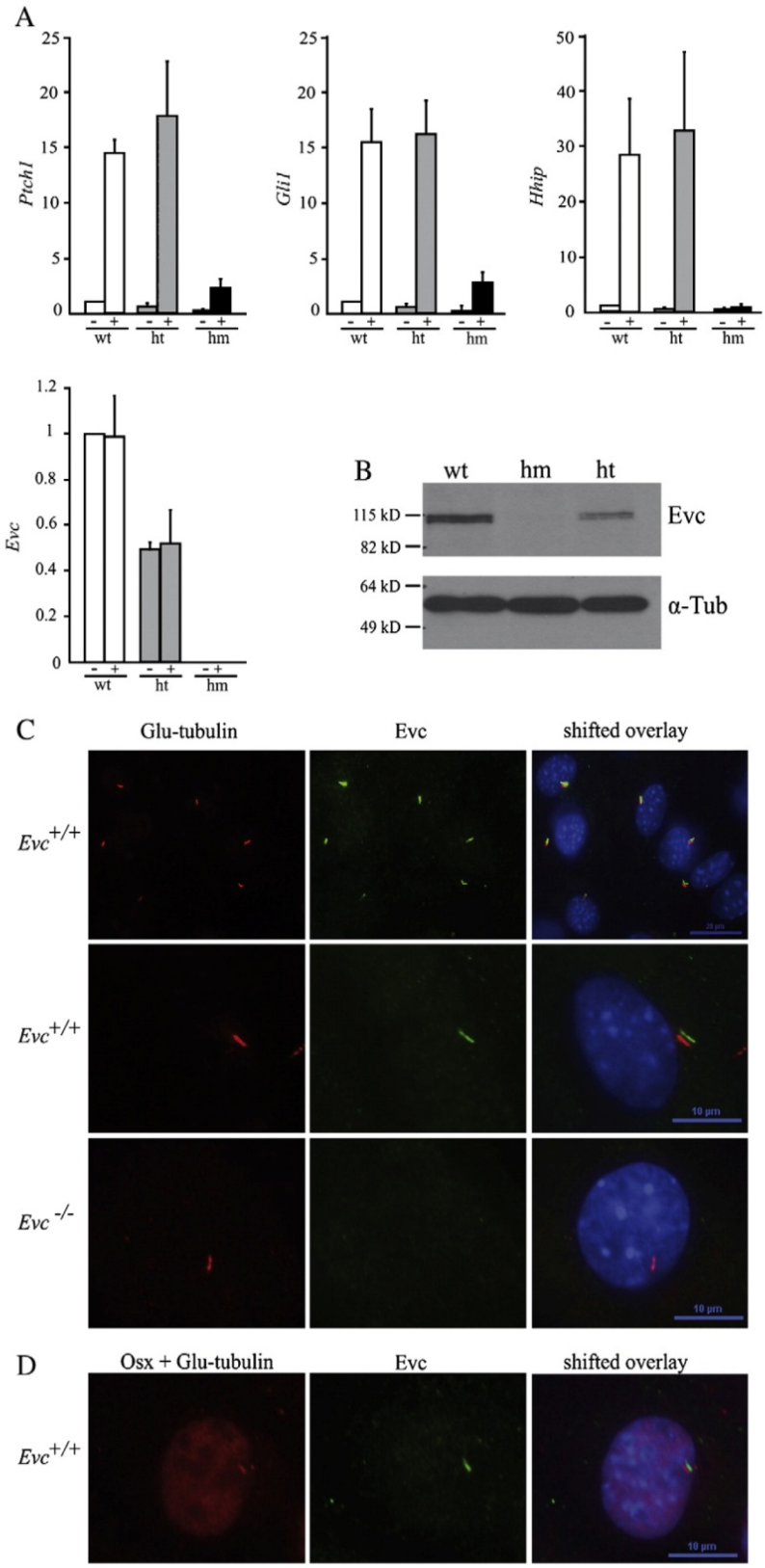

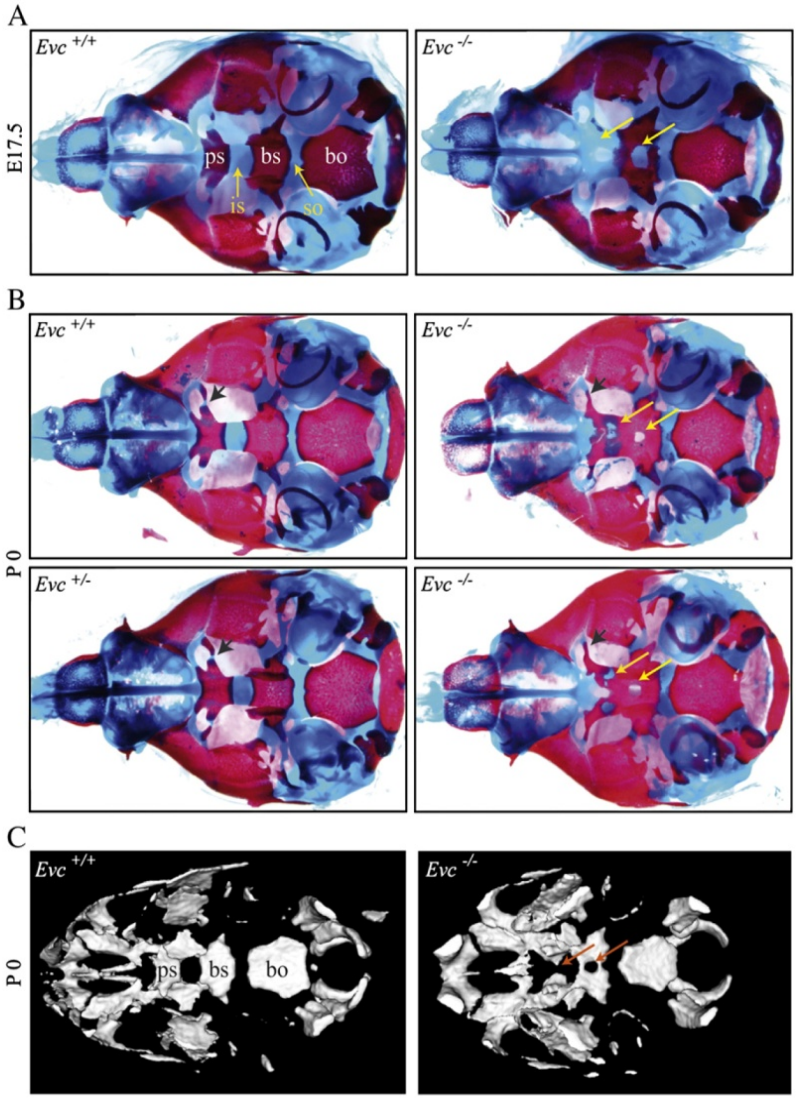

Fig. 6. Cranial base defects in $Evc^{-/-}$ mice. A–B. "Bird's-eye view" of wild type, heterozygous and $Evc^{-/-}$ cranial bases from E17.5 embryos and neonate mice (P0) analyzed by whole mount Alcian blue/Alizarin red staining. C. Micro-CT computed tomography showing the base of the skull of newborn mice. Locations of intrasphenoidal synchondrosis (is), spheno-occipital synchondrosis (so), presphenoid bone (ps), basisphenoid bone (bs) and basioccipital bone (bo) are indicated in the wild type pictures. The central hole in the basisphenoid and morphological alterations in the presphenoid bone of the $Evc^{-/-}$ genotype including midline clefts and premature synchondrosis closure are designated by yellow arrows. At E17.5 the presphenoid ossification center is not present in the mutant genotype. Small black arrows indicate early closure of a synchondrosis adjacent to the cranial base in the mutant mice. (For interpretation of the references to color in this figure legend, the reader is referred to the web version of this article.)

synchondrosis (Figs. 8A–B). Asymmetrical expression of osteoblast markers was also seen in the perichondrium of some mutant sections (Figs. 8A–B, red arrows). Proliferation measured by BrdU incorporation in SO chondrocytes was slightly reduced in the mutant mice (Fig. 8C).

Discussion

Here we have shown that Evc plays a major role in bone development by promoting all known regulatory aspects of Ihh signaling in the growth plates of the long bones and skull base. Decreased *Pthrp* expression in addition to reduced proliferation both explain the shortening of the region of columnar chondrocytes in Evc depleted mice, since low levels of Pthrp result in chondrocytes becoming hypertrophic prematurely [2]. Simultaneously, as Ihh induces chondrocyte maturation in a Pthrp-independent fashion, the hypertrophic delay of peripheral chondrocytes detected at the early ossification stages of the $Evc^{-/-}$ tubular bones and in the skull base, is in keeping with Evc augmenting also this branch of the Ihh pathway [5]. The first indication of the Ihh role in induction of hypertrophy came after the observation that chondrocyte differentiation was delayed in the

Fig. 5. Evc localizes to osteoblast primary cilia and is required for the intracellular transduction of the Hh signal in osteoblasts. A. Relative quantification of the mRNA levels of Hh target genes and *Evc* in E18.5 primary osteoblast cultures treated with purmorphamine (+) or its carrier DMSO (−) by qRT-PCR. Three genotypes, wild-type (wt), $Evc^{+/-}$ (ht) and $Evc^{-/-}$ (hm) were analyzed. The y-axis represents the mean of the $2^{-\Delta\Delta Ct}$ values ± SD for each genotype. Differences in *Ptch1*, *Gli1* and *Hhip* expression following purmorphamine treatment were only statistically significant between wild-type and homozygous littermates ($p \leq 0.005$, $n = 4$). B. Western blot analysis of protein extracts from cultured osteoblasts probed with an anti-Evc monoclonal antibody. α-Tubulin (α-Tub) loading control is shown underneath. C. Immunofluorescence analysis of primary calvarial osteoblasts stained with anti-Evc monoclonal antibody (green) and the cilia marker anti-Glu-tubulin (red). Nuclei are stained blue with DAPI. D. Same as in C except that an antibody against the osteoblast specific marker Osx (nuclear red staining) was also included in the assay demonstrating cilia localization of Evc in Osx-positive osteoblasts. (For interpretation of the references to color in this figure legend, the reader is referred to the web version of this article.)

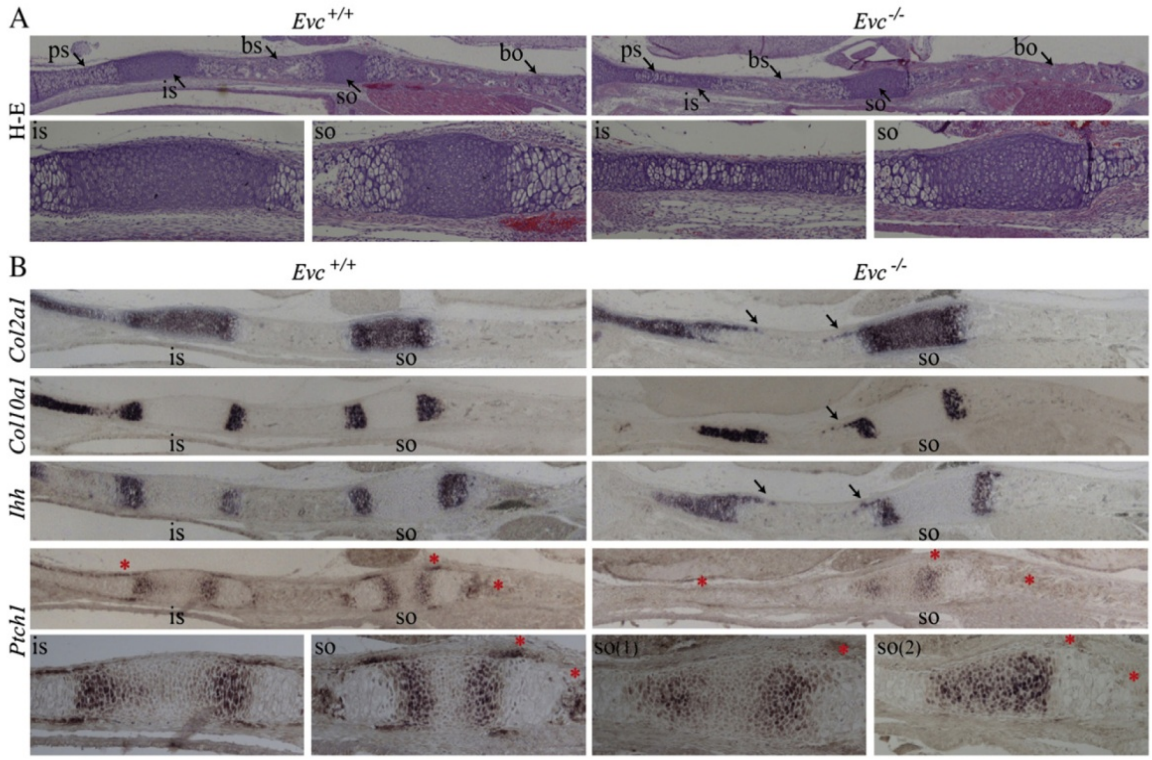

Fig. 7. *Evc*$^{-/-}$ mutants show altered synchondrosis development. A. H-E staining of sagittal sections of the base of the skull from E18.5 embryos showing lack of an organized IS synchondrosis in *Evc*$^{-/-}$ mutants. Lower panels are amplification pictures of intrasphenoidal (is, left) and spheno-occipital (so, right) synchondroses. B. Non-radioactive ISH analysis on E18.5 sagittal paraffin sections of the cranial base with the indicated probes. Residual expression of *Col2a1*, *Ihh* and *Col10a1* in the basisphenoid ossification center of *Evc*$^{-/-}$ mutants is designated with arrows. *Ptch1* expression is reduced in chondrocytes and in perichondrial and primary spongiosa osteoblasts of the mutant embryos (asterisks). For *Ptch1* magnification pictures are shown in the lower panels. There are two different sections of *Evc*$^{-/-}$ spheno-occipital synchondrosis (so(1) and so(2)) illustrating reduced *Ptch1* expression and loss of the *Ptch1* expression gradient. Intrasphenoidal synchondrosis (is), spheno-occipital synchondrosis (so), presphenoid bone (ps), basisphenoid bone (bs) and basioccipital bone (bo). Mutant sections comprising midline clefts were avoided in this figure.

humeri of E14.5 *Ihh* null embryos [4]. This is also manifested later at E18.5 in the bones of *Ihh* null and *Ihh*$^{c/c}$;*Col2a1-Cre* conditional mice by the presence of a core of hypertrophic chondrocytes surrounded by less mature cells [3,4]. Chondrocytes surrounding the primary ossification center of the E15.5 tibia from *Smo*$^{c/c}$;*Col2a1-Cre* and *Pthrp*$^{-/-}$;*Smo*$^{c/c}$;*Col2a1-Cre* embryos have been described too with delayed hypertrophic maturation [5]. Thus taking the data from all of these mutants together, we postulate that chondrocytes within the same transverse plane of the growth plate differ in their requirements to reach terminal differentiation. The requirement for Ihh signaling being greater in chondrocytes of the more outer layers of the growth plate. Consistent with this Evc-LacZ expression is higher in the outer layers of chondrocytes suggesting that increased levels of Evc could be required to potentiate signaling in these regions. Impaired chondrocyte maturation explains the delay in primary spongiosa formation of the Evc knockouts, as hypertrophic cells produce angiogenic factors such as Vegf that attract blood vessels, which are vital for primary spongiosa induction.

Ihh signaling is essential for bone collar development [3,4]. More precisely, Hh signaling was shown to be specifically required in the perichondrium for osteoblast development, since perichondrial cells lacking Smo failed to undergo osteoblast differentiation [31]. Thus the severe reduction in Hh target gene expression in the perichondrium of Evc mutants is the likely cause of the delay in bone collar formation observed in these mice at the early stages of endochondral development and the reduced number of differentiated osteoblasts in the DBPO at later stages. Advancement of the DBPO, has been described in *Trps1* $^{\Delta GT/\Delta GT}$ mice in which Ihh signaling is amplified [36]. However compared to the complete lack of osteoblasts of *Ihh*$^{-/-}$ mice, it is surprising that osteoblast differentiation is only mildly affected in the Evc knockouts. In fact excluding the DBPO, expression of osteoblast markers is normal in Evc depleted embryos. In this context ISH analysis showed some, albeit weak, expression of *Ptch1* and *Gli1* in the inner perichondrium of *Evc* $^{-/-}$ mice, indicating that loss of Evc does not totally abrogate the response to Ihh in this region (Fig. 1B). This low level of response to Ihh is then sufficient to allow osteoblast differentiation, but insufficient for normal bone collar development. It is worth mentioning that during the course of our E16.5 ISH experiments we often observed that the border between proliferative and hypertrophic chondrocytes and between these and the primary spongiosa was not a straight horizontal line, as in the normal littermates, but a curve, indicating delayed differentiation of the chondrocytes adjacent to the perichondrium also at this stage (Supplementary Fig. S2, black arrows). Thus, it is possible that, in addition to loss of Ihh signaling in perichondrial cells, delayed maturation of chondrocytes adjacent to perichondrium contributes to the bone collar defect of *Evc*$^{-/-}$ mice. As Mmp9 is involved in matrix degradation, calcification and vascularization, we cannot excluded that decreased *Mmp9* expression in the *Evc*$^{-/-}$ perichondrium is another factor influencing this process [37].

Wnt/β-catenin signaling is a key pathway of bone development that works downstream of Ihh signaling during osteoblast differentiation [27,30]. The data presented here indicates that Evc-mediated Ihh signaling regulates the onset of Wnt/β-catenin signaling in the perichondrium by determining the position at which mesenchymal cells initiate definitive osteoblast differentiation. Our observations also indicate that once mesenchymal cells are fully committed to osteogenic differentiation, β-catenin signaling functions independently of Ihh signaling. Several signaling cascades including Hh, Bmp4, Wnt7b, Pth/Pthrp and canonical Wnt/β-catenin converge at the

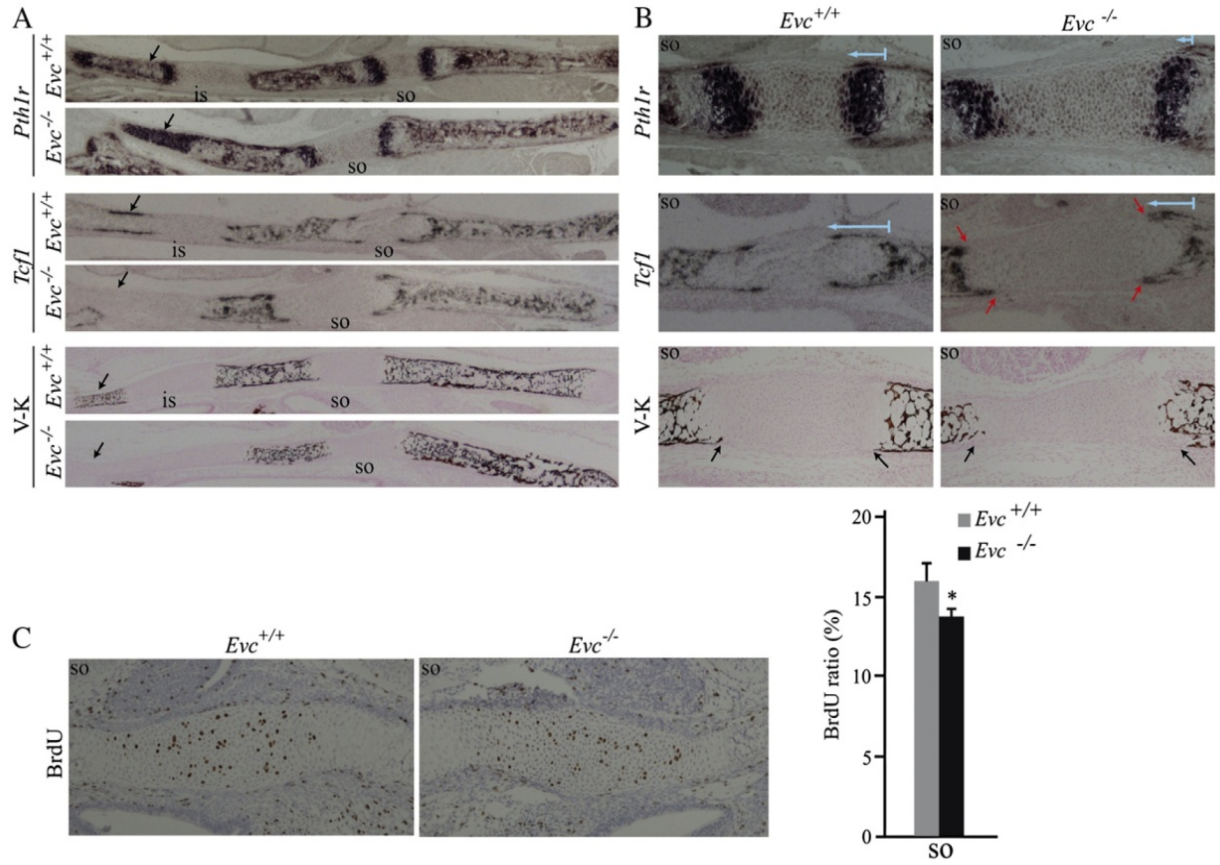

Fig. 8. Defects in osteoblast differentiation and chondrocyte proliferation in the $Evc^{-/-}$ SO synchondrosis. A. Gene expression analysis by radioactive and non-radioactive ISH of osteoblast markers and von-Kossa staining (V-K) on sagittal paraffin sections of the base of the skull at E18.5 showing delayed ossification and hypertrophy in the frontal region of the $Evc^{-/-}$ cranial base (black arrows). B. Higher magnification of the SO synchondroses shown in A. The leading edge of expression of osteoblast markers is located nearer to the primary spongiosa in the $Evc^{-/-}$ SO perichondrium (blue arrows) and bone collar mineralization is delayed (black arrows). Asymmetrical expression of osteoblast markers in the perichondrium is indicated with red arrows. C. BrdU immunohistochemistry and percentages of labeled chondrocytes in SO synchondroses at E16.5. n = 3, * = $p<0.05$. (For interpretation of the references to color in this figure legend, the reader is referred to the web version of this article.)

DBPO to promote differentiation of perichondrial cells into Osx-positive osteoprogenitors. DBPO osteoblast precursors are larger than the remaining mesenchymal cells and are arranged in a half-moon-like shape above the distal tip of the newly synthesized osteoid, an arrangement that is disturbed in $Evc^{-/-}$ mice (Figs. 4D–E, G–H and Supplementary Fig. S4). Mature osteoblasts secreting osteoid are however organized in a column next to the bone matrix (Figs. 4F, I and Supplementary Fig. S4). Therefore during mesenchyme to osteoblast differentiation there are changes in cell size, shape and organization which appear to require Ihh signaling. The non-canonical Wnt pathway has a key role in planar cell polarity [38]. As Wnt7b is a perichondrial target of Ihh signaling that has been shown to induce osteoblastogenesis via a non-cannonical mechanism it may be a mediator of these changes [27,39].

Hh-responsive cells in the outer perichondrium show robust *Ptch1*, *Gli1*, *Hhip* and *Pthrp* expression. The expression of Hh targets is upregulated in these cells in the Evc knockouts [20]. The function of the more external Hh-responsive cells of the perichondrium has not yet been studied. Whilst this layer may simply be a sink for Ihh and hence a barrier to further diffusion into surrounding tissues, it is likely that it has a more active role as cells in this layer express Pthrp. We hypothesize that the outer layer of Hh-responsive cells could play a role in shape specification and remodeling, a little understood process that is essential for integration of individual bones into a functioning skeleton.

Defects in the $Evc^{-/-}$ skull base are in agreement with the $Evc^{-/-}$ long bone phenotype. Excluding presphenoid midline clefts which have not been reported in the Ihh knockouts, $Evc^{-/-}$ mice mostly replicate the $Ihh^{-/-}$ cranial base phenotype, with both type of mutants having defects in the anterior side of the base of the skull, but not in the basioccipital region [35]. A similar hole in the center of the basisphenoid bone is present in $Gli3^{\Delta 699/\Delta 699}$ mice and in Ihh mutants indicating that this defect is also connected to diminished Hh signaling [40,41]. Given that Evc is an intracellular component of the Hh pathway, the presence of midline clefts in the anterior bones of the $Evc^{-/-}$ cranial base, which have not been noticed in the Ihh knockouts, could be explained if, as previously suggested, chondrocytes and osteoblasts of the base of the skull respond to Sonic hegehog in addition to the Ihh ligand [35].

In summary, we have demonstrated that in addition to the known function of Evc in Ihh-mediated control of hypertrophy through a Pthrp-dependent mechanism, Evc is also required for promoting hypertrophy, cell division and the incorporation of reserve chondrocytes into the columnar region. Three processes not known previously to be regulated by Evc. $Evc^{-/-}$ mice were reported earlier with delayed bone collar mineralization, but we did not identify the origin of this defect [20]. We now show that this arises from impaired osteoblast differentiation with osteoblasts at the leading edge of the bone collar relying heavily on Evc to emerge. In contrast, Evc depleted differentiated osteoblasts do not show significant variation in the expression of bone markers, regardless of having low levels of Hh signaling. From this we conclude that Evc is mainly required in the osteoblast lineage during the differentiation process. Finally, we unveil the presence of skull base defects in $Evc^{-/-}$ mice, which are more severe at the frontal region of the cranium. Although

cranial base defects have not been reported in individuals with EvC, on the light of the abnormalities described here in Evc null mice, they should be taken into consideration during clinical management of EvC patients.

Supplementary materials related to this article can be found online at doi:10.1016/j.bone.2011.08.025.

Acknowledgments

We are grateful to Fanxin Long, Matthew Hilton, Andrew McMahon, Andrea Vortkamp and Christine Hartman for ISH probes and to Danny Chan for the anti-Col X antibody. This work was funded by the Spanish Ministry of Science and Innovation (SAF-62291 and SAF-17901), the European Union (LSHM-CT-2007-03741) and the Ramón Areces Foundation.

References

[1] Kronenberg HM. Developmental regulation of the growth plate. Nature 2003;423:332–6.
[2] Vortkamp A, Lee K, Lanske B, Segre GV, Kronenberg HM, Tabin CJ. Regulation of rate of cartilage differentiation by Indian hedgehog and PTH-related protein. Science 1996;273:613–22.
[3] Razzaque MS, Soegiarto DW, Chang D, Long F, Lanske B. Conditional deletion of Indian hedgehog from collagen type 2alpha1-expressing cells results in abnormal endochondral bone formation. J Pathol 2005;207:453–61.
[4] St-Jacques B, Hammerschmidt M, McMahon AP. Indian hedgehog signaling regulates proliferation and differentiation of chondrocytes and is essential for bone formation. Genes Dev 1999;13:2072–86.
[5] Mak KK, Kronenberg HM, Chuang PT, Mackem S, Yang Y. Indian hedgehog signals independently of PTHrP to promote chondrocyte hypertrophy. Development 2008;135:1947–56.
[6] Logan CY, Nusse R. The Wnt signaling pathway in development and disease. Annu Rev Cell Dev Biol 2004;20:781–810.
[7] Day TF, Guo X, Garrett-Beal L, Yang Y. Wnt/beta-catenin signaling in mesenchymal progenitors controls osteoblast and chondrocyte differentiation during vertebrate skeletogenesis. Dev Cell 2005;8:739–50.
[8] Hill TP, Spater D, Taketo MM, Birchmeier W, Hartmann C. Canonical Wnt/beta-catenin signaling prevents osteoblasts from differentiating into chondrocytes. Dev Cell 2005;8:727–38.
[9] Huangfu D, Liu A, Rakeman AS, Murcia NS, Niswander L, Anderson KV. Hedgehog signalling in the mouse requires intraflagellar transport proteins. Nature 2003;426:83–7.
[10] Liu A, Wang B, Niswander LA. Mouse intraflagellar transport proteins regulate both the activator and repressor functions of Gli transcription factors. Development 2005;132:3103–11.
[11] Corbit KC, Aanstad P, Singla V, Norman AR, Stainier DY, Reiter JF. Vertebrate smoothened functions at the primary cilium. Nature 2005;437:1018–21.
[12] Haycraft CJ, Banizs B, Aydin-Son Y, Zhang Q, Michaud EJ, Yoder BK. Gli2 and Gli3 localize to cilia and require the intraflagellar transport protein polaris for processing and function. PLoS Genet 2005;1:e53.
[13] Rohatgi R, Milenkovic L, Scott MP. Patched1 regulates hedgehog signaling at the primary cilium. Science 2007;317:372–6.
[14] Haycraft CJ, Zhang Q, Song B, Jackson WS, Detloff PJ, Serra R, et al. Intraflagellar transport is essential for endochondral bone formation. Development 2007;134:307–16.
[15] Haycraft CJ, Serra R. Cilia involvement in patterning and maintenance of the skeleton. Curr Top Dev Biol 2008;85:303–32.
[16] Ruiz-Perez VL, Ide SE, Strom TM, Lorenz B, Wilson D, Woods K, et al. Mutations in a new gene in Ellis-van Creveld syndrome and Weyers acrodental dysostosis. Nat Genet 2000;24:283–6.
[17] Ruiz-Perez VL, Tompson SW, Blair HJ, Espinoza-Valdez C, Lapunzina P, Silva EO, et al. Mutations in two nonhomologous genes in a head-to-head configuration cause Ellis-van Creveld syndrome. Am J Hum Genet 2003;72:728–32.
[18] Tompson SW, Ruiz-Perez VL, Blair HJ, Barton S, Navarro V, Robson JL, et al. Sequencing EVC and EVC2 identifies mutations in two-thirds of Ellis-van Creveld syndrome patients. Hum Genet 2007;120:663–70.
[19] Valencia M, Lapunzina P, Lim D, Zannolli R, Bartholdi D, Wollnik B, et al. Widening the mutation spectrum of EVC and EVC2: ectopic expression of Weyer variants in NIH 3T3 fibroblasts disrupts Hedgehog signaling. Hum Mutat 2009;30:1667–75.
[20] Ruiz-Perez VL, Blair HJ, Rodriguez-Andres ME, Blanco MJ, Wilson A, Liu YN, et al. Evc is a positive mediator of Ihh-regulated bone growth that localises at the base of chondrocyte cilia. Development 2007;134:2903–12.
[21] Goodrich LV, Milenkovic L, Higgins KM, Scott MP. Altered neural cell fates and medulloblastoma in mouse patched mutants. Science 1997;277:1109–13.
[22] Lescher B, Haenig B, Kispert A. sFRP-2 is a target of the Wnt-4 signaling pathway in the developing metanephric kidney. Dev Dyn 1998;213:440–51.
[23] Hogan B. Manipulating the mouse embryo: a laboratory manual. 2nd ed. Plainview, N.Y.: Cold Spring Harbor Laboratory Press; 1994
[24] Chuang PT, McMahon AP. Vertebrate hedgehog signalling modulated by induction of a Hedgehog-binding protein. Nature 1999;397:617–21.
[25] Koziel L, Wuelling M, Schneider S, Vortkamp A. Gli3 acts as a repressor downstream of Ihh in regulating two distinct steps of chondrocyte differentiation. Development 2005;132:5249–60.
[26] Kobayashi T, Soegiarto DW, Yang Y, Lanske B, Schipani E, McMahon AP, et al. Indian hedgehog stimulates periarticular chondrocyte differentiation to regulate growth plate length independently of PTHrP. J Clin Invest 2005;115:1734–42.
[27] Hu H, Hilton MJ, Tu X, Yu K, Ornitz DM, Long F. Sequential roles of hedgehog and Wnt signaling in osteoblast development. Development 2005;132:49–60.
[28] Minina E, Wenzel HM, Kreschel C, Karp S, Gaffield W, McMahon AP, et al. BMP and Ihh/PTHrP signaling interact to coordinate chondrocyte proliferation and differentiation. Development 2001;128:4523–34.
[29] Pathi S, Rutenberg JB, Johnson RL, Vortkamp A. Interaction of Ihh and BMP/Noggin signaling during cartilage differentiation. Dev Biol 1999;209:239–53.
[30] Mak KK, Chen MH, Day TF, Chuang PT, Yang Y. Wnt/beta-catenin signaling interacts differentially with Ihh signaling in controlling endochondral bone and synovial joint formation. Development 2006;133:3695–707.
[31] Long F, Chung UI, Ohba S, McMahon J, Kronenberg HM, McMahon AP. Ihh signaling is directly required for the osteoblast lineage in the endochondral skeleton. Development 2004;131:1309–18.
[32] Hecht J, Seitz V, Urban M, Wagner F, Robinson PN, Stiege A, et al. Detection of novel skeletogenesis target genes by comprehensive analysis of a Runx2(−/−) mouse model. Gene Expr Patterns 2007;7:102–12.
[33] Sinha S, Chen JK. Purmorphamine activates the hedgehog pathway by targeting smoothened. Nat Chem Biol 2006;2:29–30.
[34] Roberts GJ, Blackwood HJ. Growth of the cartilages of the mid-line cranial base: a radiographic and histological study. J Anat 1983;136:307–20.
[35] Young B, Minugh-Purvis N, Shimo T, St-Jacques B, Iwamoto M, Enomoto-Iwamoto M, et al. Indian and sonic hedgehogs regulate synchondrosis growth plate and cranial base development and function. Dev Biol 2006;299:272–82.
[36] Napierala D, Sam K, Morello R, Zheng Q, Munivez E, Shivdasani RA, et al. Uncoupling of chondrocyte differentiation and perichondrial mineralization underlies the skeletal dysplasia in tricho-rhino-phalangeal syndrome. Hum Mol Genet 2008;17:2244–54.
[37] Vu TH, Shipley JM, Bergers G, Berger JE, Helms JA, Hanahan D, et al. MMP-9/gelatinase B is a key regulator of growth plate angiogenesis and apoptosis of hypertrophic chondrocytes. Cell 1998;93:411–22.
[38] Veeman MT, Axelrod JD, Moon RT. A second canon. Functions and mechanisms of beta-catenin-independent Wnt signaling. Dev Cell 2003;5:367–77.
[39] Tu X, Joeng KS, Nakayama KI, Nakayama K, Rajagopal J, Carroll TJ, et al. Noncanonical Wnt signaling through G protein-linked PKCdelta activation promotes bone formation. Dev Cell 2007;12:113–27.
[40] Abzhanov A, Rodda SJ, McMahon AP, Tabin CJ. Regulation of skeletogenic differentiation in cranial dermal bone. Development 2007;134:3133–44.
[41] Bose J, Grotewold L, Ruther U. Pallister–Hall syndrome phenotype in mice mutant for Gli3. Hum Mol Genet 2002;11:1129–35.

Supplementary Fig. S1. Evc deficient mice have short skeletal elements with reduced regions of proliferative and hypertrophic chondrocytes. Graphical representation of differences in the total length of the radius and in the length of the *Col2a1* and *Col10a1* expressing regions of this bone defined by ISH, between normal (wt) and *Evc*$^{-/-}$ (hm) mice at E16.5. Measurements were taken in 3 embryos of each genotype from 3 different litters. All differences were statistically significant, $p < 0.01$.

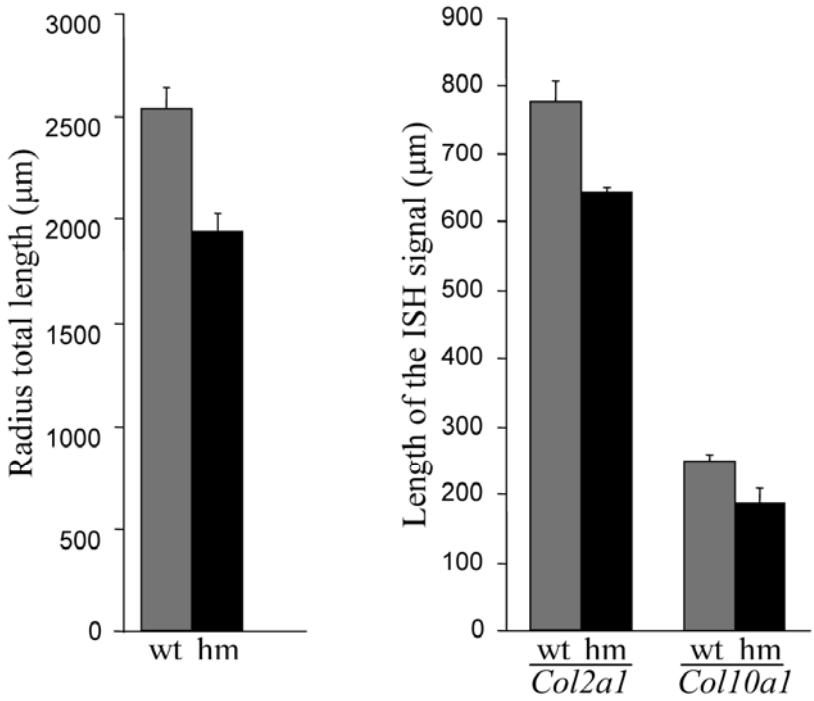

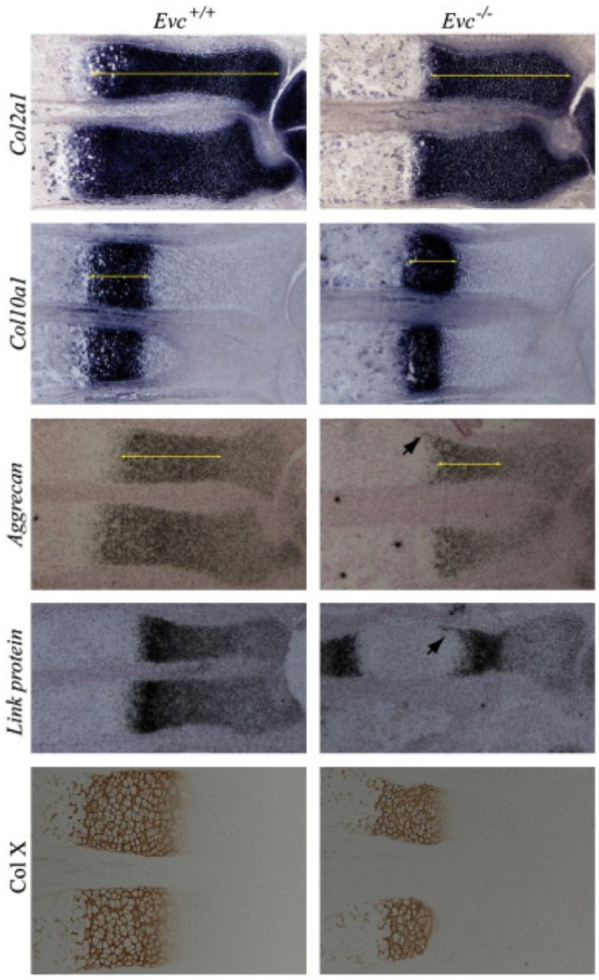

Supplementary Fig. S2. Expression of extracellular matrix markers in *Evc* $^{-/-}$ mice. **A.** ISH analysis of genes encoding extracellular matrix proteins on paraffin sections of E16.5 forelimbs. Delayed maturation of chondrocytes adjacent to the perichondrium is indicated with an arrow. **B.** Col X immunohistochemistry in E16.5 forelimbs.

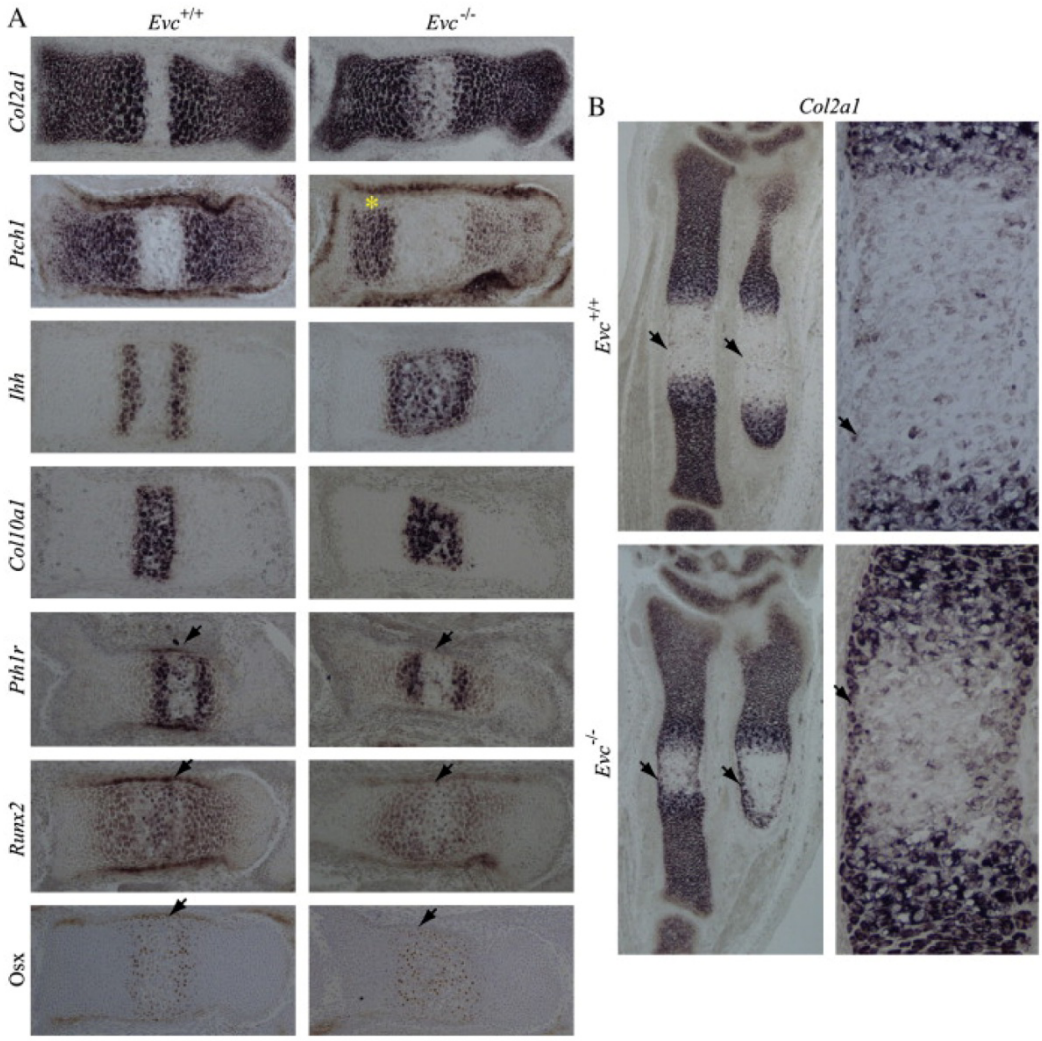

Supplementary Fig. S3. Delayed endochondral ossification in *Evc* $^{-/-}$ mice. **A**. Paraffin sections corresponding to the first phalange of the central digit of E18.5 hindpaws hybridized with the indicated probes and Osx-immunohistochemistry, showing a delay in chondrocyte hypertrophy and in bone collar development (arrow) in the mutant mice. Asterisk indicates less reduction of *Ptch1* expression in the proximal growth plate of the mutant bone. **B**. ISH for *Col2a1* on paraffin sections of E14.5 radius and ulna showing hypertrophic delay of peripheral chondrocytes in the mutant bones (arrows). Right panels are higher magnifications pictures of the normal and mutant primary ossification centers of the radius.

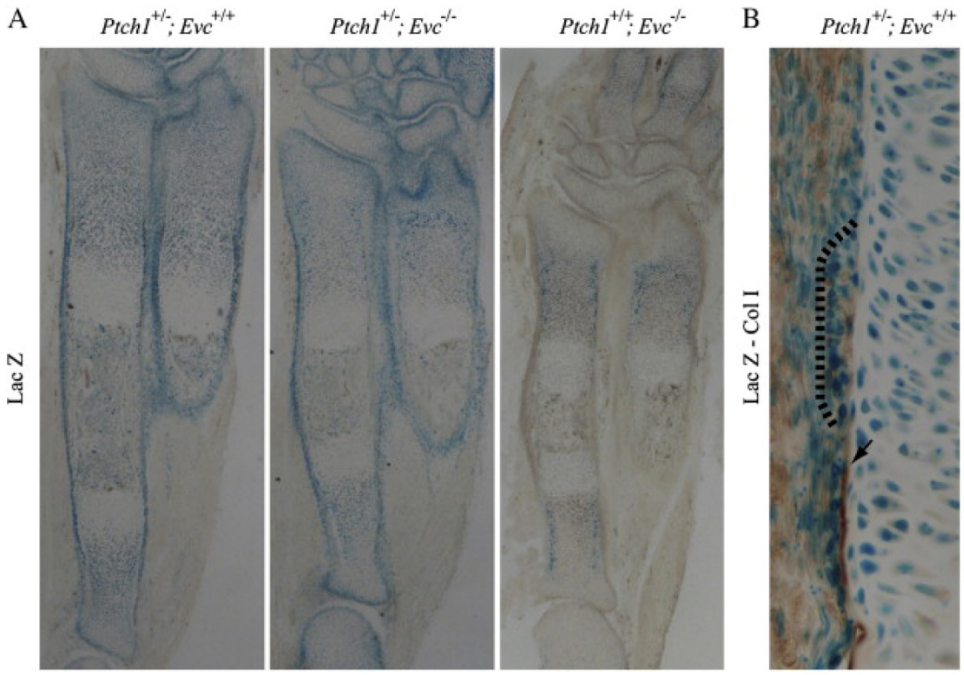

Supplementary Fig. S4. Hh-responsive cells in normal and *Evc* $^{-/-}$ perichondrium. **A**. Full view of *Ptch1*$^{+/n}$;*Evc*$^{+/+}$,*Ptch1*$^{+/n}$;*Evc*$^{-/-}$ and *Ptch1*$^{+/+}$;*Evc*$^{-/-}$ E16.5 forelimb cryosections stained with X-Gal B. X-Gal staining and Col-I immunohistochemistry co-localization in an E16.5 *Pcth1*$^{+/n}$;*Evc*$^{+/+}$ radius cryosection. DBPO cells which are bordered by a dashed line are above the distal border of Col-I-rich osteoid matrix (arrow).

Discusión

Análisis molecular en pacientes diagnosticados con Ellis-van Creveld.

Hasta la fecha los pacientes con EvC habían sido descritos con dos mutaciones en *EVC* o dos mutaciones en *EVC2* y fenotipos indistinguibles (Tompson et al., 2007), siendo una incógnita el fenotipo resultante de la inactivación simultánea de ambos genes. En el primer capítulo de este trabajo mostramos por primera vez individuos con mutaciones en *EVC* y en *EVC2* como consecuencia de una deleción mediada por retroelementos LINE-1. La deleción presente en los pacientes fue confirmada mediante técnicas de FISH, PCR e hibridación en arrays de SNPs y comprende los exones del 4 al 11 de *STK32B,* todos los exones de *C4orf6* y *EVC2* y los 11 primeros exones de *EVC*. *STK32B* codifica una proteína con dominios estructurales característicos de las quinasas (Hanks and Hunter, 1995) y *C4orf6* codifica un pequeño péptido de 93 amino ácidos sólo conservado en primates. En esta tesis demostramos que los individuos portadores de esta deleción en heterocigosis no presentan fenotipo, de lo que se deduce que una sola copia de *EVC, EVC2, C4orf6* y *STK32B* no provoca defectos clínicos. Al mismo tiempo este dato excluye la posibilidad de herencia digénica debida a mutaciones en *EVC* y *EVC2* en el síndrome de EvC, a diferencia de otras ciliopatías como es el caso del síndrome de Bardet-Biedl (Zaghloul and Katsanis, 2009).

El paciente del pedigrí italiano descrito en el primer capítulo de esta tesis heredó la deleción *STK32B-EVC* de su madre y una mutación puntual en *EVC* del cromosoma paterno no reordenado, por lo que tiene una sola copia funcional de *EVC2* y ninguna de *EVC.* Sin embargo este paciente presenta el mismo espectro de malformaciones característico de EvC. Asimismo, los pacientes del pedigrí egipcio descrito en el mismo capítulo son homocigotos para la deleción *STK32B-EVC*, es decir, carecen de copias funcionales de *EVC* y de *EVC2* y también muestran las características esqueléticas y orofaciales típicas de EvC sin agravamiento de las mismas, de hecho estos pacientes no desarrollan defectos cardíacos. Por tanto se puede deducir que la ausencia funcional de EVC y EVC2 no agrava el fenotipo EvC asociado a mutaciones en un sólo gen.

Es interesante que los tres hermanos afectados con EvC del pedigrí egipcio fuesen también diagnosticados con un bajo cociente intelectual a diferencia de sus otros dos hermanos sanos. El déficit intelectual no es una característica típica de EvC (Baujat and Le Merrer, 2007), sin embargo el hecho que esta característica co-segregue junto a EvC en este pedigrí sugiere que está asociado a la deleción *STK32B-EVC* más que a otra mutación

recesiva independiente en otro locus. Por eso analizamos la expresión de los cuatro genes afectados por la deleción *STK32B-EVC* mediante RT-PCR en cerebro fetal humano, con la intención de determinar cuál o cuáles de ellos podrían ser responsables de este defecto. Puesto que el resultado de la RT-PCR fue positivo para todos (datos no mostrados), no pudimos concluir qué gen o combinación génica es la que podría ser causante del retraso mental en esta familia. No obstante hace falta mayor número de casos con esta deleción para poder confirmar una asociación entre la deleción *STK32B-EVC* y el déficit intelectual. Lo que sí podemos afirmar a partir de nuestros datos es que la inactivación de *STK32B* o *C4Orf6*, cuya función a día de hoy es desconocida, no provoca defectos estructurales y como máximo da lugar a un ligero retraso mental. Igualmente podemos concluir que el fenotipo EvC se genera por la ausencia de proteínas EVC o EVC2.

La técnica de hibridación en chips de arrays de SNPs (*Single Nucleotide Polymorphism*) es utilizada habitualmente para detectar aberraciones cromosómicas (Steemers and Gunderson, 2007). Esta técnica proporciona una medida indirecta del número de copias de cada SNP en función de la intensidad de la hibridación (parámetro logR ratio), entendiendo por SNPs las variaciones de nucleótidos polimórficas existentes en la población (Johnson, 2009). El uso de la hibridación en chips de arrays de SNPs descrito en el primer capítulo, fue de gran utilidad para conocer el tamaño del fragmento de ADN delecionado tanto en la familia italiana como en la egipcia, el cual resultó ser de 520 kb en los dos pedigrís. Al poder determinar la última SNP no delecionada en cada extremo, diseñamos *primers* que amplificasen un fragmento de ADN que incluyera el punto de unión de ambos extremos de la deleción en individuos portadores de la misma en las dos familias. La posterior secuenciación de los fragmentos amplificados nos permitió localizar en los dos casos el punto de ruptura telomérico y el punto de ruptura centromérico dentro de dos elementos LINE-1 situados en el mismo brazo cromosómico, los cuales se habían fusionado en uno sólo tras la deleción. Un análisis detallado de la secuencia de nucleótidos del elemento L1 resultante en ambos pedigrís y contenido en el fragmento de PCR amplificado, desveló que ambas familias contenían posiciones polimórficas correspondientes a los dos elementos LINE-1 de los extremos, por lo que dedujimos que la deleción se había originado en los dos casos por recombinación entre ambos retroelementos.

Los retroelementos LINE-1 o L1 constituyen aproximadamente el 17% del genoma humano y representan una fuerza importante en su evolución, al ser los únicos elementos móviles autónomos (Kazazian, 2004; Lander et al., 2001). Estos retrotransposones son secuencias de aproximadamente 6 kb cuando se encuentran completos, si bien la gran mayoría de inserciones están truncadas en su extremo 5'. Los L1 presentan dos marcos de lectura abiertos, uno codifica para una proteína de unión a ácidos nucleicos, y el otro para una proteína con actividad endonucleasa y retrotranscriptasa, las cuales son necesarias para su retrotransposición (Kazazian et al., 1988; Kazazian, 2004). Aunque la mayor parte de los elementos L1 se localizan en regiones intergénicas o en secuencias intrónicas (Babushok and Kazazian, 2007) pueden ocasionar enfermedades si al insertarse *de novo* interrumpen la región codificante de determinados genes provocando cambios en la pauta de lectura (Kazazian et al., 1988) o si su integración va acompañada de una deleción genómica amplia que afecte a genes adyacentes al punto de inserción (Babushok and Kazazian, 2007). La frecuencia de eventos de retrotransposición espontáneos responsables de enfermedades en humanos es de 1 por cada 1.000 nacimientos (Chen et al., 2005a; Kazazian and Moran, 1998). Por otro lado los elementos L1 pueden provocar inestabilidad genómica por recombinación entre sus secuencias dando lugar a duplicaciones y/o deleciones (Burwinkel and Kilimann, 1998). Además del caso descrito en este trabajo se han documentado otros dos casos de enfermedades humanas causadas por deleciones provocadas por recombinación entre elementos L1. En uno de ellos la deleción afectó al gen que codifica la subunidad β de la fosforilasa quinasa (*PHKB*) originando la enfermedad de almacenamiento de glucógeno (Burwinkel and Kilimann, 1998). En el otro caso, la deleción afectó a los genes *COL4A5* y *COL4A6* causando el síndrome de Alport (Segal et al., 1999). En nuestro estudio los puntos de recombinación de los elementos LINE-1 en los dos pedigrís son distintos indicando que ocurrieron de forma independiente, sin embargo no parece ser un tipo de mutación recurrente en EvC puesto que hasta la fecha solo se ha descrito en estas dos familias. El reordenamiento *STK32B-EVC* tampoco se detectó en las bases de datos que almacenan información sobre las regiones de ADN sujetas a variación en el número de copias (*Copy Number Variation*, CNV) en la población normal (Redon et al., 2006).

Un estudio anterior llevado a cabo en 65 pacientes EvC, en los cuales se secuenciaron todos los exones codificantes de *EVC* y *EVC2* y la región promotora intergénica, mostró la existencia de un 31% de pacientes sin mutaciones y otros 3 pacientes EvC con sólo una mutación identificada (Tompson et al., 2007). Con la intención de confirmar estos datos y obtener una cohorte de pacientes que sirviesen de base para la búsqueda de un tercer gen, en el segundo capítulo de esta tesis llevamos a cabo el análisis molecular de *EVC* y *EVC2* en 39 pacientes (36 pacientes EvC y 3 pacientes Weyers) de distintos orígenes geográficos. Estos pacientes fueron seleccionados fijando como criterio las características condroectodérmicas típicas de EvC, excluyendo las muestras sin un diagnóstico clínico claro, como aquellas procedentes de interrupciones del embarazo. A diferencia del estudio anterior (Tompson et al., 2007) encontramos mutaciones en todos los casos analizados, identificando un total de 40 mutaciones recesivas independientes en *EVC/EVC2,* de las cuales 31 eran nuevas. Los cambios encontrados se corresponden con los datos anteriormente publicados y consistieron en sustituciones de nucleótidos, microdeleciones, microinserciones, y dos deleciones en *EVC2* que abarcaban varios exones. Al igual que en el trabajo de Tompson et al, 2007 en uno de los casos EvC la secuenciación de los exones codificantes solo detectó una mutación en el sitio donador de *splicing* del intrón 8 de *EVC*. Sin embargo al analizar el ADNc encontramos la segunda mutación en el intrón 7 de este mismo gen. Es probable que mutaciones similares se encuentren en los casos identificados por Tompson et al, 2007 con una sola mutación, ya que en estos pacientes no se estudió el ADNc.

Es importante resaltar entre el espectro de mutaciones de pacientes EvC, la existencia de deleciones que abarcan uno o varios exones de *EVC* y de *EVC2*. Puesto que este tipo de mutaciones no son detectadas mediante secuenciación directa de los exones codificantes en el caso de estar en heterocigosis, se requiere el uso de técnicas que permitan distinguir dosis génica, como MLPA (*Multiplex Ligation-dependent Probe Amplification*) (den Dunnen and White, 2006; Gouas et al., 2008). A la vista de los resultados obtenidos en esta tesis y los publicados anteriormente (Tompson et al., 2007), para el diagnóstico molecular de pacientes EvC, sería aconsejable utilizar primero secuenciación directa de las regiones codificantes, la cual detecta un elevado porcentaje de mutaciones, seguido del análisis del ADNc y MLPA cuando por secuenciación no se observen mutaciones o se detecte sólo una.

Sumando los datos de los dos estudios más extensivos realizados hasta la fecha Tompson et al, 2007 y Valencia et al, 2009 (incluido en esta tesis) de un total de 101 pacientes EvC, el 38% portaban mutaciones en *EVC*, el 40% en *EVC2* (excluyendo los tres casos con sólo una mutación detectada en *EVC2* en el estudio de Tompson et al, 2007) y en el 20% restante no se detectaron mutaciones. Hay que tener en cuenta, como se especifica en el estudio de Tompson et al, 2007, que los casos sin mutaciones detectadas pueden ser debidas a un diagnóstico clínico erróneo puesto que algunos de esos casos eran fetos de embarazos no llegados a término y existen otros síndrome CCP con fenotipo similar en estas etapas. Por eso es discutible la existencia de un tercer gen que de existir sería responsable de un número bajo de casos. En ninguno de los dos trabajos mencionados (Tompson et al., 2007) y esta tesis) se ha podido establecer una asociación fenotipo/genotipo clara y tampoco hemos podido asociar un determinado tipo de mutación con la presencia de defectos cardíacos, por lo que es posible que haya otros genes modificadores que influyan en la aparición de este tipo de defectos.

Análisis molecular en pacientes diagnosticados con Weyers e implicación de *EVC2* en la señalización Hh.

En la discusión de este punto es necesario aclarar que la maquinaria de NMD sólo degrada aquellos mensajeros con codones de terminación prematuros situados a una distancia mayor de 50-55 nucleótidos en dirección 5´ respecto de la última unión entre exón y exón. Por lo tanto aquellos transcritos que contengan codones de terminación prematuros situados en el último exón eludirían la maquinaria NMD (Hentze and Kulozik, 1999; Khajavi et al., 2006; Nagy and Maquat, 1998)

Hasta ahora hay cuatro mutaciones dominantes Weyers descritas: una sustitución de la Serina 307 por Prolina en EVC (Ruiz-Perez et al., 2000), una deleción de un nucleótido (c.3793delC) en *EVC2* (Ye et al, 2006; y en el trabajo de esta tesis) y las dos mutaciones *nonsense* (c.3797T>A y c.3797T>G) también en *EVC2* aquí reportadas. Mientras que las mutaciones Weyers en *EVC2* parecen producir consistentemente un fenotipo dominante, la mutación S307P en EVC produce defectos clínicos dependiendo del contexto genético de cada individuo, puesto que existen portadores de esta mutación en heterocigosis que sin embargo no presentan alteración del fenotipo (Tompson et al., 2007). Las tres mutaciones Weyers en *EVC2* originan codones de terminación prematuros

pero al encontrarse en el último exón del gen es de esperar que no sean degradadas vía NMD y den lugar a proteínas truncadas a las que les faltan los últimos 43 aminoácidos. Es interesante que las mutaciones que originan Weyers dan lugar a un fenotipo dominante, mientras que otras mutaciones situadas aguas arriba dentro del mismo exón y que deberían eludir el NMD son recesivas, como la mutación c.3731dupT y la mutación de mayor frecuencia en la población española c.3660delC (encontrada en el 50% de pacientes españoles EvC no relacionados), la cual origina una proteína a la que le faltan los últimos 87 aminoácidos. En este segundo capítulo demostramos experimentalmente que las variantes mutantes tanto recesivas como dominantes del último exón de *EVC2* no son degradadas, ya que la cantidad de transcrito de *EVC2* cuantificado por qRT-PCR procedente de fibroblastos en cultivo de un individuo heterocigoto c.3660delC y de un paciente Weyers, era equivalente a la cantidad registrada en los fibroblastos control. Además la secuenciación directa del ADNc verificó la presencia de los transcritos procedentes del alelo normal y del mutante en fibroblastos c.3660delC y Weyers.

Puesto que el trabajo realizado en los ratones mutantes *Evc* demuestra que EvC se produce por una disminución en la respuesta a las señales Hh, nos preguntamos si las mutaciones Weyers podrían tener un efecto similar. Utilizando células NIH3T3 como modelo, demostramos que la expresión de una proteína murina de Evc2 tipo Weyers a la que eliminamos los 43 aminoácidos finales (p.Evc2Δ43), disminuye la respuesta de estas células a la activación de la señalización Hh, mientras que la expresión de una proteína Evc2 normal u otra que mimetiza la mutación recesiva c.3660delC (p.Evc2Δ87) no tienen ese efecto. De aquí se deduce que el defecto molecular subyacente a Weyers es igual al de EvC y consiste en una menor respuesta de los tejidos a las señales Hh. Se conoce que alteraciones en esta ruta están implicadas en defectos esqueléticos, craniofaciales y dentales (Ehlen et al., 2006; McMahon et al., 2003). El hecho que la expresión de la proteína Evc2 carente de los 87 aminoácidos finales no tenga efecto sobre la señalización Hh, implica que los 44 residuos existentes entre esta mutación y la de Weyers son importantes para el funcionamiento de la proteína. Podemos especular sobre el mecanismo molecular por el cual las mutaciones Weyers tienen un efecto dominante. Es posible que Evc2 funcione como un homodímero bien solo o en asociación con otras proteínas como Evc, y que el fragmento comprendido entre Evc2Δ87 y Evc2Δ43 sea necesario para que se forme el complejo pero insuficiente para que pueda ser funcional,

por lo que de esta manera el alelo mutante interferiría con la función del normal. Alternativamente una ganancia de función podría ser también el mecanismo desencadenado por la pérdida de los 43 aminoácidos finales pero no de los 87, es decir, que las proteínas Evc2-Weyers adquieran ahora una función distinta cuyo resultado es la disminución de la respuesta a Hh. La estabilidad de la proteína podría también jugar un papel importante para explicar el patrón de herencia de las mutaciones del exón 22 de *EVC2*, ya que existe la posibilidad que los cambios recesivos en ese exón den lugar a proteínas EVC2 truncadas menos estables que las producidas por Weyers, las cuales son ligeramente más largas, y podrían tener la suficiente estabilidad para provocar un efecto dominante mediante uno de los mecanismo citados anteriormente.

Evc desempeña un papel esencial durante la osificación endocondral.

Los ratones desprovistos de *Evc* recapitulan las características esqueléticas de los pacientes y presentan extremidades y costillas cortas junto con anormalidades dentales, aunque no reproducen la polidactilia ni las malformaciones cardíacas (Ruiz-Perez et al., 2007). Un primer estudio preliminar de estos ratones se llevó a cabo en un fondo genético mixto C57BL/6J; 129 usando la tibia como hueso modelo y demostró que la ruta Ihh está disminuida en la placa de crecimiento de los ratones $Evc^{-/-}$ (Ruiz-Perez et al., 2007). El objetivo del tercer trabajo presentado en esta tesis consistió en profundizar en la función de Evc en el desarrollo del hueso para averiguar cuáles de los diferentes aspectos regulados por Ihh en la placa de crecimiento eran dependientes de Evc y en qué grado. Igualmente queríamos conocer si las placas de crecimiento distintas a las de los huesos largos, como son las sincondrosis craneales, requerían de Evc para su desarrollo. Para ello utilizamos ratones con fondo genético homógeneo C57BL/6J donde el fenotipo resulta ser más severo. A modo de ejemplo, mientras que en el fondo mixto C57BL/6J; 129 algunos son capaces de sobrevivir algunos meses sometidos a una dieta especial para ratones con defectos dentales, en el fondo puro C57BL/6J los ratones $Evc^{-/-}$ no sobreviven más allá del primer o segundo día después del parto.

En este trabajo se estudiaron las placas de crecimiento del cúbito y el radio y confirmamos mediante HIS el déficit en la expresión de las dianas de Ihh (*Ptch1, Gli1, Hhip1* y *Pthrp)* observado anteriormente en la tibia (Ruiz-Perez et al., 2007) así como un acortamiento de la región de los condrocitos columnares debido principalmente a los

bajos niveles de *Pthrp* en la región articular. También la región hipertrófica es más corta en los ratones mutantes indicando una posible aceleración en la degeneración y apoptosis de los condrocitos hipertróficos en ausencia de Evc. La incorporación de condrocitos de reserva a columnares está inducida por Ihh (Kobayashi et al., 2005; Koziel et al., 2005), por lo que analizamos este procesos en los ratones *Evc*$^{-/-}$ utilizando marcadores específicos de ambas tipos de condrocitos, *Fgfr3* para los columnares y *Fgfr1* para los condrocitos de reserva. Como resultado encontramos una expansión del dominio de expresión de *Fgfr1*, indicativo de un retraso en la diferenciación de los condrocitos de reserva a columnares en los ratones *Evc*$^{-/-}$, a la vez que comprobamos la existencia de una fuerte reducción de la región positiva para *Fgfr3.* En el primer estudio de los ratones *Evc*$^{-/-}$ de fondo mixto se describió un patrón normal para *Fgfr1* en la tibia (Ruiz-Perez et al., 2007), esta discrepancia estaría justificada por la mayor gravedad fenotípica del fondo genético usado en el trabajo presentado aquí.

A continuación estudiamos la proliferación, puesto que también es una característica dependiente de Ihh (St-Jacques et al., 1999). En este caso encontramos una reducción de la división celular de un 56% en la región de reserva y de un 33% en la región de los columnares. Esto supone de nuevo una diferencia en los ratones *Evc*$^{-/-}$ C57BL/6J respecto a los de fondo mixto en los que no se detectaron diferencias en división celular (Ruiz-Perez et al., 2007). Aunque esto también podría ser atribuido a la mayor gravedad del fenotipo en el fondo genético homogéneo, hay que tener en cuenta que el estudio de la proliferación en los ratones *Evc*$^{-/-}$ del fondo mixto se llevó a cabo contando los núcleos que habían incorporado BrdU en un área fija de la región columnar (región menos afectada) (Ruiz-Perez et al., 2007) y aquí contamos todos los núcleos en dos áreas separadas: en los condrocitos de reserva y en los columnares. La variabilidad en el fenotipo de los ratones *Evc*$^{-/-}$ según el fondo genético es esperable puesto que estaría de acuerdo con la variabilidad fenotípica observada en los pacientes EvC. El hecho que la proliferación en ausencia de Evc esté alterada es relevante ya que existe una fuerte asociación en la placa de crecimiento entre la proliferación y los niveles de Gli3-R. Así en los huesos endocondrales de ratones *Ihh*$^{-/-}$ la proliferación de los condrocitos cae un 50% y se produce un fuerte aumento de Gli3-R (Razzaque et al., 2005), mientras que en los dobles *knockouts Ihh* $^{-/-}$*; Gli3* $^{-/-}$, los cuales carecen tanto de Gli3-A como Gli3-R, la proliferación vuelve a niveles normales (Hilton et al., 2005; Koziel et al., 2005). Según

estos datos la disminución en la proliferación de los ratones *Evc* $^{-/-}$ sugiere que los niveles de Gli3-R podrían estar elevados en estos ratones.

Los ratones *Ihh* $^{-/-}$ carecen de osteoblastos, de lo que se deduce que Ihh actua promoviendo la diferenciación de este tipo celular en el pericondrio (St-Jacques et al., 1999). De acuerdo con este dato, los ratones *Evc*$^{-/-}$ muestran un retraso en la formación del collar óseo en etapas tempranas durante la formación del centro de osificación primario y también más adelante, una vez formada la placa de crecimiento en la región DBPO. Sin embargo en contraste con el fenotipo de los mutantes *Ihh*$^{-/-}$ excepto en el DBPO, la diferenciación de los osteoblastos en los ratones *Evc*$^{-/-}$ tanto en la esponjosa primaria como en el resto del collar del hueso no se encuentra fuertemente afectada, a pesar que observamos una fuerte reducción de la expresión de genes diana de la ruta Ihh (*Ptch1, Gli1* y *Pthrp1*). Esto podría explicarse porque que la ruta no está anulada por completo en el pericondrio *Evc*$^{-/-}$, ya que aún se observa una débil expresión de *Ptch1* y *Gli1* la cual sería suficiente para permitir la diferenciación de osteoblastos aunque a un ritmo ralentizado.

Ihh ejerce un control dual sobre la hipertrofia de los condrocitos. Por un lado actúa a través de Pthrp, retrasando la hipertrofia de los condrocitos y manteniéndolos en estado proliferativo, y por otro, actúa de manera independiente a Pthrp induciendo la hipertrofia (Mak et al., 2008). Ambas funciones están alteradas en los ratones *Evc*$^{-/-}$, la primera ya ha sido comentada anteriormente, y la segunda puede deducirse de los estudios histológicos y de HIS, en los cuales se observa una desincronización entre la diferenciación de los condrocitos situados en el centro de la placa de crecimiento, más avanzados en su diferenciación, y los adyacentes al pericondrio. Este fenotipo es muy claro en las fases iníciales de la osificación endocondral en la que utilizamos el metatarso como hueso modelo. Es posible que el retraso en la hipertrofia de los condrocitos adyacentes al pericondrio ejerza una influencia en la células mesenquimales pericondriales retrasando su diferenciación a osteoblastos.

Nuestro estudio con ratones *Ptch-LacZ*$^{+/-}$ y *Ptch-LacZ*$^{+/-}$*; Evc*$^{-/-}$ confirma los estudios anteriores de HIS, ya que detectamos menor actividad *β-galactosidasa* dependiente de *Ptch1* en condrocitos y osteoblastos *Evc* $^{-/-}$. Por otro lado, estos estudios revelan la existencia de dos regiones diferentes dentro del pericondrio: una región interna de la que surgen los osteoblastos del collar del hueso, y otra externa formada por

células fibroblásticas que bordean todo el elemento óseo y presentan un alto nivel de respuesta a Hh. Tanto en el estudio con fondo mixto como en el estudio llevado a cabo en esta tesis, detectamos que la expresión de genes diana de Ihh, como *Ptch1, Gli1* y *Pthrp* está incrementado en esta capa de células externas en los ratones $Evc^{-/-}$. Este fenómeno también se ha observado en otros mutantes de la vía Hh, como en los mutantes condicionales $Smo^{-/-}$, y podría estar explicado por una mayor difusión de Ihh al disminuir la cantidad de receptor Ptch1 (Long et al., 2004). La función de esta capa celular es desconocida; hipotéticamente podría actuar como aislante para atrapar el exceso de ligando y evitar su difusión a tejidos adyacentes, o puesto que estas células expresan *Pthrp* podría intervenir en la coordinación del desarrollo del elemento óseo.

Previamente se había descrito que Evc se localiza en la base del cilio primario en condrocitos utilizando un anticuerpo policlonal (Ruiz-Perez et al., 2007), aquí hemos desarrollado un anticuerpo monoclonal específico contra Evc demostrando que también se expresa en el cilio primario de osteoblastos. Este anticuerpo ha permitido detectar la proteína endógena mediante la técnica de *western blot* en los extractos proteicos de osteoblastos normales que está ausente en los mutantes. Utilizando cultivos primarios de osteoblastos derivados de calvaria de embriones normales y nulos para *Evc,* hemos confirmado mediante qRT-PCR que Evc es un mediador esencial de la vía de Hh también en osteoblastos, lo que explicaría el retraso en la diferenciación de este tipo celular en la formación del collar óseo.

Una cuestión que estaba pendiente de esclarecer es si Evc funciona como mediador generalizado de la osificación endocondral. Para ello estudiamos los huesos de la base del cráneo, ya que poseen placas de crecimiento distintas a las de los huesos largos denominadas sincondrosis. Según su disposición anatómica existen cuatro sincondrosis: etmoides, intra-esfenoidal, esfeno-occipital e intraoccipital (Young et al., 2006). Cada sincondrosis consiste en dos placas de crecimiento dispuestas a modo de imagen especular, las cuales comparten una única zona de reserva de la que surgen en direcciones opuestas capas de condrocitos proliferativos, pre-hipertróficos e hipertróficos que, como ocurre en los huesos largos, terminan degenerando para ser sustituidos por tejido óseo. (Young et al., 2006). El análisis macroscópico mediante tinción *in toto* de la base del cráneo de ratones $Evc^{-/-}$ demostró la presencia de alteraciones morfológicas importantes sólo en la región frontal, especialmente en el

preesfenoides y un orificio central en el basisfenoides. Posteriormente analizamos las sincrondrosis craneales a nivel histológico y observamos ausencia de la sincondrosis intraesfenoidal en los ratones *Evc*$^{-/-}$ y hendiduras a nivel de la línea media del preesfenoides. Los estudios de HIS confirmaron en los mutantes la disminución de la expresión de las dianas de Ihh en condrocitos y osteoblastos, retraso en la inducción del pericondrio, disminución de la proliferación y retraso en la hipertrofia de los condrocitos próximos al pericondrio tal y como ocurre en los huesos largos, indicando que en ausencia de Evc la ruta Ihh también está alterada en estos huesos.

Excluyendo la hendidura de la línea media del preesfenoides el fenotipo craneal de los ratones *Evc*$^{-/-}$ es muy similar al de los ratones *Ihh* $^{-/-}$, los cuales también presentan defectos en la parte frontal del cráneo pero no en la región basioccipital (Young et al., 2006). Tanto los ratones *Ihh*$^{-/-}$ como otros mutantes de la vía de Hh, como los ratones Gli3, presentan un orificio en el centro del hueso basiesfenoides apuntando a una asociación entre este defecto y la señalización Hh (Abzhanov et al., 2007; Bose et al., 2002). En un estudio previo en ratones *Ihh*$^{-/-}$ se detectó expresión de *Shh* en vestigios de la notocorda próximos a la sincondrosis esfeno-occipital (E13.5) (Young et al., 2006), de manera que el patrón de crecimiento y la osificación de la base del cráneo a lo largo del eje antero-posterior parece estar orquestada por Ihh y Shh. Por eso es posible que la hendidura de la línea media presente en los huesos anteriores de la base del cráneo en los ratones *Evc*$^{-/-}$ pero no en los de *Ihh*$^{-/-}$, sea debido a una deficiencia en la respuesta a *Shh* en los ratones *Evc* $^{-/-}$ y no en los *Ihh* $^{-/-}$. Aunque en los pacientes con EvC no se han descrito defectos en la base del cráneo (Baujat and Le Merrer, 2007), en vista de los datos obtenidos de este trabajo sería importante tenerlo en cuenta para el manejo de los pacientes afectados con este síndrome.

Conclusiones

1. Nuestro estudio mutacional llevado a cabo en 36 pacientes EvC y 3 pacientes Weyers ha detectado mutaciones en *EVC* o en *EVC2* en todos los casos. Este estudio ha permitido identificar 31 mutaciones nuevas en *EVC* y en *EVC2* y demuestra la existencia de un punto caliente de mutaciones Weyers en el final del último exón de *EVC2*.

2. Hemos detectado dos familias con mutaciones en *EVC* y *EVC2* causadas por deleción mediada por recombinación entre elementos LINE-1. El estudio del fenotipo de los pacientes heterocigotos para esta deleción indica que la ausencia de un alelo funcional de *EVC* junto con la ausencia de un alelo funcional de *EVC2* no produce fenotipo, lo que demuestra que no existe herencia digéncia *EVC/EVC2* en EvC. Asimismo el fenotipo de los pacientes homocigotos para la deleción muestra que la ausencia de proteínas funcionales EVC y EVC2, no agrava las características clínicas de EvC.

3. La deleción mediada por elementos LINE-1 afecta a cuatro genes (*EVC, EVC2, C4orf6* y *STK32B*) y puede estar asociada a un ligero retraso mental. Las características clínicas de los pacientes homocigotos para la deleción demuestra que la inactivación total de *STK32B* y de *C4orf6* (ambos de función desconocida) origina como máximo un ligero retraso mental.

4. Mutaciones que introducen codones de terminación prematuros en el último exón de *EVC2* eluden NMD, sin embargo mientras las mutaciones que originan proteínas truncadas carentes de los últimos 43 aminoácidos producen un fenotipo dominante Weyers las que dan lugar a proteínas sin los últimos 87 aminoácidos son recesivas, indicando que los 44 residuos existentes entre ambas mutaciones son importantes para el funcionamiento de la proteína.

5. El fenotipo dominante Weyers asociado a proteínas truncadas Evc2, se debe a una disminución en la respuesta a las señales Hh bien porque la proteína Evc2 mutante interfiere con la función del alelo normal o porque adquiere una ganancia de función, de lo que se deduce que Evc2, al igual que Evc, son mediadores positivos de la señales Hh.

6. Evc desempeña un papel esencial en la osificación endocondral de los huesos largos, ya que actúa mediando prácticamente la totalidad de los aspectos regulados por Ihh en la placa de crecimiento. Así Evc es requerido para el control dual de la hipertrofia de los condrocitos, su proliferación y su diferenciación desde la zona de reserva a la columnar y para la diferenciación de los osteoblastos en el pericondrio.

7. Las sincondrosis de los ratones *Evc* $^{-/-}$ reproducen los defectos fenotípicos observados en los huesos largos, por lo que *Evc* también es un gen esencial para el desarrollo de la base del cráneo.

Bibliografía

Abzhanov, A., Rodda, S.J., McMahon, A.P., and Tabin, C.J. (2007). Regulation of skeletogenic differentiation in cranial dermal bone. Development *134*, 3133-3144.

Ali, B.R., Akawi, N.A., Chedid, F., Bakir, M., Ur Rehman, M., Rahmani, A., and Al-Gazali, L. (2010). Molecular and clinical analysis of Ellis-van Creveld syndrome in the United Arab Emirates. BMC Med Genet *11*, 33.

Apionishev, S., Katanayeva, N.M., Marks, S.A., Kalderon, D., and Tomlinson, A. (2005). Drosophila Smoothened phosphorylation sites essential for Hedgehog signal transduction. Nat Cell Biol *7*, 86-92.

Aza-Blanc, P., Ramirez-Weber, F.A., Laget, M.P., Schwartz, C., and Kornberg, T.B. (1997). Proteolysis that is inhibited by hedgehog targets Cubitus interruptus protein to the nucleus and converts it to a repressor. Cell *89*, 1043-1053.

Babushok, D.V., and Kazazian, H.H., Jr. (2007). Progress in understanding the biology of the human mutagen LINE-1. Hum Mutat *28*, 527-539.

Bai, C.B., and Joyner, A.L. (2001). Gli1 can rescue the in vivo function of Gli2. Development *128*, 5161-5172.

Baujat, G., and Le Merrer, M. (2007). Ellis-van Creveld syndrome. Orphanet J Rare Dis *2*, 27.

Bellus, G.A., Hefferon, T.W., Ortiz de Luna, R.I., Hecht, J.T., Horton, W.A., Machado, M., Kaitila, I., McIntosh, I., and Francomano, C.A. (1995). Achondroplasia is defined by recurrent G380R mutations of FGFR3. Am J Hum Genet *56*, 368-373.

Bergmann, C. (2011). Educational paper : Ciliopathies. Eur J Pediatr.

Bi, W., Deng, J.M., Zhang, Z., Behringer, R.R., and de Crombrugghe, B. (1999). Sox9 is required for cartilage formation. Nat Genet *22*, 85-89.

Bijlsma, M.F., Spek, C.A., Zivkovic, D., van de Water, S., Rezaee, F., and Peppelenbosch, M.P. (2006). Repression of smoothened by patched-dependent (pro-)vitamin D3 secretion. PLoS Biol *4*, e232.

Bisgrove, B.W., and Yost, H.J. (2006). The roles of cilia in developmental disorders and disease. Development *133*, 4131-4143.

Blair, H.J., Tompson, S., Liu, Y.N., Campbell, J., MacArthur, K., Ponting, C.P., Ruiz-Perez, V.L., and Goodship, J.A. (2011). Evc2 is a positive modulator of Hedgehog signalling that interacts with Evc at the cilia membrane and is also found in the nucleus. BMC Biol *9*, 14.
Bose, J., Grotewold, L., and Ruther, U. (2002). Pallister-Hall syndrome phenotype in mice mutant for Gli3. Hum Mol Genet *11*, 1129-1135.

Bose, J., Grotewold, L., and Ruther, U. (2002). Pallister-Hall syndrome phenotype in mice mutant for Gli3. Hum Mol Genet 11, 1129-1135

Burwinkel, B., and Kilimann, M.W. (1998). Unequal homologous recombination between LINE-1 elements as a mutational mechanism in human genetic disease. J Mol Biol *277*, 513-517.

Buttitta, L., Mo, R., Hui, C.C., and Fan, C.M. (2003). Interplays of Gli2 and Gli3 and their requirement in mediating Shh-dependent sclerotome induction. Development *130*, 6233-6243.

Cahuana, A., Palma, C., Gonzales, W., and Gean, E. (2004). Oral manifestations in Ellis-van Creveld syndrome: report of five cases. Pediatr Dent *26*, 277-282.

Cardenas-Rodriguez, M., and Badano, J.L. (2009). Ciliary biology: understanding the cellular and genetic basis of human ciliopathies. Am J Med Genet C Semin Med Genet *151C*, 263-280.

Cohen, M., Jr. (2010). Hedgehog signaling update. Am J Med Genet Part A *152*, 1875-1914.

Cole, D.G., Diener, D.R., Himelblau, A.L., Beech, P.L., Fuster, J.C., and Rosenbaum, J.L. (1998). Chlamydomonas kinesin-II-dependent intraflagellar transport (IFT): IFT particles contain proteins required for ciliary assembly in Caenorhabditis elegans sensory neurons. J Cell Biol *141*, 993-1008.

Colvin, J.S., Bohne, B.A., Harding, G.W., McEwen, D.G., and Ornitz, D.M. (1996). Skeletal overgrowth and deafness in mice lacking fibroblast growth factor receptor 3. Nat Genet *12*, 390-397.

Corbit, K.C., Aanstad, P., Singla, V., Norman, A.R., Stainier, D.Y., and Reiter, J.F. (2005). Vertebrate Smoothened functions at the primary cilium. Nature *437*, 1018-1021.

Corcoran, R.B., and Scott, M.P. (2006). Oxysterols stimulate Sonic hedgehog signal transduction and proliferation of medulloblastoma cells. Proc Natl Acad Sci U S A *103*, 8408-8413.

Curry, C.J., and Hall, B.D. (1979). Polydactyly, conical teeth, nail dysplasia, and short limbs: a new autosomal dominant malformation syndrome. Birth Defects Orig Artic Ser *15*, 253-263.

Chen, C.P., Su, Y.N., Hsu, C.Y., Chern, S.R., Tsai, F.J., Wu, P.C., Chen, P.T., and Wang, W. (2010). Ellis-van Creveld syndrome: prenatal diagnosis, molecular analysis and genetic counseling. Taiwan J Obstet Gynecol *49*, 481-486.

Chen, J.M., Stenson, P.D., Cooper, D.N., and Ferec, C. (2005a). A systematic analysis of LINE-1 endonuclease-dependent retrotranspositional events causing human genetic disease. Hum Genet *117*, 411-427.

Chen, M.H., Gao, N., Kawakami, T., and Chuang, P.T. (2005b). Mice deficient in the fused homolog do not exhibit phenotypes indicative of perturbed hedgehog signaling during embryonic development. Mol Cell Biol *25*, 7042-7053.

Chen, M.H., Li, Y.J., Kawakami, T., Xu, S.M., and Chuang, P.T. (2004). Palmitoylation is required for the production of a soluble multimeric Hedgehog protein complex and long-range signaling in vertebrates. Genes Dev *18*, 641-659.

Day, T.F., Guo, X., Garrett-Beal, L., and Yang, Y. (2005). Wnt/beta-catenin signaling in mesenchymal progenitors controls osteoblast and chondrocyte differentiation during vertebrate skeletogenesis. Dev Cell *8*, 739-750.

Dellaporta, S.L., Xu, A., Sagasser, S., Jakob, W., Moreno, M.A., Buss, L.W., and Schierwater, B. (2006). Mitochondrial genome of Trichoplax adhaerens supports placozoa as the basal lower metazoan phylum. Proc Natl Acad Sci U S A *103*, 8751-8756.

den Dunnen, J.T., and White, S.J. (2006). MLPA and MAPH: sensitive detection of deletions and duplications. Curr Protoc Hum Genet *Chapter 7*, Unit 7 14.

Deng, C., Wynshaw-Boris, A., Zhou, F., Kuo, A., and Leder, P. (1996). Fibroblast growth factor receptor 3 is a negative regulator of bone growth. Cell *84*, 911-921.

Deretic, D., and Mazelova, J. (2009). Assay for in vitro budding of ciliary-targeted rhodopsin transport carriers. Methods Cell Biol *94*, 241-257.

Digilio, M.C., Marino, B., Ammirati, A., Borzaga, U., Giannotti, A., and Dallapiccola, B. (1999). Cardiac malformations in patients with oral-facial-skeletal syndromes: clinical similarities with heterotaxia. Am J Med Genet *84*, 350-356.

Ehlen, H.W., Buelens, L.A., and Vortkamp, A. (2006). Hedgehog signaling in skeletal development. Birth Defects Res C Embryo Today *78*, 267-279.

Ellis, R.W., and van Creveld, S. (1940). A Syndrome Characterized by Ectodermal Dysplasia, Polydactyly, Chondro-Dysplasia and Congenital Morbus Cordis: Report of Three Cases. Arch Dis Child *15*, 65-84.

Fliegauf, M., Benzing, T., and Omran, H. (2007). When cilia go bad: cilia defects and ciliopathies. Nat Rev Mol Cell Biol *8*, 880-893.

Galdzicka, M., Patnala, S., Hirshman, M.G., Cai, J.F., Nitowsky, H., Egeland, J.A., and Ginns, E.I. (2002). A new gene, EVC2, is mutated in Ellis-van Creveld syndrome. Mol Genet Metab *77*, 291-295.

Garber, K. (2008). Hedgehog drugs begin to show results. J Natl Cancer Inst *100*, 692-697.

Gehring, N.H., Lamprinaki, S., Hentze, M.W., and Kulozik, A.E. (2009). The hierarchy of exon-junction complex assembly by the spliceosome explains key features of mammalian nonsense-mediated mRNA decay. PLoS Biol *7*, e1000120.

Giknis, F.L. (1963). Single atrium and the Ellis-van Creveld syndrome. J Pediatr *62*, 558-564.

Goetz, S.C., and Anderson, K.V. (2010). The primary cilium: a signalling centre during vertebrate development. Nat Rev Genet *11*, 331-344.

Gouas, L., Goumy, C., Veronese, L., Tchirkov, A., and Vago, P. (2008). Gene dosage methods as diagnostic tools for the identification of chromosome abnormalities. Pathol Biol (Paris) *56*, 345-353.

Hahn, H., Wicking, C., Zaphiropoulous, P.G., Gailani, M.R., Shanley, S., Chidambaram, A., Vorechovsky, I., Holmberg, E., Unden, A.B., Gillies, S*., et al.* (1996). Mutations of the human homolog of Drosophila patched in the nevoid basal cell carcinoma syndrome. Cell *85*, 841-851.

Hall, T.M., Porter, J.A., Beachy, P.A., and Leahy, D.J. (1995). A potential catalytic site revealed by the 1.7-A crystal structure of the amino-terminal signalling domain of Sonic hedgehog. Nature *378*, 212-216.

Hanks, S.K., and Hunter, T. (1995). Protein kinases 6. The eukaryotic protein kinase superfamily: kinase (catalytic) domain structure and classification. FASEB J *9*, 576-596.

Hattab, F.N., Yassin, O.M., and Sasa, I.S. (1998). Oral manifestations of Ellis-van Creveld syndrome: report of two siblings with unusual dental anomalies. J Clin Pediatr Dent *22*, 159-165.

Haycraft, C.J., Banizs, B., Aydin-Son, Y., Zhang, Q., Michaud, E.J., and Yoder, B.K. (2005). Gli2 and Gli3 localize to cilia and require the intraflagellar transport protein polaris for processing and function. PLoS Genet *1*, e53.

Hentze, M.W., and Kulozik, A.E. (1999). A perfect message: RNA surveillance and nonsense-mediated decay. Cell *96*, 307-310.

Hildebrandt, F., Benzing, T., and Katsanis, N. (2011). Ciliopathies. N Engl J Med *364*, 1533-1543.

Hilton, M.J., Tu, X., Cook, J., Hu, H., and Long, F. (2005). Ihh controls cartilage development by antagonizing Gli3, but requires additional effectors to regulate osteoblast and vascular development. Development *132*, 4339-4351.

Hill, T.P., Spater, D., Taketo, M.M., Birchmeier, W., and Hartmann, C. (2005). Canonical Wnt/beta-catenin signaling prevents osteoblasts from differentiating into chondrocytes. Dev Cell *8*, 727-738.

Hills, C.B., Kochilas, L., Schimmenti, L.A., and Moller, J.H. (2011). Ellis-van Creveld syndrome and congenital heart defects: presentation of an additional 32 cases. Pediatr Cardiol *32*, 977-982.

Hooper, J. E., and Scott, M. P (2005). Communicating with Hedgehogs. Nat Rev Mol Cell Biol 6,306-317

Howard, T.D., Guttmacher, A.E., McKinnon, W., Sharma, M., McKusick, V.A., and Jabs, E.W. (1997). Autosomal dominant postaxial polydactyly, nail dystrophy, and dental abnormalities map to chromosome 4p16, in the region containing the Ellis-van Creveld syndrome locus. Am J Hum Genet *61*, 1405-1412.

Huangfu, D., Liu, A., Rakeman, A.S., Murcia, N.S., Niswander, L., and Anderson, K.V. (2003). Hedgehog signalling in the mouse requires intraflagellar transport proteins. Nature *426*, 83-87.

Humke, E.W., Dorn, K.V., Milenkovic, L., Scott, M.P., and Rohatgi, R. (2010). The output of Hedgehog signaling is controlled by the dynamic association between Suppressor of Fused and the Gli proteins. Genes Dev *24*, 670-682.

Huntzicker, E.G., Estay, I.S., Zhen, H., Lokteva, L.A., Jackson, P.K., and Oro, A.E. (2006). Dual degradation signals control Gli protein stability and tumor formation. Genes Dev *20*, 276-281.

Ide, S.E., Ortiz de Luna, R.I., Francomano, C.A., and Polymeropoulos, M.H. (1996). Exclusion of the MSX1 homeobox gene as the gene for the Ellis van Creveld syndrome in the Amish. Hum Genet *98*, 572-575.

Ingham, P.W., Nakano, Y., and Seger, C. (2011). Mechanisms and functions of Hedgehog signalling across the metazoa. Nat Rev Genet *12*, 393-406.

Jia, J. and Jiang, J. (2006). Decoding the Hedgehog signal in animal development. Cell Mol Life Sci 63, 1249-1265

Jia, J., Tong, C., and Jiang, J. (2003). Smoothened transduces Hedgehog signal by physically interacting with Costal2/Fused complex through its C-terminal tail. Genes Dev *17*, 2709-2720.

Jia, J., Tong, C., Wang, B., Luo, L., and Jiang, J. (2004). Hedgehog signalling activity of Smoothened requires phosphorylation by protein kinase A and casein kinase I. Nature *432*, 1045-1050.

Jia, J., Zhang, L., Zhang, Q., Tong, C., Wang, B., Hou, F., Amanai, K., and Jiang, J. (2005). Phosphorylation by double-time/CKIepsilon and CKIalpha targets cubitus interruptus for Slimb/beta-TRCP-mediated proteolytic processing. Dev Cell *9*, 819-830.

Jiang, J., and Struhl, G. (1998). Regulation of the Hedgehog and Wingless signalling pathways by the F-box/WD40-repeat protein Slimb. Nature *391*, 493-496.

Jockel, J.A., Reichel, H., and Nelitz, M. (2011). Correction of knee deformity in patients with Ellis-van Creveld syndrome: A case report and review of the literature. Knee.

Johnson, A.D. (2009). Single-nucleotide polymorphism bioinformatics: a comprehensive review of resources. Circ Cardiovasc Genet *2*, 530-536.

Johnson, R.L., Rothman, A.L., Xie, J., Goodrich, L.V., Bare, J.W., Bonifas, J.M., Quinn, A.G., Myers, R.M., Cox, D.R., Epstein, E.H., Jr*., et al.* (1996). Human homolog of patched, a candidate gene for the basal cell nevus syndrome. Science *272*, 1668-1671.

Kawakami, T., Kawcak, T., Li, Y.J., Zhang, W., Hu, Y., and Chuang, P.T. (2002). Mouse dispatched mutants fail to distribute hedgehog proteins and are defective in hedgehog signaling. Development *129*, 5753-5765.

Kazazian, H.H., Jr. (2004). Mobile elements: drivers of genome evolution. Science *303*, 1626-1632.

Kazazian, H.H., Jr., and Moran, J.V. (1998). The impact of L1 retrotransposons on the human genome. Nat Genet *19*, 19-24.

Kazazian, H.H., Jr., Wong, C., Youssoufian, H., Scott, A.F., Phillips, D.G., and Antonarakis, S.E. (1988). Haemophilia A resulting from de novo insertion of L1 sequences represents a novel mechanism for mutation in man. Nature *332*, 164-166.

Khajavi, M., Inoue, K., and Lupski, J.R. (2006). Nonsense-mediated mRNA decay modulates clinical outcome of genetic disease. Eur J Hum Genet *14*, 1074-1081.

Kobayashi, T., Soegiarto, D.W., Yang, Y., Lanske, B., Schipani, E., McMahon, A.P., and Kronenberg, H.M. (2005). Indian hedgehog stimulates periarticular chondrocyte differentiation to regulate growth plate length independently of PTHrP. J Clin Invest *115*, 1734-1742.

Komori, T., Yagi, H., Nomura, S., Yamaguchi, A., Sasaki, K., Deguchi, K., Shimizu, Y., Bronson, R. T., Gao, Y. H., Inada, M., Sato, M., Okamoto, R., Kitamura, Y., Yoshiki, S., and Kishimoto, T (1997).Targeted disruption of Cbfa1 results in a complete lack of bone formation owing to maturational arrest of osteoblasts. Cell 89, 755-764

Koziel, L., Wuelling, M., Schneider, S., and Vortkamp, A. (2005). Gli3 acts as a repressor downstream of Ihh in regulating two distinct steps of chondrocyte differentiation. Development *132*, 5249-5260.

Kozminski, K.G., Johnson, K.A., Forscher, P., and Rosenbaum, J.L. (1993). A motility in the eukaryotic flagellum unrelated to flagellar beating. Proc Natl Acad Sci U S A *90*, 5519-5523.

Kronenberg, H.M. (2003). Developmental regulation of the growth plate. Nature *423*, 332-336.

Lander, E.S., Linton, L.M., Birren, B., Nusbaum, C., Zody, M.C., Baldwin, J., Devon, K., Dewar, K., Doyle, M., FitzHugh, W*., et al.* (2001). Initial sequencing and analysis of the human genome. Nature *409*, 860-921.

Lee, J.J., Ekker, S.C., von Kessler, D.P., Porter, J.A., Sun, B.I., and Beachy, P.A. (1994). Autoproteolysis in hedgehog protein biogenesis. Science *266*, 1528-1537.

Lewis, P.M., Dunn, M.P., McMahon, J.A., Logan, M., Martin, J.F., St-Jacques, B., and McMahon, A.P. (2001). Cholesterol modification of sonic hedgehog is required for long-range signaling activity and effective modulation of signaling by Ptc1. Cell *105*, 599-612.

Li, C., Chi, S., and Xie, J. (2011). Hedgehog signaling in skin cancers. Cell Signal *23*, 1235-1243.

Litingtung, Y., Dahn, R.D., Li, Y., Fallon, J.F., and Chiang, C. (2002). Shh and Gli3 are dispensable for limb skeleton formation but regulate digit number and identity. Nature *418*, 979-983.

Logan, C.Y., and Nusse, R. (2004). The Wnt signaling pathway in development and disease. Annu Rev Cell Dev Biol *20*, 781-810.

Long, F., Chung, U.I., Ohba, S., McMahon, J., Kronenberg, H.M., and McMahon, A.P. (2004). Ihh signaling is directly required for the osteoblast lineage in the endochondral skeleton. Development *131*, 1309-1318.

Lum, L., and Beachy, P.A. (2004). The Hedgehog response network: sensors, switches, and routers. Science *304*, 1755-1759.

Lum, L., Zhang, C., Oh, S., Mann, R.K., von Kessler, D.P., Taipale, J., Weis-Garcia, F., Gong, R., Wang, B., and Beachy, P.A. (2003). Hedgehog signal transduction via Smoothened association with a cytoplasmic complex scaffolded by the atypical kinesin, Costal-2. Mol Cell *12*, 1261-1274.

Ma, Y., Erkner, A., Gong, R., Yao, S., Taipale, J., Basler, K., and Beachy, P.A. (2002). Hedgehog-mediated patterning of the mammalian embryo requires transporter-like function of dispatched. Cell *111*, 63-75.

Mak, K.K., Kronenberg, H.M., Chuang, P.T., Mackem, S., and Yang, Y. (2008). Indian hedgehog signals independently of PTHrP to promote chondrocyte hypertrophy. Development *135*, 1947-1956.

May, S.R., Ashique, A.M., Karlen, M., Wang, B., Shen, Y., Zarbalis, K., Reiter, J., Ericson, J., and Peterson, A.S. (2005). Loss of the retrograde motor for IFT disrupts localization of Smo to cilia and prevents the expression of both activator and repressor functions of Gli. Dev Biol *287*, 378-389.

McDermott, A., Gustafsson, M., Elsam, T., Hui, C.C., Emerson, C.P., Jr., and Borycki, A.G. (2005). Gli2 and Gli3 have redundant and context-dependent function in skeletal muscle formation. Development *132*, 345-357.

McKusick, V.A., Egeland, J.A., Eldridge, R., and Krusen, D.E. (1964). Dwarfism in the Amish I. The Ellis-Van Creveld Syndrome. Bull Johns Hopkins Hosp *115*, 306-336.

McMahon, A.P., Ingham, P.W., and Tabin, C.J. (2003). Developmental roles and clinical significance of hedgehog signaling. Curr Top Dev Biol *53*, 1-114.

Merchant, M., Evangelista, M., Luoh, S.M., Frantz, G.D., Chalasani, S., Carano, R.A., van Hoy, M., Ramirez, J., Ogasawara, A.K., McFarland, L.M*., et al.* (2005). Loss of the serine/threonine kinase fused results in postnatal growth defects and lethality due to progressive hydrocephalus. Mol Cell Biol *25*, 7054-7068.

Merchant, M., Vajdos, F.F., Ultsch, M., Maun, H.R., Wendt, U., Cannon, J., Desmarais, W., Lazarus, R.A., de Vos, A.M., and de Sauvage, F.J. (2004). Suppressor of fused regulates Gli activity through a dual binding mechanism. Mol Cell Biol *24*, 8627-8641.

Minina, E., Kreschel, C., Naski, M.C., Ornitz, D.M., and Vortkamp, A. (2002). Interaction of FGF, Ihh/Pthlh, and BMP signaling integrates chondrocyte proliferation and hypertrophic differentiation. Dev Cell *3*, 439-449.

Minina, E., Wenzel, H.M., Kreschel, C., Karp, S., Gaffield, W., McMahon, A.P., and Vortkamp, A. (2001). BMP and Ihh/PTHrP signaling interact to coordinate chondrocyte proliferation and differentiation. Development *128*, 4523-4534.

Mostafa, M.I., Temtamy, S.A., el-Gammal, M.A., and Mazen, I.M. (2005). Unusual pattern of inheritance and orodental changes in the Ellis-van Creveld syndrome. Genet Couns *16*, 75-83.

Nagy, E., and Maquat, L.E. (1998). A rule for termination-codon position within intron-containing genes: when nonsense affects RNA abundance. Trends Biochem Sci *23*, 198-199.

Nakashima, K., Zhou, X., Kunkel, G., Zhang, Z., Deng, J.M., Behringer, R.R., and de Crombrugghe, B. (2002). The novel zinc finger-containing transcription factor osterix is required for osteoblast differentiation and bone formation. Cell *108*, 17-29.

Nusslein-Volhard, C., and Wieschaus, E. (1980). Mutations affecting segment number and polarity in Drosophila. Nature *287*, 795-801.

Ocbina, P.J., and Anderson, K.V. (2008). Intraflagellar transport, cilia, and mammalian Hedgehog signaling: analysis in mouse embryonic fibroblasts. Dev Dyn *237*, 2030-2038.

Ohlmeyer, J.T., and Kalderon, D. (1998). Hedgehog stimulates maturation of Cubitus interruptus into a labile transcriptional activator. Nature *396*, 749-753.

Olsen, B.R., Reginato, A.M., and Wang, W. (2000). Bone development. Annu Rev Cell Dev Biol *16*, 191-220.

Ornitz, D.M., and Marie, P.J. (2002). FGF signaling pathways in endochondral and intramembranous bone development and human genetic disease. Genes Dev *16*, 1446-1465.

Otto, F., Thornell, A.P., Crompton, T., Denzel, A., Gilmour, K. C., Rosewell, I. R., Stamp, G. W., Beddington, R. S., Mundlos, S., Olsen, B. R., Selby, P. B., Owen, M. J. (1997). Cbfa1, a candidate gene for cleidocranial dysplasia syndrome, is essential for osteoblast differentiation and bone development. Cell 89, 765-771

Pan, Y., Bai, C.B., Joyner, A.L., and Wang, B. (2006). Sonic hedgehog signaling regulates Gli2 transcriptional activity by suppressing its processing and degradation. Mol Cell Biol *26*, 3365-3377.

Pastorino, L., Ghiorzo, P., Nasti, S., Battistuzzi, L., Cusano, R., Marzocchi, C., Garre, M.L., Clementi, M., and Scarra, G.B. (2009). Identification of a SUFU germline mutation in a family with Gorlin syndrome. Am J Med Genet A *149A*, 1539-1543.

Pathi, S., Rutenberg, J.B., Johnson, R.L., and Vortkamp, A. (1999). Interaction of Ihh and BMP/Noggin signaling during cartilage differentiation. Dev Biol *209*, 239-253.

Pedersen, L.B., and Rosenbaum, J.L. (2008). Intraflagellar transport (IFT) role in ciliary assembly, resorption and signalling. Curr Top Dev Biol *85*, 23-61.

Pedersen, L.B., Veland, I.R., Schroder, J.M., and Christensen, S.T. (2008). Assembly of primary cilia. Dev Dyn *237*, 1993-2006.

Polymeropoulos, M.H., Ide, S.E., Wright, M., Goodship, J., Weissenbach, J., Pyeritz, R.E., Da Silva, E.O., Ortiz De Luna, R.I., and Francomano, C.A. (1996). The gene for the Ellis-van Creveld syndrome is located on chromosome 4p16. Genomics *35*, 1-5.

Porter, J.A., Ekker, S.C., Park, W.J., von Kessler, D.P., Young, K.E., Chen, C.H., Ma, Y., Woods, A.S., Cotter, R.J., Koonin, E.V.*, et al.* (1996). Hedgehog patterning activity: role of a lipophilic modification mediated by the carboxy-terminal autoprocessing domain. Cell *86*, 21-34.

Preat, T. (1992). Characterization of Suppressor of fused, a complete suppressor of the fused segment polarity gene of Drosophila melanogaster. Genetics *132*, 725-736.

Razzaque, M.S., Soegiarto, D.W., Chang, D., Long, F., and Lanske, B. (2005). Conditional deletion of Indian hedgehog from collagen type 2alpha1-expressing cells results in abnormal endochondral bone formation. J Pathol *207*, 453-461.

Redon, R., Ishikawa, S., Fitch, K.R., Feuk, L., Perry, G.H., Andrews, T.D., Fiegler, H., Shapero, M.H., Carson, A.R., Chen, W.*, et al.* (2006). Global variation in copy number in the human genome. Nature *444*, 444-454.

Rohatgi, R., Milenkovic, L., and Scott, M.P. (2007). Patched1 regulates hedgehog signaling at the primary cilium. Science *317*, 372-376.

Rohatgi, R., and Scott, M.P. (2007). Patching the gaps in Hedgehog signalling. Nat Cell Biol *9*, 1005-1009.

Rosenbaum, J.L., and Witman, G.B. (2002). Intraflagellar transport. Nat Rev Mol Cell Biol *3*, 813-825.

Roubicek, M., and Spranger, J. (1984). Weyers acrodental dysostosis in a family. Clin Genet *26*, 587-590.

Rousseau, F., Bonaventure, J., Legeai-Mallet, L., Pelet, A., Rozet, J.M., Maroteaux, P., Le Merrer, M., and Munnich, A. (1994). Mutations in the gene encoding fibroblast growth factor receptor-3 in achondroplasia. Nature *371*, 252-254.

Ruiz-Perez, V.L., Blair, H.J., Rodriguez-Andres, M.E., Blanco, M.J., Wilson, A., Liu, Y.N., Miles, C., Peters, H., and Goodship, J.A. (2007). Evc is a positive mediator of Ihh-regulated bone growth that localises at the base of chondrocyte cilia. Development *134*, 2903-2912.

Ruiz-Perez, V.L., and Goodship, J.A. (2009). Ellis-van Creveld syndrome and Weyers acrodental dysostosis are caused by cilia-mediated diminished response to hedgehog ligands. Am J Med Genet C Semin Med Genet *151C*, 341-351.

Ruiz-Perez, V.L., Ide, S.E., Strom, T.M., Lorenz, B., Wilson, D., Woods, K., King, L., Francomano, C., Freisinger, P., Spranger, S.*, et al.* (2000). Mutations in a new gene in Ellis-van Creveld syndrome and Weyers acrodental dysostosis. Nat Genet *24*, 283-286.

Ruiz-Perez, V.L., Tompson, S.W., Blair, H.J., Espinoza-Valdez, C., Lapunzina, P., Silva, E.O., Hamel, B., Gibbs, J.L., Young, I.D., Wright, M.J., *et al.* (2003). Mutations in two nonhomologous genes in a head-to-head configuration cause Ellis-van Creveld syndrome. Am J Hum Genet *72*, 728-732.

Scholey, J.M. (2008). Intraflagellar transport motors in cilia: moving along the cell's antenna. J Cell Biol *180*, 23-29.

Sedmak, T., and Wolfrum, U. (2011). Intraflagellar transport proteins in ciliogenesis of photoreceptor cells. Biol Cell *103*, 449-466.

Segal, Y., Peissel, B., Renieri, A., de Marchi, M., Ballabio, A., Pei, Y., and Zhou, J. (1999). LINE-1 elements at the sites of molecular rearrangements in Alport syndrome-diffuse leiomyomatosis. Am J Hum Genet *64*, 62-69.

Shapiro, S.D., Jorgenson, R.J., and Salinas, C.F. (1984). Brief clinical report: Curry-Hall syndrome. Am J Med Genet *17*, 579-583.

Shen, W., Han, D., Zhang, J., Zhao, H., and Feng, H. (2011). Two novel heterozygous mutations of EVC2 cause a mild phenotype of Ellis-van Creveld syndrome in a Chinese family. Am J Med Genet A *155A*, 2131-2136.

Shiang, R., Thompson, L.M., Zhu, Y.Z., Church, D.M., Fielder, T.J., Bocian, M., Winokur, S.T., and Wasmuth, J.J. (1994). Mutations in the transmembrane domain of FGFR3 cause the most common genetic form of dwarfism, achondroplasia. Cell *78*, 335-342.

Shibata, T., Kawabata, H., Yasui, N., Nakahara, H., Hirabayashi, S., Nakase, T., and Ochi, T. (1999). Correction of knee deformity in patients with Ellis-van Creveld syndrome. J Pediatr Orthop B *8*, 282-284.

Silverman, M.A., and Leroux, M.R. (2009). Intraflagellar transport and the generation of dynamic, structurally and functionally diverse cilia. Trends Cell Biol *19*, 306-316.

Singla, V., and Reiter, J.F. (2006). The primary cilium as the cell's antenna: signaling at a sensory organelle. Science *313*, 629-633.

Smelkinson, M.G., and Kalderon, D. (2006). Processing of the Drosophila hedgehog signaling effector Ci-155 to the repressor Ci-75 is mediated by direct binding to the SCF component Slimb. Curr Biol *16*, 110-116.

St-Jacques, B., Hammerschmidt, M., and McMahon, A.P. (1999). Indian hedgehog signaling regulates proliferation and differentiation of chondrocytes and is essential for bone formation. Genes Dev *13*, 2072-2086.

Steemers, F.J., and Gunderson, K.L. (2007). Whole genome genotyping technologies on the BeadArray platform. Biotechnol J *2*, 41-49.

Stoll, C., Dott, B., Roth, M.P., and Alembik, Y. (1989). Birth prevalence rates of skeletal dysplasias. Clin Genet *35*, 88-92.

Svard, J., Heby-Henricson, K., Persson-Lek, M., Rozell, B., Lauth, M., Bergstrom, A., Ericson, J., Toftgard, R., and Teglund, S. (2006). Genetic elimination of Suppressor of fused reveals an essential repressor function in the mammalian Hedgehog signaling pathway. Dev Cell *10*, 187-197.

Taipale, J., Chen, J.K., Cooper, M.K., Wang, B., Mann, R.K., Milenkovic, L., Scott, M.P., and Beachy, P.A. (2000). Effects of oncogenic mutations in Smoothened and Patched can be reversed by cyclopamine. Nature *406*, 1005-1009.

Takeda, H., Takami, M., Oguni, T., Tsuji, T., Yoneda, K., Sato, H., Ihara, N., Itoh, T., Kata, S.R., Mishina, Y.*, et al.* (2002). Positional cloning of the gene LIMBIN responsible for bovine chondrodysplastic dwarfism. Proc Natl Acad Sci U S A *99*, 10549-10554.

Tavormina, P.L., Shiang, R., Thompson, L.M., Zhu, Y.Z., Wilkin, D.J., Lachman, R.S., Wilcox, W.R., Rimoin, D.L., Cohn, D.H., and Wasmuth, J.J. (1995). Thanatophoric dysplasia (types I and II) caused by distinct mutations in fibroblast growth factor receptor 3. Nat Genet *9*, 321-328.

Taylor, M.D., Liu, L., Raffel, C., Hui, C.C., Mainprize, T.G., Zhang, X., Agatep, R., Chiappa, S., Gao, L., Lowrance, A.*, et al.* (2002). Mutations in SUFU predispose to medulloblastoma. Nat Genet *31*, 306-310.

Tempe, D., Casas, M., Karaz, S., Blanchet-Tournier, M.F., and Concordet, J.P. (2006). Multisite protein kinase A and glycogen synthase kinase 3beta phosphorylation leads to Gli3 ubiquitination by SCFbetaTrCP. Mol Cell Biol *26*, 4316-4326.

Tenzen, T., Allen, B.L., Cole, F., Kang, J.S., Krauss, R.S., and McMahon, A.P. (2006). The cell surface membrane proteins Cdo and Boc are components and targets of the Hedgehog signaling pathway and feedback network in mice. Dev Cell *10*, 647-656.

The, I., Bellaiche, Y., and Perrimon, N. (1999). Hedgehog movement is regulated through tout velu-dependent synthesis of a heparan sulfate proteoglycan. Mol Cell *4*, 633-639.

Tompson, S.W., Ruiz-Perez, V.L., Blair, H.J., Barton, S., Navarro, V., Robson, J.L., Wright, M.J., and Goodship, J.A. (2007). Sequencing EVC and EVC2 identifies mutations in two-thirds of Ellis-van Creveld syndrome patients. Hum Genet *120*, 663-670.

Tukachinsky, H., Lopez, L.V., and Salic, A. (2010). A mechanism for vertebrate Hedgehog signaling: recruitment to cilia and dissociation of SuFu-Gli protein complexes. J Cell Biol *191*, 415-428.

Umm, E.K., Wasif, N., Tariq, M., and Ahmad, W. (2010). A novel missense mutation in the EVC gene underlies Ellis-van Creveld syndrome in a Pakistani family. Pediatr Int *52*, 240-246.

Valencia, M., Lapunzina, P., Lim, D., Zannolli, R., Bartholdi, D., Wollnik, B., Al-Ajlouni, O., Eid, S. S., Cox, H., Buoni, S., Hayek, J., Martinez-Frias, M. L., Antonio, P. A., Temtamy, S., Aglan, M., Goodship, J. A., and Ruiz-Perez, V. L. (2009). Widening the mutation spectrum of EVC and EVC2: ectopic expression of Weyer variants in NIH 3T3 fibroblasts disrupts Hedgehog signaling. Hum Mutat 30, 1667-1675

Varjosalo, M., Li, S.P., and Taipale, J. (2006). Divergence of hedgehog signal transduction mechanism between Drosophila and mammals. Dev Cell *10*, 177-186.

Vortkamp, A., Lee, K., Lanske, B., Segre, G.V., Kronenberg, H.M., and Tabin, C.J. (1996). Regulation of rate of cartilage differentiation by Indian hedgehog and PTH-related protein. Science *273*, 613-622.

Wang, B., Fallon, J.F., and Beachy, P.A. (2000). Hedgehog-regulated processing of Gli3 produces an anterior/posterior repressor gradient in the developing vertebrate limb. Cell *100*, 423-434.

Wang, Q.T., and Holmgren, R.A. (1999). The subcellular localization and activity of Drosophila cubitus interruptus are regulated at multiple levels. Development *126*, 5097-5106.

Weyers, H. (1952). [A correlated abnormality of the mandible and extremities (dysostosis acrofacialis)]. Fortschr Geb Rontgenstr *77*, 562-567.

Wolfrum, U., and Schmitt, A. (2000). Rhodopsin transport in the membrane of the connecting cilium of mammalian photoreceptor cells. Cell Motil Cytoskeleton *46*, 95-107.

Yao, S., Lum, L., and Beachy, P. (2006). The ihog cell-surface proteins bind Hedgehog and mediate pathway activation. Cell *125*, 343-357.

Ye, X., Song, G., Fan, M., Shi, L., Jabs, E.W., Huang, S., Guo, R., and Bian, Z. (2006). A novel heterozygous deletion in the EVC2 gene causes Weyers acrofacial dysostosis. Hum Genet *119*, 199-205.

Young, B., Minugh-Purvis, N., Shimo, T., St-Jacques, B., Iwamoto, M., Enomoto-Iwamoto, M., Koyama, E., and Pacifici, M. (2006). Indian and sonic hedgehogs regulate synchondrosis growth plate and cranial base development and function. Dev Biol *299*, 272-282.

Zaghloul, N.A., and Katsanis, N. (2009). Mechanistic insights into Bardet-Biedl syndrome, a model ciliopathy. J Clin Invest *119*, 428-437.

Zhang, C., Williams, E.H., Guo, Y., Lum, L., and Beachy, P.A. (2004). Extensive phosphorylation of Smoothened in Hedgehog pathway activation. Proc Natl Acad Sci U S A *101*, 17900-17907.

Zhang, Q., Zhang, L., Wang, B., Ou, C.Y., Chien, C.T., and Jiang, J. (2006a). A hedgehog-induced BTB protein modulates hedgehog signaling by degrading Ci/Gli transcription factor. Dev Cell *10*, 719-729.

Zhang, W., Kang, J.S., Cole, F., Yi, M.J., and Krauss, R.S. (2006b). Cdo functions at multiple points in the Sonic Hedgehog pathway, and Cdo-deficient mice accurately model human holoprosencephaly. Dev Cell *10*, 657-665.

Zhang, W., Zhao, Y., Tong, C., Wang, G., Wang, B., Jia, J., and Jiang, J. (2005). Hedgehog-regulated Costal2-kinase complexes control phosphorylation and proteolytic processing of Cubitus interruptus. Dev Cell *8*, 267-278.

Zhu, A.J., and Scott, M.P. (2004). Incredible journey: how do developmental signals travel through tissue? Genes Dev *18*, 2985-2997.

Anexos

El trabajo realizado durante el desarrollo de la tesis ha dado lugar a otras publicaciones, que se adjuntan como anexo:

Lapunzina, P.; Aglan, M.; Temtamy, S.;Caparrós-Martín, J.A.; **Valencia, M.**; Letón, R.; Martínez-Glez, V.; Elhossini, R.; Amr, K.;Vilaboa, N.; Ruiz-Perez, V.L.*"Identification of a frameshift mutation in Osterix in a patient with recessive osteogenesis imperfecta."*. Am. J. Hum. Genet. 87(1): 110-114. (2010).

Martínez-Glez, V.*; **Valencia, M**.*; Caparrós-Martín, J.A.*; Aglan, M.*; Temtamy, S.*; Tenorio, J.; Pulido, V.; Lindert, U.; Rohrbach, M.; Eyre, D.; Giunta, C.; Lapunzina, P.; Ruiz-Perez, V.L.*"Identification of a mutation causing deficient BMP1/mTLD proteolytic activity in autosomal recessive osteogenesis imperfecta."*. Hum. Mutat. 33(2): 343-350. (2012).

Identification of a Frameshift Mutation in *Osterix* in a Patient with Recessive Osteogenesis Imperfecta

Pablo Lapunzina,[1,2,7] Mona Aglan,[3,7] Samia Temtamy,[3,7] José A. Caparrós-Martín,[1,4] Maria Valencia,[1,4] Rocío Letón,[1,4,8] Victor Martínez-Glez,[1,2] Rasha Elhossini,[3] Khalda Amr,[3] Nuria Vilaboa,[5,6] and Victor L. Ruiz-Perez[1,4,*]

Osteogenesis imperfecta, or "brittle bone disease," is a type I collagen-related condition associated with osteoporosis and increased risk of bone fractures. Using a combination of homozygosity mapping and candidate gene approach, we have identified a homozygous single base pair deletion (c.1052delA) in *SP7/Osterix* (*OSX*) in an Egyptian child with recessive osteogenesis imperfecta. The clinical findings from this patient include recurrent fractures, mild bone deformities, delayed tooth eruption, normal hearing, and white sclera. *OSX* encodes a transcription factor containing three Cys2-His2 zinc-finger DNA-binding domains at its C terminus, which, in mice, has been shown to be essential for bone formation. The frameshift caused by the c.1052delA deletion removes the last 81 amino acids of the protein, including the third zinc-finger motif. This finding adds another locus to the spectrum of genes associated with osteogenesis imperfecta and reveals that *SP7/OSX* also plays a key role in human bone development.

Osteogenesis imperfecta (OI, MIM 166200, MIM 166210, MIM 259420, MIM 166220) is a bone-related genetic disorder characterized by low bone mass and bone fragility that is clinically and genetically heterogeneous. Patients with OI have clinical features that may range from mild symptoms with a scant number of fractures to severe bone deformities and neonatal lethality.[1] Most cases of OI are caused by mutations in the type I procollagen genes, *COL1A1* (MIM 120150) and *COL1A2* (MIM 120160), and follow an autosomal-dominant pattern of inheritance.[2] Type I collagen is a structural component of the connective tissue that is initially synthesized as a procollagen precursor in the endoplasmic reticulum (ER) by the combination of two procollagen a1 (I) and one procollagen a2 (I) peptide chains paired together into a triple helix, a process that is assisted by a number of molecular chaperons and ER enzymes. Type I procollagen trimers are then exported into the extracellular matrix and transformed into functionally competent type I collagen molecules by the proteolytic removal of the N-terminal and C-terminal propeptides.[3] In a minority of cases with severe or lethal autosomal-recessive OI, there have been mutations identified in the three components of the ER collagen 3-hydroxylation complex, comprising prolyl 3-hydroxylase 1 (LEPRE1, MIM 610339), cartilage-associated protein (CRTAP, MIM 605497), and peptidylprolyl isomerase B (PPIB, MIM 123841).[4–7] These three proteins are responsible for the 3-hydroxylation of a specific residue, Pro986, in the collagen a1 (I) chains.[8] Although the function of this modification is not clear, it appears to be important for the correct folding or stability of the collagen triple helix.[9] Recently, also in a family with severe OI and recessive inheritance, a homozygous missense mutation (c.233T>C, p.Leu78Pro) was found in *SERPINH1* (MIM 600943; Serpin peptidase inhibitor, clade H), the gene encoding the ER chaperone-like protein HSP47 (heat shock protein 47).[10] *SERPINH1* was first linked to OI by homozygosity mapping in a canine pedigree of Dachshunds.[11] Biochemical analysis of patient-derived primary fibroblasts demonstrated that the p.Leu78Pro HSP47 mutant variants were subjected to proteasome-mediated degradation, whereas there was accumulation of type I procollagen in the Golgi and abnormal folding of a proportion of the secreted type I collagen. Because Pro986 3-hydroxylation was found to be normal in the HSP47 mutant cells, it was concluded that this protein is required downstream of the CRTAP/LEPRE1/PPIB protein complex.[10] Finally, two mutations have been reported in *FKBP10* (MIM 607063) in patients with moderately severe OI and recessive disease transmission.[12] *FKBP10* codes for FKBP65, which is a protein with known type I procollagen chaperone function. Investigation of the FKBP65 mutations in dermal fibroblasts from affected individuals revealed normal 3-hydroxylation of the proline 986 but delayed secretion of type I procollagen.[12] Hence, so far all the genes associated with OI are involved in the synthesis, posttranslational modification, trafficking, processing, or secretion of type I collagen. Herein we report the genetic analysis of a family that has led us to the identification of an additional gene mutated in this disease.

[1]CIBER de enfermedades Raras (CIBERER), 28046 Madrid, Spain; [2]Instituto de Genética Médica y Molecular, Hospital Universitario La Paz-IdiPaz, Universidad Autónoma de Madrid, 28046 Madrid, Spain; [3]Human Genetics and Genome Research Division, National Research Centre, 12311 Cairo, Egypt; [4]Instituto de Investigaciones Biomédicas, Consejo Superior de Investigaciones Científicas-Universidad Autónoma de Madrid, 28029 Madrid, Spain; [5]Unidad de Investigación, Hospital Universitario La Paz-IdiPaz, 28046 Madrid, Spain; [6]CIBER de Bioingeniería, Biomateriales y Nanomedicina (CIBER-BBN), 28046 Madrid, Spain
[7]These authors contributed equally to this work
[8]Present address: Centro Nacional de Investigaciones Oncológicas, 28029 Madrid, Spain
*Correspondence: vlruiz@iib.uam.es
DOI 10.1016/j.ajhg.2010.05.016. ©2010 by The American Society of Human Genetics. All rights reserved.

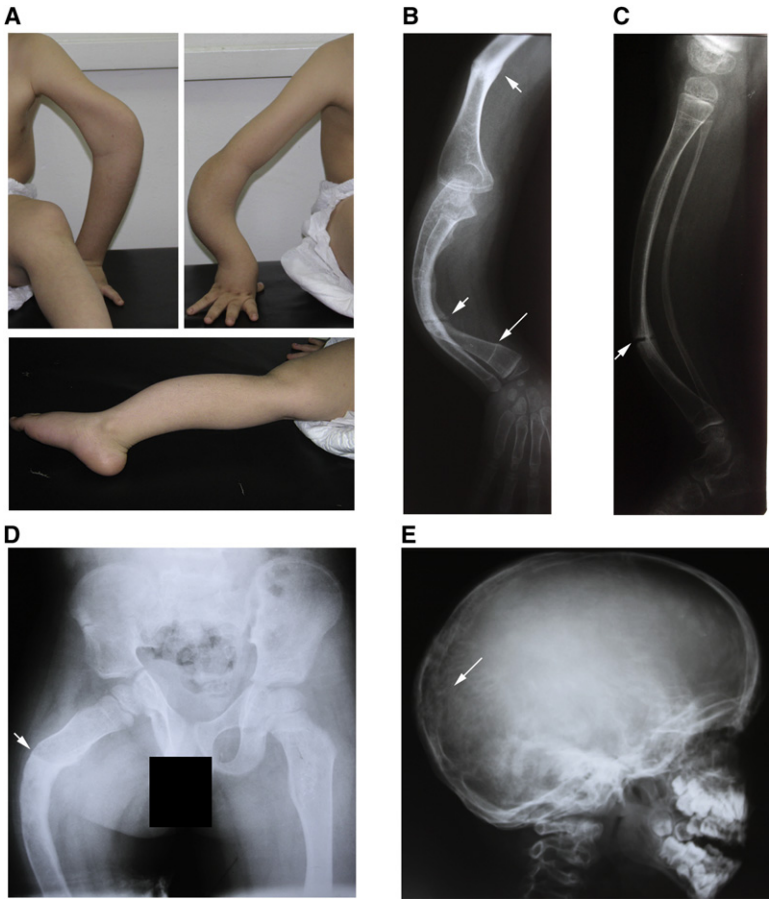

Figure 1. Clinical Findings in the Patient with an *OSX* Mutation

(A) Photographs of the reported patient showing bowing of the long bones of the arms (top) and sabre tibia (bottom).

(B–E) Radiographical findings in the proband at the age of 8 years.

(B) X-ray of the right upper limb (lateral view) demonstrating anterior bowing, deformed irregular humerus, radius, and ulna, and generalized decreased bone density. An old, improperly healed fracture at the lower third of the humerus and transverse fractures of the radius and ulna are indicated by small arrows. The long arrow designates a transverse line of arrested bone growth at the lower end of the radius.

(C) X-ray of the right leg (lateral view) showing decreased bone density with anterior bowing of the tibia and fibula and transverse fracture at the lower third of the tibia (arrow).

(D) X-ray of the pelvis and upper ends of femora (anterior-posterior view) demonstrating a deformed asymmetric pelvis with thin laterally displaced neck of the femur, bilaterally, mostly on the right side. There is an old, improperly healed fracture at the upper end of right femur with callus formation (arrow).

(E) X-ray of the skull (lateral view) showing wormian bones at the occipital region (arrow).

We have studied the case of an Egyptian 8-year-old boy with OI born to consanguineous parents related as second cousins (Figure 1; Figure 2A). The family had a history of a similarly affected sibling who, in addition to OI with repeated bone fractures, was diagnosed with a congenital heart condition and died at the age of 4 years as a result of pneumonia. We did not see the deceased child, and thus no DNA from this individual was available for molecular studies. Fractures in the proband started at 3 months of age, and since then they occurred frequently, mostly following minor trauma, with an average of 6–7 fractures per year. The number of fractures decreased after the patient began biphosphonate treatment (see Table S1 available online). The child has had delayed motor milestones: he sat at the age of 1 year, was not able to stand unsupported until the age of 6 years, and he is not able to walk independently at the age of 8 years. His hearing and sclerae were normal. Craniofacial features included a skull with wormian bones, mild asymmetry of the face, high prominent forehead with prominent supraorbital ridges more obvious on the right side, midface hypoplasia, depressed nasal bridge, microstomia, micrognathia, and high arched palate. Delayed teeth eruption was noted, but he did not have dentinogenesis imperfecta. Radiographic examination of the skeletal system revealed bowing of the upper and lower limbs; his right leg was shorter than his left leg because of bone deformities, and he also presented hyperextensibility of the interphalangeal joints, mild scoliosis, and mild pectus carinatum (Figure 1). Anthropometric measurements for length were below normal (−3.6 standard deviation [SD] at the age of 8 years), and head circumference and weight were within normal range for his age (+0.9 SD and −2.1 SD, respectively, at the age of 8 years). Bone densitometry performed by dual energy X-ray absorptiometry (DEXA) revealed generalized osteoporosis (Z score of −3.4 at the lumbar spine and −1.9 at the femur at the age of 4 years, before the start of biphosphonate treatment). Anthropometric and DEXA data related to the follow-up of this patient are listed in Table S1. Based on the phenotype, a diagnosis of OI type IV was considered following the Sillence classification guidelines.[1] All studies and investigations involving the proband and other members of his family were performed in accordance with the ethical standards of the Medical Research Ethics Committee of the National Research Centre (Egypt), and all DNA samples were obtained with appropriate informed consent.

Recurrence in a sibling and parental consanguinity suggested a recessive pattern of inheritance, and on this basis we embarked on the genetic analysis of this family. Microsatellite analysis in the proband, his father, and two of the unaffected siblings excluded linkage to *COL1A1*, *COL1A2*, *LEPRE1*, and *CRTAP* under a recessive disease model, because the patient was heterozygous for markers

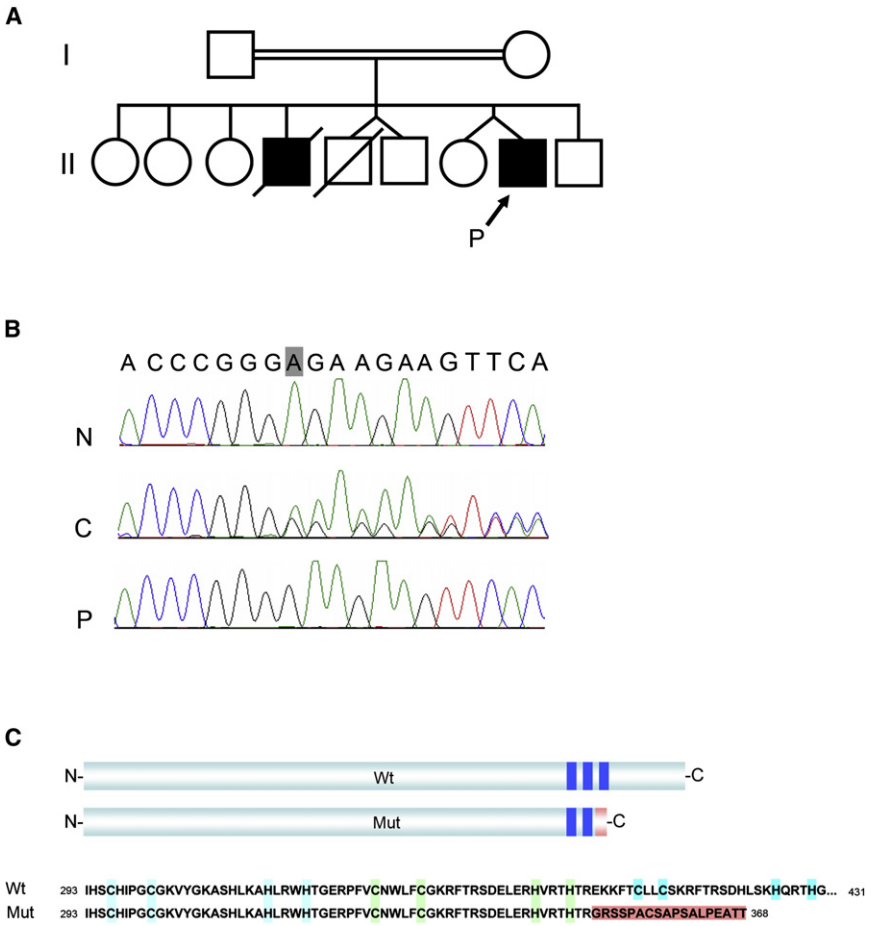

Figure 2. Identification of a Frameshift Mutation in *Osterix*

(A) Pedigree of the OI family analyzed in this study; the proband (P) is designated with an arrow.

(B) Alignment of genomic sequence chromatograms corresponding to an area encompassing the c.1052delA mutation from a normal individual (N), a heterozygous carrier (C), and the proband (P). The adenine deleted in the patient is squared in gray. Numbering of the mutation correlates to the reference sequence NM_152860.1, taking the A of the translation start site as nucleotide + 1.

(C) Protein effect of the c.1052delA mutation. The picture on the top shows the position of the three zinc fingers represented by blue rectangles in the normal (Wt) and mutant (Mut) SP7 proteins. The mutant protein is missing the third zinc finger, and the new residues incorporated after the frameshift are indicated in red. The lower panel shows the sequence of amino acids corresponding to the DNA binding region of normal and mutant OSX. Conserved cysteine and histidine residues involved in zinc ion coordination corresponding to each individual zinc finger are highlighted in different colors. The amino acids inserted after the mutation are in red. Protein numbering is related to the reference sequence NP_690599.1.

surrounding these loci. We also sequenced the five coding exons of *PPIB*, the five exons of *SERPINH1*, and all of the coding exons of *COL1A1* and *COL1A2*, including the intronic boundaries, but no pathogenic sequence variations were found in the patient DNA. To search for the causative gene, we performed homozygosity mapping in the proband and one of his unaffected sisters by using genome-wide high-density SNP arrays (Illumina Human610-Quad BeadChip). The two SNP genotypes generated by this process were then analyzed with Illumina software to look for blocks of homozygosity. Taking an arbitrary cutoff of 300 consecutive homozygous SNPs, we found five large regions of homozygosity in the patient that were not shared by his normal sibling. These regions were located on chromosome 2 (two DNA segments of 3.5 and 3.1 Mb), chromosome 4 (8.1 Mb), chromosome 11 (14.5 Mb), and chromosome 12 (19.3 Mb) and contained 29, 22, 92, 410, and 332 genes, respectively (Genome Reference Consortium Human Build 37.1). Evaluation of the transcripts comprised in each region revealed the presence of a candidate gene, *SP7/OSX* (MIM 606633), in the homozygosity block of chromosome 12 (12q13.13). We considered *OSX* to be a good candidate for the disease because it encodes an osteoblast-specific transcription factor that, in mice, has been shown to be indispensable for bone formation. Osx null mice are deficient in osteoblast differentiation and have reduced expression of osteoblast markers, including *Col1a1*, *Bone sialoprotein*, and *Osteocalcin*.[13] In addition, these mice display bone-bending deformities similar to those seen in patients with OI.[13] We screened the proband for the presence of *OSX* mutations by genomic amplification followed by direct sequencing of the two *SP7* coding exons and at least 100 bp of the adjacent intronic sequences, and we identified a homozygous single nucleotide deletion, c.1052delA, in the last exon of this gene (Figure 2B). The frameshift caused by this mutation introduces 18 novel residues at codon 351 before running into a premature termination codon (p.E351GfsX19). Segregation analysis of the mutation within the family showed that the two parents were heterozygous for the nucleotide deletion and that out of the five normal siblings from whom we could obtain DNA, three carried the mutation in the heterozygous state and two had normal sequence. We checked normal controls for the presence of the c.1052delA change by direct sequencing, but it was not found in 122 control chromosomes of the same ethnic origin or in 284 normal chromosomes from controls of mixed ethnicity.

Because the c.1052delA mutation introduces a premature stop codon within the final exon of the gene, the mutant transcript is predicted to escape the nonsense-mediated mRNA decay machinery.[14] OSX is a 431 amino acid protein that belongs to the Specificity protein (Sp)

subgroup of the Krüppel-like family of transcription factors characterized by the invariable presence of three tandem Cys2-His2 zinc-finger DNA-binding domains at their carboxy terminus.[15–17] Based on crystallography and nuclear magnetic resonance studies performed in some members of the family, it has been established that each protein finger recognizes a consecutive trinucleotide sequence, with the three zinc fingers contributing to the strength and specificity of the DNA-protein interaction.[18–20] Sp1, which is the best-characterized member of the Sp group and is closely related to SP7, binds GC-rich DNA boxes of 9 base pairs. Previous experimental studies, including DNA-binding assays, that used Sp1 peptide fragments in which either the N-terminal (1) or the C-terminal (3) zinc fingers were deleted demonstrated a greater contribution of finger 3 to the DNA-binding affinity than the other two remaining fingers.[21,22] The p.E351GfsX19 change leads to a truncated SP7 protein that lacks the last 81 amino acids, including the third Zn-finger domain, and carries instead 18 new residues downstream of codon 351 (Figure 2C). Thus, in the case in which the OSX mutant variant is not degraded by the proteasome, its DNA-binding properties are expected to be altered, and, consequently, the SP7/OSX-mediated transcription regulation will be impaired. Mutations in the third Zn finger of EGR2 (MIM 129010), a very similar Cys2-His2 transcription factor, have been described in patients with autosomal-recessive congenital hypomyelinating neuropathy (MIM 605253), proving that mutations in the third zinc finger can lead to disease.[23] A limitation of this work is that in vivo studies to assess the effect of the *OSX* mutation on transcript and protein stability and on type 1 collagen production in patient cells could not be performed because of the unavailability of additional biological material from the patient.

Sp7/Osx is specifically expressed in cortical and trabecular osteoblasts and at a lower level in the prehypertrophic chondrocytes of the growth plate.[13] This restricted expression pattern is consistent with the patient having normal white sclera. Analysis of *Osx* mouse models has revealed that Osx plays an essential role in regulating the differentiation of preosteoblasts to osteoblasts in a step downstream of *Runx2* (MIM 600211),[13] another transcription factor that is a master regulator for osteoblast differentiation and that, in humans, is responsible for cleidocranial dysplasia (MIM 119600).[24] Although *Runx2* null mice do not express *Osx*, *Runx2* expression was shown to be unaffected in the developing bones of $Osx^{-/-}$ mutants.[13] In agreement with the craniofacial features identified in our patient, both endochondral and intramembranous bone formations were found to be disrupted in the Osx null mice. Because constitutive ablation of Osx is perinatal lethal, the function of Osx in adult bone has been studied by using conditional models. Postnatal inactivation of Osx with tamoxifen inducible *Col1a1-CreERT2* mice resulted in impaired bone formation as a result of reduced expression of osteoblast-specific markers.[25] OSX function has not been explored in detail in humans, but the DNA region around *OSX* has been identified as one of the osteoporosis susceptibility loci. Several genome-wide association studies have shown significant association of common variants in the region of *OSX* with bone mineral density (BMD) and osteoporosis, although this association could not be assigned unequivocally to this gene.[26–28] To assess whether the c.1052delA *OSX* mutation could have an effect on adult BMD in the heterozygous state, we performed DEXA scans in the parents of our patient. The 39-year-old mother had normal bone density at the femur (T score −0.4) and osteopenia at the spine (T score −1.3). The 61-year-old father had borderline osteoporosis of the spine and osteoporosis of the femur (T scores −2.2 and −3.0, respectively). However, the father has been on corticosteroid therapy for the treatment of lung fibrosis since the age of 43 years and had already been identified as having progressive osteoporosis and bilateral glaucoma 2 years after the beginning of this treatment. He also has a history of partial thyroidectomy at the age of 39 years, and he is on L-thyroxine, but thyroid functions are not regulated. Because it is known that prolonged corticosteroid therapy can induce osteoporosis, we cannot conclude from these data that the low BMD of the father is a direct consequence of being a heterozygous carrier for the *OSX* mutation.

In summary, the data we present here add one more gene to the growing number of causative loci for autosomal-recessive OI and indicate that mutations in transcription factors that regulate the expression of osteoblast-specific genes can also be accountable for OI. Further testing is required to ascertain what proportion of autosomal-recessive OI cases arise from mutations in *OSX*.

Supplemental Data

Supplemental Data include one table and can be found with this article online at http://www.ajhg.org.

Acknowledgments

We thank the patient and his family for their contribution to this research. This work was funded by the Biomedical Network Research Centre on Rare Diseases (CIBERER), the Spanish Ministry of Science and Innovation (SAF-62291), and the Ramon Areces Foundation. We are grateful to Judith Goodship for the critical reading of the manuscript.

Received: April 12, 2010
Revised: May 19, 2010
Accepted: May 24, 2010
Published online: June 24, 2010

Web Resources

The URLs for data presented herein are as follows:

Ensembl Human Genome Browser, http://www.ensembl.org/index.html

Online Mendelian Inheritance in Man, http://www.ncbi.nlm.nih.gov/Omim/
Primer3 design tool, http://frodo.wi.mit.edu/primer3/
UCSC Genome Browser, http://genome.ucsc.edu/

References

1. Sillence, D.O., Senn, A., and Danks, D.M. (1979). Genetic heterogeneity in osteogenesis imperfecta. J. Med. Genet. *16*, 101–116.
2. Byers, P.H., and Steiner, R.D. (1992). Osteogenesis imperfecta. Annu. Rev. Med. *43*, 269–282.
3. Canty, E.G., and Kadler, K.E. (2005). Procollagen trafficking, processing and fibrillogenesis. J. Cell Sci. *118*, 1341–1353.
4. Cabral, W.A., Chang, W., Barnes, A.M., Weis, M., Scott, M.A., Leikin, S., Makareeva, E., Kuznetsova, N.V., Rosenbaum, K.N., Tifft, C.J., et al. (2007). Prolyl 3-hydroxylase 1 deficiency causes a recessive metabolic bone disorder resembling lethal/severe osteogenesis imperfecta. Nat. Genet. *39*, 359–365.
5. Barnes, A.M., Chang, W., Morello, R., Cabral, W.A., Weis, M., Eyre, D.R., Leikin, S., Makareeva, E., Kuznetsova, N., Uveges, T.E., et al. (2006). Deficiency of cartilage-associated protein in recessive lethal osteogenesis imperfecta. N. Engl. J. Med. *355*, 2757–2764.
6. Morello, R., Bertin, T.K., Chen, Y., Hicks, J., Tonachini, L., Monticone, M., Castagnola, P., Rauch, F., Glorieux, F.H., Vranka, J., et al. (2006). CRTAP is required for prolyl 3- hydroxylation and mutations cause recessive osteogenesis imperfecta. Cell *127*, 291–304.
7. van Dijk, F.S., Nesbitt, I.M., Zwikstra, E.H., Nikkels, P.G., Piersma, S.R., Fratantoni, S.A., Jimenez, C.R., Huizer, M., Morsman, A.C., Cobben, J.M., et al. (2009). PPIB mutations cause severe osteogenesis imperfecta. Am. J. Hum. Genet. *85*, 521–527.
8. Ishikawa, Y., Wirz, J., Vranka, J.A., Nagata, K., and Bächinger, H.P. (2009). Biochemical characterization of the prolyl 3-hydroxylase 1.cartilage-associated protein.cyclophilin B complex. J. Biol. Chem. *284*, 17641–17647.
9. Krane, S.M. (2008). The importance of proline residues in the structure, stability and susceptibility to proteolytic degradation of collagens. Amino Acids *35*, 703–710.
10. Christiansen, H.E., Schwarze, U., Pyott, S.M., AlSwaid, A., Al Balwi, M., Alrasheed, S., Pepin, M.G., Weis, M.A., Eyre, D.R., and Byers, P.H. (2010). Homozygosity for a missense mutation in SERPINH1, which encodes the collagen chaperone protein HSP47, results in severe recessive osteogenesis imperfecta. Am. J. Hum. Genet. *86*, 389–398.
11. Drögemüller, C., Becker, D., Brunner, A., Haase, B., Kircher, P., Seeliger, F., Fehr, M., Baumann, U., Lindblad-Toh, K., and Leeb, T. (2009). A missense mutation in the SERPINH1 gene in Dachshunds with osteogenesis imperfecta. PLoS Genet. *5*, e1000579.
12. Alanay, Y., Avaygan, H., Camacho, N., Utine, G.E., Boduroglu, K., Aktas, D., Alikasifoglu, M., Tuncbilek, E., Orhan, D., Bakar, F.T., et al. (2010). Mutations in the gene encoding the RER protein FKBP65 cause autosomal-recessive osteogenesis imperfecta. Am. J. Hum. Genet. *86*, 551–559.
13. Nakashima, K., Zhou, X., Kunkel, G., Zhang, Z., Deng, J.M., Behringer, R.R., and de Crombrugghe, B. (2002). The novel zinc finger-containing transcription factor osterix is required for osteoblast differentiation and bone formation. Cell *108*, 17–29.
14. Nagy, E., and Maquat, L.E. (1998). A rule for termination-codon position within intron-containing genes: When nonsense affects RNA abundance. Trends Biochem. Sci. *23*, 198–199.
15. Milona, M.A., Gough, J.E., and Edgar, A.J. (2003). Expression of alternatively spliced isoforms of human Sp7 in osteoblast-like cells. BMC Genomics *4*, 43.
16. Suske, G., Bruford, E., and Philipsen, S. (2005). Mammalian SP/KLF transcription factors: Bring in the family. Genomics *85*, 551–556.
17. Gao, Y., Jheon, A., Nourkeyhani, H., Kobayashi, H., and Ganss, B. (2004). Molecular cloning, structure, expression, and chromosomal localization of the human Osterix (SP7) gene. Gene *341*, 101–110.
18. Nardelli, J., Gibson, T.J., Vesque, C., and Charnay, P. (1991). Base sequence discrimination by zinc-finger DNA-binding domains. Nature *349*, 175–178.
19. Nardelli, J., Gibson, T., and Charnay, P. (1992). Zinc finger-DNA recognition: Analysis of base specificity by site-directed mutagenesis. Nucleic Acids Res. *20*, 4137–4144.
20. Choo, Y., and Klug, A. (1994). Selection of DNA binding sites for zinc fingers using rationally randomized DNA reveals coded interactions. Proc. Natl. Acad. Sci. USA *91*, 11168–11172.
21. Uno, Y., Matsushita, K., Nagaoka, M., and Sugiura, Y. (2001). Finger-positional change in three zinc finger protein Sp1: Influence of terminal finger in DNA recognition. Biochemistry *40*, 1787–1795.
22. Yokono, M., Saegusa, N., Matsushita, K., and Sugiura, Y. (1998). Unique DNA binding mode of the N-terminal zinc finger of transcription factor Sp1. Biochemistry *37*, 6824–6832.
23. Warner, L.E., Mancias, P., Butler, I.J., McDonald, C.M., Keppen, L., Koob, K.G., and Lupski, J.R. (1998). Mutations in the early growth response 2 (EGR2) gene are associated with hereditary myelinopathies. Nat. Genet. *18*, 382–384.
24. Mundlos, S., Otto, F., Mundlos, C., Mulliken, J.B., Aylsworth, A.S., Albright, S., Lindhout, D., Cole, W.G., Henn, W., Knoll, J.H., et al. (1997). Mutations involving the transcription factor CBFA1 cause cleidocranial dysplasia. Cell *89*, 773–779.
25. Baek, W.Y., de Crombrugghe, B., and Kim, J.E. (2010). Postnatally induced inactivation of Osterix in osteoblasts results in the reduction of bone formation and maintenance. Bone *46*, 920–928.
26. Rivadeneira, F., Styrkársdottir, U., Estrada, K., Halldórsson, B.V., Hsu, Y.H., Richards, J.B., Zillikens, M.C., Kavvoura, F.K., Amin, N., Aulchenko, Y.S., et al; Genetic Factors for Osteoporosis (GEFOS) Consortium. (2009). Twenty bone-mineral-density loci identified by large-scale meta-analysis of genome-wide association studies. Nat. Genet. *41*, 1199–1206.
27. Styrkarsdottir, U., Halldorsson, B.V., Gretarsdottir, S., Gudbjartsson, D.F., Walters, G.B., Ingvarsson, T., Jonsdottir, T., Saemundsdottir, J., Snorradóttir, S., Center, J.R., et al. (2009). New sequence variants associated with bone mineral density. Nat. Genet. *41*, 15–17.
28. Timpson, N.J., Tobias, J.H., Richards, J.B., Soranzo, N., Duncan, E.L., Sims, A.M., Whittaker, P., Kumanduri, V., Zhai, G., Glaser, B., et al. (2009). Common variants in the region around Osterix are associated with bone mineral density and growth in childhood. Hum. Mol. Genet. *18*, 1510–1517.

RESEARCH ARTICLE

Human Mutation

OFFICIAL JOURNAL HGVS HUMAN GENOME VARIATION SOCIETY www.hgvs.org

Identification of a Mutation Causing Deficient BMP1/mTLD Proteolytic Activity in Autosomal Recessive Osteogenesis Imperfecta

Víctor Martínez-Glez,[1,2,†] Maria Valencia,[1,3,†] José A. Caparrós-Martín,[1,3,†] Mona Aglan,[4,†] Samia Temtamy,[4,†] Jair Tenorio,[2] Veronica Pulido,[3] Uschi Lindert,[5] Marianne Rohrbach,[5] David Eyre,[6] Cecilia Giunta,[5] Pablo Lapunzina,[1,2] and Victor L. Ruiz-Perez[1,3*]

[1] *Centro de Investigación Biomédica en Red de Enfermedades Raras (CIBERER), Instituto de Salud Carlos III (ISCIII), Madrid, Spain;* [2] *Instituto de Genética Médica y Molecular (INGEMM), Hospital Universitario La Paz-IdiPaz, Universidad Autónoma de Madrid, Madrid, Spain;* [3] *Instituto de Investigaciones Biomédicas, Consejo Superior de Investigaciones Científicas-Universidad Autónoma de Madrid, Madrid, Spain;* [4] *Human Genetics and Genome Research Division, National Research Centre, Cairo, Egypt;* [5] *Division of Metabolism, Connective Tissue Unit, University Children's Hospital and Children's Research Center, Zurich, Switzerland;* [6] *Department of Orthopaedics and Sports Medicine, University of Washington, Seattle, Washington*

Communicated by Raymond Dalgleish

Received 12 September 2011; accepted revised manuscript 27 October 2011.
Published online 3 November 2011 in Wiley Online Library (www.wiley.com/humanmutation).DOI: 10.1002/humu.21647

ABSTRACT: Herein, we have studied a consanguineous Egyptian family with two children diagnosed with severe autosomal recessive osteogenesis imperfecta (AR-OI) and a large umbilical hernia. Homozygosity mapping in this family showed lack of linkage to any of the previously known AR-OI genes, but revealed a 10.27 MB homozygous region on chromosome 8p in the two affected sibs, which comprised the procollagen I C-terminal propeptide (PICP) endopeptidase gene *BMP1*. Mutation analysis identified both patients with a Phe249Leu homozygous missense change within the BMP1 protease domain involving a residue, which is conserved in all members of the astacin group of metalloproteases. Type I procollagen analysis in supernatants from cultured fibroblasts demonstrated abnormal PICP processing in patient-derived cells consistent with the mutation causing decreased BMP1 function. This was further confirmed by overexpressing wild type and mutant *BMP1* longer isoform (mammalian Tolloid protein [mTLD]) in NIH3T3 fibroblasts and human primary fibroblasts. While overproduction of normal mTLD resulted in a large proportion of proα1(I) in the culture media being C-terminally processed, proα1(I) cleavage was not enhanced by an excess of the mutant protein, proving that the Phe249Leu mutation leads to a BMP1/mTLD protein with deficient PICP proteolytic activity. We conclude that *BMP1* is an additional gene mutated in AR-OI.

Hum Mutat 00:1–8, 2011. © 2011 Wiley Periodicals, Inc.

KEY WORDS: osteogenesis imperfecta; *BMP1*; astacin-like metalloproteases; type I collagen

Introduction

Osteogenesis imperfecta (OI type I-XII; MIM#s 166200, 166210, 259420, 166220, 610967, 610968, 610682, 610915, 259440, 613848, 613849, 613982) is a rare genetic disorder primarily characterized by bone fragility leading to increased risk of fractures. The clinical manifestations of patients with OI vary considerably from severe bone deformities or perinatal lethality to individuals with nearly no fractures [Rauch and Glorieux, 2004; Sillence et al., 1979]. While the majority of OI cases are autosomal dominant and arise from heterozygous mutations in the structural genes coding for the two procollagen chains, proα1(I) *COL1A1* (MIM# 120150) and proα2(I) *COL1A2* (MIM# 120160), there is a less frequent group of autosomal recessive forms of OI (AR-OI), for which, the molecular bases are increasingly heterogeneous [Byers and Steiner, 1992]. So far, seven AR-OI loci have been identified, Prolyl 3-hydroxylase 1 (*LEPRE1*; MIM# 610339), cartilage-associated protein (*CRTAP*; MIM# 605497), and peptidylprolyl isomerase B (*PPIB*; MIM# 123841), which are the three components of the endoplasmic reticulum (ER) complex responsible for 3-hydroxylation of Pro 986 in the proα1(I) chain [Barnes et al., 2006; Cabral et al., 2007; Ishikawa et al., 2009; Morello et al., 2006; van Dijk et al., 2009]; *SERPINH1* (Serpin peptidase inhibitor, clade H; MIM# 600943) and *FKBP10* (Fk506-binding protein 10; MIM# 607063) that function as type I procollagen molecular chaperons [Alanay et al., 2010; Christiansen et al., 2010; Drogemuller et al., 2009]; the osteoblast specific transcription factor *SP7/OSTERIX* (MIM# 606633), implicated in the differentiation of osteoblasts [Lapunzina et al., 2010]; and the type I collagen interacting protein and antiangiogenic extracellular matrix factor *SERPINF1* (Serpin peptidase inhibitor, clade F, member 1; MIM# 172860) [Becker et al., 2011]. Except for SERPINF1, whose molecular pathomechanism remains to be elucidated, the rest of AR-OI genes identified are involved in type I collagen synthesis, posttranslational modification, or secretion.

Additional Supporting Information may be found in the online version of this article.

[†]These authors contributed equally to the work.

*Correspondence to: Victor L. Ruiz-Perez, Instituto de Investigaciones Biomédicas, Consejo Superior de Investigaciones Científicas-Universidad Autónoma de Madrid, Arturo Duperier 4, Madrid 28029, Spain. E-mail: vlruiz@iib.uam.es

Contract grant sponsors: Spanish Ministry of Science and Innovation (SAF-17901); CIBERER Programa de Investigación de Enfermedades Pediátricas; Gottfried und Julia Bangerter-Rhyner Stiftung (to C.G. and M.R.).

© 2011 WILEY PERIODICALS, INC.

Type I collagen, which is the most abundant protein in bone and other connective tissues, is initially synthesized in the ER as a precursor molecule (type I procollagen) that combines two proα1(I) and one proα2(I) peptide chains in a triple helix. Prior to helix formation, procollagen chains undergo a series of posttranslational modifications including 3 and 4-hydroxylation of proline residues and lysine hydroxylations. These modifications are necessary for the correct folding and thermal stability of the triple helix and posterior crosslinking between collagen molecules. Procollagen trimers are then secreted into the extracellular space via the Golgi network, where they are processed into mature type I collagen molecules by proteolytic cleavage of the N and C-terminal propeptides, and self-assembled into collagen fibrils and fibers [Canty and Kadler, 2005; Makareeva et al., 2011]. Type I procollagen N-propeptide is removed by the protein product of *ADAMTS-2* (A disintegrin and metalloproteinase with thrombospondin motifs 2; MIM# 604539) and mutations in this gene are associated with recessive Ehlers–Danlos syndrome type VIIC (EDS type VIIC; MIM# 225410) [Colige et al., 1999]. Two *ADAMTS-2*-related enzymes, *ADAMTS*-3 (MIM# 605011) and *ADAMTS-14* (MIM# 607506), also display some amino-peptidase activity [Colige et al., 2002; Fernandes et al., 2001]. Processing of procollagen I C-terminal propeptide (PICP) is accomplished by the family of mammalian bone morphogenetic protein 1/Tolloid-like (BMP1/TLD-like) proteinases, which is composed of four secreted proteins encoded by three different loci [Hopkins et al., 2007; Kessler et al., 1996]. BMP1 and its longer isoform mammalian Tolloid protein (mTLD) are alternative spliced products of *BMP1* (MIM# 112264), which is located on 8p21.3. The other two remaining BMP1/TLD-like members, Tolloid-like protein 1 (*TLL1*; MIM# 606742) and Tolloid-like protein 2 (*TLL2*; MIM# 606743), are transcribed from genes that lie on chromosomes 4 and 10, respectively [Scott et al., 1999; Takahara et al., 1994, 1996]. All four mammalian BMP1/TLD-like proteases share domain structure and sequence similarity with *Drosophila* tolloid (tld), a protein that is involved in dorsal–ventral patterning of the *Drosophila* embryo [Shimell et al., 1991]. BMP1/TLD-like family structure consists of a signal peptide, followed by an aminoterminal protease inhibitor prodomain, that is proteolytically removed by the subtilisin-like proprotein convertases in the mature proteins, a conserved astacin-like protease domain shared by a wider family of metalloproteases and a variable number of complement-uegf-BMP1 (CUB) domains and epidermal growth factor like domains, involved in protein–protein interactions and in certain cases in Ca^{+2} binding [Ge and Greenspan, 2006; Hopkins et al., 2007]. Although the four BMP1/TLD-like mammalian proteins can process the C-terminal propeptide of type I procollagen, they do not show the same cleavage efficiency, with BMP1 having the highest PICP-protease activity, followed by mTLD and TLL1, and TLL2 having the lowest procollagen I C-propeptidase efficiency [Pappano et al., 2003; Scott et al., 1999]. BMP1/TLD-like proteases are also known to be involved in type II, type III, and type V procollagen processing and in the activation of the lysyl oxidase zymogen (LOX; MIM# 153455) [Bonod-Bidaud et al., 2007; Ge and Greenspan, 2006]. LOX is an extracellular copper enzyme that initiates crosslinking of collagens. Furthermore, a variety of secreted factors and extracellular matrix proteins including the dorsalizing agent Chordin have been additionally described as substrates of the BMP1/TLD-like peptidases [Ge and Greenspan, 2006].

Herein, we report the identification of a homozygous missense mutation in a highly conserved residue of the protease domain of BMP1/mTLD in two siblings diagnosed with AR-OI type III and show that this change inhibits the proteolytic activity of BMP1, thus causing deficient PICP processing in patients. We propose that this mutation is the most likely cause of AR-OI in this family.

Material and Methods

Array Hybridization

DNA samples were genotyped applying 250 ng of genomic DNA obtained from peripheral blood to the Human 610-Quad chip (Illumina, San Diego, CA) following the manufacturer's instructions. Single nucleotide polymorphisms (SNPs) with call rates <0.95 were excluded. Image data were analyzed using the Chromosome Viewer tool contained in GenomeStudio V2010.3 (Illumina). Genomic positions were based upon human build GRCh37.

Genomic Sequencing

BMP1 coding exons and at least 100 bp of the flanking introns were amplified by standard PCR (primers available on request). Prior to sequencing, the PCR products were treated with shrimp alkaline phosphatase and exonuclease I (ExoSapit; GE Healthcare, Piscataway, NJ) according to the manufacturers instructions. Sequencing reactions were carried out using a dye terminator cycle sequencing kit and run on an ABI 3730 sequencer (Applied Biosystems, Foster City, CA). Chromatograms were aligned and compared with the mRNA reference nucleotide sequence of *BMP1* (NM_001199.3 and NM_006129.4) and with the corresponding genomic sequence obtained from the Ensembl genome browser using Sequencher (Gene Codes Corp, Ann Arbor, MI). Mutation name was checked using Mutalizer http://www.mutalyzer.nl/2.0/ [Wildeman et al., 2008]. Sequencing of *COL1A1* and *COL1A2* coding exons was performed following standard procedures.

Cell Culture and Western Blotting Conditions

Human primary fibroblasts generated from skin biopsies were seeded in 60-mm Petri dishes (3.5×10^5 cells/dish) in Dulbecco's Modified Eagle Medium (DMEM) supplemented with 10% foetal bovine serum, 100 units/ml penicillin, 100 μg/ml streptomycin, 0.25 μg/ml amphotericin B (Invitrogen, Carlsbad, CA), and 50μg/ml ascorbic acid for 24 hours at 37°C, 5% CO_2. After that, we took off the media, washed the cells three times in phosphate buffered saline (PBS), and kept the cultures in serum free DMEM at 37 °C for 15 minutes. Cells were then washed twice in PBS and incubated in 2 ml of DMEM with 50 μg/ml of ascorbic acid and 40 μg/ml of soybean trypsin inhibitor for 24 hours before cell culture supernatants were collected and protease inhibitors added as described previously [Pappano et al., 2003]. Supernatants were subjected to SDS-PAGE in 5% or 7% acrylamide gels to separate the high molecular weight type I procollagen variants, except for free PICP analysis that because of its small molecular size, we used 12% acrylamide gels. For cell layer analysis, cells were lysed during 10 minutes on ice in RIPA buffer (50 mM Tris-HCl pH 7.5, 150 mM NaCl, 1mM EDTA, 1%Triton X-100, 0.1% SDS, 1% Sodium Deoxycholate) containing 1 mM PMSF (Sigma (P7626), St. Louis, MO) and protease and phosphatase inhibitors (Sigma, P8340, P5726 and P0044). Lysates were cleared at 13,000 rpm for 15 minutes at 4°C and proteins quantified using the BCA protein assay (Pierce, Rockford, IL). SDS-PAGE gels of supernatants or cell extracts were transferred onto nitrocellulose membrane (GE Healthcare) and processed with ECL-Western Blotting Detection Reagents (GE Healthcare). LF antibodies were used at 1:1,500 (LF-68) or 1:3,000 (LF-42 and LF-9) dilutions, respectively. BMP1 and mTLD were detected with an anti-BMP1 (0,2μg/ml) antibody from R&D Systems (AF1927; R&D Systems, Minneapolis, MN). Anti α-Tubulin (1:15,000) obtained from Sigma (T9026)

served as loading control. Horseradish peroxidase-conjugated secondary antibodies were purchased from Jackson ImmunoResearch (West Grove, PA).

Biochemical Analyses

Collagen biochemical analysis was performed by standard methods [Steinmann et al., 1984]. Briefly, fibroblasts were grown to confluence in DMEM and 10% foetal calf serum, and then plated in 35-mm dishes. After 48 hours, medium was changed for DMEM (lacking serum, proline, and glycine) and preincubated with ascorbic acid (50 μg/ml), before overnight labeling with 20 μCi [2,3,4,5-^{3}H]-proline and 20 μCi [2-^{3}H]-glycine. The medium and cell layers were harvested separately for each sample, and a portion of them was digested with pepsin (50 μg/ml) for 2 hours at 20°C. Purified procollagens and collagens were separated on 5% SDS-PAGE with 0.05 M dithiothreitol (DTT) as reducing agent, processed for fluorography and exposed to X-ray films.

Plasmid Constructions and Retroviral Infections

Wild type and mutant *mTLD* cDNAs were generated by PCR using pfx50^{TM} DNA polymerase (Invitrogen) and cloned into pBABE-puro. Absence of nucleotide differences between normal and mutant *mTLD* cDNAs other than the c.747C>G mutation was verified by sequencing. Packaging of pBABE, pBABE-mTLD wild type, or pBABE-mTLD-mutant was performed by cotransfecting 70% confluent HEK293T cells with each one of these vectors individually and the packaging plasmid pCL-Eco (for NIH3T3 cells) or pCL-Amphos (for human primary fibroblats) using calcium phosphate. Supernatants containing retroviral particles were collected at 36, 48, and 60 hours posttransfection, passed through a 0.45 μm nitrocellulose filter, diluted 1:1 in growth medium, and applied to the cells of interest with polybrene. Three consecutive infections were performed. Twenty-four hours after the last infection, cells were selected with puromycin (2 μg/ml) for 2–3 days before they were plated at adequate density (3.5×10^5 cells/p60 for human fibroblasts or 8×10^5 cells/p60 for NIH3T3 cells) and assayed as described above for human primary fibroblasts.

Results

Clinical Characterization of Patients

Patients in this study include two siblings diagnosed with AR-OI (Fig. 1A). The proband of the family (II-3) is a 15-year-old female, the offspring of first cousin normal Egyptian parents, who was referred to us with history of recurrent fractures and bone deformities. She has a younger similarly affected brother, two normal sibs, and an older deaf mute sister who was not available for examination. After normal vaginal delivery at full term, fracture of the left tibia was noted. Since then, fractures occurred frequently and spontaneously with an average number of 10–15 fractures/year affecting both upper and lower limbs. On clinical examination, she had triangular face, broad forehead, wide palpebral fissures, long eyelashes, faint blue sclera, long philtrum, thin lips, and prominent ears. Gross motor development was delayed and she was not able to stand unsupported. Her mental development was normal. No dentinogenesis imperfecta was present. Her thorax was relatively large with increased both anteroposterior and transverse diameters compressing the abdomen. She had a large umbilical hernia, 5-cm wide and 7-cm long with abdominal content, generalized hypotonia, muscle wasting, and nocturnal enuresis. Her skin had normal stretchability with no bruising or scars. Generalized hirsutism was noted. Skeletal examination showed severe generalized deformities of all bones with consistent pain on touch, including deformed clavicles; bilateral bowed angulated humerus, radius, and ulna; arachnodactyly; and hyperextensibility of elbow, wrist, and interphalangeal (IP) joints. Lower limbs showed bowing of femora, severely angulated deformed leg bones and limited movements of the knee joints. She also had kyphoscoliosis and pectus carinatum. Radiological examination revealed deformed long bones with multiple fractures and callus formation, lack of bone modeling with wide distal metaphyses of femora, serpentine thin tibiae and fibulae in addition to S-curve scoliosis of thoracic and lumbar spine with platyspondyly, and generalized decreased bone density (Fig. 1B–G). Skull X-ray showed wormian bones. Anthropometric measurements at 13 years of age were below normal for weight (–3.8 SD), length (–11.5 SD) and head circumference (–3.0 SD). Bone densitometry (DEXA) at 15 years revealed borderline osteoporosis at the hip and spine (Z-score –2.22, –2.13, respectively).

Patient II-6 is the 5-year-old younger brother of patient II-3. Bilateral femoral bowing was detected intrauterine by fetal ultrasound and fracture of both femora was noted at birth. Recurrent fractures of both upper and lower limbs occurred with an average rate of 15/year. He had facial features, no dentinogenesis imperfecta, and normal mentality similar to his sister. He was not able to stand unsupported. Skeletal examination revealed generalized bone deformities; hyperextensibility of elbows, wrists, and IP joints; and arachnodactyly. He also had a relatively large thorax compressing the abdomen with a large umbilical hernia (4-cm wide and 5-cm long with abdominal contents). X-ray survey revealed wormian bones of skull, deformed long bones with lack of modeling, fractures and callus formation, scoliosis, platyspondyly, and wide symphyses pubis (Fig. 1B and H). Anthropometric measurements were below normal for weight (–3.7 SD) and length (–7.2 SD) with normal head circumference (–0.8 SD). Bone densitometry (DEXA) at 5 years revealed borderline osteoporosis at the spine (Z-score –1.63) and osteoporosis at the left femur (Z-score –2.75). Audiological and cardiovascular examinations of both patients were unremarkable. Serum calcium and phosphate were normal, while alkaline phosphatase levels were slightly high. Both patients were diagnosed as OI Sillence type III, and cyclic IV biphosphonate injections were started. All studies and investigations involving the proband and other members of her family were performed in accordance with the ethical standards of the Medical Research Ethics Committee of the National Research Centre (Egypt), and all DNA samples were obtained with appropriate informed consent.

Genetic Analysis

Genetic studies in this family were performed by genome-wide homozygosity mapping in the affected children and in two normal sibs. To do this genomic DNA from each individual was hybridized to whole-genome high-density SNP arrays and the four resulting SNP genotypes were analyzed with Illumina software. The result of this study showed none of the patients to be homozygous at the *CRTAP*, *PPIB*, *SERPINH1*, *SP7*, and *SERPINF1* loci, while only one of the affected children was homozygous for *LEPRE1* and *FKBP10*, thus indicating further genetic heterogeneity in AR-OI. Sequencing of *COL1A1* and *COL1A2* coding exons in patient II-6 revealed no mutations in these genes (Fig. 1A). This prompted us to search for the causative gene, and so, we used the genotypes generated by the array hybridizations to look for blocks of homozygosity shared

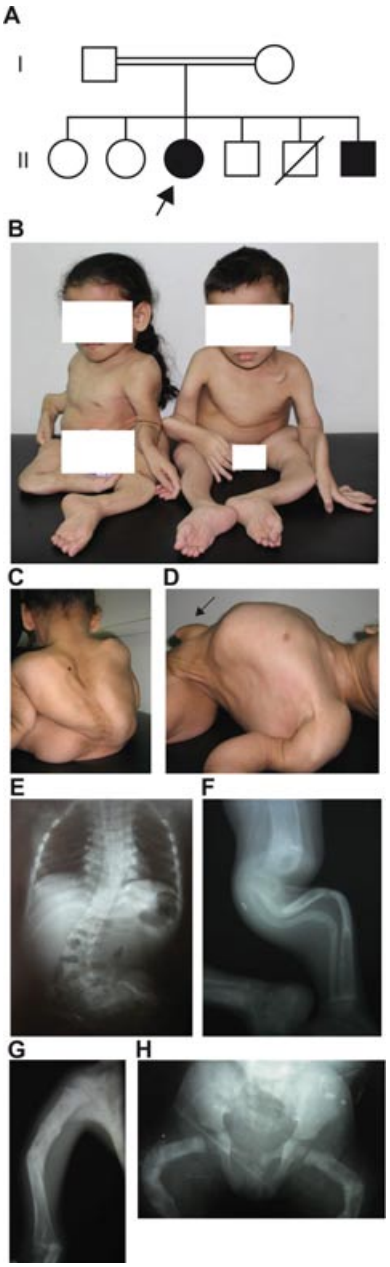

Figure 1. Clinical and radiological features of the patients studied in this report. **A:** Family pedigree showing parental consanguinity. The proband is indicated with an arrow. **B:** Severe bone deformities in both affected sibs. **C–D:** Panels illustrate severe kyphoscoliosis (C) and relatively large thorax, small abdomen and large umbilical hernia (arrow) in the proband (D). **E:** X-ray of the spine of the proband showing S-curve scoliosis of thoracic and lumbar spine and platyspondyly. **F:** X-ray of the left leg of the proband showing serpentine bowing and osteoporosis of tibia and fibula. **G:** X-ray of the right humerus showing healed fractures, angulations, and lack of bone modeling in the proband. **H:** X-ray of the pelvis and both femora of patient II-6 showing multiple healed fractures, with bowing, and lack of bone modeling.

by both individuals with OI. Taking an arbitrary cutoff of 1 MB of consecutive homozygous SNPs, we identified two large homozygous DNA regions on chromosomes 3 and 8p, which were present in the patients but absent in the other two normal siblings. The homozygous region on chromosome 3 expanded 35.4 MB around the centromere and contained 151 genes. The 8p region consisted of 10.27 MB and contained 84 genes.

Identification of a Missense Mutation in *BMP1*

Analysis of candidate genes comprised in each DNA fragment revealed the presence of *BMP1* within the chromosome 8 region. Given the nature of the disease, we considered this gene to be the best functional candidate. Moreover, a recent report has shown that dominant missense mutations in the C-terminal cleavage site of *COL1A1* or *COL1A2*, which disrupt PICP processing, cause OI [Lindahl et al., 2011]. Hence, we direct sequenced all 21 coding exons (including those that are alternatively spliced) and exon–intron boundaries of *BMP1* in the proband of the family and found a homozygous c.747C>G nucleotide change in exon 6 that causes the substitution of phenylalanine at position 249 to leucine (p.Phe249Leu) (Fig. 2A and 2B). The mutation was numbered with respect to the NM_006129.4 reference sequence taking the A of the first ATG as nucleotide +1, following the current nomenclature guidelines [den Dunnen and Antonarakis, 2000; den Dunnen and Paalman, 2003]. Phe249 is a residue contained within the peptidase domain of BMP1/mTLD that is conserved in all members of the astacin family of metalloproteases independently of their substrate and whether they are of a vertebrate or invertebrate origin (Fig. 2C). Functionally, this amino acid is thought to be involved in internal bonds within the astacin protease module [Bond and Beynon, 1995; Guevara et al., 2010]. Segregation analysis of the mutation within the family showed the two affected children to be homozygous for the c.747C>G nucleotide change, while the normal sister (II-2) and brother (II-4) from whom DNA was available and the parents carried the mutation in the heterozygous state. To exclude the possibility of c.747C>G being a rare polymorphism, we checked normal controls for the presence of the c.747C>G change by direct sequencing. The mutation was not found in 100 control chromosomes of the same ethnic origin or in 884 normal chromosomes from controls of European ethnicity. c.747C>G is not listed as a polymorphism in any of the public databases.

Deficient Procollagen I C-Terminal Processing in Patient Fibroblasts

Subsequently, we established dermal fibroblast cultures from skin biopsies of the two siblings with OI, their heterozygous normal sister (II-2), and an unrelated control individual to test whether PICP processing was altered in patients. Serum-free supernatants from cultured fibroblasts treated with ascorbic acid were analyzed by Western blotting using LF-68, LF-42, and LF-9 proα1(I) antisera. These antibodies were a generous gift from Dr. Larry Fisher (National Institute of Dental and Craniofacial Research, NIH, Bethesda, MD) and were raised specifically against proα1(I) C-telopeptide, proα1(I) C-propeptide, and proα1(I) N-propeptide, respectively [Fisher et al., 1987, 1995]. Thus, LF-68 can detect α1(I) and all forms of proα1(I), while LF-9 and LF-42 distinguish between proα1(I) chains containing the N-propeptide or C-propeptide, respectively (Fig. 3A). Western Blot analysis of supernatants from control cells using LF-68 showed a major proα1(I) band and two minor intermediately processed proα1(I) forms referred as pCα1(I) and pNα1(I), each one of these being exclusively recognized by LF-42 or LF-9 (Fig. 3B and 3C). pCα1(I) has lost the aminopropeptide but retains the larger C-terminal propeptide, whereas pN1α(I) lacks the C-terminal propeptide and retains the N-propeptide (Fig. 3A). Compared to control cells, LF-68 analysis of supernatants from patient-derived cells demonstrated a significant decrease in the amount of pNα1(I)

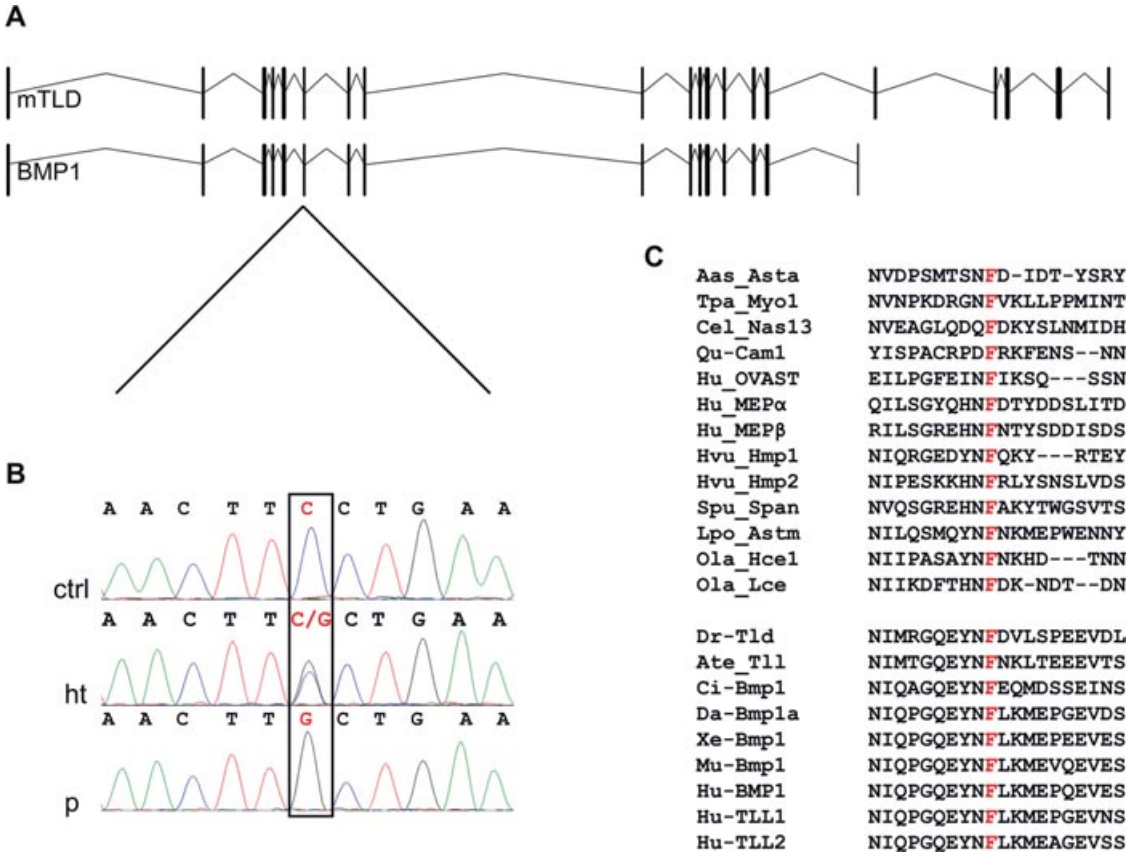

Figure 2. Identification of a missense mutation in *BMP1* in individuals with AR-OI. **A:** Exon–intron structure of the two alternative spliced isoforms (*BMP1* and *mTLD*) transcribed from the *BMP1* locus. **B:** Sequence analysis of genomic DNA from a control (ctrl), a heterozygous individual (ht), and one of the patients (p) showing the c.747C>G transversion in *BMP1* exon 6 (red and squared nucleotide). **C:** Multiple sequence alignment of a fragment from the catalytic domain of different astacin-like metalloproteases from diverse organisms showing conservation of the F249 residue labeled in red. The lower cluster of sequences corresponds to protein members of the BMP1/tolloid-like subgroup of astacin-like metalloproteases both from vertebrate and invertebrate organisms. Aaa_Asta, astacin from the crayfish *A. Astacus* (P07584), Tpa_My01 myosinase from giant squid *Todarodes pacificus* (Q8IU46), Cel_Nas13 metalloproteinase from *Caenorhabditis elegans*, (Q20191), Qu_Cam-I from quail (AAA20842.1), Hu_Ovast, human ovastacin (Q6HA08), Hu_MEPα (Q16819) and Hu_MEPβ (Q16820), human meprins α and β, Hvu_Hmp1 (AAA92361.2) and Hvu_Hmp2 (AAD33860.1) from *Hydra vulgaris*, Spu_Span from sea urchin (P98068), Lpo_Astm from the horseshoe crab *Limulus polyphemus* (B4F320), Ola_Hce1 (NP_001188427.1) and Ola_Lce1 (NP_001098292.1) from medaka fish *Oryzias latipes*, Dr_tld, *Drosophila* tolloid (NP_524487.2), Ate_tll, tolloid-like peptidase from the spider *Achaearanea tepidariorum* (Q75UQ6), Ci_Bmp1 from *Ciona intestinalis* (NP_001071840.1), Da_Bmp1a from *Danio rerio* (NP_001035126.1), Xe_Bmp1 from *Xenopus laevis* (AAI70427.1), Mu_Bmp1 from *Mus musculus* (NP_033885.2), Hu_BMP1/mTLD, Hu_TLL1 and Hu_TLL2 human BMP1/TLD-like proteases (NP_001190.1/NP_006120.1, NP_036596.3 and NP_036597.1). For most of the proteins shown here, a wider sequence alignment of the catalytic domain and information about substrate specificity have been described previously [Bond and Beynon, 1995; Guevara et al., 2010].

with respect to pCα1(I) in both patients, thus indicating diminished PICP-peptidase activity in homozygous mutant cells (Fig. 3B and C). In agreement with this, we also detected decreased concentration of free PICP in the supernatants of patient cells after probing an equivalent loaded gel made at a higher percentage of acrylamide with LF-42 (Fig. 3B). Nevertheless, pNα1(I) and free PICP were both detected in patient fibroblasts, and so there is residual PICP-peptidase activity from the mutant enzyme or from other proteases in the culture. Cell cultures derived from heterozygous individual II-2 were found slightly impaired in procollagen I C-terminal processing as the pCα1(I)/pNα1(I) ratio in LF-68 blots was increased in these cells (1.7) with respect to control fibroblasts (0.9) (Fig. 3B). Steady-state procollagen processing was additionally analyzed in fibroblast cultures. This showed diminished pNα1(I), pNα2(I) and fully processed α1(I) and α2(I) in the supernatants of patient fibroblasts compared to the heterozygous control culture, hence corroborating impaired processing of type I procollagen in patient cells (Supp. Figure S1A). Pepsin-treated procollagens purified from the medium and cell layers of both patient and heterozygous fibroblasts showed a normal migration patterns of collagen type I, III, and V, indicating lack of collagen overmodification (Supp. Figure S1B). Next, we checked whether the Phe249Leu mutation could trigger BMP1/mTLD degradation due to possible missfolding, however no significant differences in the intensity of bands corresponding to mTLD or BMP1 were detected between cell extracts from control and mutant fibroblasts on western blot analysis using an anti-BMP1 antibody (Supp. Figure S2).

Mutant mTLD Shows Impaired Proteolytic Activity

To confirm that the Phe249Leu substitution inhibits BMP1/mTLD-mediated PICP cleavage, we used puromycin-resistant retroviral vectors to deliver normal or mutant *mTLD* cDNA under control of a constitutive promoter into NIH3T3 mouse

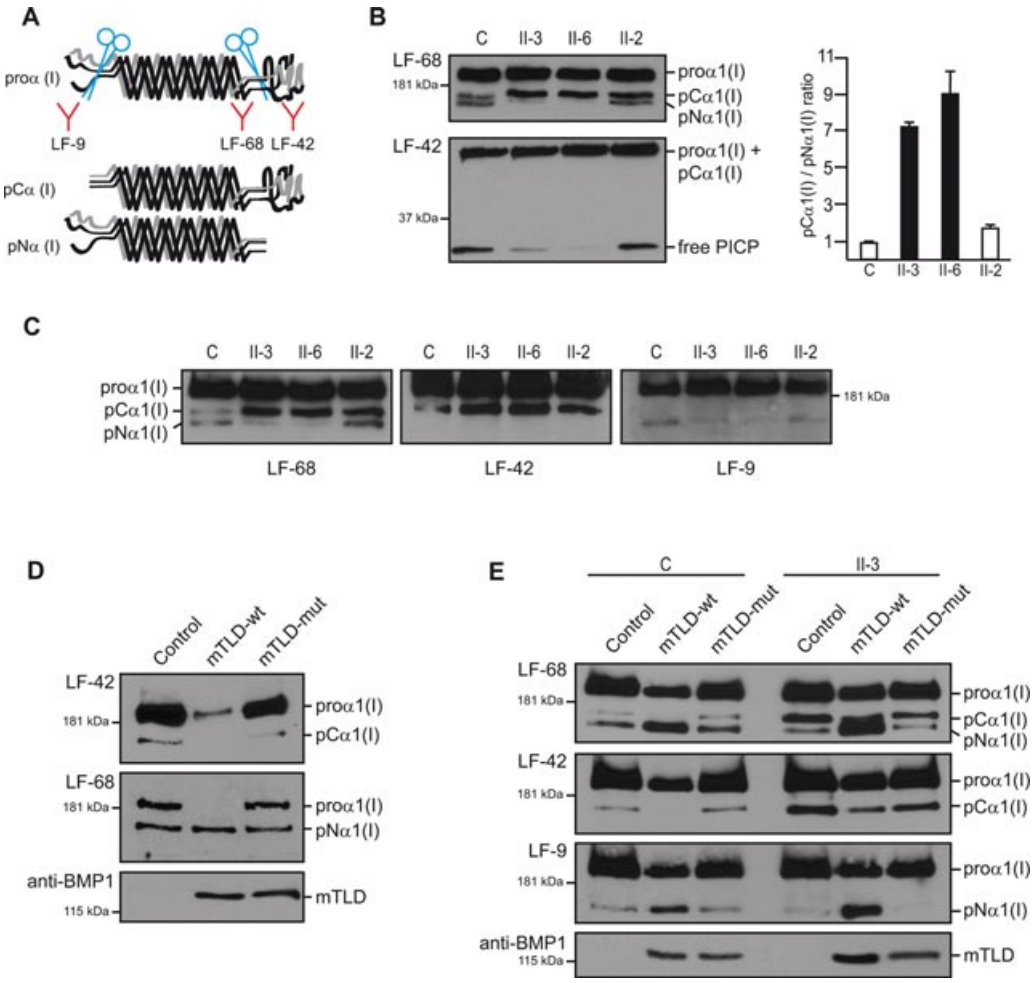

Figure 3. Phe249Leu impairs type I procollagen C-propeptide protease activity of BMP1/mTLD. **A:** Diagram representing unprocessed type I procollagen and intermediate variants following removal of the N or C-terminal propeptides. LF antibodies are shown underneath their corresponding epitope. **B:** Western blot analysis of supernatants from fibroblasts derived from patients II-3 and II-6, their heterozygous sibling (II-2), and an unrelated normal control (C) incubated with the indicated LF antibodies to monitor proteolytic processing of proα1(I). For each sample the volume of supernatant loaded per total amount of protein in the cell extracts of the corresponding culture was the same (15 μl, 14 μl, 15 μl, and 18 μl were loaded for samples C, II-3, II-6, and II-2, respectively). Analysis of proα1(I) variants is shown in the upper panel and free PICP analysis with LF-42 is in the lower panel. Compared to controls, patients have lower levels of pNα(I) and free PICP, while pCα1(I) is accumulated. Slight impairment of PICP-processing is detected in the heterozygous individual II-2. Quantification of the pCα1(I)/pNα1(I) ratio in each lane using densitometry data from two independent LF-68 blots is shown in the graph on the right. **C:** Western blot analysis of supernatants run in parallel and probed with the indicated antibodies demonstrating the propeptide composition of each of the intermediately processed proα1(I) bands. **D:** Western blot analysis of supernatants from NIH3T3 cell cultures overexpressing wild type mTLD (mTLD-wt) or Phe249Leu mTLD (mTLD-mut). Cells infected with the empty retroviral vector (pBABE-puro) were used as control (Control). 30 μl of supernatant from each culture with the same number of cells were loaded in each lane. Both LF-68 and LF-42 antibodies detected a dramatic decrease in unprocessed proα1(I) that is converted into a smaller size C-terminally processed variant when mTLD-wt is overexpressed. Since LF-9 does not crossreact with the murine N-propeptide, we could not use this antibody, and hence, the processed variant detected by LF-68 is assumed to correspond to pNα1(I) because of its size and because it is not recognized by LF-42. The amount of mTLD-wt and mTLD-mut in the media of the corresponding culture was demonstrated by reprobing the upper LF-blots with anti-BMP1. **E:** Western blot of supernatants from a control individual (C) and patient II-3 fibroblast cultures infected with retroviral vectors as in panel D and probed against LF antibodies. Only expression of mTLD-wt strongly improves PICP-protease activity both in patient and control cells as demonstrated by the augmented pNα1(I)/pCα1(I) ratio and reduction of unprocessed proα1(I). Levels of mTLD variants in the media were monitored with anti-BMP1.

fibroblasts. Following viral infection, puromycin was added to the media to generate homogenous cultures, in which all surviving cells carry the recombinant vector integrated into their genome. After antibiotic selection, cells were plated at 8×10^5/p60 dish density and treated in the same way as described for human primary fibroblasts. Western blotting of serum-free supernatants using LF-68 and LF-42 showed that the vast majority of proα1(I) secreted into the media by NIH3T3 fibroblasts overexpressing wild-type mTLD, had lost the C-terminal propeptide and had been processed into a smaller size proα1(I) variant. In contrast, the supernatants of cells overexpressing mutant mTLD were found with similar levels of proα1(I) C-terminal processing as the control cells transduced with the empty retroviral vector, thus indicating that the Phe249Leu mutation causes strong reduction of the BMP1/mTLD proteolytic function and confirming the pathogenicity of the mutation (Fig. 3D). The presence of equivalent levels of normal or mutant mTLD in the media of NIH3T3 cultures was verified by reprobing the LF-68 and LF-42 blots with anti-BMP1 (Fig. 3D). We repeated the same

experiment using retroviral-mediated expression of normal and mutant mTLD in human primary fibroblasts and found the same result with only expression of the wild-type protein being able to rescue the phenotype of mutant fibroblasts (Fig. 3E).

Discussion

Two OI patients have been recently reported by Lindahl et al., one with a dominant missense mutation in the *COL1A1* C-propeptide cleavage site and another one with a dominant missense mutation in the C-propeptide cleavage site of *COL1A2*. Both patients were described with a mild phenotype including fractures, radiographic osteopenia, and wormian bones. Mild tibial bowing was found in one of the cases. Biochemical analysis of collagens in cells derived from these patients showed minimal alteration of the triple helix folding process, but delayed processing of type I procollagen secreted into the media, hence indicating that abnormal PICP processing is a cause of OI in humans [Lindahl et al., 2011]. As PICP is critical for the initiation of chain folding, these mutations differ from those placed in the C-terminal propeptide region that interferes with the formation of the triple helix [Chessler et al., 1993; Khoshnoodi et al., 2006]. The patients we report here have a more severe phenotype than the cleavage site mutation patients described by Lindahl et al. [2011]. This could be explained by the fact that deficient BMP1/mTLD function alters C-terminal processing of both procollagen (I) chains simultaneously leading to low levels of fully processed type I collagen, which in our patients according to the negligible BMP1/mTLD activity detected in the overexpression experiments, will be essentially depending on the activity of TLD-like proteins. Furthermore, since the Phe249Leu change lies within the BMP1/mTLD catalytic protease domain, it is highly probable that processing of other BMP1/mTLD substrates including fibrillar type II and III procollagens, activation of LOX zymogen, as well as processing of other secreted factors and extracellular matrix proteins is compromised in our patients [Ge and Greenspan, 2006]. In addition, the possibility of other genome variants contributing to the phenotype spectrum in this family cannot be ruled out.

Our data indicate that the phenotype resulting from diminished function of BMP1 in human diverges from that of *Bmp1*$^{-/-}$ mice. This is similar to the *SERPINF1* situation, as no features resembling OI were described in *SerpinF1*-deficient mice [Becker et al., 2011; Doll et al., 2003]. *Bmp1* homozygous knockout mice are perinatal lethal and although it is unknown whether they could have developed OI later in life, they do not show gross skeletal abnormalities at the time of birth excepting for reduced ossification of some skull bones [Suzuki et al., 1996]. In contrast, patient II-6 was detected with femoral bowing during intrauterine examination and bone fractures were noted at birth in both patients. C-terminal processing of type I procollagen secreted into the media by *Bmp1*$^{-/-}$ mouse embryonic fibroblasts (MEFs) was demonstrated to be reduced, nevertheless these cells were still producing fully processed type I collagen chains [Suzuki et al., 1996]. We also detected residual PICP-protease activity in the fibroblasts from our patients, however further experiments comparing human and mouse cells under the same methodology are necessary to understand whether the remaining PICP-protease activity in mutant human fibroblasts is lower than that of the *Bmp1* knockout cells. PICP processing was nearly undetectable in double knockout *Bmp1*$^{-/-}$*;Tll1*$^{-/-}$ fibroblasts and thus Tll1 is the protein designated to be accountable for the remaining PICP activity of *Bmp1*$^{-/-}$ MEFs. *Bmp1*$^{-/-}$*;Tll1*$^{-/-}$ mice are embryonic lethal owing to cardiac failure and evaluation of skeletal abnormalities in this genotype was not achieved [Pappano et al., 2003]. A possible explanation for the human/mouse phenotypic differences could be a more essential role for BMP1/mTLD in protein processing in the human skeletal system than in mice, or in other words TLD-like proteases could compensate less in the human skeleton. It is also possible that the process of collagen fibril assembly in mice is more resilient to the presence of unprocessed type I procollagen molecules. There is however one phenotypic aspect in common between *Bmp1* knockout mice and the human phenotype. *Bmp1*$^{-/-}$ mice were reported with consistent herniation of the gut and both the proband and her affected brother have large umbilical hernias with intestinal content. It was suggested that this mouse phenotype could be due to lack of tensile strength in the ventral body wall secondary to abnormal collagen fibril formation. Additionally, since BMP1 is involved in processing dorso-ventral patterning factors such as Chordin, this could also play a role in this particular phenotypic feature [Ge and Greenspan, 2006; Suzuki et al., 1996]. The broad function of *BMP1* includes processing of type III and type V procollagens that are associated with specific forms of EDS ([EDS type III–IV; MIM#s 130020, 130050] and [EDS type I–II; MIM#s 130000, 130010] linked to collagen III and V, respectively). Our patients lack the skin increased stretchability and fragility and the joint hyperextensibility characteristic of EDS but have in common blue sclera, kyphoscoliosis, and presence of hernia that in EDS is usually inguinal but umbilical in our cases.

In summary, we describe a mutation associated to severe AR-OI (OI type III) in an additional gene, *BMP1*, which extends further the list of genes that are mutated in this heterogeneous disorder.

Acknowledgments

This work was supported by the Spanish Ministry of Science and Innovation SAF-17901 and the CIBERER Programa de Investigación de Enfermedades Pediátricas. We are very grateful to our patients and their family who were very cooperative during this study. We also wish to thank the National Society of Human Genetics in Egypt, which provided the biphosphonate injections for the patients. We thank Dr. Larry Fisher (NIH, Bethesda, MD) for the kind gift of LF-9, LF-42, and LF-68 antibodies that were so useful in this study and Dr. Ignacio Palmero (IIB, CSIC-UAM) for helping with the retroviral infection technique. The technical assistance of Angelika Schwarze is kindly acknowledged. Biochemical analysis of collagens was supported by a grant from the Gottfried und Julia Bangerter-Rhyner Stiftung to C.G. and M.R. M.A. and S.T. analyzed data, performed diagnoses, and phenotyping, V. M-G., J.T., V.P, P.L., and V.L.R-P. conducted genetic and mutational studies, J.A.C-M., M.V., and V.L.R-P performed procollagen functional analysis on primary fibroblasts and retroviral experiments; D.E. and M.R contributed to the discussion and interpretation of experiments; and C.G. and U.L. carried out procollagen biochemical analyses. P.L. and V.L.R.-P. led the group. All authors contributed to the writing of the manuscript.

References

Alanay Y, Avaygan H, Camacho N, Utine GE, Boduroglu K, Aktas D, Alikasifoglu M, Tuncbilek E, Orhan D, Bakar FT, Zabel B, Superti-Furga A, Bruckner-Tuderman L, Curry CJ, Pyott S, Byers PH, Eyre DR, Baldridge D, Lee B, Merrill AE, Davis EC, Cohn DH, Akarsu N, Krakow D. 2010. Mutations in the gene encoding the RER protein FKBP65 cause autosomal-recessive osteogenesis imperfecta. Am J Hum Genet 86:551–559.

Barnes AM, Chang W, Morello R, Cabral WA, Weis M, Eyre DR, Leikin S, Makareeva E, Kuznetsova N, Uveges TE, Ashok A, Flor AW, Mulvihill JJ, Wilson PL, Sundaram UT, Lee B, Marini JC. 2006. Deficiency of cartilage-associated protein in recessive lethal osteogenesis imperfecta. N Engl J Med 355:2757–2764.

Becker J, Semler O, Gilissen C, Li Y, Bolz HJ, Giunta C, Bergmann C, Rohrbach M, Koerber F, Zimmermann K, de Vries P, Wirth B, Schoenau E, Wollnik B, Veltman JA, Hoischen A, Netzer C. 2011. Exome sequencing identifies truncating mutations in human SERPINF1 in autosomal-recessive osteogenesis imperfecta. Am J Hum Genet 88:362–371.

Bond JS, Beynon RJ. 1995. The astacin family of metalloendopeptidases. Protein Sci 4:1247–1261.

Bonod-Bidaud C, Beraud M, Vaganay E, Delacoux F, Font B, Hulmes DJ, Ruggiero F. 2007. Enzymatic cleavage specificity of the proalpha1(V) chain processing analysed by site-directed mutagenesis. Biochem J 405:299–306.

Byers PH, Steiner RD. 1992. Osteogenesis imperfecta. Annu Rev Med 43:269–282.

Cabral WA, Chang W, Barnes AM, Weis M, Scott MA, Leikin S, Makareeva E, Kuznetsova NV, Rosenbaum KN, Tifft CJ, Bulas DI, Kozma C, Smith PA, Eyre DR, Marini JC. 2007. Prolyl 3-hydroxylase 1 deficiency causes a recessive metabolic bone disorder resembling lethal/severe osteogenesis imperfecta. Nat Genet 39:359–365.

Canty EG, Kadler KE. 2005. Procollagen trafficking, processing and fibrillogenesis. J Cell Sci 118(Pt 7):1341–1353.

Colige A, Sieron AL, Li SW, Schwarze U, Petty E, Wertelecki W, Wilcox W, Krakow D, Cohn DH, Reardon W, Byers PH, Lapière CM, Prockop DJ, Nusgens BV. 1999. Human Ehlers-Danlos syndrome type VII C and bovine dermatosparaxis are caused by mutations in the procollagen I N-proteinase gene. Am J Hum Genet 65:308–317.

Colige A, Vandenberghe I, Thiry M, Lambert CA, Van Beeumen J, Li SW, Prockop DJ, Lapiere CM, Nusgens BV. 2002. Cloning and characterization of ADAMTS-14, a novel ADAMTS displaying high homology with ADAMTS-2 and ADAMTS-3. J Biol Chem 277:5756–5766.

Chessler SD, Wallis GA, Byers PH. 1993. Mutations in the carboxyl-terminal propeptide of the pro alpha 1(I) chain of type I collagen result in defective chain association and produce lethal osteogenesis imperfecta. J Biol Chem 268(24):18218–18225.

Christiansen HE, Schwarze U, Pyott SM, AlSwaid A, Al Balwi M, Alrasheed S, Pepin MG, Weis MA, Eyre DR, Byers PH. 2010. Homozygosity for a missense mutation in SERPINH1, which encodes the collagen chaperone protein HSP47, results in severe recessive osteogenesis imperfecta. Am J Hum Genet 86:389–398.

den Dunnen JT, Antonarakis SE. 2000. Mutation nomenclature extensions and suggestions to describe complex mutations: a discussion. Hum Mutat 15:7–12.

den Dunnen JT, Paalman MH. 2003. Standardizing mutation nomenclature: why bother? Hum Mutat 22:181–182.

Doll JA, Stellmach VM, Bouck NP, Bergh AR, Lee C, Abramson LP, Cornwell ML, Pins MR, Borensztajn J, Crawford SE. 2003. Pigment epithelium-derived factor regulates the vasculature and mass of the prostate and pancreas. Nat Med 9:774–780.

Drogemuller C, Becker D, Brunner A, Haase B, Kircher P, Seeliger F, Fehr M, Baumann U, Lindblad-Toh K, Leeb T. 2009. A missense mutation in the SERPINH1 gene in Dachshunds with osteogenesis imperfecta. PLoS Genet 5:e1000579.

Fernandes RJ, Hirohata S, Engle JM, Colige A, Cohn DH, Eyre DR, Apte SS. 2001. Procollagen II amino propeptide processing by ADAMTS-3. Insights on dermatosparaxis. J Biol Chem 276:31502–31509.

Fisher LW, Hawkins GR, Tuross N, Termine JD. 1987. Purification and partial characterization of small proteoglycans I and II, bone sialoproteins I and II, and osteonectin from the mineral compartment of developing human bone. J Biol Chem 262:9702–9708.

Fisher LW, Stubbs JT, 3rd, Young MF. 1995. Antisera and cDNA probes to human and certain animal model bone matrix noncollagenous proteins. Acta Orthop Scand Suppl 266:61–65.

Ge G, Greenspan DS. 2006. Developmental roles of the BMP1/TLD metalloproteinases. Birth Defects Res C Embryo Today 78:47–68.

Guevara T, Yiallouros I, Kappelhoff R, Bissdorf S, Stocker W, Gomis-Ruth FX. 2010. Proenzyme structure and activation of astacin metallopeptidase. J Biol Chem 285:13958–13965.

Hopkins DR, Keles S, Greenspan DS. 2007. The bone morphogenetic protein 1/Tolloid-like metalloproteinases. Matrix Biol 26(7):508–523.

Ishikawa Y, Wirz J, Vranka JA, Nagata K, Bachinger HP. 2009. Biochemical characterization of the prolyl 3-hydroxylase 1.cartilage-associated protein.cyclophilin B complex. J Biol Chem 284:17641–17647.

Kessler E, Takahara K, Biniaminov L, Brusel M, Greenspan DS. 1996. Bone morphogenetic protein-1: the type I procollagen C-proteinase. Science 271:360–362.

Khoshnoodi J, Cartailler JP, Alvares K, Veis A, Hudson BG. 2006. Molecular recognition in the assembly of collagens: terminal noncollagenous domains are key recognition modules in the formation of triple helical protomers. J Biol Chem 281:38117–38121.

Lapunzina P, Aglan M, Temtamy S, Caparros-Martin JA, Valencia M, Leton R, Martinez-Glez V, Elhossini R, Amr K, Vilaboa N, Ruiz-Perez VL. 2010. Identification of a frameshift mutation in Osterix in a patient with recessive osteogenesis imperfecta. Am J Hum Genet 87:110–114.

Lindahl K, Barnes AM, Fratzl-Zelman N, Whyte MP, Hefferan TE, Makareeva E, Brusel M, Yaszemski MJ, Rubin CJ, Kindmark A, Roschger P, Klaushofer K, McAlister WH, Mumm S, Leikin S, Kessler E, Boskey AL, Ljunggren O, Marini JC. 2011. COL1 C-propeptide cleavage site mutations cause high bone mass osteogenesis imperfecta. Hum Mutat 32:598–609.

Makareeva E, Aviles NA, Leikin S. 2011. Chaperoning osteogenesis: new protein-folding disease paradigms. Trends Cell Biol 21:168–176.

Morello R, Bertin TK, Chen Y, Hicks J, Tonachini L, Monticone M, Castagnola P, Rauch F, Glorieux FH, Vranka J, Bächinger HP, Pace JM, Schwarze U, Byers PH, Weis M, Fernandes RJ, Eyre DR, Yao Z, Boyce BF, Lee B. 2006. CRTAP is required for prolyl 3- hydroxylation and mutations cause recessive osteogenesis imperfecta. Cell 127:291–304.

Pappano WN, Steiglitz BM, Scott IC, Keene DR, Greenspan DS. 2003. Use of Bmp1/Tll1 doubly homozygous null mice and proteomics to identify and validate in vivo substrates of bone morphogenetic protein 1/tolloid-like metalloproteinases. Mol Cell Biol 23:4428–4438.

Rauch F, Glorieux FH. 2004. Osteogenesis imperfecta. Lancet 363:1377–1385.

Scott IC, Blitz IL, Pappano WN, Imamura Y, Clark TG, Steiglitz BM, Thomas CL, Maas SA, Takahara K, Cho KW, Greenspan DS. 1999. Mammalian BMP-1/Tolloid-related metalloproteinases, including novel family member mammalian Tolloid-like 2, have differential enzymatic activities and distributions of expression relevant to patterning and skeletogenesis. Dev Biol 213:283–300.

Shimell MJ, Ferguson EL, Childs SR, O'Connor MB. 1991. The Drosophila dorsal-ventral patterning gene tolloid is related to human bone morphogenetic protein 1. Cell 67:469–481.

Sillence DO, Rimoin DL, Danks DM. 1979. Clinical variability in osteogenesis imperfecta-variable expressivity or genetic heterogeneity. Birth Defects Orig Artic Ser 15:113–129.

Steinmann B, Rao VH, Vogel A, Bruckner P, Gitzelmann R, Byers PH. 1984. Cysteine in the triple-helical domain of one allelic product of the alpha 1(I) gene of type I collagen produces a lethal form of osteogenesis imperfecta. J Biol Chem 259:11129–11138.

Suzuki N, Labosky PA, Furuta Y, Hargett L, Dunn R, Fogo AB, Takahara K, Peters DM, Greenspan DS, Hogan BL. 1996. Failure of ventral body wall closure in mouse embryos lacking a procollagen C-proteinase encoded by Bmp1, a mammalian gene related to Drosophila tolloid. Development 122:3587–3595.

Takahara K, Brevard R, Hoffman GG, Suzuki N, Greenspan DS. 1996. Characterization of a novel gene product (mammalian tolloid-like) with high sequence similarity to mammalian tolloid/bone morphogenetic protein-1. Genomics 34:157–165.

Takahara K, Lyons GE, Greenspan DS. 1994. Bone morphogenetic protein-1 and a mammalian tolloid homologue (mTld) are encoded by alternatively spliced transcripts which are differentially expressed in some tissues. J Biol Chem 269:32572–32578.

van Dijk FS, Nesbitt IM, Zwikstra EH, Nikkels PG, Piersma SR, Fratantoni SA, Jimenez CR, Huizer M, Morsman AC, Cobben JM, van Roij MH, Elting MW, Verbeke JI, Wijnaendts LC, Shaw NJ, Högler W, McKeown C, Sistermans EA, Dalton A, Meijers-Heijboer H, Pals G. 2009. PPIB mutations cause severe osteogenesis imperfecta. Am J Hum Genet 85:521–527.

Wildeman M, van Ophuizen E, den Dunnen JT, Taschner PE. 2008. Improving sequence variant descriptions in mutation databases and literature using the mutalyzer sequence variation nomenclature checker. Hum Mutat 29:6–13.

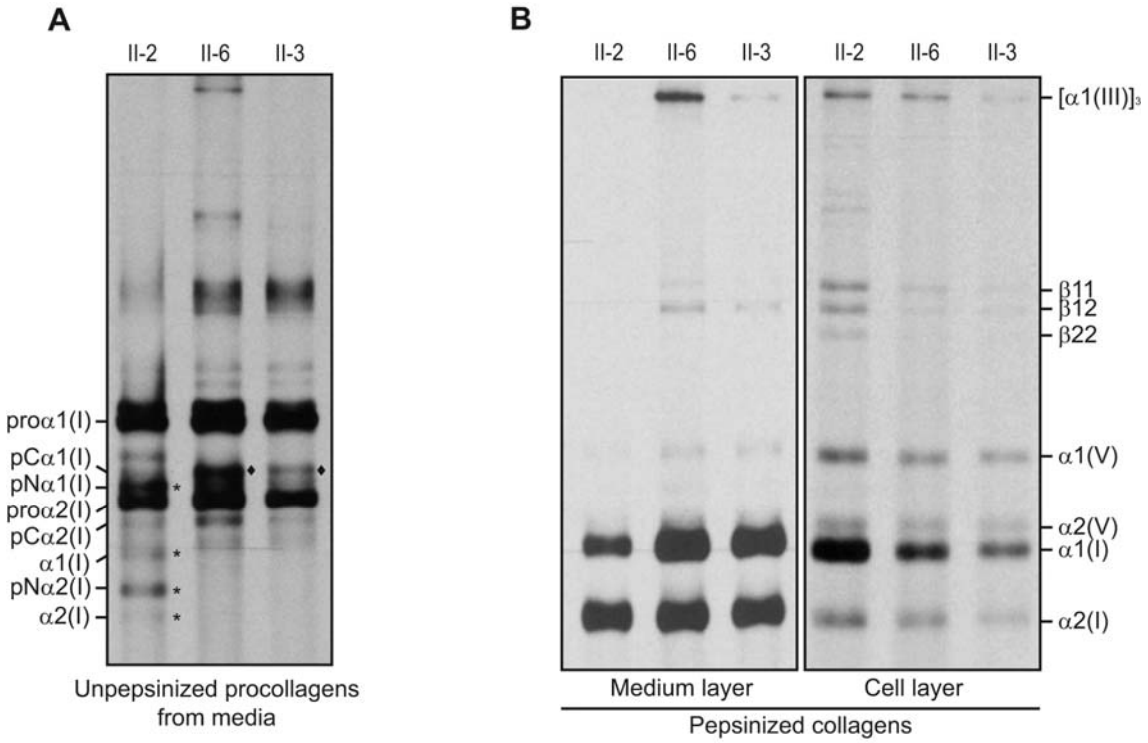

Supp. Figure S1. Steady-state analysis of procollagen processing. **A-B**. Medium and cell layers from confluent fibroblast cultures of the heterozygous sister (II-2) and patients (II-3 and II-6) were radiolabeled for 16 hours, harvested separately and split into two equal amounts for the analysis of unpepsinized (A) and pepsinized (B) procollagens. Ethanol precipitated procollagens were run in reduced (+DTT) conditions. The results in A are indicative of abnormal procollagen processing in the patients as evidenced by the near absence of fully processed α1(I) and α2(I) and diminished amount of pNα1(I) and pNα2(I) in patient cells (asterisks). Diamonds designate increased pCα1(I) in the patient lanes. Normal electromobility of pepsinized collagens is shown in B.

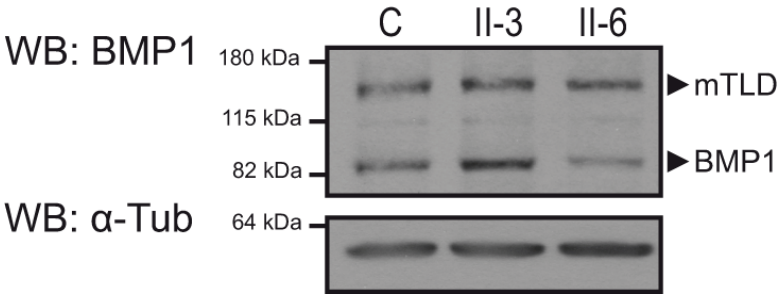

Supp. Figure S2. Endogenous BMP1 and mTLD levels in primary fibroblasts. Western blot showing similar levels of BMP1 and mTLD in whole-cell protein extracts from control (C) and patient (II-3 and II-6) fibroblasts. 50 µg of total protein were loaded in each lane. The band labelled as mTLD migrates to the same position on the gel as the overexpressed mTLD (see figure 3D). α-Tubulin used as loading control is shown in the lower panel.